Dissertation zur Erlangung des Doktorgrades
der Fakultät für Chemie und Pharmazie
der Ludwig-Maximilians-Universität München

Development of Efficient and Low-Scaling Coupled Cluster and Algebraic Diagrammatic Construction Methods

Filippo Sacchetta

aus

Montepulciano, Italy

2023

Erklärung

Diese Dissertation wurde im Sinne von §7 der Promotionsordnung vom 28. November 2011 von Herrn Prof. Dr. Christian Ochsenfeld betreut.

Eidesstattliche Versicherung

Diese Dissertation wurde eigenständig und ohne unerlaubte Hilfe erarbeitet.

München, 11.12.2023

Filippo Sacchetta

Dissertation eingereicht am:	23.10.2023
1. Gutachterin/Gutachter:	Prof. Dr. Christian Ochsenfeld
2. Gutachterin/Gutachter:	Prof. Dr. Andreas Dreuw
Mündliche Prüfung am:	07.12.2023

Danksagung

First of all, I would like to express my sincere gratitude to Prof. Dr. Christian Ochsenfeld for giving me the opportunity to complete this dissertation in his working group and under his supervision, as well as for his support over the years. I also could not have undertaken this journey without the generous support from the Marie Skłodowska-Curie European Training Network "COSINE - COmputational Spectroscopy In Natural sciences and Engineering," Grant Agreement No. 765739 which financed my research. In addition, I am grateful to Prof. Dr. Andreas Dreuw for his contributions to my research.

Of course, this endeavor would not have been possible without the help of Dr. Joerg Kussmann, without whom I would not have been able to complete my research. Additionally, I want to thank all my colleagues for their moral support. In particular, I am grateful to Dr. Daniel Graf, Dr. Henryk Laqua, Felix Bangerter, Yannick Lemke, Viktoria Drontschenko, and Dr. Maximilien Ambroise for their contributions to my research and the inspiring scientific discussions. Moreover, I would like to extend my sincere thanks to Dr. Dirk Rehn for his help in debugging part of the code in the ongoing projects.

Lastly, special thanks to my family and my girlfriend for their constant support and their belief in me over the past five years.

Summary

Molecular electronic structure theory attempts to find approximate solutions to the electronic Schrödinger equation for molecules, and decades of research provided scientists with a plethora of methods of increasing accuracy and cost. Coupled cluster linear response (LR-CC) and algebraic diagrammatic construction (ADC) scheme for the polarization propagator are among the most accurate and hence successful methods for the *in silico* study of excited state properties. However, the steep scaling in the computational and storage demands are prohibitive and limit their application to small molecules. Even in the most cost-effective variants of LR-CC and ADC, i.e., LR-CC2 and ADC(2), the computational effort and the storage demands scale with the fifth and fourth power of the system size, respectively. In the past two decades, several approximations have been made to mitigate the drawbacks of LR-CC2 and ADC(2) and to extend their application to molecular systems of interest. Rank-reduction techniques for the electron-repulsion integrals (ERIs) paved the way for efficient implementations based on the canonical molecular orbitals (MOs), and their combination with the Laplace transformation technique as well as the semi-empirical scaled opposite-spin (SOS) approximation allowed for a diminution of the computational scaling to quartic or even cubic. More recently, local excited state implementations based on spatially confined orbital representations have been proposed showing low-scaling behavior. Nowadays, state-specific local molecular orbitals (LMOs), natural orbitals (NOs), natural transition orbitals (NTOs), or combinations thereof are employed. However, the localization procedures yielding these orbitals increase the prefactor and make the methods less robust. In this thesis, we present efficient and low-scaling reformulations of SOS-LR-CC2 and SOS-ADC(2) that, contrary to the current local excited state methods, do not require expensive localization techniques. Inspired by the preceding low-scaling second-order Møller-Plesset (MP2) energy approaches, we reformulate the SOS-LR-CC2 and SOS-ADC(2) methods in the local atomic orbitals (AO) basis and derive expressions for the excitation energies based on Cholesky decomposed density matrices (CDD). For systems with a significant HOMO-LUMO gap, the computational effort, I/O effort, memory and storage demands, as well as their scaling, are reduced by block-sparse linear algebra that takes advantage of the sparsity manifested by the density matrices and the AO-based ERIs decomposed within the resolution of the identity (RI) and tensor hypercontraction (THC) ansatz. For systems with a local electronic structure and local excitations, the presented local ω-CDD-RI-SOS-LR-CC2/ADC(2) implementations show asymptotical linear scaling computational behavior and memory demands when a local metric is used. On the other hand, the CDD-THC-SOS-LR-CC2/ADC(2) implementations show a quadratic scaling behavior in the asymptotic limit and exhibit considerably reduced computational effort and memory demands with respect to the RI-based variants. Finally, low-scaling reformulations for computing the one-particle reduced density matrix of excited states and transition density matrix are provided enabling, e.g., the analysis of the electronic structure of excited states and transition properties for molecules with hundreds of atoms at the ADC(2) level of theory.

List of Publications

The present work is a cumulative dissertation comprising 3 articles (labeled I-III) published in peer-reviewed Journals. In addition, a Chapter is provided discussing the ongoing projects. All articles and the author's contribution to each of them are stated below:

I **F. Sacchetta**, D. Graf, H. Laqua, M. A. Ambroise, J. Kussmann, A. Dreuw, C. Ochsenfeld.
"An effective sub-quadratic scaling atomic-orbital reformulation of the scaled opposite-spin RI-CC2 ground-state model using Cholesky-decomposed densities and an attenuated Coulomb-metric"
J. Chem. Phys. **157**, 104104 (2022).
Contribution by the author: *Most of the theory, most of the implementation, implementation of the block-sparse matrix algebra in cooperation with H. Laqua, all of the test calculations and the writing.*

II M. A. Ambroise, **F. Sacchetta**, D. Graf, C. Ochsenfeld, A. Dreuw.
"Scaled opposite-spin atomic-orbital based algebraic diagrammatic construction scheme for the polarization propagator with asymptotic linear-scaling effort: Theory and implementation"
J. Chem. Phys **158**, 124121 (2023).
Contribution by the author: *Shared first authorship. Development of the theory in cooperation with M. A. Ambroise and D. Graf. Contributions to the manuscript.*

III **F. Sacchetta**, F. Bangerter, H. Laqua, C. Ochsenfeld.
"Efficient Low-scaling Calculation of THC-SOS-LR-CC2 and THC-SOS-ADC(2) Excitation Energies Through Density-based Integral-direct Tensor Hypercontraction"
To be submitted (2023).
Contribution by the author: *Shared first authorship. Development and implementation in cooperation with F. Bangerter and H. Laqua. Most of the test calculations. Equal contribution to the writing.*

Contents

1 Introduction **1**

2 Electronic Structure Methods for the Ground State **5**
2.1 Hartree-Fock Approximation 6
2.1.1 Roothaan-Hall equations 7
2.2 Electron-Correlation Methods 8
2.3 Second Quantization 9
2.4 Coupled Cluster Theory 10
2.4.1 Pair Clusters 10
2.4.2 The Coupled Cluster wave function 11
2.4.3 The projected Coupled Cluster Schrödinger equations 12
2.5 Second-Order Møller-Plesset Perturbation Theory: MP2 14
2.5.1 Explicit expressions for the closed-shell MP2 energy 15
2.6 Coupled Cluster Perturbation Theory 16
2.6.1 The approximate CCSD method: CC2 17
2.6.2 Explicit expressions for the closed-shell CC2 method 18

3 Electronic Structure Methods for the Excited States **21**
3.1 Coupled Cluster Response Theory 22
3.1.1 Linear Response CC2 24
3.2 Algebraic Diagrammatic Construction Theory 24
3.2.1 Intermediate State Representation 25
3.2.2 Second-Order Algebraic Diagrammatic Construction Theory: ADC(2) . 27
3.3 Solution of the LR-CC2 and ADC(2) eigenvalue problems 27
3.3.1 Explicit expressions for closed-shell CC2 and ADC(2) matrix-vector products 28
3.4 Relation between LR-CC2 and ADC(2) 30

4 Tensor Decomposition and Sparse Linear-Algebra **33**
4.1 Resolution of the Indentity 33
4.2 Tensor Hypercontraction 35
4.3 Block-Sparse Linear Algebra 37

5 Publications **39**
5.1 Publication I: An effective sub-quadratic scaling atomic-orbital reformulation of the scaled opposite-spin RI-CC2 ground-state model using Cholesky-decomposed densities and an attenuated Coulomb metric 39

5.2 Publication II: Scaled opposite-spin atomic-orbital based algebraic diagrammatic construction scheme for the polarization propagator with asymptotic linear-scaling effort: Theory and implementation 60
5.3 Publication III: Efficient Low-scaling Calculation of THC-SOS-LR-CC2 and THC-SOS-ADC(2) Excitation Energies Through Density-based Integral-direct Tensor Hypercontraction 85

6 Ongoing Projects **153**
6.1 Linear-Scaling Evaluation of Closed-Shell RI-SOS-LR-CC2 and RI-SOS-ADC(2) Excitation Energies 153
6.1.1 Low-scaling reformulation: ω-SOS-RI-CDD-LR-CC2 and ω-SOS-RI-CDD-ADC(2) 154
6.1.2 Outline of the implementation 159
6.1.3 Scaling Behavior 164
6.2 Low-scaling Evaluation of Closed-Shell SOS-ADC(2) Density Matrices 168
6.2.1 Closed-shell expressions of the one-particle density matrices 169
6.2.2 Quartic-scaling RI-MO-based formulation of the one-particle density matrices 170
6.2.3 Low-scaling RI-CDD-based formulation of the one-particle density matrices 173
6.2.4 Cubic-scaling THC-MO-based formulation of the one-particle density matrices 177
6.2.5 Low-scaling THC-CDD-based formulation of the one-particle density matrices 180

7 Conclusion **185**

8 Appendix **189**

List of Figures

2.1 Hierarchy of correlation methods. 9

4.1 Block-sparsity patterns of the density matrices for linear carboxylic acid with 160 carbon atoms (LCA_{160}) in the def2-SVP basis.[162] The relevant blocks are in red, while the non-significant block are in white. The cutoff threshold was $\vartheta_a = 10^{-7}$. (A) occupied one-particle density matrix. (B) Cholesky decomposed occupied one-particle density matrix. (C) virtual one-particle density matrix. (D) AO-based singles transition vector to the lowest singlet state of LCA_{160}. 37

4.2 Schematic representation of a block-sparse matrix. The red blocks are the significant and allocated blocks. Each block has a defined maximum row and column dimension, **x** and **y**, respectively. 38

6.1 Number FLOP for the evaluation of the matrix-vector product of MO-RI-SOS-LR-CC2 and MO-RI-SOS-ADC(2) (MO) and ω-CDD-SOS-RI-SOS-LR-CC2 ω-CDD-SOS-RI-SOS-ADC(2) with $\omega = 0.0$ (CDD-0) and $\omega = 0.1$ (CDD-1) in the def2-SVP basis. The computational scaling and speedups are also reported. 164

6.2 Number of relevant blocks in the most important intermediates of ω-CDD-RI-SOS-ADC(2) with $\omega = 0.0$ (A) and $\omega = 0.1$ (B) for the def2-SVP basis. 167

List of Tables

6.1 Formal and asymptotic computational scaling (with the number of orbitals N) for key steps of ω-CDD-RI-SOS-LR-CC2 and ω-CDD-RI-SOS-ADC(2) within the RI standard-Coulomb metric ($\omega = 0$) and overlap metric ($\omega \to \infty$). 163

1 Introduction

Non-relativistic quantum chemistry has at its center the Schrödinger equation[1] whose solutions describe all non-relativistic properties of any physical system, e.g., molecules. However, it can not be solved analytically for molecular systems containing more than one electron. Therefore, since the publication of the Schrödinger equation in 1926, scientists relied on approximations to systematically approach the exact solutions – many-particle wave functions – for any many-electron molecular system. Within the Born-Oppenheimer approximation,[2] the Schrödinger equation is reduced to the so-called electronic Schrödinger equation. Its solutions describe the correlated motion of the electrons in a field of fixed atoms. Thus, the electronic Schrödinger equation yields a potential energy surface for the nuclei to move on. Despite its reduced space, not even the electronic Schrödinger equation can be solved exactly, and a hierarchy of wave function-based – ab initio – schemes was proposed to systematically approach the exact electronic wave function.[3] The simplest representation of the electronic motion is provided by the Hartree-Fock (HF) wave function, where the electronic interactions are described in a mean-field approach. The HF method is known to account for 99% of the electron correlation, the remaining 1% is, however, crucial for describing chemical properties accurately. The missing correlation effects are recovered by ab initio methods devised upon the HF wave function and hence called post-HF methods. Amongst the most popular we list the coupled cluster[4–11] (CC) and Møller-Plesset[4,12,13] perturbation theory (MPPT).
The main difficulties associated with the hierarchy of quantum chemical methods are the large computational effort and memory demands, as well as their steep increase with the size of the system M defined by, e.g., the number of atoms or atom-centered orbitals (AOs). The computational effort for solving the simplest ab initio scheme, the HF method, scales conventionally as $\mathcal{O}(M^3)$, where $\mathcal{O}()$ denotes the order of the asymptotic scaling behavior.[14] That means the computational cost of HF increases 1000-fold if the size of the system is 10 times larger. Accounting for the electron correlation effects vastly increases both the prefactor and the scaling behavior because it typically requires the evaluation of several four-index electron-repulsion integrals (ERIs) and the solution of the equations involving them. Among the less expensive and yet often chemically accurate post-HF methods, the so-called second-order Møller-Plesset[12] (MP2) and the approximated coupled cluster singles and doubles[15] (CC2) methods show $\mathcal{O}(M^5)$ computational scaling behavior and $\mathcal{O}(M^4)$ scaling behavior for the memory demands – in their conventional, canonical molecular orbital (MO)-based formulations. The more accurate coupled cluster singles and doubles[9] (CCSD) approach shows $\mathcal{O}(M^6)$ computational scaling behavior. Due to the computational cost and memory demands in their conventional formulations, these methods can be routinely applied to systems with only a few atoms.

Among the ab initio methods listed so far, scientists have shown particular interest in CC2 as it provides ground state energies and properties at a level similar to MP2 and as it grants access

to excited states within the linear response[15–18] (LR) – or equation-of-motion[19–21] (EOM) – framework retaining the $\mathcal{O}(M^5)$ computational scaling behavior. In addition, the possibility of obtaining explicit equations for the closely related and more compact second-order algebraic diagrammatic constructor scheme,[22] ADC(2) as a by-product of LR-CC2,[23–25] piqued the interest in this method. Despite the LR-CC2 and ADC(2) methods profiting from the fast improvement of computer technology, their application to large systems is still hampered by the scaling behavior of their computational (and storage) demands. An important role in reducing the prefactor and the scaling behavior with the system size of LR-CC2 and ADC(2) was played by the decomposition of the ERIs via the resolution of the identity[26,27] (RI) and the tensor hyper-contraction[28–31] (THC). Indeed, they mitigated the bottleneck represented by the storage demands and reduced the cost of computing the electron integrals in the MO basis.[23,24,32] In addition, the combination of the scaled opposite-spin[33] (SOS) – that neglects the calculation of the contributions from electrons with the same spin and scales the opposite spin part by a factor (i.e., $c_{\text{os}} = 1.3$) – and the Laplace transformation of the energy denominators[34–37] decreased the scaling of the MO-based LR-CC2 and ADC(2) methods to $\mathcal{O}(M^4)$[25,38] within the RI framework – here named MO-RI-SOS-LR-CC2 and MO-RI-SOS-ADC(2), respectively. Alternatively, a cubic scaling implementation of SOS-EOM-CC2 within the THC approximation was proposed[32,39] – here named MO-THC-SOS-EOM-CC2. Such approximations extended the routine application of these schemes to molecular systems with $\sim$150 atoms and increased their popularity.
The application of LR-CC2 and ADC(2) to the thousand atoms region is achieved by exploiting the locality of the electronic structure of systems with a significant HOMO-LUMO gap[14,40] as well as the locality of the electronic excitation. The description of the electronic structure of such systems is often unphysical when the canonical molecular orbitals are used, i.e., these orbitals are delocalized over the molecular systems, and the sparsity of the electronic structure is not well represented. On the other hand, the use of localized orbitals such as local molecular orbitals (LMOs) and projected atomic orbitals[41–44] (PAOs) was first introduced for MP2 to decrease its computational scaling since they account for the locality of the electronic structure. Later, these orbitals have been used within CC2 and ADC(2) methods[45–48] as well as natural orbitals[49–57] (NOs), natural transition orbitals[58,59] (NTOs), and correlated natural transition orbitals[60] (CNTOs) reducing their scaling behavior. The major drawback of these local approaches is that they are often state-specific and hence the set of local orbitals needs to be recomputed for each excited state – or even each iteration – and it may become a limiting factor for multi-state calculations.[59,60] As an alternative to both MOs and localized orbitals of the above kind, one can rely on the sparsity of the ERIs expressed in terms of AOs and on the one-particle density matrix that contains information about the electronic structure while properly reflecting its sparsity. In fact, the density matrix decays rapidly with the size of systems characterized by a local electronic[40] structure and hence it contains a linearly growing number of significant – non-zero – elements in the asymptotic limit.[14,40]

The aim of the present work is the development of efficient and linear scaling algorithms for the evaluation of molecular energies and properties at the LR-CC2 and ADC(2) level of theory, by reformulating their equations in terms of Cholesky decomposed one-particle density (CDD) matrices and avoiding any kind of localization or integral-screening technique. In order to exploit the sparsity of the tensors, we implemented fast block-sparse linear algebra routines which greatly reduce the number of operations as well as the storage demands for systems with

a significant HOMO-LUMO gap (see Sec. 4.3) and local excitations. In addition, we aim to develop efficient algorithms that show linear computational behavior and an early crossover with the existing MO-based implementations. Note that the crossover point indicates the system size beyond which a certain method is faster than another one, and it depends both on the prefactors and the scaling of the compared methods. In Chapter 2, we set the theoretical foundations of the methods that account for the correlated motion of the electrons in the ground state. In Chapter 3, we discuss the linear response coupled cluster (LR-CC) theory and algebraic diagrammatic construction (ADC) scheme that extends the CC and MPPT methods to the description of excited states. In Chapter 4, a description of the integral decomposition techniques and an outline of the sparse linear algebra routines are provided. The last two chapters constitute the main part of this cumulative dissertation. Chapter 5 reproduces **Publication I-III** in their entirety, while the unfinished projects are discussed in Chapter 6.

Publication I (in Chapter 5) focuses on reformulating in the AO basis the problem for the scaled opposite-spin CC2 ground state energy within the RI approximation (RI-SOS-CC2) to extend its applicability to molecules with several hundreds of atoms and large basis sets. We exploit sparse linear algebra and, for the first time, a local RI Coulomb metric to achieve an asymptotic sub-quadratic computational and storage scaling with the size of the system. The three-index electron integrals obtained via RI decomposition are treated by our sparse algebra routines and the number of significant elements grows linearly with the size of systems with sparse electronic structure. Despite the $\mathscr{O}(N)$ behavior of the three-index integrals, the I/O of these tensors eventually becomes an important bottleneck in our local reformulation and hence a Lagrangian-based minimal-overhead batching scheme[61] is introduced to alleviate the I/O cost. In addition, we introduce the Cholesky decomposed density matrices[62–64] (CDD), significantly reducing the memory requirements of the method on a single node as well as the computational effort. Hence, an early crossover with the MO-based formulation is achieved. The resulting ω-CDD-RI-SOS-CC2 method proved to be as accurate as the MO-based implementation for small- to medium-size systems while it shows a linear scaling growth in the error for larger systems with sparse electronic structures. Both performance and accuracy are controlled by the sparsity thresholds used within our sparse linear algebra and set by the user (see Sec. 4.3). The importance of the results achieved in this work relies on the possibility of extending such local reformulation to the equations for the RI-SOS-LR-CC2 and RI-SOS-ADC(2) excited states energies as well as their properties. Furthermore, we showed the efficiency and accuracy of our sparse linear algebra routines that do not present negative effects on the convergence of the iterative optimization of the CC2 amplitudes. Notice that the algorithms discussed in **Publication I** are implemented in the FERMIONS++[65–67] program.

Publication II (in Chapter 5) provides a local reformulation of the scaled opposite-spin second-order algebraic diagrammatic construction SOS-ADC(2) scheme within the RI approximation, for singlet and triplet states. The equations of the RI-SOS-ADC(2) problem are derived from RI-SOS-LR-CC2 in order to reduce the size of the RI-SOS-ADC(2) secular matrix[25] and hence the computational effort with respect to the more rigorous intermediate state representation (ISR)-RI-SOS-ADC(2) matrix. The reformulation strategy proposed in **Publication I** is used to rewrite the MO-based equations – for both singlet and triplet excitation energies – in terms of Cholesky decomposed density matrices (CDD). By exploiting the sparsity of the electronic structure and, additionally, the locality of the electronic excitation, the new CDD-RI-SOS-ADC(2) implemen-

tation shows a $\mathcal{O}(N^2)$ computational scaling behavior when the standard RI Coulomb metric is used. As in **Publication I**, we take advantage of a local RI Coulomb metric to increase the sparsity within the three-index integrals and further decrease the effort and the memory demands to asymptotically linear – for local excitations and sparse electronic structures. The linear scaling implementation – ω-CDD-RI-SOS-ADC(2) – is applied to both linear and three-dimensional systems in order to test its behavior and accuracy. Furthermore, we propose a CDD-RI-SOS-ADC(2) implementation based on the so-called quasi-robust[68] RI approximation which provides a sparse RI metric while retaining the accuracy of the standard (and dense) Coulomb metric. The presented ω-CDD-RI-SOS-ADC(2) method is implemented in a developmental quantum chemistry package called MEGALOCHEM of M. Ambroise, which is open source and available at `https://github.com/ambmax00/megalochem`.
Publication III (in Chapter 5) presents a highly efficient and low-scaling reformulation of the SOS-CC2 and SOS-ADC(2) equations – for singlet and triplet states – where the ERIs are decomposed via least-squares (LS)-THC. Furthermore, a density-based integral-direct approach for the formation of LS-THC fitting metric is presented. The density-based reformulation allows the use of existing codes for Coulomb matrix builds facilitating the implementation of LS-THC in quantum chemistry packages since only the ability to evaluate basis functions on a real-space DFT-like grid is required. In addition, an optimized kernel for the calculation of the THC metric improves the efficiency of the THC fitting step. Notice that, in order to obtain chemically accurate results, different THC-fitting matrices are computed for different kinds of ERIs.
The use of tensor hypercontraction vastly scales down both the memory demands and computational cost of these methods because the ERIs are decomposed into two-index tensors (matrices). Contrary to the RI-approximated formulations, the computational scaling of SOS-ADC(2) and SOS-CC2 is reduced to cubic by introducing the THC decomposition. In order to further extend the applicability of MO-THC-SOS-LR-CC2 and MO-THC-SOS-ADC(2), we reformulated the equations for the ground and excited state energies by introducing the Cholesky decomposed density matrices (CDD), as previously proposed in **Publications I-II** and made use of our sparse linear algebra routines. The computational effort to evaluate the excitation energies with the newly derived CDD-THC-SOS-ADC(2) and CDD-THC-SOS-LR-CC2 formulations scales as $\mathcal{O}(N^2)$ for systems with local electronic structure and local excitations. On the other hand, the solution of the ground state equations – i.e., SOS-MP2 and SOS-CC2 energies – shows a sub-cubic computational scaling behavior for the studied systems. The CDD-THC-SOS-ADC(2) model is applied to linear and three-dimensional systems (e.g., LCAs and DNA fragments) in order to assess its accuracy and performance. The algorithms and equation presented in **Publication III** are implemented in the FERMIONS++[65–67] program.

Finally, in Chapter 6 we provide an improved linear scaling algorithm for the evaluation of the RI-SOS-ADC(2) and RI-SOS-LR-CC2 excitation energies (see Sec. 6.1). In addition, in Section 6.2 we propose a low-scaling reformulation, based on the Cholesky decomposed ground state density matrices (CDD), of the equations for the formation of the one-particle reduced density matrices and transition density matrices for SOS-MP2 and SOS-ADC(2) by using either the RI and THC decomposition of the ERIs.

2 Electronic Structure Methods for the Ground State

The movement of electrons and nuclei in molecules is described by the time-dependent Schrödinger equation[1]

$$\hat{H}\Psi(\{x_i\},\{R_A\},t) = i\frac{h}{2\pi}\frac{\delta}{\delta t}\Psi(\{x_i\},\{R_A\},t) \tag{2.1}$$

where h is Planck's constant and Ψ is the molecular wave function depending on the coordinates (including spin) of all electrons x_i and the coordinates of all nuclei R_A, and the time t. The Hamilton operator $\hat{H}$

$$\hat{H} = \hat{T}_\mathrm{n} + \hat{T}_\mathrm{e} + \hat{V}_\mathrm{nn} + \hat{V}_\mathrm{en} + \hat{V}_\mathrm{ee} \tag{2.2}$$

describes the movements and interactions of all particles as the kinetic energy of the nuclei $\hat{T}_\mathrm{n}$ and the electrons $\hat{T}_\mathrm{e}$, the Coulomb repulsion between nuclei $\hat{V}_\mathrm{nn}$ and between electrons $\hat{V}_\mathrm{ee}$, as well as the Coulomb attraction between electrons and nuclei $\hat{V}_\mathrm{en}$. The stationary solutions of eq. (2.1) can be separated into a time-independent wave function and a time-dependent phase-factor

$$\Psi(\{x_i\},\{R_A\},t) = \Psi(\{x_i\},\{R_A\})e^{-\frac{i2\pi}{h}Et} \tag{2.3}$$

where the wave function $\Psi(\{x_i\},\{R_A\})$ solves the time-independent Schrödinger equation:[1]

$$\hat{H}\Psi(\{x_i\},\{R_A\}) = E\Psi(\{x_i\},\{R_A\}) \tag{2.4}$$

with E being the constant energy of the state described by $\Psi(\{x_i\},\{R_A\})$. The exact solution of eq. (2.4) is precluded by the two-particle operators $\hat{V}_\mathrm{nn}$, $\hat{V}_\mathrm{en}$, and $\hat{V}_\mathrm{ee}$ in the Hamiltonian $\hat{H}$.
Since the nuclei are much heavier than electrons and therefore move significantly slower, one can consider the electrons in a molecule to be moving in a field of fixed nuclei (Born-Oppenheimer approximation).[2] Within this approximation, T_n and V_nn are considered constants, and the remaining terms of the Hamilton operator result in the electronic Hamilton operator $\hat{H}_\mathrm{e}$. The Schrödinger equation in the Born-Oppenheimer approximation

$$\hat{H}_\mathrm{e}\Psi_\mathrm{e}(\{x_i\}) = E_\mathrm{e}\Psi_\mathrm{e}(\{x_i\}) \tag{2.5}$$

is solved by the electronic wave function Ψ_e that depends explicitly on the electronic coordinates and only parametrically on the position of the nuclei. The total energy of the system is the sum of E_e and the nuclear-nuclear repulsion energy V_nn. Despite the complexity of eq. (2.4) being reduced within the Born-Oppenheimer approximation, its solution quickly becomes unfeasible to be handled computationally because of the electron-electron repulsion term $\hat{V}_{ee}$. Therefore, additional approximations are required to efficiently determine the electronic energy.

2.1 Hartree-Fock Approximation

The simplest way to handle the many-electron problem is to consider a system of non-interacting electrons (independent particle model, IPM) whose Hamiltonian is given by a sum of effective one-electron operators and hence is described by a wave function that is a simple anti-symmetrized product of one-electron wave functions (molecular orbitals, MO) $\phi_i(x_j)$, the so-called Slater determinant:[69]

$$\Phi_0 = |\mathrm{HF}\rangle = \frac{1}{\sqrt{n!}} \det \begin{pmatrix} \phi_1(x_1) & \phi_2(x_1) & \dots & \phi_n(x_1) \\ \phi_1(x_2) & \phi_2(x_2) & \dots & \phi_n(x_2) \\ \vdots & \vdots & \ddots & \vdots \\ \phi_1(x_n) & \phi_2(x_n) & \dots & \phi_n(x_n) \end{pmatrix} = |\Phi_0\rangle \tag{2.6}$$

where n is the number of electrons, ϕ_i the spin-orbital i, and x_j the space-spin coordinates of electron j. It is easily shown that the Slater determinant wave function satisfies the Pauli principle (antisymmetry principle), which a Fermionic wave function has to satisfy:[70]

$$\Psi_\mathrm{e}(x_1,\dots,x_i,\dots,x_j,\dots,x_n) = -\Psi_\mathrm{e}(x_1,\dots,x_j,\dots,x_i,\dots,x_n), \tag{2.7}$$

Solving the electronic Schrödinger equation – in eq. (2.5) – for $|\mathrm{HF}\rangle$ results in the Hartree-Fock (HF) method. According to the Slater-Condon rules,[71] the expectation value of the electronic Hamiltonian yields the Hartree-Fock ground state energy

$$E_\mathrm{HF} = \langle \mathrm{HF}|\hat{H}_\mathrm{e}|\mathrm{HF}\rangle = \sum_i^{N_\mathrm{occ}} \langle i|\hat{h}|i\rangle + \frac{1}{2}\sum_{ij}^{N_\mathrm{occ}} \langle ij||ij\rangle = \sum_i^{N_\mathrm{occ}} (i|\hat{h}|i) + \frac{1}{2}\sum_{ij}^{N_\mathrm{occ}} (ii||jj) \tag{2.8}$$

where N_occ is the number of occupied orbitals. The one-electron integrals

$$\langle i|\hat{h}|i\rangle = (i|\hat{h}|i) = \int \mathrm{d}x_1 \phi_i^*(x_1)\hat{h}(r_1)\phi_i(x_1) \tag{2.9}$$

$$\hat{h} = -\frac{1}{2}\nabla_1^2 - \sum_A^{N_\mathrm{atoms}} \frac{Z_A}{r_{1A}} \tag{2.10}$$

and the two-electron integrals are given in both Dirac notation

$$\langle ij|ij\rangle = \iint \mathrm{d}x_1 \mathrm{d}x_2 \phi_i^*(x_1)\phi_i(x_1)\frac{1}{|r_1 - r_2|}\phi_j^*(x_2)\phi_j(x_2) \tag{2.11}$$

$$\langle ij||ij\rangle = \langle ij|ij\rangle - \langle ij|ji\rangle \tag{2.12}$$

$$\tag{2.13}$$

and Mulliken notation

$$\langle ij|ij\rangle = (ii|jj) \qquad\qquad (ii||jj) = (ii|jj) - (ij|ji) \tag{2.14}$$

Minimizing eq. (2.8) with respect to the one-particle functions (the MOs) according to the variational principle and ensuring the MO orthonormality leads - after unitary transformation - to the canonical HF equations[71]

$$\hat{F}\phi_i = \varepsilon_i \phi_i \tag{2.15}$$

Since the Fock operator

$$\hat{F} = \hat{h} + \sum_{j}^{N_{\text{occ}}} \left[\hat{J}_j - \hat{K}_j \right] \tag{2.16}$$

depends on the molecular orbitals through the Coulomb operator

$$\hat{J}_j \phi_i(x_1) = \int \mathrm{d}x_2 \phi_i(x_1) \frac{1}{r_{12}} \phi_j^*(x_2) \phi_j(x_2) \tag{2.17}$$

and the exchange operator

$$\hat{K}_j \phi_i(x_1) = \int \mathrm{d}x_2 \phi_j(x_1) \frac{1}{r_{12}} \phi_j^*(x_2) \phi_i(x_2) \tag{2.18}$$

the HF equations must be solved iteratively by employing the self-consistent field (SCF) method.

2.1.1 Roothaan-Hall equations

The molecular orbitals can be expanded in a fixed, finite set of atom-centered basis functions χ_ν (atomic orbitals, AOs) in the linear combination of atomic orbital (LCAO) ansatz

$$\phi_i(r) = \sum_{\nu} C_{\nu i} \chi_\nu, \tag{2.19}$$

employing the linear expansion coefficients $C_{\nu i}$. Inserting this ansatz into 2.16 and projecting onto one trial orbital χ_μ, leads to the Roothaan-Hall equations[72]

$$\sum_{\nu} \langle \chi_\mu | \hat{F} | \chi_\nu \rangle C_{\nu i} = \sum_{\nu} \langle \chi_\mu | \chi_\nu \rangle C_{\nu i} \varepsilon_i, \tag{2.20}$$

which represents a non-orthogonal matrix eigenvalue problem

$$\mathbf{FC} = \mathbf{SC}\boldsymbol{\varepsilon} \tag{2.21}$$

where $\mathbf{S}$ is the overlap metric, $\mathbf{C}$ are the molecular orbital coefficients and the diagonal matrix $\boldsymbol{\varepsilon}$ contains the orbital energies. The Fock matrix is given by

$$F_{\mu\nu} = h_{\mu\nu} + \sum_{\mu\nu} P_{\lambda\sigma} \left[\langle \mu\lambda | \nu\sigma \rangle - \frac{1}{2} \langle \mu\lambda | \sigma\nu \rangle \right] \tag{2.22}$$

with the matrix $\mathbf{P}$ being the matrix representation of the one-particle density (or Fock-Dirac density) in the given AO basis.

$$P_{\mu\nu} = \sum_{i} C_{\mu i} C_{\nu i} \tag{2.23}$$

The HF energy is computed as

$$E_{\text{HF}} = \frac{1}{2} \text{Tr}[\mathbf{P}(\mathbf{H} + \mathbf{F})] \tag{2.24}$$

with the matrix **H** representing the core Hamiltonian. The formal scaling behavior with the number of basis functions N of the HF method is $\mathscr{O}(N^4)$ due to the computation of the Coulomb matrix **J** and **K**:

$$J_{\mu\nu} = \sum_{\lambda\sigma} P_{\lambda\sigma}(\mu\nu|\lambda\sigma) = \sum_{\lambda\sigma} P_{\lambda\sigma} \iint \mathrm{d}r_1 \mathrm{d}r_2 \chi_\mu^*(r_1)\chi_\nu(r_1)\frac{1}{r_{12}}\chi_\lambda^*(r_2)\chi_\sigma(r_2) \tag{2.25}$$

$$K_{\mu\nu} = \sum_{\lambda\sigma} P_{\lambda\sigma}(\mu\sigma|\nu\lambda) = \sum_{\lambda\sigma} P_{\lambda\sigma} \iint \mathrm{d}r_1 \mathrm{d}r_2 \chi_\mu^*(r_1)\chi_\sigma(r_1)\frac{1}{r_{12}}\chi_\lambda^*(r_2)\chi_\nu(r_2) \tag{2.26}$$

The use of direct SCF methods[73] and the introduction of integral screening techniques allow to form the Fock matrix with a computational effort scaling asymptotically as $\mathscr{O}(N^2)$. Further reduction to $\mathscr{O}(N)$[14] is possible by fast multiple methods[74–77] and exploiting the coupling with the one-particle density matrix **P**[78,79] for systems with significant HOMO-LUMO gap.[14,40] The diagonalization of the Fock matrix scales with the system size and hence different diagonalization alternatives exist, achieving asymptotic linear scaling for very large systems.[80–83]

2.2 Electron-Correlation Methods

The HF energy accounts only for $\sim 99\%$ of the non-relativistic energy. The error results from the use of a single determinantal wave function describing the spatial distribution of the electrons by a set of orbitals. In other words, the motions of two electrons are not correlated as the probability of finding electron 2 at r_2 does not depend on the position r_1 of electron one. Although the antisymmetry of the Slater determinant introduces a partial correlation between electrons with parallel spins, the Coulomb interaction between two electrons is accounted for in an average fashion. The missing $\sim 1\%$ energy is important to describe chemical properties accurately and is defined as correlation energy, i.e., the difference between the exact non-relativistic energy E_{ex} and the HF energy:

$$E_{\mathrm{corr}} = E_{\mathrm{ex}} - E_{\mathrm{HF}} \tag{2.27}$$

It is important to stress that the correlation energy is an artificial concept originating from the independent particle approximation. In order to determine the correlation energy, the description of the Coulomb repulsion between two electrons (Coulomb correlation) must be improved. Notice that the electron correlation associated with the Pauli principle is called the Fermi correlation and is already included in the HF reference and therefore is excluded by the definition of eq. (2.27). In addition, one can distinguish between dynamic and static correlation. The dynamic correlation is generally associated with the correlated motion of electrons due to their "instantaneous repulsion". The static correlation is associated with the electrons avoiding each other as they occupy different spatial orbitals. The second one becomes important when multiple and nearly degenerate configurations contribute to the wave function. The conceptually simplest method to recover the correlation energy is the well-known *Configuration Interaction (CI)*, where the N-electron Hamiltonian is diagonalized in a basis of all possible Slater determinants (configurations) generated from the one-electron functions obtained as solution of the HF problem. That is the exact wave function is expressed as a linear combination of N-electron Slater determinants

$$\Psi_{\mathrm{FCI}} = c_0\Phi_0 + \sum_{ia} c_i^a \Phi_i^a + \sum_{ijab} c_{ij}^{ab}\Phi_{ij}^{ab} + \sum_{ijkabc} c_{ijk}^{abc}\Phi_{ijk}^{abc} + \ldots. \tag{2.28}$$

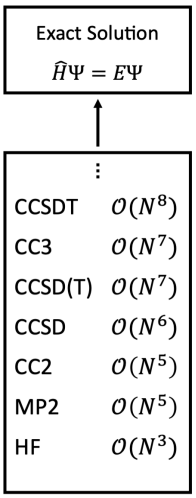

Figure 2.1: Hierarchy of correlation methods.

whose expansion coefficients c are variationally determined. The single (Φ_i^a), double (Φ_{ij}^{ab}), triple (Φ_{ijk}^{abc}), etc. excited determinants describe the electronic configurations generated by the instantaneous repulsion of the electrons. If all possible excited determinants are considered, this full configuration-interaction (FCI) ansatz represents the correlated wave function exactly. The correlation energy is given by

$$E_{\text{corr}}^{\text{FCI}} = \sum_{i>j} \sum_{a>b} c_{ij}^{ab} \langle \Psi_{\text{HF}} | \hat{H} | \Psi_{ij}^{ab} \rangle \tag{2.29}$$

where the coefficients c_{ij}^{ab} are obtained as a solution of equations involving the contributions from all excited state determinants that interact with the doubly excited state.
The prohibitive computational effort to form c_{ij}^{ab} makes the evaluation of the correlation energy (i.e., the description of the electron correlation) challenging, and hence a hierarchy of methods has been developed to approximate eq. (2.29) – see Figure 2.1. These methods like truncated CI, many-body perturbation theory (MBPT), and coupled cluster theory (CC) are usually known as post-HF methods as they improve the description of the electronic repulsion provided by the uncorrelated HF reference wave function. Due to the steep scaling and the lack of size consistency in the truncated CI approximations, these have fallen out of favor.[71]

2.3 Second Quantization

The formalism of second quantization[4,84–86] simply rewrites the Schrödinger equation in terms of elementary creation $\hat{a}_p^\dagger$ and annihilation $\hat{a}_p$ operators. The antisymmetry of the electronic wave function follows from the algebra of these operators.
In second quantization, each determinant is represented by an occupation-number (ON) vector $|\mathbf{k}\rangle$,

$$|\mathbf{k}\rangle = |k_1, k_2, \ldots, k_{\text{n}}\rangle \tag{2.30}$$

where the occupation number k_i is 1, if ϕ_i is present in the determinant (occupied) and 0 if it is absent (unoccupied). The creation and annihilation operators raise and lower the respective occupation number by one and satisfy the following anticommutation rules:[87]

$$\left[\hat{a}_p^\dagger, \hat{a}_q^\dagger\right]_+ = \left[\hat{a}_p, \hat{a}_q\right]_+ = 0 \tag{2.31}$$

$$\left[\hat{a}_p^\dagger, \hat{a}_q\right]_+ = \hat{a}_p^\dagger \hat{a}_q + \hat{a}_q \hat{a}_p^\dagger = \delta_{pq} \tag{2.32}$$

with δ_{pq} denoting the Kronecker delta. Using eqs. (2.31) and (2.32) and introducing the vacuum state, it can be shown that the antisymmetry property of the wave function has been transferred to the algebraic properties of the creation and annihilation operators:

$$|k_i, k_j\rangle = \hat{a}_i^\dagger \hat{a}_j^\dagger |vac\rangle = -\hat{a}_j^\dagger \hat{a}_i^\dagger |vac\rangle = -|k_j, k_i\rangle \tag{2.33}$$

In addition, the creation and annihilation operators are used to rewrite the electronic Hamilton operator

$$\hat{H}_\mathrm{e} = \sum_{pq} h_{pq} \hat{a}_p^\dagger \hat{a}_q + \frac{1}{2} \sum_{pqrs} g_{pqrs} \hat{a}_p^\dagger \hat{a}_r^\dagger \hat{a}_q \hat{a}_s \tag{2.34}$$

where the first term is the one-electron operator, and the second is the two-electron operator. From now on, the second quantization formalism will be employed.

2.4 Coupled Cluster Theory

The coupled-cluster (CC) theory represents the most successful way to approach the exact solution to the electronic Schrödinger equation. It is a size-consistent and size-extensive approach that recovers a large part of the correlation energy. However, it requires a suitable single-determinant wave function (e.g., the HF wave function) as a reference and yields poor results, for truncated CC, when applied to systems with nearly degenerate (or degenerate) electronic configurations. Thus, the application of the CC approximation is best suited for describing the dynamic correlation, rather than the static correlation.[4]

2.4.1 Pair Clusters

As an improvement to the HF wave function, one may consider that the motion of two interacting electrons – occupying the orbitals ϕ_i and ϕ_j – is disturbed by their instantaneous repulsion which leads to the excitation of the electrons to a different set of orbitals ϕ_a and ϕ_b, initially unoccupied. With each excitation, we associate an amplitude t_{ij}^{ab}, representing the probability that this particular excitation will occur as a result of interactions among the electrons. This excitation process is mathematically described by the so-called pair cluster expansion:

$$\hat{a}_i^\dagger \hat{a}_j^\dagger + \sum_{a>b} t_{ij}^{ab} \hat{a}_a^\dagger \hat{a}_b^\dagger = \left(1 + t_{ij}^{ab} \hat{\tau}_{ij}^{ab}\right) \hat{a}_i^\dagger \hat{a}_j^\dagger \tag{2.35}$$

where $\hat{\tau}_{ij}^{ab}$ is the operator describing the "correlation process" of two electrons occupying the orbitals ϕ_i and ϕ_j

$$\hat{\tau}_{ij}^{ab} = \hat{a}_a^\dagger \hat{a}_i \hat{a}_b^\dagger \hat{a}_j \tag{2.36}$$

Assuming a Hartree-Fock reference state and introducing cluster expansions for all pairs of occupied orbitals, we arrive at the following expression for the wave function:[5]

$$|\mathrm{CCD}\rangle = \Big[\prod_{a>b,i>j}(1+t_{ij}^{ab}\hat{\tau}_{ij}^{ab})\Big]|\mathrm{HF}\rangle \tag{2.37}$$

This approximation is also known as coupled cluster doubles (CCD) wave function, in which only double excitations are allowed and the pair clusters interact with each other.

2.4.2 The Coupled Cluster wave function

The pair clusters dominate the description of the correlated motion of interacting electrons, since at most two electrons (with opposite spins) may coincide in space and the correlated motion is especially important for spatially close electrons. Nevertheless, an accurate treatment of the correlation is achieved by considering clusters of all sizes. Thus, for the three-electron clusters, we consider the interaction of three electrons resulting in the excitation of three electrons from three occupied orbitals to three unoccupied ones. The amplitude associated with this process is t_{ijk}^{abc}. In addition, one should allow one-electron processes that represent a relaxation of the orbitals. A general expression for the coupled cluster wave function is given as:

$$|\mathrm{CC}\rangle = \Big[\prod_{\mu}(1+t_\mu\hat{\tau}_\mu)\Big]|\mathrm{HF}\rangle = |\mathrm{HF}\rangle + \sum_{\mu} t_\mu|\mu\rangle + \sum_{\mu>\nu} t_\mu t_\nu|\mu\nu\rangle \tag{2.38}$$

where $\hat{\tau}_\mu$ is the excitation operator of unspecified excitation level μ and t_μ is the associated amplitude.[5] It should be noted that in the CC wave function the excitation operator $\hat{\tau}_\mu$ not only generates the determinant $|\mu\rangle$ but a large number of determinants in collaboration with the other excitation operators (e.g., $|\mu\nu\rangle$).
In general, high-order excited determinants (e.g., $|\mu\nu\rangle$) can be generated by an operator of the same excitation level (e.g., $\hat{\tau}_{\mu\nu}$) and by a composite operator equivalent to the product of separate excitations

$$\hat{\tau}_{\mu\nu} = \hat{\tau}_\mu\hat{\tau}_\nu \tag{2.39}$$

with an overall amplitude equal to the sum of the individual amplitudes

$$t_{\mu\nu}^{\mathrm{tot}} = t_{\mu\nu} + t_\mu t_\nu \tag{2.40}$$

where $t_{\mu\nu}$ and $t_\mu t_\nu$ are named connected amplitudes and disconnected amplitudes, respectively. It follows that a CC wave function – generated, for example, by all possible single- and double-excitation operators – contains contributions from all determinants entering the FCI wave function.

The exponential ansatz

The coupled cluster wave function can be expressed as the exponential of an operator acting on the Hartree-Fock determinant

$$|\mathrm{CC}\rangle = e^{\hat{T}}|\mathrm{HF}\rangle \tag{2.41}$$

known as the exponential ansatz, where the cluster operator is a linear combination of excitation operators multiplied by the associated (connected) cluster amplitudes:[6–8]

$$\hat{T} = \sum_{\mu} t_{\mu} \hat{\tau}_{\mu} \tag{2.42}$$

The excitations are included in eq. (2.42) by partitioning the cluster operator into classes comprising all single (one-electron) excitations, all double (two-electron) excitations, all triple (three-electron) excitations, and so on. We may then write the cluster operator as

$$\hat{T} = \hat{T}_1 + \hat{T}_2 + \hat{T}_3 + \cdots + \hat{T}_N \tag{2.43}$$

where N is the number of electrons and

$$\hat{T}_1 = \sum_{ai} t_i^a \hat{a}_a^\dagger \hat{a}_i = \sum_{ai} t_i^a \hat{\tau}_i^a \tag{2.44}$$

$$\hat{T}_2 = \sum_{a>b} \sum_{i>j} t_{ij}^{ab} \hat{a}_a^\dagger \hat{a}_i \hat{a}_b^\dagger \hat{a}_j = \sum_{a>b} \sum_{i>j} t_{ij}^{ab} \hat{\tau}_{ij}^{ab} = \frac{1}{4} \sum_{abij} t_{ij}^{ab} \hat{\tau}_{ij}^{ab} \tag{2.45}$$

The Coupled Cluster hierarchy

Truncating the cluster operator to include only excitations up to a certain level yields a hierarchy of CC methods named CCSD,[9] CCSDT[10,11] etc. The excitation processes that contribute at each excitation level i are:

$$e^{\hat{T}_1} = 1 + \hat{T}_1 + \frac{1}{2}\hat{T}_1^2 + \ldots \tag{2.46}$$

$$e^{\hat{T}_1 + \hat{T}_2} = 1 + \hat{T}_1 + (\hat{T}_2 + \frac{1}{2}\hat{T}_1^2) + \ldots \tag{2.47}$$

$$e^{\hat{T}_1 + \hat{T}_2 + \hat{T}_3} = 1 + \hat{T}_1 + (\hat{T}_2 + \frac{1}{2}\hat{T}_1^2) + (\hat{T}_3 + \hat{T}_1\hat{T}_2 + \frac{1}{6}\hat{T}_1^3) + \ldots \tag{2.48}$$

Thus, triple configurations for example are generated by three mechanisms: $\hat{T}_3 + \hat{T}_1\hat{T}_2 + \frac{1}{6}\hat{T}_1^3$. The advantages of the cluster parametrization are apparent upon truncation because even at the truncated level, the CC wave function contains contributions from all determinants in the FCI wave function, with weights obtained from the different excitation processes leading to the determinants.

2.4.3 The projected Coupled Cluster Schrödinger equations

The truncated CC wave function satisfies the Schrodinger equation projected onto the Hartree-Fock state and onto the excited determinants $\langle\mu| = \langle \mathrm{HF}|\tau_\mu^\dagger$ that enter the coupled cluster wave function with connected amplitudes

$$\langle \mathrm{HF}|\hat{H}^T|\mathrm{HF}\rangle = E \tag{2.49}$$

$$\langle \mu|\hat{H}^T|\mathrm{HF}\rangle = 0 \tag{2.50}$$

where the so-called similarity-transformed Hamiltonian is equal to:

$$\hat{H}^T = e^{-\hat{T}} \hat{H} e^{\hat{T}} \tag{2.51}$$

The electronic energy in eq. (2.49) can be written as

$$E_{\mathrm{CC}} = \langle \mathrm{HF}|\hat{H}(1+\hat{T}+\frac{1}{2}\hat{T}^2+\ldots)|\mathrm{HF}\rangle = \langle \mathrm{HF}|\hat{H}(1+\hat{T}_2+\frac{1}{2}\hat{T}_1^2)|\mathrm{HF}\rangle \tag{2.52}$$

after expanding the exponential ansatz.[4] Notice that cluster operators higher than doubles do not contribute to the energy since the $\hat{H}$ is a two-particle operator. In addition, the one-particle operators contribute only to second-order, because of the Brillouin theorem. As a result, the coupled cluster energy is no higher than quadratic in the cluster amplitudes – irrespective of the truncation level. Of course, the higher-order excitations contribute indirectly since all amplitudes are coupled by the projected equations.
The CC connected amplitudes are computed by iteratively solving eq. (2.50) for a set of excitation manifolds μ. Using the Baker–Campbell–Hausdorff (BCH) formula, we can rewrite eq. (2.51) as

$$e^{-\hat{T}} \hat{H} e^{\hat{T}} = \hat{H} + [\hat{H},\hat{T}] + \frac{1}{2}[[\hat{H},\hat{T}],\hat{T}] + \frac{1}{6}[[[\hat{H},\hat{T}],\hat{T}],\hat{T}] + \frac{1}{24}[[[[\hat{H},\hat{T}],\hat{T}],\hat{T}],\hat{T}] \tag{2.53}$$

Thus, the projected equations yield at most quartic equations in the cluster amplitudes, with the BCH expansions terminating because of the special structure of the cluster operators. Introducing the so-called T1-similarity transformed Hamilton operator[88]

$$\hat{\tilde{H}} = e^{-\hat{T}_1} \hat{H} e^{\hat{T}_1} \tag{2.54}$$

which does not affect the particle rank of the Hamiltonian, the expressions for the CCSD amplitudes are:

$$0 = \langle \mu_1 | \hat{\tilde{H}} + [\hat{\tilde{H}}, \hat{T}_2] | \mathrm{HF} \rangle \tag{2.55}$$

$$0 = \langle \mu_2 | \hat{\tilde{H}} + [\hat{\tilde{H}}, \hat{T}_2] + \frac{1}{2}[[\hat{\tilde{H}}, \hat{T}_2], \hat{T}_2] | \mathrm{HF} \rangle \tag{2.56}$$

It is clear from eq. (2.55) and eq. (2.56) that the solution of the CCSD projected equations is complicated. In fact, the computational effort required to solve these equations formally scales as N^6. In particular, the last two terms from eq. (2.56) scale as N^6, while the other terms required for the solution of eq. (2.55) and eq. (2.56) scale as the fifth or lower powers of the system size. In addition, the memory and disk storage demands on the computing machines represent an important bottleneck. In order to overcome such bottlenecks and widen the application of CCSD, approximations have been proposed. Integral-direct implementations of CCSD avoid the storage of integrals in the atomic orbital (AO) basis by recomputing them when needed, thus reducing the storage bottleneck.[88,89] In addition, tensor decomposition techniques reduced the computational effort as well as the memory demands – e.g. the tensor hypercontraction which also reduces the scaling by two orders.[90] As discussed in Sec. 2.6, the complexity of the CC equations can be reduced by exploiting the perturbation theory approach to approximate the highest-rank excitation amplitudes while retaining part of the correlation in the energy.

2.5 Second-Order Møller-Plesset Perturbation Theory: MP2

Perturbation theory[13] (PT) represents a different way to systematically approach the exact wave function. Contrary to CC and CI theories, it is based on the idea that the exact solution differs only slightly from a previously solved problem for a simpler, related system. In Møller-Plesset perturbation theory (MPPT),[4,12] the Hamilton operator is partitioned as:

$$\hat{H} = \hat{H}_0 + \hat{\Phi} \tag{2.57}$$

where $\hat{H}_0$ is the zero-order Hamiltonian with known eigensolutions $E^{(0)}$, $|\Psi^{(0)}\rangle$ and

$$\hat{\Phi} = \hat{H} - \hat{H}_0 \tag{2.58}$$

is the perturbation. Since the zero-order Hamiltonian of MPPT is the Fock operator

$$\hat{H}_0 = \hat{f} = \sum_p \varepsilon_p \hat{a}_p^\dagger \hat{a}_p \tag{2.59}$$

the zero-order wave function corresponds to the Hartree-Fock wave function $|\mathrm{HF}\rangle$ and the perturbation operator takes the form:

$$\hat{\Phi} = \hat{H} - \hat{f} \tag{2.60}$$

Notice that the Hartree-Fock wave function satisfies the zero-order Schrödinger equation

$$\hat{f}|\mathrm{HF}\rangle = \sum_i \varepsilon_i |\mathrm{HF}\rangle = E_{\mathrm{MP}}^{(0)} |\mathrm{HF}\rangle \tag{2.61}$$

and that the zero-order MPPT energy is equal to the sum of orbital energies. In order to calculate higher-order corrections in MPPT, one must expand the wave function $|\Psi\rangle$ and the energy E in orders of the perturbations n and collect terms to order n in the perturbation – choosing $|\Psi\rangle$ to fulfill intermediate normalization.[4,12] Note that the wave function to order $(n-1)$ determines the energy to order n, and the exact energy is recovered by summing all energy corrections. The first-order correction to the energy is

$$E_{\mathrm{MP}}^{(1)} = \langle \Psi^{(0)} | \hat{\Phi} | \Psi^{(0)} \rangle = \langle \mathrm{HF} | \hat{\Phi} | \mathrm{HF} \rangle \tag{2.62}$$

Thus, the HF energy is equal to the sum of the zero- and first-order Møller-Plesset energies:

$$E_{\mathrm{HF}} = E_{\mathrm{MP}}^{(0)} + E_{\mathrm{MP}}^{(1)} \tag{2.63}$$

For a first estimate of the electron correlation energy, we consider the MP2 energy

$$E_{\mathrm{MP}}^{(2)} = \langle \Psi^{(0)} | \hat{\Phi} | \Psi^{(1)} \rangle = \langle \mathrm{HF} | \hat{H} \hat{T}_2^{(1)} | \mathrm{HF} \rangle = \langle \mathrm{HF} | [\hat{H}, \hat{T}_2^{(1)}] | \mathrm{HF} \rangle \tag{2.64}$$

where the $|\Psi^{(1)}\rangle$ wave function is expressed as generated by the application of an operator to the HF state:

$$|\Psi^{(1)}\rangle = \hat{T}_2^{(1)} |\mathrm{HF}\rangle \tag{2.65}$$

$$\hat{T}_2^{(1)} = \sum_{\mu_2} t_{\mu_2} \hat{\tau}_{\mu_2} = \sum_{a>b} \sum_{i>j} t_{ij}^{ab^{(1)}} \hat{a}_a^\dagger \hat{a}_i \hat{a}_b^\dagger \hat{a}_j \tag{2.66}$$

$$t_{ij}^{ab^{(1)}} = -\frac{\langle \mu_2 | \hat{H} | \mathrm{HF} \rangle}{\varepsilon_{\mu_2}} = -\frac{\langle \mathrm{HF} | [\hat{a}_j \hat{a}_b^\dagger \hat{a}_i \hat{a}_a^\dagger, \hat{H}] | \mathrm{HF} \rangle}{\varepsilon_a - \varepsilon_i + \varepsilon_b - \varepsilon_j} \tag{2.67}$$

Notice that the total energy at the MP2 level of theory is equal to

$$E_{\mathrm{MP2}} = E_{\mathrm{HF}} + E_{\mathrm{MP}}^{(2)} \tag{2.68}$$

and the wave function corrected up to first-order is:

$$|\mathrm{MP1}\rangle = (1 + \hat{T}_2^{(1)})|\mathrm{HF}\rangle \tag{2.69}$$

Contrary to the CI energy, which is determined variationally and therefore has a lower bound, the same is not true for MP theory. Also, it does not converge monotonically towards the correct limit with increasing order of perturbation:[4,91,92] due to the irregular convergence behavior of MPPT, higher-order corrections like MP3 or MP4 have fallen out of favor in recent years. Moreover, the requirement of the single-determinant HF wave function being a suitable starting guess makes MPPT, as CC theory, ill-suited to describe static correlation effects.

2.5.1 Explicit expressions for the closed-shell MP2 energy

To calculate the energy to second-order, we must determine the singlet wave function to first-order, introducing the doubles cluster operator in the singlet spin symmetry

$$\hat{T}_2 = \frac{1}{2} \sum_{aibj} t_{ij}^{ab} E_{ai} E_{bj} \tag{2.70}$$

where E_{ai} is the singlet excitation operator[4] and $t_{ij}^{ab} = t_{ji}^{ba}$. Insertion of eq. (2.70) in equation eq. (2.64) leads to the closed-shell formula for MP2 energy

$$E_{\mathrm{MP}}^{(2)} = \sum_{aibj} \left(2t_{ij}^{ab} - t_{ji}^{ab}\right)(ia|jb) \tag{2.71}$$

where the closed-shell first-order doubles amplitudes are equal to:

$$t_{ij}^{ab} = -\frac{(ai|bj)}{\varepsilon_a - \varepsilon_i + \varepsilon_b - \varepsilon_j} \tag{2.72}$$

The MO-based electron-repulsion integrals are formed as

$$(pq|rs) = g_{pqrs} = \sum_{\mu\nu\sigma\lambda} C_{\mu p} C_{\nu q} C_{\sigma r} C_{\lambda s} (\mu\nu|\sigma\lambda) \tag{2.73}$$

where $\mu, \nu, \sigma, \lambda$ are the indices for the AO orbitals and $\mathbf{C}$ are the solutions to the Roothaan-Hall equations. The solution of the MP2 problem formally scales as N^5 with the system size, due to the formation of the MO-based four-index integrals in eq. (2.72). The formation of the amplitudes and the calculation of the energy formally scale as N^4, as well as the memory demands. In order to extend the application of MP2 to large molecules, several reduced-scaling approaches have been proposed based on, e.g., the use of localized molecular orbitals (LMOs)[41,44,93–96] or atomic orbitals (AOs).[97–101] With the help of a Laplace transform[34,35,37] for decomposing the orbital energy denominator in eq. (2.72), and in combination with integral screening approaches or sparse

linear algebra, the scaling behavior of AO-MP2 can be reduced to linear in the asymptotic limit. In addition, the RI-CDD-MP2 method[102,103] further increases the efficiency of AO-MP2 by using the resolution of the identity (RI) approximation (see Sec. 4.1) and Cholesky decomposed pseudo-density matrices.[63,103–106] More recently, the RI-CDD-MP2 has been improved further by introducing a local attenuated Coulomb metric[107–110] for the RI and by efficiently exploiting the resulting additional sparsity in the three-index integrals (see Sec. 4.1). Furthermore, the tensor hypercontraction (THC, see Sec. 4.2) – has been employed to efficiently reduce both computational effort and scaling of the MP2 method.[111–114]
In the past decades, variations of the conventional MP2 theory have been proposed. In spin-component scaled MP2 (SCS-MP2) from Grimme,[115] the Coulomb and exchange type contributions to the MP2 energy are scaled using different constant factors, which has been shown to further improve the accuracy. In the related scaled opposite-spin MP2 (SOS-MP2) from Jung et al.,[33] the computationally demanding exchange contributions can be neglected entirely without degrading the accuracy of MP2. The THC approximation has been applied to SCS-MP2 and SOS-MP2 as well.[31,113,114,116]

2.6 Coupled Cluster Perturbation Theory

Contrary to MP perturbation theory, we assume an exponential parametrization for the perturbed wave function

$$|\mathrm{CC}\rangle = e^{\hat{T}}|\mathrm{HF}\rangle \tag{2.74}$$

where $\hat{T}$ is the cluster operator defined as in eq. (2.42). The Hamilton operator is again separated into the zero-order Fock operator $\hat{f}$ and first-order fluctuation potential $\hat{\Phi}$

$$\hat{H} = \hat{f} + \hat{\Phi} \tag{2.75}$$

The zero-order wave functions are the HF determinant, $|\mathrm{HF}\rangle$, and the excited determinants, $|\mu\rangle$. We expand the full CC wave function, the CC electronic energy in eq. (2.49), and the amplitude equation in eq. (2.50) in orders of the fluctuation potential, generating in this way expressions that are equivalent to those of MPPT. The general expression for the amplitudes and the energy correction within CCPT are:

$$\varepsilon_\mu t_\mu^{(n)} = -\langle\mu|[\hat{\Phi}^T]^{(n)}|\mathrm{HF}\rangle \tag{2.76}$$

$$E^{(n)} = \langle\mathrm{HF}|[\hat{\Phi}^T]^{(n)}|\mathrm{HF}\rangle \tag{2.77}$$

where $[\hat{\Phi}^T]^{(n)}$ contains the nth-order part of the similarity-transformed fluctuation potential. Since the fluctuation potential contains no terms to zero order:

$$t_\mu^{(0)} = 0 \tag{2.78}$$

To third order in the perturbation, eq. (2.76) becomes

$$\varepsilon_\mu t_\mu^{(1)} = -\langle\mu|\hat{\Phi}|\mathrm{HF}\rangle \tag{2.79}$$

$$\varepsilon_\mu t_\mu^{(2)} = -\langle\mu|[\hat{\Phi}, \hat{T}^{(1)}]|\mathrm{HF}\rangle \tag{2.80}$$

$$\varepsilon_\mu t_\mu^{(3)} = -\langle\mu|[\hat{\Phi}, \hat{T}^{(2)}]|\mathrm{HF}\rangle - \frac{1}{2}\langle\mu|[[\hat{\Phi}, \hat{T}^{(1)}], \hat{T}^{(1)}]|\mathrm{HF}\rangle \tag{2.81}$$

and the CCPT energies are given by

$$E^{(0)} = E_0 \tag{2.82}$$

$$E^{(1)} = \langle \mathrm{HF}|\hat{\Phi}|\mathrm{HF}\rangle \tag{2.83}$$

$$E^{(2)} = \langle \mathrm{HF}|[\hat{\Phi}, \hat{T}_2^{(1)}]|\mathrm{HF}\rangle \tag{2.84}$$

$$E^{(3)} = \langle \mathrm{HF}|[\hat{\Phi}, \hat{T}_2^{(2)}]|\mathrm{HF}\rangle \tag{2.85}$$

The CC wave function can be calculated to any order according to the expression

$$|\Phi^{(n)}\rangle = [e^{\hat{T}}]^{(n)}|\mathrm{HF}\rangle \tag{2.86}$$

Expanding the exponential and collecting terms to the same order in the fluctuation potential, the perturbed CC wave functions are, up to third order:

$$|\Psi^{(0)}\rangle = |\mathrm{HF}\rangle \tag{2.87}$$

$$|\Psi^{(1)}\rangle = \hat{T}^{(1)}|\mathrm{HF}\rangle \tag{2.88}$$

$$|\Psi^{(2)}\rangle = (\hat{T}^{(2)} + \frac{1}{2}\hat{T}^{(1)}\hat{T}^{(1)})|\mathrm{HF}\rangle \tag{2.89}$$

$$|\Psi^{(3)}\rangle = (\hat{T}^{(3)} + \hat{T}^{(2)}\hat{T}^{(1)} + \frac{1}{6}\hat{T}^{(1)}\hat{T}^{(1)}\hat{T}^{(1)})|\mathrm{HF}\rangle \tag{2.90}$$

After some manipulation of the previous equations for the energy and the amplitudes, we would demonstrate that, for the CCSD approximation, the singles and doubles amplitudes are correct to second-order in the fluctuation, while the wave function is correct to only to first-order.[4] In addition, we conclude that the CCSD energy is correct to third-order in the fluctuation potential.

2.6.1 The approximate CCSD method: CC2

Perturbational approaches may also be used to obtain approximate hybrid coupled cluster methods. For example, we can simplify the equations for the CC amplitudes while retaining some approximate description of the highest-rank excitations. Therefore, we may approximate the doubles equations of CCSD to first-order in the fluctuation potential. The resulting method is known as approximate coupled cluster singles and doubles (CC2),[15] whose energy is correct to second-order in the fluctuation potential. It is important to stress that the singles cluster operators are treated as zero-order operators, thus ensuring that any large adjustments in the orbitals may be incorporated into our perturbational treatment at any stage. This is important when properties are considered and, in particular, for the treatment of time-dependent properties.[16,117]

As stated before, the CC2 equations are obtained from their CCSD counterpart by treating the doubles equations to first order:

$$\varepsilon_{\mu_1} t_{\mu_1} = -\langle \mu_1|\tilde{\hat{\Phi}}|\mathrm{HF}\rangle - \langle \mu_1|[\tilde{\hat{\Phi}}, \hat{T}_2]|\mathrm{HF}\rangle \tag{2.91}$$

$$\varepsilon_{\mu_2} t_{\mu_2} = -\langle \mu_2|\tilde{\hat{\Phi}}|\mathrm{HF}\rangle \tag{2.92}$$

where we introduced the tilde notation for the T1-similarity transformed fluctuation potential. By solving for the doubles, we can rewrite the CC2 equations as

$$\varepsilon_{\mu_1} t_{\mu_1} = -\langle \mu_1 | \tilde{\hat{\Phi}} | \mathrm{HF} \rangle - \langle \mu_1 | [\tilde{\hat{\Phi}}, \hat{Q}_2] | \mathrm{HF} \rangle \tag{2.93}$$

where we introduced the approximated doubles cluster operator:

$$\hat{Q}_2 = -\sum_{\mu_2} \varepsilon_{\mu_2}^{-1} \langle \mu_2 | \tilde{\hat{\Phi}} | \mathrm{HF} \rangle \hat{\tau}_{\mu_2} \tag{2.94}$$

Similarly, the CC2 wave function may be written as

$$|\mathrm{CC}\rangle = e^{(\hat{T}_1 + \hat{Q}_2)} |\mathrm{HF}\rangle \tag{2.95}$$

The CC2 wave function can be considered as intermediate in quality between those of MP2 and CCSD theories. Most of the correlation energy is recovered at the MP2 and CC2 levels, which are similar in quality and cost except that CC2 is iterative. Indeed, the attraction of the CC2 method relative to MP2 lies not so much in the calculation of the energy as in the calculation of various molecular properties.

2.6.2 Explicit expressions for the closed-shell CC2 method

As for MP2 theory, to formulate the CC2 equation in closed-shell expressions, we must introduce the needed cluster operators in the singlet spin symmetry[4]

$$\hat{T}_1 = \sum_{ai} t_i^a E_{ai} \tag{2.96}$$

$$\hat{T}_2 = \frac{1}{2} \sum_{aibj} t_{ij}^{ab} E_{ai} E_{bj} \tag{2.97}$$

where E_{ai} is the singlet excitation operator and $t_{ij}^{ab} = t_{ji}^{ba}$. By inserting eq. (2.96) and eq. (2.97) in eq. (2.49), one obtains the following closed-shell expression for the CC2 energy:

$$\begin{aligned} E_{\mathrm{CC2}} &= E_{\mathrm{HF}} + \frac{1}{2} \sum_{aibj} t_i^a t_j^b \langle \mathrm{HF} | [[\hat{H}, E_{ai}], E_{bj}] | \mathrm{HF} \rangle + \frac{1}{2} t_{ij}^{ab} \langle \mathrm{HF} | [\hat{H}, E_{ai} E_{bj}] | \mathrm{HF} \rangle \\ &= E_{\mathrm{HF}} + (t_i^a t_j^b + t_{ij}^{ab}) \Big[2(ia|jb) - (ib|ja) \Big] = E_{\mathrm{HF}} + (t_i^a t_j^b + t_{ij}^{ab}) L_{iajb} \end{aligned} \tag{2.98}$$

The singles and doubles amplitudes are required to compute the CC2 energy. As stated in Sec. 2.6.1, we can explicitly solve for the doubles and solve for the singles iteratively. The CC2 doubles amplitudes are computed from eq. (2.92)

$$t_{ij}^{ab} = -\frac{(ai\tilde{|}bj)}{\varepsilon_a - \varepsilon_i + \varepsilon_b - \varepsilon_j} \tag{2.99}$$

formed as in MP2, but we used the T1-similarity transformed two-electron integrals:[4,15]

$$(pq\tilde{|}rs) = \tilde{g}_{pqrs} = \sum_{\mu\nu\sigma\lambda} \Lambda_{\mu p}^{\mathrm{p}} \Lambda_{\nu q}^{\mathrm{h}} \Lambda_{\sigma r}^{\mathrm{p}} \Lambda_{\lambda s}^{\mathrm{h}} (\mu\nu|\sigma\lambda) \tag{2.100}$$

with p,q,r,s indicating general MO orbitals. The transformation matrices are given by

$$\mathbf{\Lambda}^{\mathrm{p}} = \mathbf{C}(\mathbf{1} - \mathbf{t}_1^T) \tag{2.101}$$

$$\mathbf{\Lambda}^{\mathrm{h}} = \mathbf{C}(\mathbf{1} + \mathbf{t}_1) \tag{2.102}$$

and the matrix for the singles is:

$$\mathbf{t}_1 = \begin{pmatrix} 0 & 0 \\ t_i^a & 0 \end{pmatrix} \tag{2.103}$$

The right hand side of eq. (2.93), is solved as:

$$\Omega_{ai} = \langle \mu_1 | \hat{\tilde{H}} + [\hat{\tilde{H}}, \hat{T}_2] | \mathrm{HF} \rangle = \sum_{ckd} u_{ik}^{cd} \tilde{g}_{ackd} - \sum_{ckl} u_{kl}^{ac} \tilde{g}_{kilc} + \sum_{ck} u_{ik}^{ac} \tilde{F}_{kc} + \tilde{F}_{ai} \tag{2.104}$$

where $u_{ij}^{ab} = 2t_{ij}^{ab} - t_{ji}^{ab}$ and $\tilde{\mathbf{F}}$ is the T1-similarity transformed inactive Fock matrix:

$$\tilde{F}_{pq} = \tilde{h}_{pq} + \sum_j [2(pq\tilde{|}jj) - (pj\tilde{|}jq)] \tag{2.105}$$

The overall formal computational scaling behavior of CC2 is N^5. On the other hand, the memory demands formally scale N^4 with the system size.[15] Both RI and THC approximations have been used to improve the efficiency of CC2.[23,32,39] In addition, SCS-CC2, and SOS-CC2 approximations have been proposed,[38,118–120] with a formal N^4 computational scaling for the opposite-spin contributions. Alternatively, as for MP2, several local approaches have been implemented to further reduce the scaling behavior of CC2 methods.[46,47,52,53,59,60,121,122]
In **Publication I**, we reformulated the SOS-CC2 method, within the resolution of the identity framework (RI), into the AO basis and expressed its equations in terms of ground state one-particle density matrices. For systems with a significant HOMO-LUMO gap, it was possible to take advantage of the sparsity of both the electron integrals and density matrices[14,40] via block-sparse linear algebra and hence reduce the computational scaling behavior to $\mathscr{O}(N^3)$. Moreover, we employed an attenuated RI Coulomb metric which increased the sparsity of the three-index integrals, resulting in an effective asymptotic sub-quadratic computational scaling. As for RI-CDD-MP2, the Cholesky decomposition of density matrices[63,64,104] improved the efficiency of the method – accordingly named CDD-RI-SOS-CC2 – both computationally and memory-wise. In **Publication III**, we decomposed the four-index electron integrrals using the tensor hypercontraction (THC) approximation directly reducing the computational scaling of the method and providing a considerable diminution of both the computational effort (the prefactor) and memory demands. As previously proposed by Hohenstein *et al.*[32] the cost for solving the MO-based SOS-CC2 equations scales cubically with the system size and only two-index tensors are stored reducing the memory demands scaling behavior to quadratic. In addition, we derived a low-scaling formulation of the THC-SOS-CC2 method in terms of Cholesky decomposed densities,[63,64,104] as in **Publication I**, and hence proposed an efficient CDD-THC-SOS-CC2 method showing a sub-cubic scaling behavior in the asymptotic limit and for systems with a significant HOMO-LUMO gap. Note that the methods presented in **Publication I** and **Publication III** are implemented in FERMIONS++.[65–67]

3 Electronic Structure Methods for the Excited States

A quantum system is said to be in an excited state if that state is at a higher energy level than the ground state, for example by absorption of one or more photons. Excited states display chemical and structural properties usually different than the ground state. Moreover, the system in an excited state will eventually decay back to the ground state via several different mechanisms.[123] In order to describe the properties of excited states, as well as the various decay mechanisms, a plethora of methods have been developed, each with its strengths and weaknesses. This chapter will only treat the coupled cluster (CC) and algebraic diagrammatic construction (ADC) methods,[4,71] which are single-reference methods, with a focus on the approximate second-order truncations.

As discussed in Sec. 2.2, the correlated CI methods, except full CI, are not size-consistent. Similarly to the ground state correlation energy, excitation energies, transition moments, and excited state properties are also not size-consistent.[4] However, the advantage of these methods relies on the Hermiticity of the CI problem which allows for a straightforward computation of excited state properties and transition moments. The CC-based excited state methods comprise four related methods referred to as linear response coupled cluster (LR-CC),[16,17,117,124–126] equation-of-motion coupled cluster (EOM-CC),[127–131] symmetry-adapted cluster configuration interaction (SAC-CI),[132–134] and unitary coupled cluster (UCC),[135–137] which yield identical algebraic expressions for the excitation energies but differ in the calculation of properties.[4,138] All CC methods are non-Hermitian and thus lead to a dual wave function representation of the excited states, corresponding to right and left eigenvectors of the CC Jacobian matrix. This means that, for a rigorous calculation of excited state properties, both the right and left excited states are required – i.e., the CC problem for excited states must be solved twice. Notice that the accuracy of the properties is not affected by non-Hermiticity. In contrast to CC methods, the ADC secular matrix is Hermitian and the ADC equations need to be solved only once. Hence, the computation of excited states and of their properties is simpler than CC.

The LRCC and ADC methods are fully size-consistent, thus the excitation energies, ground state transition moments and excited state properties are all size-consistent.[139] For the remaining CC methods, only the excitation energies are size-consistent.[117] An additional advantage of LR-CC and ADC over CI methods is their compactness, defined as the size of the configuration space needed for a consistent perturbation-theoretical description of the singly excited states to specific order n.[140,141] However, it should be specified that the ADC methods are the most compact ones.

As we consider approximations higher in the hierarchy, the biggest advantage of CC over ADC methods is the improved description of the ground state. However, due to the higher compactness of ADC, the scaling of the computational effort with the system size is more favorable for the ADC schemes. For instance, both CC2 and ADC(2) methods show the same N^5 computational scaling. However, the computational cost of the ADC(3) scheme scales as N^6 – as CCSD –, while the CC3 method scales as N^7 with the system size.[126,142–144]

Finally, the most remarkable advantage of ADC methods is the consistently high order of perturbation-theoretical treatment of the excited state properties, which is always as high as the one of the singly excited configurations.[145]

3.1 Coupled Cluster Response Theory

The response function formalism offers a consistent approach for deriving expressions for the physically observable quantities, based on the idea that if a system is known to be in the ground state in the limit of vanishing perturbation (an adiabatically switched-on external field) we gain knowledge of the unperturbed excited states by studying its time evolution. Information about the excited states will be obtained from the response functions, only requiring the ground state wave function to be determined.[16,17,117,124–126] In particular, the CC excitation energies are known to be found at the poles of the CC linear response function, which occur at the poles of the firs-order amplitude responses.[15,126] In order to obtain the expressions for the CC amplitude responses, the quasi-energy Lagrangian approach is used, starting from the time evolution of a CC state, described by the time-dependent CC wave function

$$|\mathrm{CC}(t)\rangle = e^{\hat{T}(t)}|\mathrm{HF}\rangle e^{i\varepsilon(t)} = |\widetilde{\mathrm{CC}}\rangle e^{i\varepsilon(t)} \tag{3.1}$$

where $\hat{T}(t)$ is the time-dependent cluster operator and $\varepsilon(t)$ is a time-dependent phase.[117,126] Notice that the reference wave function is fixed and not time-dependent, hence the following approach is said to be "unrelaxed". The perturbation of the external field has the following form:

$$\hat{V}(t) = \sum_{j=-N}^{N} \sum_{A} \varepsilon_A(\omega_j)\hat{A}e^{-i\omega_j t} \tag{3.2}$$

where the set $\{\hat{A}\}$ contains frequency-independent Hermitian operators and $\varepsilon_A(\omega_j)$ is a strength parameter.[117,126] For finite N, the perturbation is T-periodic – $V(t+\mathrm{T}) = V(t)$ – and T is the least common multiple of periods for the terms of $V(t)$.[117] By projection of the time-dependent Schrödinger equation for $|\mathrm{CC}(t)\rangle$ onto $\langle\mathrm{HF}|$ and $\langle\mu|$, one determines the quasi-energy Lagrangian:[16,17,117,124–126]

$$L(t) = \langle\mathrm{HF}|\hat{H}|\widetilde{\mathrm{CC}}\rangle + \sum_{k,\mu_k} \bar{t}_{\mu_k}(t)\langle\mu_k|e^{-\hat{T}(t)}\left(\hat{H} - i\frac{\delta}{\delta t}\right)|\widetilde{\mathrm{CC}}\rangle \tag{3.3}$$

with $\hat{H} = \hat{H}_0 + \hat{V}(t)$ as the perturbed Hamiltonian and $\bar{\mathbf{t}}$ as the Lagrangian multipliers. Notice that $\hat{H}_0$ is the time-independent Hamilton operator.

Introducing the time-averaged Lagrangian

$$\Big\{L(t)\Big\}_T = \frac{1}{T}\int_{t_0}^{t_0+T} L(t)dt \tag{3.4}$$

and expanding the quasi-energy Lagrangian, the CC amplitudes, and the CC multipliers in orders of the time-dependent perturbation, we can obtain the expression for the CC response equations by requiring the Lagrangian to be optimal with respect to variations[125,126]

$$\delta\Big\{L(t)\Big\}_T = 0 \tag{3.5}$$

The zeroth-order amplitudes t_μ and multipliers $\bar{t}_\mu$ are given by:

$$\langle \mu_k | e^{-\hat{T}^{(0)}} \hat{H}_0 | \mathrm{CC}\rangle = 0 \tag{3.6}$$

$$\bar{\mathbf{t}}^{(0)}\mathbf{A} = -\eta \tag{3.7}$$

with the CC Jacobian matrix $\mathbf{A}$ and the vector η given by:

$$\eta_{\nu_j} = \langle \mathrm{HF} | [\hat{H}_0, \hat{\tau}_{\nu_j}] | \mathrm{CC}\rangle \tag{3.8}$$

$$A_{\mu_i \nu_j} = \langle \mu_i | e^{-\hat{T}^{(0)}} [\hat{H}_0, \hat{\tau}_{\nu_j}] | \mathrm{CC}\rangle \tag{3.9}$$

Notice that the zeroth-order equations for the amplitudes are equivalent to those discussed in the previous Chapter, i.e., the ground state amplitudes. On the other hand, the first-order amplitude response equations are obtained as:

$$(\omega\mathbf{I} - \mathbf{A})\mathbf{t}^A = -\xi^A \tag{3.10}$$

with

$$\xi^A_{\mu_i} = \langle \mu_i | e^{-\hat{T}^{(0)}} \hat{A} | \mathrm{CC}\rangle \tag{3.11}$$

From eq. (3.10) it is seen that the excitation energies become the eigenvalues of the nonsymmetric CC Jacobian matrix $\mathbf{A}$, computed by solving either the left or the right eigenvalue problem:

$$\mathbf{AR} = \omega\mathbf{R} \tag{3.12}$$

$$\mathbf{LA} = \mathbf{L}\omega \tag{3.13}$$

where the vectors are chosen to fulfill the biorthonormality condition

$$L^I R^J = \delta_{IJ} \tag{3.14}$$

where I,J refer to excited states. Although the determination of the excitation energies only requires the solution of either the left or the right eigenvectors, when we wish to determine other properties, for example, one- or two-photon transition probabilities or excited-state properties, we need both the left and the right eigenvectors. In addition, since the Jacobian is nonsymmetric, it may have complex eigenvalues.

3.1.1 Linear Response CC2

For approximate CC models, response functions are simply obtained by introducing the corresponding approximated CC equations as constraints for the Lagrangian.[17,117,126] Thus, considering a time-dependent one-electron perturbation, the CC2 quasi-energy Lagrangian can be written as:

$$L(t) = \langle \mathrm{HF}|\hat{H}e^{\hat{T}_1(t)+\hat{T}_2(t)}|\mathrm{HF}\rangle + \sum_{\mu_1}\bar{t}_{\mu_1}(t)\langle\mu_1|e^{-\hat{T}_1(t)-\hat{T}_2(t)}\left(\hat{H}-i\frac{\delta}{\delta t}\right)e^{\hat{T}_1(t)+\hat{T}_2(t)}|\mathrm{HF}\rangle$$
$$+\sum_{\mu_2}\bar{t}_{\mu_2}(t)\langle\mu_2|[\hat{F}+\hat{V}(t)-i\frac{\delta}{\delta t},\hat{T}_2(t)]+(\hat{\Phi}+\hat{V}(t))|\mathrm{HF}\rangle \tag{3.15}$$

In linear response CC2, the operator $\hat{F}$ is considered as the zeroth-order problem perturbated by two distinct perturbations $\hat{V}(t)$ and $\hat{\Phi}$. The singles amplitudes are, thus, treated as zeroth-order parameters in the fluctuation potential $\hat{\Phi}$ and first-order in the perturbation $\hat{V}(t)$. The doubles are approximated to first order in the fluctuation potential and all terms are kept in $\hat{V}(t)$.[15,126] This approach provides an alternative to explicit orbital relaxation due to the particular treatment of the singles. If orbital relaxation is treated explicitly – i.e. when describing geometrical derivatives – the Lagrangian needs to be modified to allow for this.[126]
The response equations for the CC2 amplitudes have the form of eq. (3.10). As stated in the previous section, only zeroth-order quantities are needed to compute the properties of excited states. The excitation energies at the CC2 level are found by solving eq. (3.12), where the Jacobian matrix is built as

$$A^{\mathrm{CC2}}_{\mu_i,\nu_j} = \begin{pmatrix} \langle\mu_1|[\tilde{\hat{H}}_0,\hat{\tau}_{\nu_1}]+[[\tilde{\hat{H}}_0,\hat{\tau}_{\nu_1}],\hat{T}_2^{(0)}]|\mathrm{HF}\rangle & \langle\mu_1|[\tilde{\hat{H}}_0,\hat{\tau}_{\nu_2}]|\mathrm{HF}\rangle \\ \langle\mu_2|[\tilde{\hat{H}}_0,\hat{\tau}_{\nu_1}]|\mathrm{HF}\rangle & \langle\mu_2|[\hat{F},\hat{\tau}_{\nu_2}]|\mathrm{HF}\rangle \end{pmatrix} \tag{3.16}$$

Notice that we used the T1-similarity transformed Hamiltonian in eq. (3.16). Since the singles amplitudes are correct to second-order, the single-single block of the CC2 Jacobian is correct to second-order. The coupling blocks in eq. (3.16) are correct to first-order because the lowest-order coupling to the singles is retained. At the end, singly-excited states are correct through second-order. On the other hand, doubly-excited states are included in zeroth-order and the double-double block contains only diagonal elements that are orbital energy differences.[15,126]

3.2 Algebraic Diagrammatic Construction Theory

The algebraic diagrammatic construction (ADC) schemes originate from Green's functions, also known as propagators.[22,146] The kind of propagator determines which property of the system will be described. The one-electron propagator, for example, describes the time evolution of one electron within an N-electron system. Accordingly, they are used to obtain ionization potentials and electron affinities of a molecular system.[147,148] Finally, the polarization propagator acts on the time-dependent ground-state wave function and propagates time-dependent density fluctuations of the many-body system.[149] The latter propagator can be expressed in the well-

known spectral representation

$$\Pi_{pq,rs}(\omega) = \sum_{k\neq 0} \frac{\langle\Psi_0|\hat{a}_q^\dagger \hat{a}_p|\Psi_k\rangle\langle\Psi_k|\hat{a}_r^\dagger \hat{a}_s|\Psi_0\rangle}{\omega + E_0 - E_k} + \sum_{k\neq 0} \frac{\langle\Psi_0|\hat{a}_r^\dagger \hat{a}_s|\Psi_k\rangle\langle\Psi_n|\hat{a}_q^\dagger \hat{a}_p|\Psi_0\rangle}{-\omega + E_0 - E_k} \tag{3.17}$$

where Ψ_0 is the ground-state wave function with energy E_0. The sum is carried out over all electronically excited states $|\Psi_k\rangle$ with total energy E_k. It is clear from eq. (3.17) that the polarization propagator carries information about the exact excited states of the many-electron system. In fact, the poles are found at $\omega_k = E_k - E_0$ and the residues are the transition probabilities of the corresponding excitation. Since both parts in the right-hand of eq. (3.17) contain identical physical information, it is sufficient to consider only one of them. The polarization propagator can be written in the general algebraic form (ADC form):[22]

$$\Pi(\omega) = \mathbf{f}^\dagger(\omega - \mathbf{M})^{-1}\mathbf{f} \tag{3.18}$$

where the physical information of interest is obtained from the ADC matrix $\mathbf{M}$, the shifted Hamiltonian matrix, and the matrix $\mathbf{f}$ which corresponds to the effective transition moments. The excitation energies are obtained as a solution to the following problem:

$$\mathbf{MX} = \mathbf{X\Omega} \qquad\qquad \mathbf{X}^\dagger\mathbf{X} = \mathbf{1} \tag{3.19}$$

where $\mathbf{\Omega}$ is the diagonal matrix of eigenvalues and $\mathbf{X}$ is the matrix of eigenvectors that gives access to the spectroscopic amplitudes $\mathbf{y}$ according to:

$$\mathbf{y} = \mathbf{X}^\dagger\mathbf{f} \tag{3.20}$$

The ADC procedure expands the perturbation-theoretical expressions for the polarization propagator following the MP partitioning of the Hamiltonian, which then contains only approximate information on the excited states.[22] Following the ADC procedure, algebraic expressions are derived by expanding the matrices $\mathbf{M}$, $\mathbf{f}$, and the propagator in orders of perturbation in the fluctuation potential:

$$\mathbf{\Pi} = \mathbf{\Pi}^{(0)} + \mathbf{\Pi}^{(1)} + \mathbf{\Pi}^{(2)} + \ldots \tag{3.21}$$

$$\mathbf{M} = \mathbf{M}^{(0)} + \mathbf{M}^{(1)} + \mathbf{M}^{(2)} + \ldots \tag{3.22}$$

$$\mathbf{f} = \mathbf{f}^{(0)} + \mathbf{f}^{(1)} + \mathbf{f}^{(2)} + \ldots \tag{3.23}$$

For ADC schemes derived from the polarization propagators, only transition energies and properties between the ground state and excited states are theoretically accessible.[150] Thus, explicit expressions for the excited state wave functions are elusive.

3.2.1 Intermediate State Representation

A simpler way of deriving the algebraic ADC expressions is through the so-called intermediate state representation (ISR),[140,148,151–154] which does not require knowledge about propagators.

The unknown set of exact excited states Ψ_n in eq. (3.17) can be expanded in terms of a complete set of intermediate states:

$$\Psi_k = \sum_J X_{kI} \tilde{\Psi}_I \tag{3.24}$$

The intermediate states are required to be orthonormal and orthogonal to the ground state. Thus, starting from the correlated wave function $|\Psi_0\rangle$, a correlated excited state basis $\{\bar{\Psi}_I\}$ can be generated by acting on it with excitation operators $\{\hat{C}_I\}$ representing the excitation classes:

$$\bar{\Psi}_I = \hat{C}_I \Psi_0 \tag{3.25}$$

The definition of $\{\hat{C}_I\}$ determines the kind of ADC scheme, i.e., whether a PP, IP, or EA scheme is obtained:

$$\{\hat{C}_I\}^{PP} \equiv \{\hat{a}_a^\dagger \hat{a}_k; \hat{a}_a^\dagger \hat{a}_b^\dagger \hat{a}_k \hat{a}_l; \dots\} \tag{3.26}$$

$$\{\hat{C}_I\}^{IP} \equiv \{\hat{a}_k; \hat{a}_a^\dagger \hat{a}_k \hat{a}_l; \dots\} \tag{3.27}$$

$$\{\hat{C}_I\}^{EA} \equiv \{\hat{a}_a^\dagger; \hat{a}_a^\dagger \hat{a}_b^\dagger \hat{a}_k; \dots\} \tag{3.28}$$

These correlated excited states $\{\bar{\Psi}_I\}$ are not orthogonal but can be successively orthogonalized via Gram-Schmidt procedure yielding directly the orthogonal intermediate state basis $\{\tilde{\Psi}_J\}$. The ADC matrices $\mathbf{M}$ and $\mathbf{f}$ can be expressed by employing the IS basis as follows:

$$(M)_{IJ} = \langle \tilde{\Psi}_I | \hat{H} - E_0 | \tilde{\Psi}_J \rangle \tag{3.29}$$

$$(f)_{I,pq} = \langle \tilde{\Psi}_I | \hat{a}_p^\dagger \hat{a}_q | \Psi_0 \rangle \tag{3.30}$$

Thus, once the eigenvalue problem is solved by diagonalization, the excitation energies, IPs, or EAs are known, and the ADC vectors of the excited states can be used to construct the explicit wave function of the corresponding states via eq. (3.24). The eq. (3.30) can be contracted with the dipole operator to obtain transition dipole moments.[150] In addition, the ISR framework enables the computation of excited states properties because any one-particle operator $\hat{O}$ can be represented in the intermediate states basis as

$$(O)_{IJ} = \langle \tilde{\Psi}_I | \hat{O} | \tilde{\Psi}_J \rangle \tag{3.31}$$

and the corresponding expectation value is evaluated by contraction with the ADC eigenvectors according to:

$$\langle O \rangle_{kj} = \sum_{IJ} X_{kI} (O)_{IJ} X_{kJ} \tag{3.32}$$

Choosing the nth-order MP ground state as a starting point for the derivation of the IS basis, one arrives at the ADC(n) scheme for excitation energies and excited state properties.

3.2.2 Second-Order Algebraic Diagrammatic Construction Theory: ADC(2)

The perturbation-theoretical expansion of ADC matrices is given as

$$\mathbf{M}^{\mathrm{ADC}(n)} = \mathbf{K} + \mathbf{C}^{(1)} + \mathbf{C}^{(2)} + \mathbf{C}^{(3)} + \dots \tag{3.33}$$

where $\mathbf{K}$ corresponds to the zeroth-order contributions, and $\mathbf{C}^{(1)}$ to $\mathbf{C}^{(n)}$ are the first to nth-order corrections. At zeroth-order, the ADC matrix is diagonal and the matrix elements are orbital energy differences of the occupied and virtual molecular orbitals involved in the electronic transition. The ADC matrix up to second-order comprises the singly excited states and doubly excited states.[145,150] For the well-known strict ADC(2)-s scheme, which is rigorously derived when starting from the MP2 ground state, the single-single block of $\mathbf{M}$ is expanded to the second order of perturbation theory.[155]

$$M^{\mathrm{ADC}(2)}_{ia,jb} = K_{ia,jb} + C^{(1)}_{ia,jb} + C^{(2)}_{ia,jb} \tag{3.34}$$

On the other hand, the single-double coupling blocks are expanded to first order:[155]

$$M^{\mathrm{ADC}(2)}_{ia,klcd} = C^{(1)}_{ia,klcd} \tag{3.35}$$

$$M^{\mathrm{ADC}(2)}_{ijab,kc} = C^{(1)}_{ijab,kc} \tag{3.36}$$

Finally, since the double-double block of $\mathbf{M}$ is expanded to zeroth-order, it contains only diagonal elements:[155]

$$M^{\mathrm{ADC}(2)}_{ijab,klcd} = K_{ijab,klcd} = (\varepsilon_a - \varepsilon_i + \varepsilon_b - \varepsilon_j)\delta_{ac}\delta_{ik}\delta_{bd}\delta_{lj} \tag{3.37}$$

As discussed for LR-CC2, the singly-excited states are correct through second-order, while the doubly-excited states are included in zeroth-order.

3.3 Solution of the LR-CC2 and ADC(2) eigenvalue problems

As discussed in Sec. 3.1 and Sec. 3.2, the excitation energy, at the CC2 and ADC(2) levels, is obtained as an eigenvalue of the following problem:

$$\mathbf{A}\mathbf{X}^I = \omega^I \mathbf{X}^I \tag{3.38}$$

where $\mathbf{A}$ can be either the CC2 Jacobian or the ADC(2) secular matrix, $\mathbf{X}^I$ is the eigenvector for the state I, and ω^I is the excitation energy. We will consider only the right eigenvalue problem of CC2.

The eigenvalue problem is typically solved using the Davidson procedure to extract the first few eigenvalues. Instead of forming the whole matrix $\mathbf{A}$, one computes the matrix-vector products (MVP) of the different blocks with a trial vector $\mathbf{X}$. We can write the MVP Separating the singles and doubles excitations parts of the $\mathbf{X}$ vector:

$$\sigma_{\mu_1} = A_{\mu_1 \nu_1} x_{\nu_1} + A_{\mu_1 \mu_2} x_{\mu_2} \tag{3.39}$$

$$\sigma_{\mu_2} = A_{\mu_2 \nu_1} x_{\nu_1} + A_{\mu_2 \nu_2} x_{\nu_2} \tag{3.40}$$

Although the usage of eq. (3.39) and eq. (3.40) avoid the storage of the entire **A** matrix, storing $\mathbf{X}_{\mu_2}$ and σ_{μ_2} for the aimed excited states can easily become a major bottleneck. Therefore, most implementations of CC2 and ADC(2) take advantage of the diagonality of the double-double block of **A** and partition the CC2 eigenvalue problem as:

$$\left[A_{\mu_1\nu_1} - \sum_{\mu_2} \frac{A_{\mu_1\mu_2}A_{\mu_2\nu_1}}{\varepsilon_{\mu_2} - \omega}\right] x_{\nu_1} = \omega x_{\mu_1} \tag{3.41}$$

$$x_{\mu_2} = -\frac{A_{\mu_2\nu_1}}{\varepsilon_{\mu_2} - \omega} \tag{3.42}$$

where we directly solved for the doubles part of the excitation vector in eq. (3.42) and eq. (3.41) is the effective, but nonlinear, eigenvalue equation in the singles manifold that we must solve iteratively.[23,38] The MVP in the singles manifold, thus, reads as:

$$\sigma_{\mu_1}(x_{\nu_1}, \omega) = \sum_{\nu_1} A^{\text{eff}}_{\mu_1\nu_1}(\omega) x_{\nu_1} = \sum_{\nu_1} \left[A_{\mu_1\nu_1} - \sum_{\mu_2} \frac{A_{\mu_1\mu_2}A_{\mu_2\nu_1}}{\varepsilon_{\mu_2} - \omega}\right] x_{\nu_1} \tag{3.43}$$

In addition to the Davidson procedure – that must be modified for the problem in eq. (3.41) – the DIIS technique is often used to find and optimize the eigensolutions.[23]

3.3.1 Explicit expressions for closed-shell CC2 and ADC(2) matrix-vector products

Inserting the singlet cluster operator from eq. (2.96) and eq. (2.97) into the blocks of the CC2 Jacobian matrix, we obtain the following expression for the MVP in the singles manifold[23]

$$\begin{aligned}\sigma_{ai}^{\text{CC2}} = {} & \hat{F}_{ab}x_i^b - x_j^a\hat{F}_{ji} - \sum_b E_{ab}x_i^b - \sum_j x_j^a E_{ji} + \sum_{ck}[2\tilde{g}_{aikc} - \tilde{g}_{acki}]x_k^c \\ & + \sum_{ldc}[2x_{il}^{cd} - x_{li}^{cd}]\tilde{g}_{ldac} - \sum_{ldk}[2x_{kl}^{ad} - x_{lk}^{ad}]\tilde{g}_{ldki} \\ & + \sum_{ld}[2x_{il}^{ad} - x_{li}^{ad}]\tilde{F}_{ld} + \sum_{ld}[2t_{il}^{ad} - t_{li}^{ad}]\bar{F}_{ld}\end{aligned} \tag{3.44}$$

with the similarity transformed integrals and amplitudes are computed as in Sec. 2.6.2. The doubles amplitudes for CC2 are similarity transformed as well – see eq. (2.99). The $E_{ab}, E_{ij}, \bar{F}_{ld}$ intermediates are given by:[23]

$$E_{ab} = \sum_{ldk}[2t_{kl}^{ad} - t_{lk}^{ad}]g_{ldkb} \tag{3.45}$$

$$E_{ij} = \sum_{ldc}[2t_{il}^{cd} - t_{li}^{cd}]g_{ld\,jc} \tag{3.46}$$

$$\bar{F}_{ld} = \sum_{ck}[2\tilde{g}_{ldkc} - \tilde{g}_{lckd}]x_k^c \tag{3.47}$$

The doubles part of the excitation vector is:[23]

$$x_{ij}^{ab} = -\frac{\bar{g}_{aibj}}{\varepsilon_a - \varepsilon_i + \varepsilon_b - \varepsilon_j - \omega} \tag{3.48}$$

where the modified two-electron integrals are

$$\bar{g}_{aibj} = (ai|\bar{b}j) = \hat{S}_{ij}^{ab} \sum_{\mu\nu\sigma\lambda} (\bar{\Lambda}^{\mathrm{p}}_{\mu a}\Lambda^{\mathrm{h}}_{\nu i} + \Lambda^{\mathrm{p}}_{\mu a}\bar{\Lambda}^{\mathrm{h}}_{\nu i})\Lambda^{\mathrm{p}}_{\sigma b}\Lambda^{\mathrm{h}}_{\lambda j}(\mu\nu|\sigma\lambda) \tag{3.49}$$

The symmetrization operator $\hat{S}_{ij}^{ab}$ acts as: $\hat{S}_{ij}^{ab}Y_{ij}^{ab} = Y_{ij}^{ab} + Y_{ji}^{ba}$. The transformation matrices are formed as follows:

$$\bar{\mathbf{\Lambda}}^{\mathrm{p}} = -\mathbf{C}\mathbf{x}_{\mu_1}^{T} \tag{3.50}$$

$$\bar{\mathbf{\Lambda}}^{\mathrm{h}} = \mathbf{C}\mathbf{x}_{\mu_1} \tag{3.51}$$

From the equations in Sec. 3.2.2, the ADC(2) MVP for the singles manifold is formed:[23]

$$\begin{aligned}\sigma_{ai}^{\mathrm{ADC(2)}} = {} & (\varepsilon_a - \varepsilon_i)x_i^a - \sum_b D_{ab}x_i^b - \sum_j x_j^a D_{ji} + \sum_{ck}[2g_{aikc} - g_{acki}]x_k^c \\ & + \sum_{ldc}[2x_{il}^{cd} - x_{li}^{cd}]g_{ldac} - \sum_{ldk}[2x_{kl}^{ad} - x_{lk}^{ad}]g_{ldki} \\ & + \frac{1}{2}\sum_{ld}[2t_{il}^{ad} - t_{li}^{ad}]\bar{F}_{ld} + \frac{1}{2}\sum_{ck}[2g_{iald} - g_{idkl}]D_{ld}\end{aligned} \tag{3.52}$$

with

$$D_{ab} = \frac{1}{2}\sum_{ldk}\left[(2t_{kl}^{ad} - t_{lk}^{ad})g_{ldkb} + (2t_{kl}^{bd} - t_{lk}^{bd})g_{ldka}\right] \tag{3.53}$$

$$D_{ij} = \frac{1}{2}\sum_{ldc}\left[(2t_{il}^{cd} - t_{li}^{cd})g_{ldjb} + (2t_{jl}^{cd} - t_{lj}^{cd})g_{ldib}\right] \tag{3.54}$$

$$D_{ld} = \sum_{ck}(2t_{lk}^{dc} - t_{kl}^{dc})x_k^c \tag{3.55}$$

Contrary to CC2, the doubles amplitudes t_{ij}^{ab} in the MVP of eq. (3.52) are the MP2 amplitudes and the canonical MO coefficients are used instead of $\mathbf{\Lambda}$. The number of operations required to form $\sigma_{\mu_1}^{\mathrm{ADC(2)}}$ and $\sigma_{\mu_1}^{\mathrm{CC2}}$, as well as the x_{μ_2}, scales with the fifth power of the system size (i.e., N^5). Due to the interest in excited states, great efforts have been made to decrease the scaling of ADC(2) and CC2 and improve their efficiency. As for ground state energies, the Cholesky decomposition of the electronic integrals, as well as the RI approximation, are employed to reduce the effort in building the MVP.[23,24,38,96] The tensor hypercontraction approach has been proven to additionally reduce the computational scaling of CC2 in the canonical MO basis.[39] Low-scaling CC2, as well as ADC(2), implementations have been proposed which are based on local orbital representations.[41–47,52,55,56,59,60,156] The main drawback of these approaches is the state-specificity of the localization, thus, requiring different localization procedures for each investigated excited state. As discussed for ground state MP2 and CC2 methods, a scaled opposite-spin (SOS) approximation of both CC2 and ADC(2) schemes have been presented to show N^4 scaling behavior with the system size.[25,38,119]

3.4 Relation between LR-CC2 and ADC(2)

The previous sections made clear how much the ADC(2)-s and LR-CC2 methods are closely related both from a theoretical and computational point of view. Not only the perturbation-theoretical treatment of singly- and doubly-excited states is the same in both LR-CC2 and ADC(2)-s methods but, in addition, the ADC(2)-s secular matrix $\mathbf{M}^{\mathrm{ADC(2)}}$ can be mathematically derived from the CC2 Jacobian matrix $\mathbf{A}^{\mathrm{CC2}}$.[23–25,38] First, neglecting the t_{μ_1} amplitudes present in the CC2 Jacobian yields the so-called CIS(D_∞) Jacobian $\mathbf{A}^{\mathrm{CIS(D}_\infty)}$:

$$A^{\mathrm{CIS(D}_\infty)}_{\mu_i,\nu_j} = \begin{pmatrix} \langle\mu_1|[\hat{H}_0,\hat{\tau}_{\nu_1}]+[[\hat{H}_0,\hat{\tau}_{\nu_1}],\hat{T}_2^{(0)}]|\mathrm{HF}\rangle & \langle\mu_1|[\hat{H}_0,\hat{\tau}_{\nu_2}]|\mathrm{HF}\rangle \\ \langle\mu_2|[\hat{H}_0,\hat{\tau}_{\nu_1}]|\mathrm{HF}\rangle & \langle\mu_2|[\hat{F},\hat{\tau}_{\nu_2}]|\mathrm{HF}\rangle \end{pmatrix} \tag{3.56}$$

Finally, the ADC(2)-s secular matrix is obtained by symmetrization:

$$\mathbf{M}^{\mathrm{ADC(2)}} = \frac{1}{2}\left[\mathbf{A}^{\mathrm{CIS(D}_\infty)} + \mathbf{A}^{\mathrm{CIS(D}_\infty),\dagger}\right] \tag{3.57}$$

It must be noted that, if the HF determinant fulfills the Brillouin condition, the symmetrization in equation eq. (3.57) affects only the second-order contribution to the single-single block.[24] All other contributions to the matrix $\mathbf{M}^{\mathrm{ADC(2)}}$ are already Hermitian.

For canonical ADC(2)-s schemes, the secular matrix in eq. (3.57) is equivalent to the ISR-ADC(2)-s matrix in eq. (3.33). However, contrary to the ISR derivation, obtaining the secular matrix from the CC2 Jacobian results in important computational savings when the SCS-ADC(2)-s and SOS-ADC(2)-s schemes are employed. Within the rigorous ISR approach, only the single-single block of $\mathbf{M}^{\mathrm{ADC(2)}}$ is affected by the SOS approximation, showing a N^4 computational scaling.[25] On the other hand, the removal of the same-spin components in the double-double block in eq. (3.57) is retained from the SOS-LR-CC2 Jacobian matrix:[25]

$$A^{\mathrm{SOS\text{-}CC2}}_{\mu_i,\nu_j} = \begin{pmatrix} \langle\mu_1|[\tilde{\hat{H}}_0,\hat{\tau}_{\nu_1}]+c_{\mathrm{os}}[[\tilde{\hat{H}}_0,\hat{\tau}_{\nu_1}],\hat{T}_2^{\mathrm{os}}]|\mathrm{HF}\rangle & \langle\mu_1|c_{\mathrm{os}}[\tilde{\hat{H}}_0,\hat{\tau}^{\mathrm{os}}_{\nu_2}]|\mathrm{HF}\rangle \\ \langle\mu_2^{\mathrm{os}}|[\tilde{\hat{H}}_0,\hat{\tau}_{\nu_1}]|\mathrm{HF}\rangle & \langle\mu_2^{\mathrm{os}}|[\hat{F},\hat{\tau}^{\mathrm{os}}_{\nu_2}]|\mathrm{HF}\rangle \end{pmatrix} \tag{3.58}$$

Although the formal scaling is not affected by the reduced dimension of $\mathbf{M}^{\mathrm{ADC(2)}}$, the prefactor is reduced. **Publication II** presents a reformulation of the SOS-ADC(2)-s scheme, within the RI-approximation (see Sec. 4.1), based on the Cholesky decomposed densities.[63,64,104] For systems with a significant HOMO-LUMO gap and local electronic excitations, the computational and memory scaling behaviors are reduced to $\mathscr{O}(N^2)$ with the system size. The resulting method can be referred to as CDD-RI-SOS-ADC(2). For the first time, the attenuated RI Coulomb metric was employed to increase the sparsity of the three-index integrals and hence further reduce the scaling behavior of the method. The resulting implementation shows computational and memory demands scaling linearly with the size of systems with a local electronic structure and local excitation. In alternative, and for the first time, we proposed a linear scaling quasi-robust RI approach to reduce the scaling of CDD-RI-SOS-ADC(2) while retaining the accuracy of the standard Coulomb RI metric. The reformulation proposed in **Publication II** is extended to RI-SOS-LR-CC2 in Sec. 6.1, except the quasi-robust approach. In addition, the improved

algorithm for CDD-RI-SOS-ADC(2) (and CDD-RI-SOS-CC2), based on our block-sparse linaer algebra and implemented in FERMIONS++,[65–67] is discussed. Finally, **Publication III** proposes reduced-cost and low-scaling reformulations of the SOS-LR-CC2 and SOS-ADC(2) equations for the excitation energies based on the THC decomposition (see Sec. 4.2). The MO-based THC-SOS-LR-CC2 and THC-SOS-ADC(2) methods show computational effort and memory demands scaling as $\mathscr{O}(N^3)$ and $\mathscr{O}(N^2)$, respectively. On the other hand, the new implementations based on the Cholesky decomposed density matrices – CDD-THC-SOS-LR-CC2 and CDD-THC-SOS-ADC(2) – show $\mathscr{O}(N^2)$ computational scaling behavior for systems with local electronic structure and excitations. Note that the CDD-THC-SOS-LR-CC2 and CDD-THC-SOS-ADC(2) methods presented in **Publication III** are implemented in FERMIONS++.[65–67]

4 Tensor Decomposition and Sparse Linear-Algebra

As stated in the introductory part, the aim of this work is to extend the application of LR-CC2 and ADC(2) to systems with ~ 1000 atoms by developing highly memory- and computational-efficient low-scaling algorithms. In particular, we focused on the scaled opposite-spin contributions to the LR-CC2 and ADC(2) energies and properties. In their conventional MO-based formulations, the major bottlenecks of these methods are the transformation of the ERIs from the atomic orbital (AO) to the molecular orbital (MO) basis, the evaluation of the working equations involving them, and the storage of such ERIs-dependent quantities that would easily exceed the storage capability on a computing node. Rank-reduction approaches like the resolution of the identity (RI) and tensor hypercontraction (THC) decompose the two-electron integral tensor into lower-rank tensors and reduce the computational cost and the memory demands. The reduction of the memory and computational scaling – and the additional diminution of both computational and memory demands – is achieved by reformulating the RI- and THC-SOS-CC2/ADC(2) in term of Cholesky decomposed density matrices and by taking advantage of the sparsity in the decomposed ERIs and density matrices. The cost- and scaling-reduction are achieved via block-sparse linear algebra.
In Sec. 4.1, we outline the RI approximation of the four-index two-electron integrals into three-index integrals which played an important role in the development of efficient SOS-LR-CC2 and SOS-ADC(2) algorithms. In Sec. 4.2, we discuss the main aspects of the THC approximation that decomposes the two-electron integrals in two-index tensors vastly reducing the memory demands and I/O, and directly affecting the scaling of the treated methods. In Sec. 4.3, we briefly discuss the sparsity of the ERIs and density matrices. Moreover, the main features of our block-sparse linear algebra are outlined.

4.1 Resolution of the Indentity

The four-index two-electron integrals in the AO basis can be expressed in terms of the one-electron charge densities:[157]

$$(\mu\nu|\lambda\sigma) = \iint \chi_\mu(r_1)\chi_\nu(r_1)\frac{1}{r_{12}}\chi_\lambda(r_2)\chi_\sigma(r_2)dr_1dr_2 = \iint \Omega_{\mu\nu}(r_1)\frac{1}{r_{12}}\Omega_{\lambda\sigma}(r_2)dr_1dr_2 \quad (4.1)$$

Within the RI-approximation, the charge densities ρ are written as

$$\Omega_{\mu\nu}(r) = \sum_\alpha B^\alpha_{\mu\nu}\chi_\alpha(r) \quad (4.2)$$

where χ_α is a set of auxiliary functions and $B^\alpha_{\mu\nu}$ are fitting coefficients found by solving the following set of linear equations:

$$B^\alpha_{\mu\nu} = \sum_\beta (J^{-1})_{\alpha\beta}(\beta|\mu\nu) \tag{4.3}$$

with

$$(\beta|\mu\nu) = \iint \chi_\beta(r_1)\frac{1}{r_{12}}\chi_\mu(r_2)\chi_\nu(r_2)dr_1dr_2 \tag{4.4}$$

$$(J)_{\alpha\beta} = (\alpha|\beta) = \iint \chi_\alpha(r_1)\frac{1}{r_{12}}\chi_\beta(r_2)dr_1dr_2 \tag{4.5}$$

Notice that $(J^{-1})_{\alpha\beta}$ are the elements of the inverse Coulom metric. The three-index integrals in eq. (4.4) decay exponentially with the square of the distance between μ and ν, but decay only with r_{12}^{-1} as a function of the bra-ket distance. The number of non-negligible elements, therefore, scales with $\mathcal{O}(N^2)$. The two-center integrals – i.e., the Coulomb metric – as well as its inverse are not sparse and scale with $\mathcal{O}(N^2)$, which also imposes at best a quadratic scaling for the number of non-negligible elements in the fitting coefficients in eq. (4.3). The standard Coulomb metric has the disadvantage of introducing an unphysical long-range behavior between the charge density and the auxiliary functions. Introducing a short-range metric addresses this problem. For example, the overlap metric shows an exponential decay of the overlap metric and hence the number of non-zero elements in eq. (4.3) scales linearly with the system size. Such a sparse metric is bound to decrease the accuracy of the RI-approximation and its application is not recommended for most applications.[64,109,110,158] The attenuated Coulomb metric represents a compromise between the standard and the overlap metrics. The three- and two-index integrals are given by:

$$(\beta|\mu\nu)_\omega = \iint \chi_\beta(r_1)\frac{\mathrm{erfc}(\omega r_{12})}{r_{12}}\chi_\mu(r_2)\chi_\nu(r_2)dr_1dr_2 \tag{4.6}$$

$$(S_\omega)_{\alpha\beta} = (\alpha|\beta)_\omega = \iint \chi_\alpha(r_1)\frac{\mathrm{erfc}(\omega r_{12})}{r_{12}}\chi_\beta(r_2)dr_1dr_2 \tag{4.7}$$

where `erfc` is the complementary error function with an attenuation factor ω. The fitting coefficients are now obtained as[109,110,158]

$$B^\alpha_{\mu\nu} = \sum_\beta (J_\omega)_{\alpha\beta}(\beta|\mu\nu)_\omega \tag{4.8}$$

with

$$\mathbf{J}_\omega = \mathbf{S}_\omega^{-1}\mathbf{J}\mathbf{S}_\omega^{-1} \tag{4.9}$$

When $\omega \to 0$ or $\omega \to \infty$, the standard Coulomb metric or the overlap metric are recovered, respectively. The attenuation factor ω thus controls the degree of sparsity and numerical accuracy. A value of $\omega = 0.1$ was found to grant a linear number of elements significant[110] in the integrals of eq. (4.6) while providing accurate results. In **Publication I** the erfc-Coulomb metric was

applied for the first time to the SOS-CC2 method achieving a sub-quadratic scaling behavior in the calculation of the ground state energy, as discussed. In addition, in **Publication II**, the attenuated metric has been applied for the first time to the SOS-ADC(2) scheme to reduce its computational scaling to $\mathscr{O}(N)$ with the system size. In Chapter 6, we exploit again the locality of the attenuated Coulomb metric to develop a $\mathscr{O}(N)$ scaling algorithm for the calculation of SOS-LR-CC2 excitation energies. Moreover, the linear scaling algorithm proposed in **Publication II** has been improved and extended to the formation of the transition density between the ground and the excited states at the ADC(2) level.
As discussed in **Publications II**, the use of the local attenuated Coulomb metric introduces an error in the RI procedure which can become problematic within iterative procedures. Therefore, we used a quasi-robust formulation of the RI approximation[68] that introduces locality in the three- and two-index integrals while retaining the accuracy of the standard Coulomb metric approach. Despite the promising accuracy-locality ratio, the computational time of the existing quasi-robust algorithms may exceed the time for HF, MP2, and even ADC(2) steps in the case of large systems with dense electronic structures or large basis sets.

4.2 Tensor Hypercontraction

Within the THC framework, we approximate the four-index electron repulsion integral tensor as a product of five factor matrices $\mathbf{X}$[28,29,111,159]

$$(\mu\nu|\lambda\sigma) \approx \sum_{PQ} X_\mu^P X_\nu^P Z^{PQ} X_\lambda^Q X_\sigma^Q \tag{4.10}$$

where P indicates the grid points and the $\mathbf{X}$ correspond to the AO basis functions evaluated on a real-space grid:

$$X_\mu^P = \sqrt[n]{w_P}\phi_\mu(r_P) \tag{4.11}$$

The index of the radical is chosen, so that multiplying X_μ^P n times gives back the grid weights w_P. The matrix $\mathbf{Z}$ represents the interaction operator. Since evaluating its elements as $Z^{PQ} = ||r_{PQ}^{-1}||$ would lead to singularities for $(P = Q)$, the least-squares (LS) method[111] is recommended to evaluate $\mathbf{Z}$.
The $\mathbf{Z}$ matrix is obtained by minimizing the Euclidean norm of the residual

$$\mathscr{O} = \frac{1}{2}||(\mu\nu|\lambda\sigma) - \sum_{PQ} X_\mu^P X_\nu^P Z^{PQ} X_\lambda^Q X_\sigma^Q||^2 \tag{4.12}$$

with the following stationary condition:

$$\frac{\delta\mathscr{O}}{\delta Z^{P'Q'}} = -\sum_{\mu\nu\lambda\sigma} X_\mu^{P'} X_\nu^{P'} \Big[(\mu\nu|\lambda\sigma) - \sum_{PQ} X_\mu^P X_\nu^P Z^{PQ} X_\lambda^Q X_\sigma^Q\Big] X_\lambda^{Q'} X_\sigma^{Q'} = 0 \tag{4.13}$$

Inserting eq. (4.12) in the stationary condition and introducing the following notation for pairs of $\mathbf{X}$ matrices

$$R_{\mu\nu}^P = X_\mu^P X_\nu^P \tag{4.14}$$

yield the analytical solution to $\mathbf{Z}$[29,159]

$$\begin{aligned} Z^{PQ} &= \sum_{P'Q'} \Big[\sum_{\mu'\nu'} R^{P}_{\mu'\nu'} R^{P'}_{\mu'\nu'} \Big]^{-1} \Big[\sum_{\mu\nu\lambda\sigma} R^{P'}_{\mu\nu} (\mu\nu|\lambda\sigma) R^{Q'}_{\lambda\sigma} \Big] \Big[\sum_{\lambda'\sigma'} [R^{Q'}_{\lambda'\sigma'} R^{Q}_{\lambda'\sigma'} \Big]^{-1} \\ &= \sum_{P'Q'} \left(S^{-1}\right)^{PP'} E^{P'Q'} \left(S^{-1}\right)^{Q'Q} \end{aligned} \tag{4.15}$$

where $\left(S^{-1}\right)^{PP'}$ are the elements of the pseudo-inverse grid metric matrix. In **Publication III**, we compute the matrix $\mathbf{S^{-1}}$ via pivoted Cholesky decomposition of $\mathbf{S}$, automatically determining optimized (pruned) grids.[160] The matrix $\mathbf{E}$ can either be computed by using the ERIs or their three-index RI approximation.[30,113,114,116] In addition, it is possible to avoid the explicit calculation of the matrix $\mathbf{Z}$ by forming the $\mathbf{\Gamma}$ intermediates:[113,114,116]

$$\Gamma^{P}_{\alpha} = \sum_{P'\beta} \sum_{\mu\nu} \left(S^{-1}\right)^{PP'} R^{P'}_{\mu\nu} (\mu\nu|\beta) (J^{-\frac{1}{2}})_{\beta\alpha} \tag{4.16}$$

$$Z^{PQ} = \sum_{\alpha} \Gamma^{P}_{\alpha} \Gamma^{Q}_{\alpha} \tag{4.17}$$

where $(J^{-\frac{1}{2}})_{\beta\alpha}$ are the elements of the inverse square root of the standard or attenuated Coulomb RI metric. In **Publication III**, we propose for the first time density-based integral-direct algorithms for the calculation of the $\mathbf{\Gamma}$ matrix of transformed ERIs, based on the J-engine,[103] RI-J,[161] and natural-blocking[113,114] approaches as well as a newly implemented routine that is discussed in details in said publication. It is important to stress that the first two algorithms allow for a straightforward implementation of a THC algorithm in any quantum chemistry software.

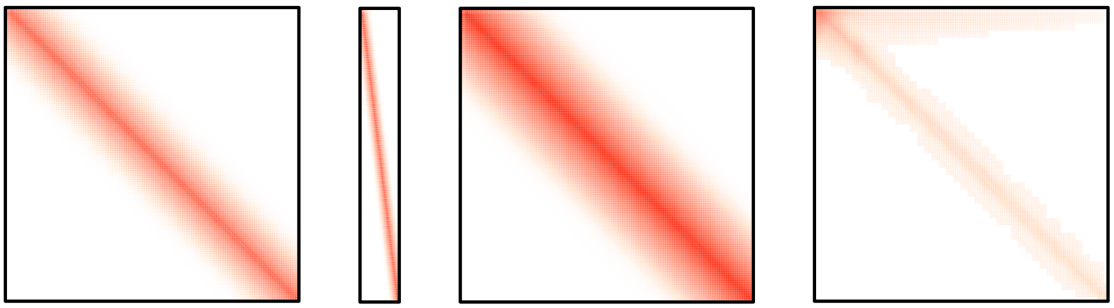

Figure 4.1: Block-sparsity patterns of the density matrices for linear carboxylic acid with 160 carbon atoms (LCA_{160}) in the def2-SVP basis.[162] The relevant blocks are in red, while the non-significant block are in white. The cutoff threshold was $\vartheta_a = 10^{-7}$. (A) occupied one-particle density matrix. (B) Cholesky decomposed occupied one-particle density matrix. (C) virtual one-particle density matrix. (D) AO-based singles transition vector to the lowest singlet state of LCA_{160}.

4.3 Block-Sparse Linear Algebra

Even within the RI and THC frameworks, several rank-two and rank-three tensors (T_{ij} and T^l_{ij}, respectively) are stored and several tensor operations are performed to evaluate the SOS-LR-CC2 and SOS-ADC(2) energies and properties. Some of these tensors are sparse, i.e., a large number of elements has a very small or zero value. For instance, the AO-based three-index integrals are sparse – due to the locality of the basis functions[14] – and the number of relevant elements $(\mu\nu|\alpha)$ scales as $\mathcal{O}(N^2)$ and $\mathcal{O}(N)$ in the standard and attenuated Coulomb metric, respectively (see Sec. 4.1). Similarly, the AO-based THC $\mathbf{X}$ matrices are sparse and the number of relevant elements X^P_μ grows linearly with the system size.[113] Since these tensors become dense upon transformation to the MO basis, we reformulate SOS-LR-CC2 and SOS-ADC(2) in terms of ground state sparse one-particle density matrices and Cholesky decomposed density matrices,[63,64,104] whose number of relevant elements grows linearly with the size of systems with a significant HOMO-LUMO gap – see Figure 4.1 A, B, and C. Moreover, we use the singles part of the transition vector in the AO basis representing the locality of the excitation, i.e., it contains a constant number of relevant numbers in the asymptotic limit for local excitations – see Figure 4.1 D.
Linear algebra operations involving sparse tensors can be accelerated significantly by avoiding the negligible elements during the calculation, hence reducing the required number of floating point operations (FLOP). For instance, many operations are omitted during the transformation of the decomposed AO-based integrals with the one-particle densities. In addition, the transformed decomposed integrals are still sparse and thus significant memory savings are achieved because we only allocate the relevant information. In practical implementations the use of sparse algebra can lead to a significant computational overhead compared to highly optimized routines for dense tensors. Therefore, efficient algorithms to exploit the sparsity of the tensors are crucial for any implementation of ab initio methods formulated in the AO basis, in order to achieve low-scaling

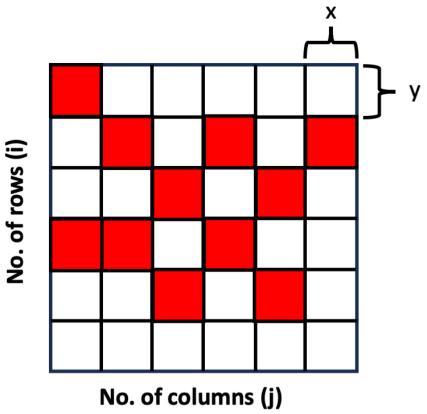

Figure 4.2: Schematic representation of a block-sparse matrix. The red blocks are the significant and allocated blocks. Each block has a defined maximum row and column dimension, **x** and **y**, respectively.

behaviors with the smallest possible overhead.
Our block-sparse linear algebra was implemented in FERMIONS++[65–67] to efficiently control memory demands, accuracy, and performance when the tensors are sparsely occupied. Considering the rank-two tensor T_{ij} (i.e., a matrix) in Figure 4.2, it is divided into blocks of defined sizes **x**,**y** (e.g., 96x96). A so-called block-allocator takes care of the allocation of each block storing them in one large and dynamically growing "memory pool", hence improving the performance for the allocation substantially (>20x). A memory pool is unique for each matrix, however, in the case of three-dimensional tensors T^l_{ij} (l matrices with i rows and j columns), we allocate the blocks from all l matrices in the same pool. Whether or not a block is allocated depends on the allocation threshold ϑ_a. Thus, only the blocks with L2-norm $\geq \vartheta_a$ are stored (red blocks in Figure 4.2). A second screening threshold ϑ_m is used within the matrix-matrix multiplication routine, whose pseudo-code is provided in the Supporting Information of **Publication I**. In this algorithm, we multiply only the elements of two allocated blocks if the product of their L2-norms is bigger than ϑ_m. If such criterium is not met, the operation will not be performed. Overall, the use of our block-sparse linear algebra comes with a small overhead of $\sim$1.6 due to the use of such a block-based structure.

5 Publications

5.1 Publication I: An effective sub-quadratic scaling atomic-orbital reformulation of the scaled opposite-spin RI-CC2 ground-state model using Cholesky-decomposed densities and an attenuated Coulomb metric

F. Sacchetta, D. Graf, H. Laqua, M. A. Ambroise, J. Kussmann, A. Dreuw, C. Ochsenfeld
J. Chem. Phys. **157**, 104104 (2022).

Abstract

An atomic-orbital reformulation of the Laplace-transformed scaled opposite-spin (SOS) coupled cluster singles and doubles (CC2) model within the resolution of the identity (RI) approximation (SOS-RI-CC2) is presented that extends its applicability to molecules with several hundreds of atoms and triple-zeta basis sets. We exploit sparse linear algebra and an attenuated Coulomb metric to decrease the disk space demands and the computational efforts. In this way, an effective sub-quadratic computational scaling is achieved with our ω-SOS-CDD-RI-CC2 model. Moreover, Cholesky decomposition of the ground-state one-electron density matrix reduces the prefactor, allowing for an early crossover with the molecular orbital formulation. The accuracy and performance of the presented method are investigated for various molecular systems.

`https://doi.org/10.1063/5.0098719`

The Journal of Chemical Physics ARTICLE scitation.org/journal/jcp

An effective sub-quadratic scaling atomic-orbital reformulation of the scaled opposite-spin RI-CC2 ground-state model using Cholesky-decomposed densities and an attenuated Coulomb metric

Cite as: J. Chem. Phys. 157, 1041 04 (2022); doi: 10.1063/5.0098719
Submitted: 11 May 2022 • Accepted: 28 July 2022 •
Published Online: 8 September 2022

F. Sacchetta,[1] D. Graf,[1] H. Laqua,[1] M. A. Ambroise,[2] J. Kussmann,[1] A. Dreuw,[2] and C. Ochsenfeld[1,a)]

AFFILIATIONS

[1] Chair of Theoretical Chemistry, Department of Chemistry, University of Munich (LMU), Munich, Germany
[2] Chair of Theoretical and Computational Chemistry, Interdisciplinary Center for Scientific Computing, Heidelberg University, Heidelberg, Germany

[a)] Author to whom correspondence should be addressed: christian.ochsenfeld@cup.uni-muenchen.de

ABSTRACT

An atomic-orbital reformulation of the Laplace-transformed scaled opposite-spin (SOS) coupled cluster singles and doubles (CC2) model within the resolution of the identity (RI) approximation (SOS-RI-CC2) is presented that extends its applicability to molecules with several hundreds of atoms and triple-zeta basis sets. We exploit sparse linear algebra and an attenuated Coulomb metric to decrease the disk space demands and the computational efforts. In this way, an effective sub-quadratic computational scaling is achieved with our ω-SOS-CDD-RI-CC2 model. Moreover, Cholesky decomposition of the ground-state one-electron density matrix reduces the prefactor, allowing for an early crossover with the molecular orbital formulation. The accuracy and performance of the presented method are investigated for various molecular systems.

I. INTRODUCTION

Coupled cluster (CC) theory[1,2] is among the most successful approaches to obtain accurate correlation energies.[3,4] However, the large computational and memory demands prohibit its routine application to large molecular systems. Among the most popular models are, e.g., CCSD and CCSD(T), whose computational effort scales as $\mathcal{O}(M^6)$ and $\mathcal{O}(M^7)$, respectively,[5,6] where M is a measure for the system size. In an effort to reduce the computational scaling associated with the accurate CCSD model, the second-order approximate coupled cluster singles and doubles model (CC2) was proposed by Christiansen *et al.*[7] in 1995. The CC2 ground-state energy is expected to be of similar quality as the MP2 energy[7] and is computed with $\mathcal{O}(M^5)$ computational scaling (as canonical MP2). Moreover, despite being the simplest approximation of the coupled cluster hierarchy, the space demand and I/O effort needed for CC2 are severe bottlenecks, scaling as $\mathcal{O}(M^4)$. While low scaling MP2 methods[8–18] are now widely used to compute ground-state properties of systems with hundreds of atoms and large basis sets, CC2 is not limited to ground-state properties, highlighting the importance of developing efficient low scaling CC2 methods. An important step in the CC2 progress has been the use of the resolution of the identity (RI) approximation,[19,20] largely reducing the storage requirements needed for two-electron integrals while maintaining $\mathcal{O}(M^5)$ computational scaling.[21] As an alternative, the Cholesky decomposition of the two-electron integral matrix can be used.[22–25] In 2004, a simplified variant of Grimme's spin-component scaled (SCS)-MP2 method[26] was proposed by Jung *et al.*[8] in order to reduce the computational complexity. The so-called scaled opposite-spin (SOS)-MP2 method[8] completely neglects the calculation of the same-spin contributions and scales the opposite spin part by a factor $c_{os} = 1.3$, providing an accuracy comparable to that of the unscaled models.[8,9] Later, the combination of this SOS approximation[8,9] employing also the Laplace transform of the energy denominator[27–29] within

the RI-approximation led to an efficient fourth-order scaling CC2 implementation by Winter and Hättig,[30] providing computational and memory/disk space savings already for small systems. Although the promising scaling behavior of the SOS-RI-CC2 model allows routine calculations of energies for systems with a few hundreds of atoms and large basis sets, it is essential to develop low or even linear scaling formulations in order to extend the CC2 applicability to even larger systems. To that end, approaches based on local molecular orbitals[31–34] and natural orbitals[35–37] have been used in the context of CC2 showing reduced computational scaling. However, to the best of our knowledge, atomic-orbital (AO) reformulations of CC2 have not yet been considered in literature and will be proposed in the present work for the ground-state energies as a first step toward reformulating CC2 excited state energies and properties. We reformulate the ground-state SOS-RI-CC2 equations presented by Winter and Hättig[30] in a pure atomic-orbital basis (Sec. II B), taking as reference the previous studies on RI-MP2,[14,16,18,38,39] CC,[40] and CPSCF[41] theory. The AO approach has the crucial advantage of depending explicitly on the one-particle density matrix **P** (and its virtual counterpart **Q**) that contains all the necessary information regarding the reference determinant and becomes sparse for growing system sizes in contrast to molecular orbitals. Such an AO-SOS-RI-CC2 approach can be further improved by introducing the Cholesky factorization of the one-particle density matrix, as previously shown by our group.[14,18,41–44] The resulting SOS-CDD-RI-CC2 model, described in Sec. II D, is based on so-called Cholesky orbitals inheriting the locality from the density matrix and whose number is equal to the number of MOs in the occupied space. Consequently, the SOS-CDD-RI-CC2 implementation features a lower prefactor and reduced memory demands[14,18] with respect to AO-SOS-RI-CC2 and shows an early crossover with the MO formulation. Additional improvements in terms of locality (and, therefore, performance) are gained by employing the RI Coulomb metric attenuated by the complementary error function that introduces only small errors.[18,45] As a result, quadratic or even sub-quadratic scaling is obtained by exploiting the locality of the atomic/Cholesky orbitals and efficient sparse algebra routines, bypassing localization procedures of any kind. This allows for a more direct control of the accuracy, contrary to previous studies on local CC2 implementations[31,32,46] based on the Pulay and Saebø approach,[10,11] where excitations between spatially distant orbitals are neglected if their contributions to the correlation energy are negligible. Accordingly, *a priori* restricted local MO (LMO) pair lists and pair specific excitation subspaces of projected AO (PAO) are specified and amplitudes outside these lists are neglected.[31,32] The downsides are the strong dependence on a successful localization procedure and the larger size of the correlation domains required for small errors.[46]

This article is structured as follows: First, in Sec. II A, we summarize the key components of the ground-state MO-SOS-RI-CC2 model proposed by Winter and Hättig.[30] Section II B describes the reformulation of the equations in the atomic-orbital basis. In Sec. II C, we introduce the Coulomb metric attenuated by the complementary error function for the RI-approximation, which moves the scaling toward sub-quadratic. The Cholesky decomposition of density matrices is introduced in Sec. II D, significantly reducing the prefactor of the AO implementation. Then, we provide an outline of our ω-SOS-CDD-RI-CC2 method in Sec. II E and discuss the accuracy (Sec. IV A), scaling behavior (Sec. IV B), and performance (Sec. IV C). Finally, we show the performance of our ω-SOS-CDD-RI-CC2 method when applied to systems of chemical interest.

II. THEORY

The CC2 model has been introduced by Christiansen *et al.*[7] as an approximation to the CCSD model, where the singles are treated as zeroth-order parameters in terms of the fluctuation potential. On the other hand, the double excitations are treated at first order in the fluctuation potential as in the MP2 theory.[7] The SOS-CC2 energy is given by

$$E^{\mathrm{sos}} = \langle \mathrm{HF}|\hat{H} + c_{\mathrm{os}}[\hat{H}, T_2^{\mathrm{os}}]|\mathrm{HF}\rangle, \tag{1}$$

where $\hat{H}$ is the similarity-transformed Hamiltonian and T_2^{os} is the two-electron excitation operator, which acts on two electrons with different spins.[8,30] The cluster amplitudes are determined by solving the coupled cluster equations,

$$\Omega_{\mu_1} = \langle \mu_1|\hat{H} + c_{\mathrm{os}}[\hat{H}, T_2^{\mathrm{os}}]|\mathrm{HF}\rangle = 0, \tag{2}$$

$$\Omega_{\mu_2} = \langle \mu_2^{\mathrm{os}}|\hat{H} + [F, T_2^{\mathrm{os}}]|\mathrm{HF}\rangle = 0, \tag{3}$$

where Ω_μ are the so-called coupled cluster vector functions and F is the Fock operator. We use the same scaling factor as for SOS-MP2,[8,30] $c_{\mathrm{os}} = 1.3$. Since the CC2 singles (t_{μ_1}) and doubles (t_{μ_2}) amplitudes depend on each other, the nonlinear Eqs. (2) and (3) must be solved iteratively. The CC2 calculations start with an initial guess for the singles amplitudes that are usually set to zero. The optimization scheme is based on the quasi-Newton equation for the nth iteration,[47]

$$\Delta t_{ai}^{(n)} = -\frac{\Omega_{ai}(t^{(n)})}{\varepsilon_a - \varepsilon_i}. \tag{4}$$

The correction $\Delta t_{ai}^{(n)}$ is then used to obtain the new singles amplitudes $t_{ai}^{(n+1)}$ by

$$t_{ai}^{(n+1)} = t_{ai}^{(n)} + \Delta t_{ai}^{(n)}. \tag{5}$$

The convergence may be improved significantly by application of the DIIS acceleration scheme[48] and it is reached when the norm of Ω_{μ_1} and the variation of the energy are below the given thresholds $\vartheta_{\mathrm{oconv}}$ (i.e., 10^{-5}) and $\vartheta_{\mathrm{econv}}$ (i.e., 10^{-6}), respectively.

A. MO-SOS-RI-CC2

In 2011, Winter and Hättig proposed an efficient fourth-order scaling implementation to compute the SOS-RI-CC2 ground-state energies,[30] given as the sum of the HF energy (E_{HF}) and the disconnected (E_{D}) and connected (E_{C}) double amplitudes contributions as follows:

$$\begin{aligned} E_{\mathrm{CC2}}^{\mathrm{SOS}} &= E_{\mathrm{HF}} + E_{\mathrm{D}} + E_{\mathrm{C}} \\ &= E_{\mathrm{HF}} + c_{\mathrm{os}} \sum_{aibj} t_{ai} t_{bj} (ai|bj) + c_{\mathrm{os}} \sum_{aibj} t_{aibj} (ai|bj). \end{aligned} \tag{6}$$

In order to solve Eq. (6) with a fourth-order scaling, the t_{aibj} orbital energy denominator is factorized using the Laplace transform technique followed by a numerical quadrature according to

$$\frac{1}{\varepsilon_{aibj}} = \int_0^\infty e^{-\varepsilon_{aibj}} dt = \sum_\tau^{N_\tau} w_\tau e^{-\varepsilon_{aibj} t_\tau}, \tag{7}$$

where $\varepsilon_{aibj} = \varepsilon_a - \varepsilon_i + \varepsilon_b - \varepsilon_j$ is the MO energy denominator and w_τ and the t_τ are the weights and grid points of the numerical quadrature procedure, respectively, which are optimized using, e.g., the minimax approximation in order to reduce the error.[49,50] In addition, the RI-approximation decomposes the four-index electron repulsion integrals (ERIs) to bypass an expensive four-index AO to MO transformation,[20,21,30]

$$(pq|rs) = \sum_P B^P_{pq} B^P_{rs}, \tag{8}$$

$$B^P_{pq} = \sum_{\mu\nu,Q} C_{\mu p} C_{\nu q} (\mu\nu|Q) J^{-1/2}_{QP}, \tag{9}$$

$$J_{PQ} = \left(P\left|\frac{1}{r_{12}}\right|Q\right), \tag{10}$$

using the Mulliken notation for two-, three-, and four-center integrals. In Eqs. (8) and (9), p, q, r, and s are MO indices, μ, ν are AO indices, and P, Q are auxiliary functions for the RI-approximation. $\mathbf{C}$ is the MO coefficient matrix. Moreover, some of the CC2 three-center integrals are modified according to

$$\hat{B}^P_{pq} = \sum_{\mu\nu} \Lambda^{\mathrm{p}}_{\mu p} \Lambda^{\mathrm{h}}_{\nu q} (\mu\nu|P), \tag{11}$$

with the transformation matrices Λ^{p} and Λ^{h} given by

$$\Lambda^{\mathrm{p}} = \mathbf{C}(\mathbf{I} - \mathbf{t}_1^T) \qquad \Lambda^{\mathrm{h}} = \mathbf{C}(\mathbf{I} + \mathbf{t}_1) \qquad \mathbf{t}_1 = \begin{pmatrix} 0 & 0 \\ \{t_{ai}\} & 0 \end{pmatrix}. \tag{12}$$

The t_1-dependent doubles amplitudes are then calculated as

$$t^{ab}_{ij} = -\sum_\tau^{N_\tau} w_\tau \sum_P \hat{B}^P_{ai} e^{-\varepsilon_{ai} t_\tau} \cdot \hat{B}^P_{bj} e^{-\varepsilon_{bj} t_\tau}, \tag{13}$$

and the expression for the MO-SOS-RI-CC2 correlation energy can be rewritten as

$$E_{\mathrm{D}} = c_{\mathrm{os}} \sum_{aibj} t_{ai} t_{bj} \sum_Q B^Q_{ai} B^Q_{bj}, \tag{14}$$

$$\begin{aligned} E_{\mathrm{C}} &= -c_{\mathrm{os}} \sum_\tau w_\tau \sum_{aibj} \sum_{PQ} \hat{B}^P_{ai} \hat{B}^P_{bj} e^{-\varepsilon_{ai} t_\tau} e^{-\varepsilon_{bj} t_\tau} B^Q_{ai} B^Q_{bj} \\ &= -c_{\mathrm{os}} \sum_\tau w_\tau \sum_{PQ} N^{QP}_\tau N^{QP}_\tau, \end{aligned} \tag{15}$$

where N^{QP}_τ is given in Table I. The converged t_1-amplitudes are obtained at the end of the iterative optimization, where, in each iteration, doubles amplitudes are computed "on-the-fly" by inserting Eq. (13) into the singles part of the vector function [Eq. (2)], yielding the working expressions in terms of computational convenient intermediates,

$$\Omega_{ai}(t^{(n)}) = \Omega^G_{ai}(t^{(n)}) + \Omega^H_{ai}(t^{(n)}) + \Omega^I_{ai}(t^{(n)}) + \Omega^J_{ai}(t^{(n)}), \tag{16}$$

whose explicit expressions are listed in Table I. The solution of Eq. (16) requires a considerable amount of memory and disk space for the calculation of intermediates. The memory limitations are overcome by employing batching algorithms to evaluate the three-center integrals and the intermediates (see the algorithm proposed by Winter and Hättig[30]).

The MO-SOS-RI-CC2 equations in Table I have been implemented in the FermiONs++[51–53] program as proposed by Winter and Hättig.[30] In contrast, we do not batch over the Laplace quadrature points (see the supplementary material).

TABLE I. Explicit expressions of the singles amplitudes vector function terms for SOS-RI-CC2 in the MO and the SOS-CDD-RI-CC2 formulation. The Einstein notation is used.

MO-SOS-RI-CC2	SOS-CDD-RI-CC2
$\Omega^G_{ai} = \hat{B}^Q_{ac} \hat{Y}^Q_{ci}$	$\Omega^G_{\mu\nu} = \hat{Q}_{\mu\mu'} (B^Q_{\mu'\nu'} \hat{Y}^Q_{\nu' i}) L_{\nu i}$
$\Omega^H_{ai} = -\hat{Y}^Q_{ak} \hat{B}^Q_{ki}$	$\Omega^H_{\mu\nu} = (-\hat{Y}^Q_{\mu k} \hat{B}^Q_{ki}) L_{\nu i}$
$\Omega^I_{ai} = -c_{\mathrm{os}} w_\tau n^P_\tau \hat{B}^P_{ai} e^{-\varepsilon_{ai} t_\tau}$	$\Omega^I_{\mu\nu} = (-c_{\mathrm{os}} \tilde{n}^{P\tau}_\tau \hat{B}^P_{\mu i}) L_{\nu i}$
$\Omega^J_{ai} = \hat{F}_{ai}$	$\Omega^J_{\mu\nu} = \hat{Q}_{\mu\mu'} \hat{F}_{\mu'\nu'} \hat{P}_{\nu'\nu}$
$\hat{Y}^Q_{ai} = -c_{\mathrm{os}} w_\tau \hat{B}^P_{ai} N^{QP}_\tau e^{-\varepsilon_{ai} t_\tau}$	$\hat{Y}^Q_{\mu i} = -c_{\mathrm{os}}{}^\tau \hat{B}^P_{\mu i} \tilde{N}^{QP}_\tau$
$N^{QP}_\tau = B^Q_{bj} \hat{B}^P_{bj} e^{-\varepsilon_{bj} t_\tau}$	$N^{RS}_\tau = B^{R\,\tau}_{\mu j} \hat{B}^S_{\mu j}$
$n^P_\tau = \hat{B}^P_{bj} \hat{F}_{jb} e^{-\varepsilon_{bj} t_\tau}$	$n^R_\tau = {}^\tau \hat{B}^R_{\mu j} \hat{F}_{j\mu}$
$\hat{B}^P_{ai} = \Lambda^p_{\mu a} \Lambda^h_{\nu i} B^P_{\mu\nu} J^{-1/2}_{PQ}$	$\tilde{N}^{QP}_\tau = J^{-1}_{QR} N^{RS}_\tau J^{-1}_{SP}$
	$\tilde{n}^P_\tau = J^{-1}_{PR} n^R_\tau$

B. Reformulation of the SOS-RI-CC2 method in the AO basis

In order to extend the applicability of the SOS-RI-CC2 model to systems with hundreds of atoms and large basis sets, we reformulated the MO-expressions summarized in Table I in the AO basis. The quasi-Newton expression for the correction of the CC2 singles amplitudes [Eq. (4)] has an important role during this reformulation. Indeed, we can back-transform $\Delta t^{(n)}_{ai}$ [Eq. (4)] to the AO basis [Eq. (17)] via the Laplace transform of the energy denominator $(\varepsilon_a - \varepsilon_i)$, along the lines of Beer and Ochsenfeld[41] for the U^x_{ai} matrix,

$$\sum_{ai} C_{\mu a} \Delta t^{(n)}_{ai} C_{\nu i} = -\sum_\alpha^{N_\alpha} w_\alpha \sum_{ai} e^{-\varepsilon_a t_\alpha} C_{\mu a} \Omega_{ai} C_{\nu i} e^{\varepsilon_i t_\alpha}. \tag{17}$$

In that way, the SOS-RI-CC2 equations are rewritten in the AO basis employing a convenient transformation that generates a formulation where all integrals and excitation amplitudes are written with AO indices. Even though this procedure allows us to completely avoid the canonical MO basis,[41] it increases the computational effort by a factor of N_α, that is, the number of Laplace quadrature points employed in [Eq. (17)] (generally 6–10 points). In order to overcome

this drawback, we limited the back-transformation to the vector function for the singles amplitudes [the numerator in Eq. (4)],

$$\sum_{ai} C_{\mu a}\Omega_{ai}(t^{(n)})C_{vi} = \Omega_{\mu\nu}(t^{(n)}) = \Omega^{G}_{\mu\nu}(t^{(n)}) + \Omega^{H}_{\mu\nu}(t^{(n)}) + \Omega^{I}_{\mu\nu}(t^{(n)}) + \Omega^{J}_{\mu\nu}(t^{(n)}). \tag{18}$$

Such a strategy enables the reformulation of the intermediates in the AO basis, while the use of canonical MOs is limited only to Eq. (4) and does not affect the overall efficiency of the method. In the following, the most important steps in the reformulation of the CC2 method in the AO basis will be presented. The computational scaling of the main SOS-RI-CC2 steps is reported in Table II. The Einstein summation convention is used in the following equations.

The first two contributions to the vector function are reformulated according to

$$\Omega^{G}_{\mu\nu} = C_{\mu a}\Omega^{G}_{ai}C_{vi} = C_{\mu a}\hat{B}^{Q}_{ac}\hat{Y}^{Q}_{ci}C_{vi} = \hat{Q}_{\mu\sigma}B^{Q}_{\sigma\lambda}\hat{Y}^{Q}_{\lambda\nu}, \tag{19}$$

$$\Omega^{H}_{\mu\nu} = C_{\mu a}\Omega^{H}_{ai}C_{vi} = -C_{\mu a}\hat{Y}^{Q}_{ak}\hat{B}^{Q}_{ki}C_{vi} = -\hat{Y}^{Q}_{\mu\sigma}B^{Q}_{\sigma\lambda}\hat{P}_{\lambda\nu}, \tag{20}$$

with the CC2 virtual ($\hat{Q}$) and occupied ($\hat{P}$) densities given by

$$\hat{Q}_{\mu\nu} = C_{\mu d}\Lambda^{p}_{vd} = Q_{\mu\nu} - Q_{\mu\mu'}S_{\mu'\sigma}t_{\sigma\lambda}S_{\lambda\nu'}P_{\nu'\nu}, \tag{21}$$

$$\hat{P}_{\mu\nu} = \Lambda^{h}_{\mu l}C_{vl} = P_{\mu\nu} + Q_{\mu\mu'}S_{\mu'\sigma}t_{\sigma\lambda}S_{\lambda\nu'}P_{\nu'\nu}, \tag{22}$$

where $Q_{\mu\nu} = \sum_a C_{\mu a}C_{va}$ and $P_{\mu\nu} = \sum_i C_{\mu i}C_{vi}$ are the virtual and occupied ground-state densities and $\mathbf{S}$ is the overlap matrix. The formation of the densities scales cubically with the system size, but its computational cost is negligible compared to other steps. The intermediate $\hat{\mathbf{Y}}$ is computed as

$$\hat{Y}^{Q}_{\mu\nu} = -c_{\text{os}}{}^{\tau}\hat{B}^{P}_{\mu\nu}\tilde{N}^{QP}_{\tau}, \tag{23}$$

where the three-center integrals and the intermediates $\tilde{N}^{QP}_{\tau}$ depending on the Laplace quadrature points τ are given by

$${}^{\tau}\hat{B}^{P}_{\mu\nu} = \hat{Q}^{\tau}_{\mu\mu'}B^{P}_{\mu'\nu'}\hat{P}^{\tau}_{\nu'\nu}, \tag{24}$$

$$\tilde{N}^{QP}_{\tau} = J^{-1}_{QR}N^{RS}_{\tau}J^{-1}_{SP}, \tag{25}$$

$$N^{RS}_{\tau} = B^{R}_{bj}\hat{B}^{S}_{bj}e^{-\varepsilon_{bj}t_{\tau}} = B^{R}_{\mu\nu}\hat{Q}^{\tau}_{\mu\sigma}B^{S}_{\sigma\lambda}\hat{P}^{\tau}_{\lambda\nu} = B^{R}_{\mu\nu}{}^{\tau}\hat{B}^{S}_{\mu\nu}. \tag{26}$$

The matrices $\hat{Q}^{\tau}$ and $\hat{P}^{\tau}$ are the CC2 virtual and occupied pseudo-densities, respectively,

$$\hat{Q}^{\tau}_{\mu\nu} = w^{\frac{1}{4}}_{\tau}C_{\mu d}e^{-\varepsilon_{d}t_{\tau}}\Lambda^{p}_{vd} = Q^{\tau}_{\mu\nu} - Q^{\tau}_{\mu\mu'}S_{\mu'\sigma}t_{\sigma\lambda}S_{\lambda\nu'}P_{\nu'\nu}, \tag{27}$$

$$\hat{P}^{\tau}_{\mu\nu} = w^{\frac{1}{4}}_{\tau}\Lambda^{h}_{\mu l}e^{\varepsilon_{l}t_{\tau}}C_{vl} = P^{\tau}_{\mu\nu} + Q_{\mu\mu'}S_{\mu'\sigma}t_{\sigma\lambda}S_{\lambda\nu'}P^{\tau}_{\nu'\nu}, \tag{28}$$

with

$$Q^{\tau}_{\mu\nu} = w^{\frac{1}{4}}_{\tau}C_{\mu a}e^{-\varepsilon_{a}t_{\tau}}C_{va}, \tag{29}$$

$$P^{\tau}_{\mu\nu} = w^{\frac{1}{4}}_{\tau}C_{\mu i}e^{\varepsilon_{i}t_{\tau}}C_{vi}. \tag{30}$$

An example of the sparsity pattern of $\hat{Q}^{\tau}_{\mu\nu}$ for the first Laplace quadrature point is displayed in Fig. 1 for the linear alkane $C_{320}H_{642}$. The remaining contributions to the singles vector function are given by

$$\Omega^{I}_{\mu\nu} = C_{\mu a}\Omega^{I}_{ai}C_{vi} = -c_{\text{os}}\tilde{n}^{P\tau}_{\tau}\hat{B}^{P}_{\mu\nu}, \tag{31}$$

$$\Omega^{J}_{\mu\nu} = C_{\mu a}\Omega^{J}_{ai}C_{vi} = \hat{Q}_{\mu\mu'}\hat{F}_{\mu'\nu'}\hat{P}_{\nu'\nu}, \tag{32}$$

where

$$\tilde{n}^{P}_{\tau} = n^{R}_{\tau}J^{-1}_{RP}, \tag{33}$$

$$n^{R}_{\tau} = \hat{F}_{jb}\hat{B}^{R}_{bj}e^{-\varepsilon_{bj}t_{\tau}} = \hat{F}_{\mu\nu}\hat{Q}^{\tau}_{\nu\sigma}B^{R}_{\sigma\lambda}\hat{P}^{\tau}_{\lambda\mu} = \hat{F}_{\mu\nu}{}^{\tau}\hat{B}^{R}_{\mu\nu}. \tag{34}$$

Moreover, the modified Fock matrix is built from the CC2 density, showing an asymptotically quadratic scaling for the calculation of the Coulomb contributions:

$$\hat{F}_{\mu\nu} = h_{\mu\nu} + \sum_{\sigma\lambda}\hat{P}_{\sigma\lambda}[2(\mu\nu|\lambda\sigma) - (\mu\sigma|\lambda\nu)]. \tag{35}$$

Due to the long-range nature of the electron–electron interaction operator ($\frac{1}{r_{12}}$), the formation of the three- and two-center integrals ($B^{P}_{\mu\nu}$ and J_{PQ}) shows a quadratic scaling with system size while the inversion of the two-center integrals scales cubically. These steps are carried out only once and the time demands are not significant as compared to the rest of the CC2 calculation. In order to retain the sparsity of the three-center integrals, the multiplication with the dense J^{-1}_{PQ} matrix is delayed until the N^{RS}_{τ} and n^{R}_{τ} intermediates are formed.

TABLE II. Formal and asymptotic computational scaling (with the number of orbitals N) for key steps of ω-SOS-CDD-RI-CC2 models within the RI standard Coulomb metric ($\omega = 0$) and overlap metric ($\omega \to \infty$).

		Asymptotic scaling	
Step	Formal scaling	$\omega = 0$	$\omega \to \infty$
Cholesky decompose $\mathbf{P}$	N^3	$\mathcal{O}(N)$	$\mathcal{O}(N)$
Form $\mathbf{J}$	N^2	$\mathcal{O}(N^2)$	$\mathcal{O}(N^2)$
Invert $\mathbf{J}$	N^3	$\mathcal{O}(N^3)$	$\mathcal{O}(N^3)$
Form $B^{P}_{\mu\nu}$	N^2	$\mathcal{O}(N^2)$	$\mathcal{O}(N^2)$
Form $\hat{B}^{P}_{\mu i}$ and $B^{P}_{\mu\underline{i}}$	N^4	$\mathcal{O}(N^2)$	$\mathcal{O}(N)$
Form ${}^{\tau}\hat{B}^{P}_{\mu i}$	N^3	$\mathcal{O}(N^2)$	$\mathcal{O}(N)$
Form N^{RS}_{τ}	N^4	$\mathcal{O}(N^3)$	$\mathcal{O}(N)$
Form n^{R}_{τ}	N^3	$\mathcal{O}(N^2)$	$\mathcal{O}(N)$
Form $\tilde{N}^{QP}_{\tau}$	N^3	$\mathcal{O}(N^3)$	$\mathcal{O}(N^3)$
Form $\tilde{n}^{P}_{\tau}$	N^2	$\mathcal{O}(N^2)$	$\mathcal{O}(N^2)$
Form $\Omega^{I}_{\mu\nu}$	N^3	$\mathcal{O}(N^2)$	$\mathcal{O}(N)$
Form $\hat{Y}^{Q}_{\mu i}$	N^4	$\mathcal{O}(N^3)$	$\mathcal{O}(N^2)$
Form $\hat{B}^{Q}_{\underline{ki}}$	N^4	$\mathcal{O}(N^2)$	$\mathcal{O}(N)$
Form $\Omega^{G}_{\mu\nu}$	N^4	$\mathcal{O}(N^3)$	$\mathcal{O}(N)$
Form $\Omega^{H}_{\mu\nu}$	N^4	$\mathcal{O}(N^3)$	$\mathcal{O}(N)$
Form $\Omega^{J}_{\mu\nu}$	N^3	$\mathcal{O}(N^3)$	$\mathcal{O}(N^3)$

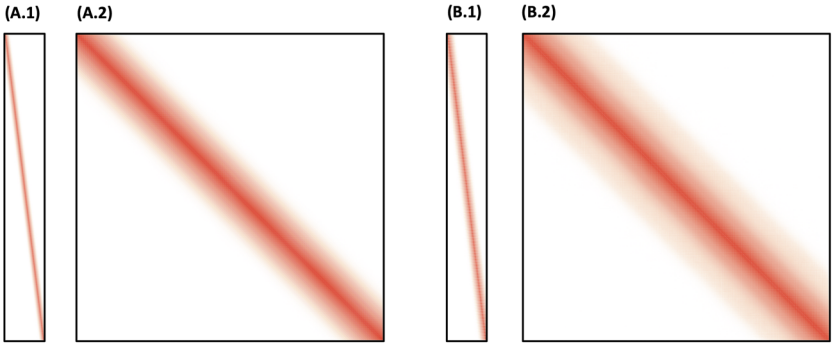

FIG. 1. Sparsity patterns of occupied and virtual CC2 pseudo-densities for the linear alkane $C_{320}H_{642}$, in the def2-svp (a) and def-tzvp (b) basis sets with a cut-off threshold equal to 10^{-10}. (a.1, b.1) $\hat{P}^{\tau}_{\underline{\mu i}}$ from Eq. (46) and (a.2, b.2) $\hat{Q}^{\tau}_{\mu\nu}$ from Eq. (27).

Once all the contributions to $\Omega_{\mu\nu}$ are computed, we transform the vector function to the MO basis according to

$$\Omega_{ai}(t^{(n)}) = C_{\mu a} S_{\mu\mu'} \Omega_{\mu'\nu'}(t^{(n)}) S_{\nu'\nu} C_{\nu i}, \tag{36}$$

and the correction Δt_{ai} is then given as in the canonical MO implementation [Eq. (4)]. The updated CC2 single amplitudes in the AO basis are finally given by

$$\Delta t^{(n)}_{\mu\nu} = C_{\mu a} \Delta t^{(n)}_{ai} C_{\nu i}, \tag{37}$$

$$t^{(n+1)}_{\mu\nu} = t^{(n)}_{\mu\nu} + \Delta t^{(n)}_{\mu\nu}. \tag{38}$$

C. Using the erfc-attenuated Coulomb metric: ω-SOS-AO-RI-CC2

The presented reformulation in the atomic-orbital basis results in a cubic asymptotic scaling $\mathcal{O}(M^3)$ with molecular size, since the auxiliary functions couple to the AO basis-function pairs with a $\frac{1}{r_{12}}$ decay within the standard Coulomb metric (see Table II). Density fitting calculations are generally performed with the Coulomb metric because it yields the most accurate results for the commonly employed auxiliary basis sets.[9,43,45] The slow long-range decay of this metric has no disadvantage when transforming to the canonical MO basis. However, in local bases (i.e., Cholesky and atomic orbitals), no sparsity can be gained. Therefore, the overlap metric represents a promising alternative due to the increased locality and sparsity.[43,45] The drawback is the decreased accuracy. A third choice would be a metric that combines the accuracy of the Coulomb metric and the sparsity of the local overlap metric. The attenuated Coulomb metric given by

$$g = \frac{\mathrm{erfc}(\omega r_{12})}{r_{12}} \tag{39}$$

has this property, as described by Jung *et al.*[45] in SOS-MP2 calculations. The three-, two-, and four-center integrals are then given by

$$(\mu\nu|P) = \left(\mu\nu\left|\frac{\mathrm{erfc}(\omega r_{12})}{r_{12}}\right|P\right), \tag{40}$$

$$(S_\omega)_{PQ} = \left(P\left|\frac{\mathrm{erfc}(\omega r_{12})}{r_{12}}\right|Q\right), \tag{41}$$

$$\mathbf{J}_{\boldsymbol{\omega}} = \mathbf{S}_{\omega}^{-1}\mathbf{J}\mathbf{S}_{\omega}^{-1}, \tag{42}$$

$$(\mu\nu|\sigma\lambda) = (\mu\nu|P) J^{PQ}_{\omega} (Q|\sigma\lambda). \tag{43}$$

As with the standard Coulomb metric, we postpone the multiplication with the two-center integrals to the step in Eq. (33) in order to preserve locality through the previous time-determining steps. The extent of locality is controlled by the parameter ω, recovering the Coulomb metric at $\omega = 0$ and approaching the overlap metric as ω increases. If $\omega \to \infty$, we recover the overlap metric. Of course, the larger ω is, the less accurate are the results[45] (at least when standard RI basis sets are employed). In the present work, we employ the erfc-Coulomb metric within CC2 for the first time, increasing the sparsity of the intermediates and allowing a further reduction of the scaling in all time-determining steps. Indeed, the effective computational scaling of ω-SOS-CDD-RI-CC2 is sub-quadratic for $\omega > 0$.

D. Reduction of the basis set scaling: ω-SOS-CDD-RI-CC2

Despite the above formulation being suited for large systems and moderate basis sets, its applicability to large basis sets is hampered by the scaling with the basis set size N_{basis} and auxiliary basis set size N_{aux}. The formal scaling is increased from $\mathcal{O}(N_{virt}N_{occ}N^2_{aux})$ to $\mathcal{O}(N^2_{basis}N^2_{aux})$ for a fixed molecular size. In order to reduce the complexity and improve the performance, we employ Cholesky decomposition of the occupied ground-state density matrix with complete pivoting[54,55] and the idempotency relation of the occupied pseudo-density matrix, as proposed by Graf *et al.*[44] and Glasbrenner *et al.*,[18]

$$\mathbf{P} = \mathbf{L}\mathbf{L}^T \quad \mathbf{P}^{\boldsymbol{\tau}} = \mathbf{P}^{\boldsymbol{\tau}}\mathbf{S}\mathbf{P} = \mathbf{P}^{\boldsymbol{\tau}}\mathbf{S}\mathbf{L}\mathbf{L}^T. \tag{44}$$

The Cholesky factorization scales formally as N^3, but it has a very low prefactor. Moreover, it can be carried out with asymptotic linear scaling.[56] The columns of $\mathbf{L}$ can be considered as the coefficients of localized occupied MOs that we will call Cholesky orbitals[14] and tag with $\underline{i}, \underline{j}, \underline{k}$ indices. They inherit the locality from the density matrix[57] and their number is equal to the number of MOs. Like the pseudo-density matrices, the CC2 occupied density matrix is invariant with respect to projection onto the occupied space and can now be written as

$$\hat{P}^{\tau}_{\mu\nu} = \hat{P}^{\tau}_{\mu\nu} S_{\nu\sigma} L_{\sigma\underline{i}} L_{\nu\underline{i}} = \hat{P}^{\tau}_{\mu\underline{i}} L_{\nu\underline{i}}, \tag{45}$$

$$\hat{P}^{\tau}_{\mu\underline{i}} = P_{\mu\sigma}S_{\sigma\lambda}P^{\tau}_{\lambda\underline{i}} + Q_{\mu\mu'}S_{\mu'\sigma}t_{\sigma\lambda}S_{\lambda\nu'}P_{\nu'\sigma'}S_{\sigma'\lambda'}P^{\tau}_{\lambda'\underline{i}}$$
$$= (L_{\mu\underline{j}} + Q_{\mu\mu'}S_{\mu'\sigma}t_{\sigma\lambda}S_{\lambda\nu'}L_{\nu'\underline{j}})L_{\sigma'\underline{j}}S_{\sigma'\lambda'}P^{\tau}_{\lambda'\underline{i}}, \quad (46)$$

and its sparsity pattern is depicted in Fig. 1 for $C_{320}H_{642}$. The derived ω-SOS-CDD-RI-CC2 expressions for the vector function contributions are given in Table I, where the three-center integrals, then, read

$$B^{Q}_{\mu\underline{i}} = B^{Q}_{\mu\nu}L_{\nu\underline{i}}, \quad (47)$$

$$\hat{B}^{Q}_{\underline{k}\underline{i}} = L_{\mu\underline{k}}B^{Q}_{\mu\nu}\hat{P}_{\nu\underline{i}}, \quad (48)$$

$${}^{\tau}\hat{B}^{P}_{\mu\underline{i}} = \hat{Q}^{\tau}_{\mu\mu'}B^{P}_{\mu'\nu'}\hat{P}^{\tau}_{\nu'\underline{i}}. \quad (49)$$

The introduction of Cholesky orbitals reduces the formal scaling behavior to $\mathcal{O}(N_{\text{basis}}N_{\text{occ}}N^2_{\text{aux}})$. The half-transformed three-center integrals $B^{Q}_{\mu\underline{i}}$ do not depend on the singles amplitudes and, hence, can be computed only once at the beginning and stored on disk. On the other hand, ${}^{\tau}\hat{B}^{P}_{\mu\underline{i}}$ in Eq. (49) is computed for each Laplace point and each iteration. We decided to use the idempotency relation in Eq. (44) not only to improve the efficiency but also to reduce the memory requirements. Each $B^{Q}_{\mu\nu}$ matrix is precontracted as shown in Eq. (50) and the resulting half-transformed $\hat{B}^{P}_{\mu\underline{i}}$ quantity is independent of the Laplace points. The Laplace point-dependent three-center integrals are then obtained from the half-transformed integrals reducing both I/O and computational effort, as shown in Eq. (51),

$$\hat{B}^{P}_{\mu\underline{j}} = B^{P}_{\mu\nu}(L_{\nu\underline{j}} + Q_{\nu\nu'}S_{\nu'\sigma}t_{\sigma\lambda}S_{\lambda\nu''}L_{\nu''\underline{j}}), \quad (50)$$

$${}^{\tau}\hat{B}^{P}_{\mu\underline{i}} = \hat{Q}^{\tau}_{\mu\mu'}B^{Q}_{\mu'\underline{j}}(L_{\sigma\underline{j}}S_{\sigma\lambda}P^{\tau}_{\lambda\underline{i}}). \quad (51)$$

The reason why we avoided Cholesky factorization of the virtual density matrix is twofold. First, the sparsity of the virtual density is not well preserved and, hence, the rank reduction is often counteracted by this loss of sparsity. Second, correlation methods such as CC2 require large basis sets for accurate results, in which case, $N_{\text{basis}} \approx N_{\text{virt}}$ and the rank reduction from factorization is negligible.

Finally, the ω-SOS-CDD-RI-CC2 ground-state energy is computed as

$$E^{\text{SOS}}_{\text{CC2}} = E_{\text{D}} + E_{\text{C}} = c_{\text{os}}t_{\mu\underline{i}}B^{P}_{\mu\underline{i}}J^{PQ}_{\omega}t_{\nu\underline{j}}B^{Q}_{\nu\underline{j}} - c_{\text{os}}\tilde{N}^{QP}_{\tau}N^{QP}_{\tau}, \quad (52)$$

with

$$t_{\mu\underline{i}} = Q_{\mu\mu'}S_{\mu'\sigma}t_{\sigma\lambda}S_{\lambda\nu'}L_{\nu'\underline{i}} \quad (53)$$

and $\tilde{N}^{QP}_{\tau}$ and N^{QP}_{τ} given by Eqs. (25) and (26).

E. Outline of the low scaling implementation: A minimal-overhead batching

The available memory on a single computing node is easily exceeded by CC2 memory requirements in both MO and AO basis. Therefore, we introduced batching schemes for evaluating intermediates as three-center integrals, intermediates N^{QP}_{τ}, $\hat{Y}^{Q}_{\mu\underline{i}}$, and contributions to the vector function. The MO implementation is not discussed here; its algorithms are provided in the supplementary material.

First, we compute the $B^{P}_{\mu\nu}$ and half-transformed $B^{P}_{\underline{i}\mu}$ matrices and store them on disk. These three-center integrals are computed only once because they do not depend on the single amplitudes. Moreover, in each iteration, the half-transformed three-center integrals $\hat{B}^{P}_{\mu\underline{i}}$ are computed and stored on disk in order to alleviate the memory limitation problem.

We introduce an optimized batching scheme based on a Lagrangian formulation, where the optimal number of batches is computed by minimizing the batching overhead.[58]

- As proposed in the optimal batching scheme by Drontschenko *et al.*[58] for the response function in RPA, we compute the intermediates N^{QP}_{τ} (and n^{P}_{τ}) as shown

```
1: for aux-batch-1 do
2:   for P ∈ aux-batch-1 do
3:     read B^P_μν ∀μ, ν
4:     B^Q_iμ = L_μi B^P_μν ∀i, μ;
5:     B̂^P_μj = B^P_μν (L_νj + Q_νν' S_ν'σ t_σλ S_λν'' L_ν''j) ∀j, μ
6:     write B^Q_iμ and B̂^P_μj on disk
7:   end for
8: end for
9: for aux-batch-1 do
10:   for AO-batch do
11:     for P ∈ aux-batch-1 do
12:       read B̂^P_μ'j ∀μ', j
13:       for all τ do
14:         τB̂^P_μi = Q̂^τ_μμ' B̂^P_μ'j (L_σj S_σλ P^τ_λi) ∀i, μ ∈ AO-batch;
15:       end for
16:     end for
17:     for all τ do
18:       for P ∈ aux-batch-1 do
19:         n^P_τ += τB̂^P_μi F̂_μi ∀i, μ ∈ AO-batch
20:       end for
21:     end for
22:     for aux-batch-2 do
23:       for Q ∈ aux-batch-2 do
24:         read B^Q_iμ ∀i, μ ∈ AO-batch;
25:       end for
26:       for all τ do
27:         for i ∈ rank_occ do
28:           N^QP_τ += B^Q_μi τB̂^P_μi ∀μ ∈ AO-batch and P, Q ∈ aux-batch-1/-2
29:         end for
30:       end for
31:     end for
32:   end for
33: end for
34: Ñ^QP_τ = J^QR_ω N^RS_τ J^SP_ω ∀τ
35: ñ^P_τ = n^R_τ J^RP_ω ∀τ
```

FIG. 2. Algorithm for the calculation of $\tilde{N}^{QP}_{\tau}$ and $\tilde{n}^{P}_{\tau}$ intermediates within the ω-SOS-CDD-RI-CC2 implementation.

in Fig. 2 by reading $\hat{B}^P_{\mu\underline{i}}$ (line 12) and $B^Q_{\underline{i}\mu}$ (line 24) by batches of auxiliary and basis functions indices, at the cost of a batching overhead proportional to the number of auxiliary and basis functions batches b_{aux} and b_{AO}, respectively. In the optimal batching, b_{aux} and b_{AO} are equal. Once the intermediates are formed, we multiply them with $\mathbf{J}_\omega$.

- The intermediates $\hat{Y}^Q_{\mu\underline{i}}$ and $\Omega^I_{\mu\underline{i}}$ are computed by batching over auxiliary and occupied indices. The three-center integrals $\hat{B}^P_{\mu\underline{j}}$ are read with an overhead proportional to the number of occupied batches b_{occ}, while $\hat{Y}^Q_{\mu\underline{i}}$ is read b_{aux} times (see Fig. 3). Notice that b_{aux} is generally smaller than b_{occ} in order to minimize the I/O effort. In addition, lines 1, 12, and 13 are optional and limited to cases with minor sparsity in the three-center integrals matrices. At the end, the contribution to the vector function is scaled by $-c_{os}$.
- The G and H contributions to the vector function are computed in batches of auxiliary indices. In this case, the three-center integrals $B^Q_{\underline{k}\underline{i}}$ and $B^Q_{\mu\nu}$ are not read redundantly, as reported in Fig. 4. At the end, the contributions to the vector function are scaled by $-c_{os}$.

1: **for** aux-batch-1 **do**
2: **for** occ-batch **do**
3: **for all** P ∈ aux-batch-1 **do**
4: read $\hat{B}^P_{\mu'\underline{j}}\ \forall\mu', \underline{j}$
5: **for all** τ **do**
6: ${}^{\tau}\hat{B}^P_{\mu\underline{i}} = \hat{Q}^{\tau}_{\mu\mu'}\hat{B}^P_{\mu'\underline{j}}(L_{\sigma\underline{j}}S_{\sigma\lambda}P^{\tau}_{\lambda\underline{i}})\forall\mu, \underline{i} \in$ occ-batch;
7: **end for**
8: **end for**
9: **for all** τ **do**
10: $\Omega^I_{\mu\underline{i}} += {}^{\tau}\hat{B}^P_{\mu\underline{i}}n^P_{\tau}\forall\mu, \underline{i} \in$ occ-batch, $\forall P \in$ aux-batch-1
11: **end for**
12: **for** aux-batch-2 **do**
13: read $\hat{Y}^Q_{\mu\underline{i}}\ \forall Q \in$ aux-batch-2, $\forall \underline{i} \in$ occ-batch
14: **for all** τ **do**
15: **for all** $\underline{i} \in$ occ-batch **do**
16: $\hat{Y}^Q_{\mu\underline{i}} += {}^{\tau}\hat{B}^P_{\mu\underline{i}}\tilde{N}^{QP}_{\tau}\forall P, Q \in$ aux-batch-1 and -2
17: **end for**
18: **end for**
19: write $\hat{Y}^Q_{\mu\underline{i}}\ \forall Q \in$ aux-batch-2, $\forall\mu, \underline{i} \in$ occ-batch
20: **end for**
21: **end for**
22: **end for**
23: scale $\Omega^I_{\mu\underline{i}}$ by $-c_{os}$

FIG. 3. Algorithm for the calculation of $\hat{Y}^Q_{\mu\underline{i}}$ and $\Omega^I_{\mu\underline{i}}$ intermediates within the ω-SOS-CDD-RI-CC2 implementation.

1: **for** aux-batch **do**
2: **for** Q ∈ aux-batch **do**
3: read $\hat{B}^Q_{\underline{k}\underline{i}}$ and $\hat{Y}^Q_{\mu\underline{k}}\ \forall\underline{k}, \underline{i}, \mu$
4: **end for**
5: **for** Q ∈ aux-batch **do**
6: $\Omega^H_{\mu\underline{i}} += \hat{Y}^Q_{\mu\underline{k}}\hat{B}^Q_{\underline{k}\underline{i}}\forall\mu, \underline{i}$
7: **end for**
8: **for** Q ∈ aux-batch **do**
9: read $B^Q_{\mu\nu}\forall\mu, \nu$
10: $\bar{\Omega}^G_{\mu\underline{i}} += B^Q_{\mu\nu}\hat{Y}^Q_{\nu\underline{i}}\forall\mu, \underline{i}$
11: **end for**
12: **end for**
13: $\Omega^G_{\mu\underline{i}} = \hat{Q}_{\mu\mu'}\bar{\Omega}^G_{\mu'\underline{i}}$
14: scale $\Omega^G_{\mu\underline{i}}$ and $\Omega^H_{\mu\underline{i}}$ by $-c_{os}$

FIG. 4. Algorithm for the calculation of $\Omega^G_{\mu\underline{i}}$ and $\Omega^H_{\mu\underline{i}}$ intermediates within the ω-SOS-CDD-RI-CC2 implementation.

As can be seen in Figs. 2 and 3, the minimal overhead is obtained if there is only one τ-batch containing all Laplace quadrature points.[58] Finally, in order to increase the efficiency, the three-center integrals are read and simultaneously transformed in parallel using all the available threads (i.e., line 11 in Fig. 2 and line 3 in Fig. 3).

III. COMPUTATIONAL DETAILS

Our ω-SOS-CDD-RI-CC2 method as well as the MO-SOS-RI-CC2 equations by Winter and Hättig[30] were implemented in the FermiONs++ program.[51–53] We checked our MO-SOS-RI-CC2 implementation against the implementation in Turbomole7.3[59] to verify comparable performance and accuracy (error in energy in the range of 10^{-4}–10^{-5} a.u. and very similar computational times). The underlying Hartree–Fock calculations have been converged to a maximum element of the error matrix in the direct inversion in the iterative subspace (DIIS) procedure below 10^{-7}. We employed the RI-approximated integrals by Kussmann *et al.*[60] for the evaluation of the Coulomb and the $\mathcal{O}(N)$ semi-numerical sn-LinK method by Laqua *et al.*[61,62] to compute the exchange integrals of the Fock matrix.

Furthermore, our CC2 model does not make use of any explicit integral screening. The reduction of the scaling and the consequent performance improvement are based on the use of efficient sparse matrix algebra in the steps involving the three-center integrals. The present implementation exploits block-sparse (BS) matrices, which divide the matrices in smaller blocks, whose maximum size is 96 × 96. The screening is twofold: First, we employ a sparsity criterion (ϑ_a) that screens the matrices upon allocation with a default threshold $\vartheta_a = 10^{-7}$. This means that every block with a

L2-norm lower than ϑ_a is discarded. Consequently, both memory and disk space requirements are reduced. Second, the threshold ϑ_m is used to improve the performance of matrix–matrix multiplications. In fact, if the product of the L2-norms of two multiplied matrix-blocks is lower than a given threshold, that multiplication step is not performed. The default value is $\vartheta_m = 10^{-9}$. Additional information about our BS matrices and the algorithm for the matrix–matrix multiplication are provided in the supplementary material.

The optimization of the singles cluster amplitudes is carried out via the DIIS procedure, which terminates when the L2-norm of the singles vector function is lower than 10^{-5}. As atomic basis sets, the def2-SVP and the def2-TZVP basis sets[63,64] are employed. For the resolution of identity used to approximate the four-center integrals, the corresponding auxiliary basis sets[9,45,65] are used. If nothing else is indicated, we use optimized minimax grids with seven quadrature points for the Laplace expansion. In addition, we set $\omega = 0.1$ a.u. for the attenuated RI-metric, which has been found sufficient for the metric[43] to start being local while there is no significant loss in accuracy. All calculations are performed using multi-core computing nodes and an OpenMP parallelized code. We used a computing node with one Dual AMD EPYC 7302 32-Core 3.0 GHz CPUs, 1 TB of RAM, and 5.5 TB of disk space. All runtimes given are wall times, not CPU times.

IV. RESULTS

A. Accuracy

We performed benchmark calculations on the S22 and L7 test sets of complexes.[66,67] The interaction energies obtained with the ω-SOS-CDD-RI-CC2 method are compared to a MO-SOS-RI-CC2 reference and the errors are summarized in Table III. The use of sparse algebra yields results as accurate as standard dense algebra for both test sets since the sparsity of the density matrices associated with these systems is low. The error introduced by the attenuation factor is negligible for the S22 set, with MAE and MAX equal to 0.002 and 0.007 kcal mol^{-1}, respectively, and slightly increases for the larger systems in the L7 set. In fact, the error for L7 samples is 0.02 and 0.03 kcal mol^{-1} in MAE and RMSD, respectively, and 0.06 kcal mol^{-1} in MAX. For the C3A, C3GC (and the monomers A, GC, and C3) systems, using the RI-approximation to compute the Coulomb contribution to the Fock matrix caused numerical instability during both HF and CC2 iterative procedures. Specifically, although HF

TABLE III. Root mean square deviation (RMSD), mean absolute error (MAE), and maximum error (MAX) for interaction energies computed with ω-SOS-CDD-RI-CC2 in the def2-TZVP basis compared to MO-SOS-RI-CC2 results for the S22[66] and L7[67] test sets with different RI-attenuation factors ω, and both sparse/dense linear algebra.

	$\vartheta_a = 10^{-7}$, $\vartheta_m = 10^{-9}$		$\vartheta_a = 0.0$, $\vartheta_m = 0.0$	
	$\omega = 0.0$	$\omega = 0.1$	$\omega = 0.0$	$\omega = 0.1$
	S22			
RMSD (μH)	0.3	5.1	0.3	5.0
MAE (μH)	0.3	3.9	0.3	3.8
MAX (μH)	0.8	11.3	0.8	11.3
	L7			
RMSD (μH)	0.7	49.8	0.6	50.0
MAE (μH)	0.5	36.9	0.5	37.0
MAX (μH)	1.5	96.0	1.2	96.3

TABLE IV. Absolute energy error of ω-SOS-CDD-RI-CC2 with respect to MO-SOS-RI-CC2 results for different attenuation factors ω, as well as for sparse and dense linear algebra. The number of basis functions is given for each system. The structure files of the selected systems are available for download from our website.[68]

		Error (μH)		Error (μH)	
	No. of bf	$\vartheta_a = 10^{-7}$, $\vartheta_m = 10^{-9}$		$\vartheta_a = 0.0$, $\vartheta_m = 0.0$	
Sample	def2-TZVP	$\omega = 0.0$	$\omega = 0.1$	$\omega = 0.0$	$\omega = 0.1$
$C_{40}H_{82}$	1732	0.02	23.00	0.03	7.90
$C_{80}H_{162}$	3452	0.50	48.20	0.50	15.30
$C_{100}H_{202}$	4312	0.71	62.60	0.74	18.42
$C_{160}H_{322}$	6892	1.06	108.00	1.36	28.90
AT01	1247	0.57	7.25	0.60	7.30
AT02	2680	0.80	17.50	0.70	16.90
Diamond 102	1662	0.004	28.00	0.03	28.01
Water 68	2924	0.14	19.30	0.14	19.30
Angiotensin	2751	0.05	31.60	0.10	30.50
Angiotensin deprotonated	2739	0.40	51.50	0.50	50.10
Angiotensin zwitterion	2751	0.50	40.00	0.50	39.00
K2 vitamine (90°)	1263	0.60	0.50	0.57	0.56
K2 vitamine (180°)	1263	0.50	1.40	0.50	1.50
CNT (C_{20})	680	1.19	3.77	1.21	3.78

calculations converged using tighter thresholds and larger auxiliary basis set for the three-center integrals, the CC2 calculations did not reach convergence for monomers or dimers if the RI-approximation was used in Eq. (35). Moreover, even using the RI-approximation only for HF calculations, and so avoiding it in Eq. (35), the CC2 calculations did not converge for monomers or dimers.

Therefore, for the mentioned systems, we did not employ the RI-approximation during neither HF nor CC2, since the computation of the Coulomb term with J-engine is not a computational bottleneck regardless. In addition, we used ten Laplace quadrature points for the C3 monomer for the same reason. In order to further investigate the behavior of ω-SOS-CDD-RI-CC2, we computed the absolute energies for random large systems from our own benchmark set[68] (see Table IV). In contrast to the observations for the S22 and the L7 test sets, the use of sparse linear algebra slightly decreases the accuracy of the obtained results. Thus, the accuracy of ω-SOS-CDD-RI-CC2 with both dense and sparse algebra is compared in order to display the influence of the sparse linear algebra screening and the RI-metric attenuation factor ω.

Again, it is clear from Table IV that the smaller systems are not affected by sparse algebra and yield results similar to the dense algebra implementation, as for the L7 and S22 sets. Moreover, the combined use of sparse algebra and the moderately attenuated Coulomb metric ($\omega = 0.1$) reduces the accuracy by a maximum of 0.1 kcal/mol. Therefore, the default screening thresholds ensure accurate results with both metrics; hence, they will be used in all further calculations. Of course, larger molecules are more sensitive to the choice of the RI-metric and are, in general, more sparse. For instance, the error introduced by either sparse linear algebra or the attenuation factor increases with the system size for the linear alkanes. Nonetheless, the accuracy of ω-SOS-CDD-RI-CC2 is under complete control using the two screening parameters ϑ_a and ϑ_m, and the attenuation factor ω.

B. Scaling behavior: Linear alkanes

The sparsity of the one-electron densities is closely related to the HOMO–LUMO gap of molecular systems.[69] Especially, the asymptotic linear scaling behavior holds only for systems with a nonvanishing HOMO–LUMO gap.[69,70] Accordingly, we investigated the computational and storage scaling of ω-SOS-CDD-RI-CC2 with $\omega = 0$ and $\omega = 0.1$ (with $\frac{1}{r_{12}}$ and $\frac{\mathrm{erfc}(\omega r_{12})}{r_{12}}$ operators for the RI-approximation, respectively) on electronically local systems such as linear alkanes. Of course, they represent optimal systems for calculations in a local basis (as shown by Fig. 1), but the same behavior is transferred to three-dimensional systems that are large enough. We carried out the analysis of the computational scaling, taking into account the number of floating-point operations (FLOPS) during the first iteration (with $t_{ai} \neq 0$). The results obtained using the def2-TZVP basis set are summarized in Fig. 5. As can be seen, the scaling exponents meet the expectations for both standard and ω-Coulomb ($\omega = 0.1$) metrics with values equal to ~2.8 and ~1.8 for the largest system. In the asymptotic limit, the computational scaling is cubic for $\omega = 0$. With a moderate attenuation factor ($\omega = 0.1$), the asymptotic scaling of almost all steps is reduced to linear. However, the number of FLOPS scales sub-quadratically $\mathcal{O}(N^{1.9})$ for the time-determining calculation of the $\hat{Y}^{Q}_{\underline{\mu i}}$ intermediate [Eq. (23)]. This

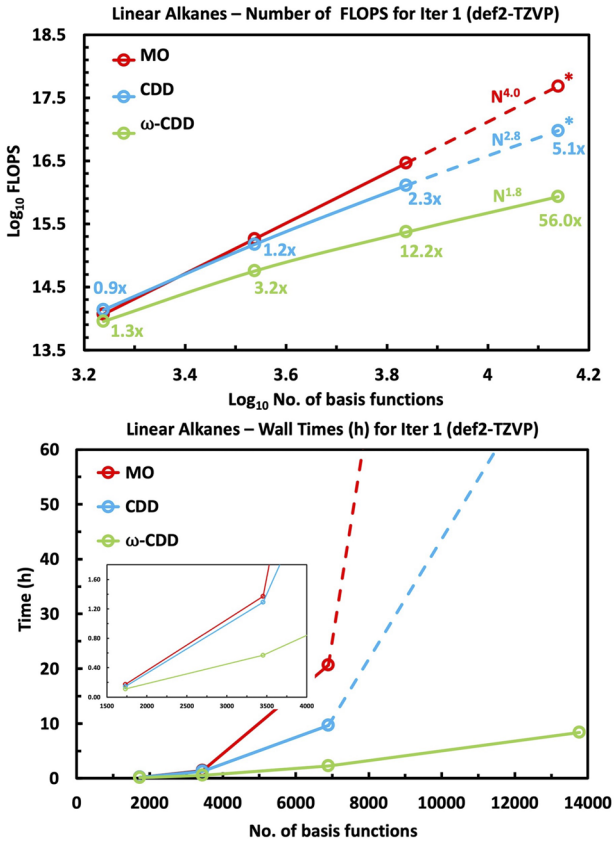

FIG. 5. Plots of FLOPS (top) and wall times (bottom) against number of basis functions showing the computational complexity of the MO and ω-SOS-CDD-RI-CC2 formulations ($\omega = 0$: "CDD" and $\omega = 0.1$: "ω-CDD") for linear alkanes in the def2-TZVP basis. In the top plot, speedups with respect to MO calculations are given. We used ϑ_a and ϑ_m equal to 10^{-7} and 10^{-9}, respectively. Top: Log-log plot. Bottom: Linear plot. The dashed lines and asterisks indicate that the points have been extrapolated.

is due to the multiplications of N_τ^{QP} matrices with $\mathbf{J}_\omega$ [Eq. (25)], which is not sparse. Notice that there are other steps with cubic or quadratic scaling in the algorithm (see Table II). Among these, the quadratic calculation of all $B_{\mu\nu}$ integrals is performed only once at the beginning and does not affect the overall efficiency (see Fig. 6). Some cubic and quadratic steps are repeated in each iteration (i.e., the formation of the Fock matrix and pseudo-densities). Nonetheless, it can be seen in Fig. 6 that these nonlinear scaling steps do not affect the overall efficiency of our method because the time demands are negligible if compared to steady times of one iteration or the entire CC2 calculation. The same behavior appears in the disk space requirements that are summarized in Table V. Since the number of basis functions is close to the number of virtual orbitals, the disk space demands of ω-SOS-CDD-RI-CC2 are formally similar to MO-SOS-RI-CC2 for smaller systems. Of course, as soon as the systems become large enough, the use of sparse matrices reduces the storage requirements along with the CPU costs. Indeed, the space needed for the matrices of the half-transformed

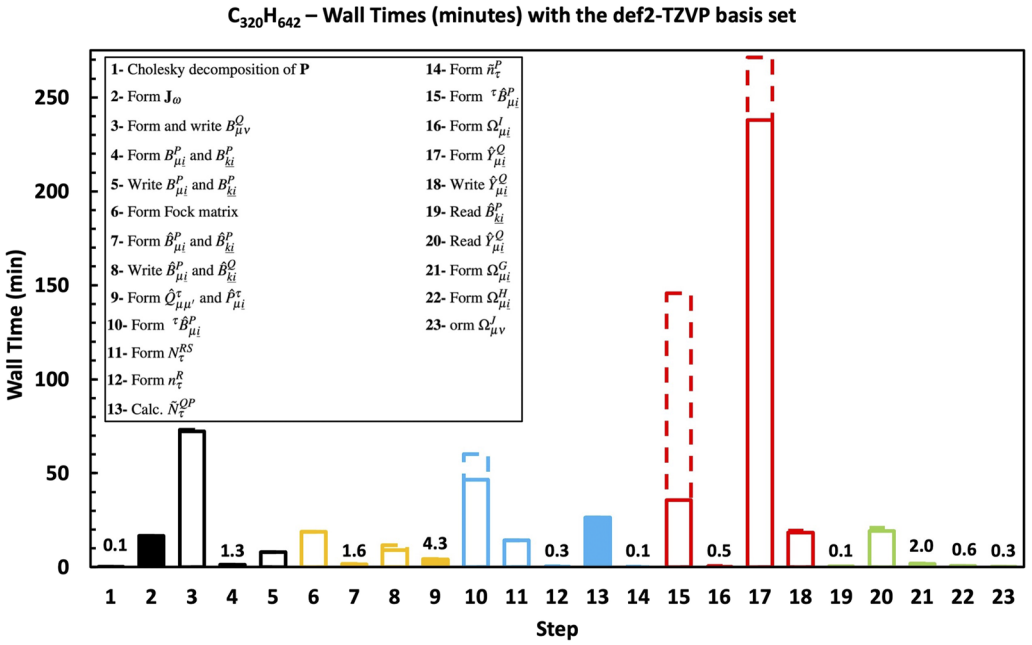

FIG. 6. Plot of wall times (minutes) for each step of ω-SOS-CDD-RI-CC2 ($\omega = 0.1$) for the linear alkane $C_{320}H_{642}$. Fully colored rectangles indicate the use of dense matrices for that specific step. In black (1–5): Steps performed only once at the beginning. In orange (6–9): Steps performed in each iteration as preparation of the following time-determining calculations. In light blue (10–14): Time-determining steps involved in Fig. 2 where Step 10 refers to lines 11–16. In red (15–18): Time-determining steps involved in Fig. 3 where Step 15 refers to lines 3–8. In green (19–23): Steps involved in Fig. 4. The dashed lines indicate the timings obtained when we reduce the available memory from ~900 to ~450 GB.

TABLE V. Disk space demands (GB) for MO-SOS-RI-CC2 ("MO") and ω-SOS-CDD-RI-CC2 with $\omega = 0$ ("CDD") and $\omega = 0.1$ ("ω-CDD"). We do not store the AO three-center integrals in the MO implementation. The $*$ highlights when sparse matrices are not used to store them on disk. The sparsity thresholds ϑ_a and ϑ_m are equal to 10^{-7} and 10^{-9}, respectively.

		$B^P_{\mu\nu}$ (GB)		$\hat{B}^P_{ai}/\hat{B}^P_{\mu\bar{i}}$ (GB)			$\hat{Y}^Q_{ai}/\hat{Y}^Q_{\mu\bar{i}}$ (GB)		
Sample	No. of bf def2-SVP	CDD	ω-CDD	MO	CDD	ω-CDD	MO	CDD	ω-CDD
$C_{40}H_{82}$	970	2.5	*2.5	2.3	2.6	1.7	2.2	2.7	2.7
$C_{80}H_{162}$	1930	10.0	7.2	17.6	16.0	6.3	17.6	17.5	17.2
$C_{160}C_{322}$	3850	40.2	15.0	140.2	68.5	15.8	140.2	80.9	69.2

		$B^P_{\mu\nu}$ (GB)		$\hat{B}^P_{ai}/\hat{B}^P_{\mu\bar{i}}$ (GB)			$\hat{Y}^Q_{ai}/\hat{Y}^Q_{\mu\bar{i}}$ (GB)		
Sample	No. of bf def2-TZVP	CDD	ω-CDD	MO	CDD	ω-CDD	MO	CDD	ω-CDD
$C_{40}H_{82}$	1732	10.6	*10.6	6.1	6.4	4.0	6.1	6.7	6.7
$C_{80}H_{162}$	3452	44.5	25.0	47.8	42.7	16.8	47.8	52.7	52.7
$C_{160}C_{322}$	6892	176.3	52.0	380.6	220.0	54.4	380.6	378.0	338.3

three-center integrals ($\hat{B}^P_{\mu\bar{i}}$) is significantly decreased and scales linearly in the asymptotic limit (with $\omega = 0.1$). On the other hand, the disk space requirements for the $\hat{Y}^Q_{\mu\bar{i}}$ matrices are only reduced for the largest system because of their decreased sparsity and scale as $\mathcal{O}(N^2)$. The symmetric AO three-center integrals are treated differently. For MO-SOS-RI-CC2, these integrals are computed and transformed in each iteration. Thus, they are not stored on disk. For ω-SOS-CDD-RI-CC2 with $\omega = 0.0$, we store only the upper triangles that require $\frac{1}{2}N_{aux}N_{basis}(N_{basis}+1)$ of disk space. On the other hand, for $\omega = 0.1$, we store the significant blocks within the upper triangle of the BS matrices, showing an asymptotic linear scaling $\mathcal{O}(N)$. The integral-direct transformation of the AO three-center integrals is possible also for ω-SOS-CDD-RI-CC2, avoiding the storage of this quantity.

C. Timings

1. Linear alkanes

The use of sparse linear algebra reduces the number of FLOPS carried out in one iteration and considerable runtime speedups over MO-SOS-RI-CC2 are expected when our ω-SOS-CDD-RI-CC2 is used. We performed the calculations in the def2-TZVP basis and the results are summarized in Table VI and Fig. 5. Moreover, all calculations were performed with the same number of batches. The runtime speedups are always smaller than the speedups obtained when comparing FLOPS, due to a runtime overhead of ~1.6 associated with the use of our block-matrices. Nevertheless, the crossover with the MO implementation is at ~50 carbon atoms, as one can see in Fig. 5. Indeed, our ω-SOS-CDD-RI-CC2 method ($\omega = 0.1$) is already twice as fast for $C_{80}H_{162}$. Doubling the size, our implementation is ~9 times faster than the MO formulation. Whether or not the runtime speedups meet the trend in the FLOPS speedups critically depends on the number of batches (b_{ao} and b_{occ}) in Figs. 2 and 3. In fact, although efficient, in general, the formation of the Laplace point-dependent three-center integrals (line 12, Fig. 2, and line 3, Fig. 3) in ω-SOS-CDD-RI-CC2 is negatively affected by the batching overhead. However, since $\hat{B}^{P}_{\mu\tilde{j}}$ is sparse, this downside is mitigated until b_{ao} and b_{occ} get large, i.e., when the memory requirements exceed the available memory of the computing node by several times. The dashed lines in Fig. 6 display such a behavior for the linear alkane $C_{320}H_{642}$, where the computation time for Step 15 is quadrupled when the available memory is halved. The AO reformulation is ~37 times faster with $\omega = 0.1$ (see Table VI) and it outperforms the MO implementation even if the number of batches is increased. Furthermore, we want to stress that one can decrease the batching overhead (and increase the runtime speedups) either by using a computing node with a larger memory or by performing CC2 calculations on multiple nodes, distributing both CPU and I/O efforts. However, we did not exploit the second solution in the present paper.

TABLE VI. Wall times (h) for the first iteration ($t_{ai} \neq 0$) of MO and ω-SOS-CDD-RI-CC2 formulations ($\omega = 0$: "CDD" and $\omega = 0.1$: "ω-CDD") for linear alkanes in the def2-TZVP basis. We employ sparsity thresholds ϑ_a and ϑ_m equal to 10^{-7} and 10^{-9}, respectively. Values marked with an asterisk (*) are extrapolated conservatively.

Sample	No. of bf def2-TZVP	MO Time (h)	CDD		ω-CDD	
			Time (h)	Speedup	Time (h)	Speedup
$C_{40}H_{82}$	1 732	0.17	0.15	×1.2	0.11	×1.6
$C_{80}H_{162}$	3 452	1.37	1.29	×1.1	0.57	×2.2
$C_{160}C_{322}$	6 892	20.63	9.62	×2.1	2.27	×9.1
$C_{320}H_{642}$	13 772	*309.00	*85.00	×3.6	8.38	×36.9

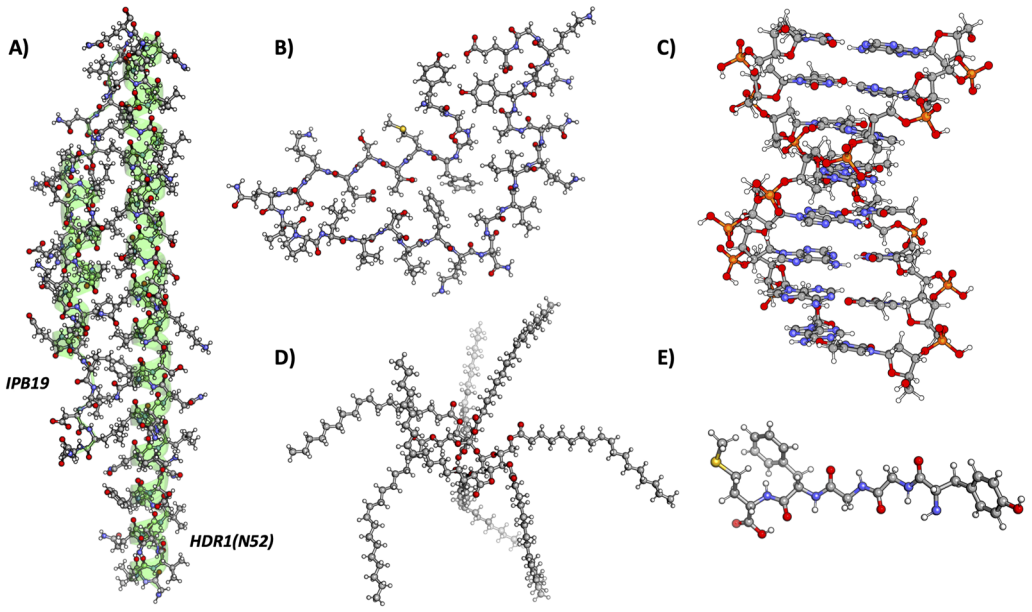

FIG. 7. Test set for the performance of the ω-SOS-CDD-RI-CC2 model ($\omega = 0.1$): (a) IPB19/N52 complex[71] (its alpha-helix structure is highlighted in green), (b) beta-endorphin,[72] (c) AT08 pairs,[68] (d) olestra,[73] (e) metenkephalin.[34] We employed MolProbity[74] with default settings in order to add the missing hydrogens to the IPB19/N52 complex.

TABLE VII. Runtime speedups for the first iteration of ω-SOS-CDD-RI-CC2 ($\omega = 0.1$) against MO-SOS-RI-CC2 in both def2-SVP and def2-TZVP bases. We employ sparsity thresholds ϑ_a and ϑ_m equal to 10^{-7} and 10^{-9}, respectively.

Sample	No. of atoms	No. of bf def2-SVP	MO-SOS-RI-CC2 Time (h)	ω-SOS-CDD-RI-CC2	
				Time (h)	Speed up
HDR1(N52)	746	7069	66.76	11.93	×5.6
DNA8	524	5574	29.25	18.42	×1.6
Beta-endorphin	495	4675	14.07	6.55	×2.1
Olestra	453	3840	5.27	3.94	×1.3
IPB19	441	4149	8.77	3.48	×2.5
Metenkephalin	75	739	0.02	0.03	×0.7

Sample	No. of atoms	No. of bf def2-TZVP	MO-SOS-RI-CC2 Time (h)	ω-SOS-CDD-RI-CC2	
				Time (h)	Speed up
Beta-endorphin	495	9076	61.32	46.24	×1.3
Olestra	453	7093	23.68	18.45	×1.3
IPB19	441	8046	40.27	26.04	×1.5
Metenkephalin	75	1456	0.08	0.09	×0.8

2. Three-dimensional systems

The ω-SOS-CDD-RI-CC2 method has proven to be efficient if applied to optimal systems such as linear alkanes. In fact, the introduction of the Cholesky-decomposed density matrices resulted in an early crossover with the MO-SOS-RI-CC2 model, as shown in Fig. 5. A reduction of the number of FLOPS and a consequent runtime speedup are also obtained when ω-SOS-CDD-RI-CC2 is applied to real-life organic systems, which do not always display sparse density matrices. We used as test set six different systems illustrated in Fig. 7, but it was not possible to perform calculations in the def2-TZVP basis for some systems due to disk space limitations. Table VII shows the wall times and speedups (with $\omega = 0.1$) for the first iteration in both def2-SVP and def2-TZVP basis sets. For HDR1(N52) in the def2-SVP basis, our ω-SOS-CDD-RI-CC2 provides a speedup of 5.6, so that one iteration is carried out in ~12 h instead of ~67 h. The speedups for the def2-TZVP basis set are lower due to the use of more diffuse functions. For instance, the ω-SOS-CDD-RI-CC2 speedups for the beta-endorphin are 2.1 and 1.3 with def2-SVP and def2-TZVP basis, respectively. In general, the ω-SOS-CDD-RI-CC2 model provides speedups that are expected to become larger for increasing system sizes due to the reduced scaling. On the other hand, ω-SOS-CDD-RI-CC2 timings are comparable to the MO-based implementation for the smaller systems (e.g., metenkephalin).

V. SUMMARY

We presented a reformulation of the SOS-RI-CC2 method in the AO basis that shows cubic scaling in the asymptotic limit. We further employed an attenuated Coulomb metric for the RI-approximation decreasing the scaling to sub-quadratic for $\omega = 0.1$. The Cholesky decomposition of the ground-state occupied density matrix provides local occupied molecular orbitals that allow for the reduction of the basis set scaling. Moreover, it leads to a reduced prefactor and an early crossover with the MO implementation. Our memory-efficient ω-SOS-CDD-RI-CC2 method is based on a minimal-overhead batching scheme and on efficient sparse linear algebra routines, providing complete control of the error via the ϑ_a and ϑ_m thresholds while significantly speeding up the calculations. Such control results in small errors as shown for calculations on the S22 and L7 test sets and a selection of systems from our own benchmark.[68] The performance of our reformulation has been assessed for both SVP and TZVP basis sets with three-dimensional systems of up to 700 atoms. The timings show that our method provides considerable advantages if there is enough sparsity to be exploited. On the other hand, ω-SOS-CDD-RI-CC2 timings are comparable to MO-SOS-RI-CC2 wall times for smaller systems, whose density matrices are not sparse.

The disk space demand will be further reduced by implementing an integral-direct algorithm, which avoids the storage of some three-dimensional tensors and will be subject of a future publication. In addition, increasing the runtime speedups may be possible by distributing the computational and I/O efforts among multiple nodes. Finally, we want to stress that the presented ω-SOS-CDD-RI-CC2 approach provides the basis for the AO reformulation of the SOS-RI-CC2 and ADC(2) equations for excited states energies. An implementation is currently in progress in our group and will be the subject of a forthcoming publication.

SUPPLEMENTARY MATERIAL

See the supplementary material for details about the reformulation of cluster equations in the AO basis, the operation of our block-sparse matrices, the scaling behavior, and our implementation of MO-SOS-RI-CC2.

ACKNOWLEDGMENTS

This project received funding from the European Union's Horizon 2020 research and innovation program under Marie Skłodowska-Curie Grant Agreement No 765739. C.O. further acknowledges financial support from the Max-Planck Fellowship Program at the MPI-FKF Stuttgart.

AUTHOR DECLARATIONS

Conflict of Interest

The authors have no conflicts to disclose.

Author Contributions

F. Sacchetta: Investigation (equal); Methodology (equal); Writing – original draft (equal). **D. Graf**: Conceptualization (equal); Investigation (equal); Writing – original draft (equal). **H. Laqua**: Conceptualization (equal); Methodology (equal); Writing – review & editing (equal). **M. A. Ambroise**: Conceptualization (equal); Investigation (equal). **J. Kussmann**: Conceptualization (equal); Investigation (equal); Methodology (equal); Writing – review & editing (equal). **A. Dreuw**: Conceptualization (equal); Supervision (equal); Writing – review & editing (equal). **C. Ochsenfeld**: Conceptualization (equal); Supervision (equal); Writing – review & editing (equal).

DATA AVAILABILITY

The data that support the findings of this study are available within the article and its supplementary material.

REFERENCES

[1] J. Čížek and J. Paldus, "Correlation problems in atomic and molecular systems III. Rederivation of the coupled-pair many-electron theory using the traditional quantum chemical methods," Int. J. Quantum Chem. **5**, 359–379 (1971).
[2] J. Čížek, "On the use of the cluster expansion and the technique of diagrams in calculations of correlation effects in atoms and molecules," Adv. Chem. Phys. **14** 35–89 (1969).
[3] R. J. Bartlett, "The coupled-cluster revolution," Mol. Phys. **108**, 2905–2920 (2010).
[4] T. D. Crawford and H. F. Schaefer, "An introduction to coupled cluster theory for computational chemists," Rev. Comput. Chem. **14**, 33–136 (2000).
[5] G. D. Purvis III and R. J. Bartlett, "A full coupled-cluster singles and doubles model: The inclusion of disconnected triples," J. Chem. Phys. **76**, 1910–1918 (1982).
[6] H. Koch, A. Sánchez de Merás, T. Helgaker, and O. Christiansen, "The integral-direct coupled cluster singles and doubles model," J. Chem. Phys. **104**, 4157–4165 (1996).
[7] O. Christiansen, H. Koch, and P. Jørgensen, "The second-order approximate coupled cluster singles and doubles model CC2," Chem. Phys. Lett. **243**, 409–418 (1995).
[8] Y. Jung, R. C. Lochan, A. D. Dutoi, and M. Head-Gordon, "Scaled opposite-spin second order Møller-Plesset correlation energy: An economical electronic structure method," J. Chem. Phys. **121**, 9793–9802 (2004).
[9] Y. Jung, Y. Shao, and M. Head-Gordon, "Fast evaluation of scaled opposite spin second-order Møller-Plesset correlation energies using auxiliary basis expansions and exploiting sparsity," J. Comput. Chem. **28**, 1953–1964 (2007).
[10] P. Pulay, "Localizability of dynamic electron correlation," Chem. Phys. Lett. **100**, 151–154 (1983).
[11] P. Pulay and S. Saebø, "Orbital-invariant formulation and second-order gradient evaluation in Møller-Plesset perturbation theory," Theor. Chim. Acta **69**, 357–368 (1986).
[12] S. Saebø and P. Pulay, "A low-scaling method for second order Møller-Plesset calculations," J. Chem. Phys. **115**, 3975–3983 (2001).
[13] H.-J. Werner, F. R. Manby, and P. J. Knowles, "Fast linear scaling second-order Møller-Plesset perturbation theory (MP2) using local and density fitting approximations," J. Chem. Phys. **118**, 8149–8160 (2003).
[14] S. A. Maurer, L. Clin, and C. Ochsenfeld, "Cholesky-decomposed density MP2 with density fitting: Accurate MP2 and double-hybrid DFT energies for large systems," J. Chem. Phys. **140**, 224112 (2014).
[15] P. Y. Ayala and G. E. Scuseria, "Linear scaling second-order Moller-Plesset theory in the atomic orbital basis for large molecular systems," J. Chem. Phys. **110**, 3660–3671 (1999).
[16] S. A. Maurer, D. S. Lambrecht, J. Kussmann, and C. Ochsenfeld, "Efficient distance-including integral screening in linear-scaling Moller-Plesset perturbation theory," J. Chem. Phys. **138**, 014101 (2013).
[17] S. Schweizer, B. Doser, and C. Ochsenfeld, "An atomic orbital-based reformulation of energy gradients in second-order Møller-Plesset perturbation theory," J. Chem. Phys. **128**, 154101 (2008).
[18] M. Glasbrenner, D. Graf, and C. Ochsenfeld, "Efficient reduced-scaling second-order Møller-Plesset perturbation theory with Cholesky-decomposed densities and an attenuated Coulomb metric," J. Chem. Theory Comput. **16**, 6856–6868 (2020).
[19] R. A. Kendall and H. A. Früchtl, "The impact of the resolution of the identity approximate integral method on modern *ab initio* algorithm development," Theor. Chem. Acc. **97**, 158–163 (1997).
[20] M. Feyereisen, G. Fitzgerald, and A. Komornicki, "Use of approximate integrals in *ab initio* theory. An application in MP2 energy calculations," Chem. Phys. Lett. **208**, 359–363 (1993).
[21] C. Hättig and F. Weigend, "CC2 excitation energy calculations on large molecules using the resolution of the identity approximation," J. Chem. Phys. **113**, 5154–5161 (2000).
[22] H. Koch, A. Sánchez de Merás, and T. B. Pedersen, "Reduced scaling in electronic structure calculations using Cholesky decompositions," J. Chem. Phys. **118**, 9481–9484 (2003).
[23] J. Boström, M. Pitoňák, F. Aquilante, P. Neogrády, T. B. Pedersen, and R. Lindh, "Coupled cluster and Møller–Plesset perturbation theory calculations of noncovalent intermolecular interactions using density fitting with auxiliary basis sets from Cholesky decompositions," J. Chem. Theory Comput. **8**, 1921–1928 (2012).
[24] P. Baudin, J. S. Marín, I. G. Cuesta, and A. M. J. Sánchez de Merás, "Calculation of excitation energies from the CC2 linear response theory using Cholesky decomposition," J. Chem. Phys. **140**, 104111 (2014).
[25] S. D. Folkestad, E. F. Kjønstad, L. Goletto, and H. Koch, "Multilevel CC2 and CCSD in reduced orbital spaces: Electronic excitations in large molecular systems," J. Chem. Theory Comput. **17**, 714–726 (2021).
[26] S. Grimme, "Improved second-order Møller-Plesset perturbation theory by separate scaling of parallel-and antiparallel-spin pair correlation energies," J. Chem. Phys. **118**, 9095–9102 (2003).
[27] M. Häser, "Møller-Plesset (MP2) perturbation theory for large molecules," Theor. Chim. Acta **87**, 147–173 (1993).
[28] J. Almlöf, "Elimination of energy denominators in Møller-Plesset perturbation theory by a Laplace transform approach," Chem. Phys. Lett. **181**, 319–320 (1991).
[29] M. Häser and J. Almlöf, "Laplace transform techniques in Møller-Plesset perturbation theory," J. Chem. Phys. **96**, 489–494 (1992).
[30] N. O. C. Winter and C. Hättig, "Scaled opposite-spin CC2 for ground and excited states with fourth order scaling computational costs," J. Chem. Phys. **134**, 184101 (2011).
[31] D. Kats, T. Korona, and M. Schütz, "Local CC2 electronic excitation energies for large molecules with density fitting," J. Chem. Phys. **125**, 104106 (2006).
[32] D. Kats and M. Schütz, "A multistate local coupled cluster CC2 response method based on the Laplace transform," J. Chem. Phys. **131**, 124117 (2009).
[33] K. Ledermüller and M. Schütz, "Local CC2 response method based on the Laplace transform: Analytic energy gradients for ground and excited states," J. Chem. Phys. **140**, 164113 (2014).

[34]P. Baudin and K. Kristensen, "LoFEx—A local framework for calculating excitation energies: Illustrations using RI-CC2 linear response theory," J. Chem. Phys. **144**, 224106 (2016).
[35]F. Neese, A. Hansen, and D. G. Liakos, "Efficient and accurate approximations to the local coupled cluster singles doubles method using a truncated pair natural orbital basis," J. Chem. Phys. **131**, 064103 (2009).
[36]F. Neese, F. Wennmohs, and A. Hansen, "Efficient and accurate local approximations to coupled-electron pair approaches: An attempt to revive the pair natural orbital method," J. Chem. Phys. **130**, 114108 (2009).
[37]B. Helmich and C. Hättig, "A pair natural orbital implementation of the coupled cluster model CC2 for excitation energies," J. Chem. Phys. **139**, 084114 (2013).
[38]F. Weigend and M. Häser, "RI-MP2: First derivatives and global consistency," Theor. Chem. Acc. **97**, 331–340 (1997).
[39]R. C. Lochan, Y. Shao, and M. Head-Gordon, "Quartic-scaling analytical energy gradient of scaled opposite-spin second-order Møller- Plesset perturbation theory," J. Chem. Theory Comput. **3**, 988–1003 (2007).
[40]G. E. Scuseria and P. Y. Ayala, "Linear scaling coupled cluster and perturbation theories in the atomic orbital basis," J. Chem. Phys. **111**, 8330–8343 (1999).
[41]M. Beer and C. Ochsenfeld, "Efficient linear-scaling calculation of response properties: Density matrix-based Laplace-transformed coupled-perturbed self-consistent field theory," 2008.
[42]M. Beuerle, D. Graf, H. F. Schurkus, and C. Ochsenfeld, "Efficient calculation of beyond RPA correlation energies in the dielectric matrix formalism," J. Chem. Phys. **148**, 204104 (2018).
[43]A. Luenser, H. F. Schurkus, and C. Ochsenfeld, "Vanishing-overhead linear-scaling random phase approximation by Cholesky decomposition and an attenuated Coulomb-metric," J. Chem. Theory Comput. **13**, 1647–1655 (2017).
[44]D. Graf, M. Beuerle, and C. Ochsenfeld, "Low-scaling self-consistent minimization of a density matrix based random phase approximation method in the atomic orbital space," J. Chem. Theory Comput. **15**, 4468–4477 (2019).
[45]Y. Jung, A. Sodt, P. M. W. Gill, and M. Head-Gordon, "Auxiliary basis expansions for large-scale electronic structure calculations," Proc. Natl. Acad. Sci. U. S. A. **102**, 6692–6697 (2005).
[46]T. D. Crawford, A. Kumar, A. P. Bazanté, and R. Di Remigio, "Reduced-scaling coupled cluster response theory: Challenges and opportunities," Wiley Interdiscip. Rev.: Comput. Mol. Sci. **9**, e1406 (2019).
[47]R. J. Bartlett and G. D. Purvis, "Many-body perturbation theory, coupled-pair many-electron theory, and the importance of quadruple excitations for the correlation problem," Int. J. Quantum Chem. **14**, 561–581 (1978).
[48]P. Pulay, "Improved SCF convergence acceleration," J. Comput. Chem. **3**, 556–560 (1982).
[49]A. Takatsuka, S. Ten-No, and W. Hackbusch, "Minimax approximation for the decomposition of energy denominators in Laplace-transformed Møller-Plesset perturbation theories," J. Chem. Phys. **129**, 044112 (2008).
[50]B. Helmich-Paris and L. Visscher, "Improvements on the minimax algorithm for the Laplace transformation of orbital energy denominators," J. Comput. Phys. **321**, 927–931 (2016).
[51]J. Kussmann and C. Ochsenfeld, "Pre-selective screening for matrix elements in linear-scaling exact exchange calculations," J. Chem. Phys. **138**, 134114 (2013).
[52]J. Kussmann and C. Ochsenfeld, "Preselective screening for linear-scaling exact exchange-gradient calculations for graphics processing units and general strong-scaling massively parallel calculations," J. Chem. Theory Comput. **11**, 918–922 (2015).
[53]J. Kussmann and C. Ochsenfeld, "Hybrid CPU/GPu integral engine for strong-scaling *ab initio* methods," J. Chem. Theory Comput. **13**, 3153–3159 (2017).
[54]N. J. Higham, "Cholesky factorization," Wiley Interdiscip. Rev.: Comput. Stat. **1**, 251–254 (2009).
[55]H. Harbrecht, M. Peters, and R. Schneider, "On the low-rank approximation by the pivoted Cholesky decomposition," Appl. Numer. Math. **62**, 428–440 (2012).
[56]S. Schweizer, J. Kussmann, B. Doser, and C. Ochsenfeld, "Linear-scaling Cholesky decomposition," J. Comput. Chem. **29**, 1004–1010 (2008).
[57]F. Aquilante, T. Bondo Pedersen, A. Sánchez de Merás, and H. Koch, "Fast noniterative orbital localization for large molecules," J. Chem. Phys. **125**, 174101 (2006).
[58]V. Drontschenko, D. Graf, H. Laqua, and C. Ochsenfeld, "Lagrangian-based minimal-overhead batching scheme for the efficient integral-direct evaluation of the RPA correlation energy," J. Chem. Theory Comput. **17**, 5623–5634 (2021).
[59]V. Turbomole, 7.3, TURBOMOLE GmbH 2018, TURBOMOLE is a development of University of Karlsruhe and Forschungszentrum Karlsruhe 2007, 1989.
[60]J. Kussmann, H. Laqua, and C. Ochsenfeld, "Highly efficient resolution-of-identity density functional theory calculations on central and graphics processing units," J. Chem. Theory Comput. **17**, 1512–1521 (2021).
[61]H. Laqua, T. H. Thompson, J. Kussmann, and C. Ochsenfeld, "Highly efficient, linear-scaling seminumerical exact-exchange method for graphic processing units," J. Chem. Theory Comput. **16**, 1456–1468 (2020).
[62]H. Laqua, J. Kussmann, and C. Ochsenfeld, "Accelerating seminumerical Fock-exchange calculations using mixed single-and double-precision arithmethic," J. Chem. Phys. **154**, 214116 (2021).
[63]F. Weigend, F. Furche, and R. Ahlrichs, "Gaussian basis sets of quadruple zeta valence quality for atoms H–Kr," J. Chem. Phys. **119**, 12753–12762 (2003).
[64]F. Weigend and R. Ahlrichs, "Balanced basis sets of split valence, triple zeta valence and quadruple zeta valence quality for H to Rn: Design and assessment of accuracy," Phys. Chem. Chem. Phys. **7**, 3297–3305 (2005).
[65]F. Weigend, M. Häser, H. Patzelt, and R. Ahlrichs, "RI-MP2: Optimized auxiliary basis sets and demonstration of efficiency," Chem. Phys. Lett. **294**, 143–152 (1998).
[66]P. Jurečka, J. Šponer, J. Černý, and P. Hobza, "Benchmark database of accurate (MP2 and CCSD (T) complete basis set limit) interaction energies of small model complexes, DNA base pairs, and amino acid pairs," Phys. Chem. Chem. Phys. **8**, 1985–1993 (2006).
[67]R. Sedlak, T. Janowski, M. Pitoňák, J. Řezáč, P. Pulay, and P. Hobza, "Accuracy of quantum chemical methods for large noncovalent complexes," J. Chem. Theory Comput. **9**, 3364–3374 (2013).
[68]Structures available online from http://www.cup.lmu.de/pc/ochsenfeld/.
[69]P. E. Maslen, C. Ochsenfeld, C. A. White, M. S. Lee, and M. Head-Gordon, "Locality and sparsity of *ab initio* one-particle density matrices and localized orbitals," J. Phys. Chem. A **102**, 2215–2222 (1998).
[70]C. Ochsenfeld, J. Kussmann, and D. S. Lambrecht, "Linear-scaling methods in quantum chemistry," Rev. Comput. Chem. **23**, 1 (2007).
[71]D. Yu, Y. Zhu, T. Jiao, T. Wu, X. Xiao, B. Qin, Y. Hu, H. Chong, X. Lei, L. Ren *et al.*, "Structure-based design and characterization of novel fusion-inhibitory lipopeptides against SARS-CoV-2 and emerging variants," Emerging Microbes Infect. **10**, 1227–1240 (2021).
[72]C. Seuring, J. Verasdonck, J. Gath, D. Ghosh, N. Nespovitaya, M. A. Wälti, S. K. Maji, R. Cadalbert, P. Güntert, B. H. Meier, and R. Riek, "The three-dimensional structure of human β-endorphin amyloid fibrils," Nat. Struct. Mol. Biol. **27**, 1178–1184 (2020).
[73]Structures available online from http://www.petachem.com/products.html.
[74]C. J. Williams, J. J. Headd, N. W. Moriarty, M. G. Prisant, L. L. Videau, L. N. Deis, V. Verma, D. A. Keedy, B. J. Hintze, V. B. Chen *et al.*, "Molprobity: More and better reference data for improved all-atom structure validation," Protein Sci. **27**, 293–315 (2018).

An effective sub-quadratic scaling atomic-orbital reformulation of the scaled opposite-spin RI-CC2 ground-state model using Cholesky-decomposed densities and an attenuated Coulomb-metric (Supporting Information).

F. Sacchetta,[1] D. Graf,[1] H. Laqua,[1] M. A. Ambroise,[2] J. Kussmann,[1] A. Dreuw,[2] and C. Ochsenfeld[1, a)]

[1)] *Chair of Theoretical Chemistry, Department of Chemistry, University of Munich (LMU), Munich, Germany.*

[2)] *Chair of Theoretical and Computational Chemistry, Interdisciplinary Center for Scientific Computing, Heidelberg University, Heidelberg, Germany.*

(Dated: 25 July 2022)

[a)] Electronic mail: christian.ochsenfeld@cup.uni-muenchen.de

I. DERIVATION OF AO-BASED EXPRESSIONS FOR THE CONTRIBUTIONS TO THE SINGLES VECTOR FUNCTION.

In this section we provide the steps for reformulating the vector function terms of MO-SOS-RI-CC2 in the AO basis. The explicit expressions for the ground state densities can be found in the article.

$$\begin{aligned}
\Omega^G_{\mu\nu} &= \sum_{ai} C_{\mu a}\Omega^G_{ai}C_{\nu i} = -c_{os}\sum_{aci,Q} C_{\mu a}C_{\nu i}\hat{B}^Q_{ac}Y^Q_{ci} \\
&= -c_{os}\sum_{aci,Q}\sum_{\tau}^{n} w_\tau \sum_P N^{QP}_\tau \sum_{\substack{\mu'\nu'\\ \sigma\lambda}} C_{\mu a}\Lambda^p_{\mu' c}\Lambda^h_{\nu' i}B^P_{\mu'\nu'}\Lambda^p_{\sigma a}C_{\lambda c}B^Q_{\sigma\lambda}e^{-\varepsilon_{ci}t_\tau}C_{\nu i} \\
&= -c_{os}\sum_{\tau}^{n}\sum_P\sum_{\substack{\mu'\nu'\\ \sigma\lambda}} \hat{Q}^\tau_{\lambda\mu'}B^P_{\mu'\nu'}\hat{P}^\tau_{\nu'\nu}N^{QP}_\tau\hat{Q}_{\mu\sigma}B^Q_{\sigma\lambda} \\
&= \sum_{\lambda,Q}\hat{B}^Q_{\mu\lambda}Y^Q_{\lambda\nu} \qquad (1)
\end{aligned}$$

$$\begin{aligned}
\Omega^H_{\mu\nu} &= \sum_{ai} C_{\mu a}\Omega^H_{ai}C_{\nu i} = -c_{os}\sum_{aik,Q} C_{\mu a}C_{\nu i}Y^Q_{ak}\hat{B}^Q_{ki} \\
&= -c_{os}\sum_{aik,Q}\sum_{\tau}^{n} w_\tau \sum_P N^{QP}_\tau \sum_{\substack{\mu'\nu'\\ \sigma\lambda}} C_{\mu a}\Lambda^p_{\mu' a}\Lambda^h_{\nu' k}B^P_{\mu'\nu'}C_{\sigma k}\Lambda^h_{\lambda i}B^Q_{\sigma\lambda}e^{-\varepsilon_{ak}t_\tau}C_{\nu i} \\
&= -c_{os}\sum_{\tau}^{n}\sum_P\sum_{\substack{\mu'\nu'\\ \sigma\lambda}} \hat{Q}^\tau_{\mu\mu'}B^P_{\mu'\nu'}\hat{P}^\tau_{\nu'\sigma}N^{QP}_\tau B^Q_{\sigma\lambda}\hat{P}_{\lambda\nu} \\
&= \sum_{\sigma,Q} Y^Q_{\mu\sigma}\hat{B}^Q_{\sigma\nu} \qquad (2)
\end{aligned}$$

$$\begin{aligned}
\Omega^I_{\mu\nu} &= \sum_{ai} C_{\mu a}\Omega^I_{ai}C_{\nu i} = -c_{os}\sum_{\tau}^{n} w_\tau \sum_{ai,P} C_{\mu a}n^P_\tau\hat{B}^P_{ai}C_{\nu i} \\
&= -c_{os}\sum_{\tau}^{n} w_\tau \sum_{\mu'\nu',P}\sum_{ai} C_{\mu a}n^P_\tau\Lambda^p_{\mu' a}\Lambda^h_{\nu' i}B^P_{\mu'\nu'}e^{-\varepsilon_{ai}t_\tau}C_{\nu i} \\
&= -c_{os}\sum_{\tau}^{n}\sum_{\mu'\nu',P} n^P_\tau\hat{Q}^\tau_{\mu\mu'}B^P_{\mu'\nu'}\hat{P}^\tau_{\nu'\nu} = -c_{os}\sum_{\tau}^{n}\sum_P n^P_\tau B^P_{\mu\nu} \qquad (3)
\end{aligned}$$

$$\begin{aligned}
\Omega^J_{\mu\nu} &= \sum_{ai} C_{\mu a}\Omega^J_{ai}C_{\nu i} = \sum_{ai,\mu'\nu'} C_{\mu a}\Lambda^p_{\mu' a}\hat{F}_{\mu'\nu'}\Lambda^h_{\nu' i}C_{\nu i} \\
&= \sum_{\mu'\nu'}\hat{Q}_{\mu\mu'}\hat{F}_{\mu'\nu'}\hat{P}_{\nu'\nu} = \hat{F}_{\mu\nu} \qquad (4)
\end{aligned}$$

II. BLOCK-SPARSE MATRICES

Our block-sparse algebra are implemented to efficiently control memory demands, accuracy, and performance when the matrices are sparsely occupied. These matrices are divided in blocks of defined size, whose maximum is 96x96 in the present work. The allocation of each block is carried out by employing a *block allocator* which stores the block in one large, and dynamically growing *memory pool*, improving the performance for the allocation substantially (>20x). A *memory pool* is unique for each matrix, however, in case of three-dimensional tensors T^l_{ij} (l matrices with i rows and k columns), we allocate the blocks from all l matrices in the same pool.

Whether or not a block is allocated depends on the allocation threshold ϑ_a. Thus, only the blocks with L2-norm $\geq \vartheta_a$ are stored. The second screening threshold ϑ_m is used within the matrix-matrix multiplication routine, whose pseudo-code is summarized in Algorithm 1. Within this algorithm we multiply only the elements of the blocks that meet the screening criterium (line 6-9). The loops in lines 1-2 can be parallelized in a single loop over all ib- and jb indices. If the workload is not enough, the loop over k indices (line 3) is also parallelized and each thread computes its local Z block (line 7) according to the multiplication in line 8.

Algorithm 1 BSMat - Multiplication of two three-dimensional tensors: $C_{ij} = \sum_k A_{ik}\, B_{kj}$. $nb_i =$ number of row-blocks of A and C, $nb_j =$ number of column-blocks of B and C, $nb_k =$ number of column- and row-blocks of A and B respectively,

1: **for** block jb$\in nb_j$ **do**
2: **for** block ib $\in nb_i$ **do**
3: **for** block kb $\in nb_k$ **do**
4: X = A.block(ib,kb)
5: Y = B.block(kb,jb)
6: **if** $(||X||*||Y||) \geq \vartheta_m$ **then**
7: Z = C.block(ib,jb)
8: $Z_{pq} += \sum_r X_{pr} Y_{rq}$
9: **end if**
10: **end for**
11: **end for**
12: **end for**

III. THEORETICAL COMPUTATIONAL SCALING AND SPEEDUPS FOR LINEAR ALKANES

TABLE I. Computational scaling of a single optimization iteration for linear alkanes. We take into account the number of FLOPS of MO-SOS-RI-CC2 and ω-SOS-CDD-RI-CC2 in the def2-TZVP basis and two different density fitting metrics. We employ sparsity thresholds ϑ_a and ϑ_m equal to 10^{-7} and 10^{-9}, respectively. Values marked with an asterisk (*) are extrapolated conservatively.

Sample	No. of bf	MO-SOS-RI-CC2	ω-SOS-CDD-RI-CC2 ($\omega = 0$)			ω-SOS-CDD-RI-CC2 ($\omega = 0.1$)		
	def2-TZVP	FLOPS	FLOPS	Scaling	Speed Up	FLOPS	Scaling	Speed Up
$C_{40}H_{82}$	1732	1.2E+14	1.4E+14	—	x0.9	8.98E+13	—	x1.3
$C_{80}H_{162}$	3452	1.8E+15	1.5E+15	**3.50**	x1.2	5.67E+14	**2.70**	x3.2
$C_{160}C_{322}$	6892	2.9E+16	1.3E+16	**3.10**	x2.3	2.4E+15	**2.10**	x12.2
$C_{320}H_{642}$	13772	*4.8E+17	*9.5E+16	**2.80**	x5.1	8.6E+15	**1.85**	x56.0

IV. MO-SOS-RI-CC2 ALGORITHMS

for occ-batch **do**
  for all P $\in$ aux **do**
    read B^Q_{bj} $\forall b, j \in$ occ-batch
  end for
  for all P $\in$ aux **do**
    read $\hat{B}^P_{bj}$ $\forall b$
    for all τ **do**
      ${}^{\tau}\hat{B}^P_{bj} = \hat{B}^P_{bj} e^{-\varepsilon_{bj} t\tau} \forall b, j \in$ occ-batch;
    end for
  end for
  for all τ **do**
    for all P $\in$ aux **do**
      $n^P_\tau += {}^{\tau}\hat{B}^P_{bj} \hat{F}_{jb} \forall b, j \in$ occ-batch;
    end for
  end for
  for all τ **do**
    for $j \in$ occ-batch **do**
      $N^{QP}_\tau += B^Q_{bj}\ {}^{\tau}\hat{B}^P_{bj} \forall P, Q, b$
    end for
  end for
end for
scale n^P_τ and N^{QP}_τ by $-c_{os} w_\tau$

FIG. 1. Algorithm for the calculation of N^{QP}_τ and n^P_τ intermediates within the MO-SOS-RI-CC2 implementation.

for occ-batch **do**
  for all P $\in$ aux **do**
    read $\hat{B}^P_{ai}$ $\forall b$
    for all τ **do**
      ${}^{\tau}\hat{B}^P_{ai} = \hat{B}^P_{ai} e^{-\varepsilon_{ai} t\tau} \forall a, i \in$ occ-batch;
    end for
  end for
  for all τ **do**
    for p $\in$ aux **do**
      $\Omega^I += {}^{\tau}\hat{B}^P_{ai} n^P_\tau \forall a, i \in$ occ-batch
    end for
  end for
  for all τ **do**
    for all i $\in$ occ-batch **do**
      $Y^Q_{ai} += {}^{\tau}\hat{B}^P_{ai} N^{QP}_\tau \forall P, Q, \mu$
    end for
  end for
  for all $i \in$ occ-batch **do**
    write $Y^Q_{ai} \forall Q, \mu$
  end for
end for

FIG. 2. Algorithm for the calculation of Y^Q_{ai} Ω^I_{ai} intermediates within the MO-SOS-RI-CC2 implementation.

1: **for** aux-batch **do**
2: **for** Q $\in$ aux-batch **do**
3: read $Y_{ai}^{Q} \forall a, i$
4: $Y_{\mu i}^{Q} = C_{\mu a} Y_{ai}^{Q} \forall \mu, i$
5: **end for**
6: **for** Q $\in$ aux-batch **do**
7: calc. $B_{\mu\nu}^{Q} \forall \mu, \nu$
8: $\bar{\Omega}_{\mu i}^{G} = B_{\mu\nu}^{Q} Y_{\nu i} \forall \mu, i$
9: **end for**
10: **for** Q $\in$ aux-batch **do**
11: read $B_{ki}^{Q} \forall \mu, \nu$
12: $\Omega_{ai}^{H} = Y_{ak}^{Q} \hat{B}_{ki}^{Q} \forall a, i$
13: **end for**
14: **end for**
15: $\Omega_{ai}^{G} = \Lambda_{\mu a}^{p} \bar{\Omega}_{\mu i}^{G}$

FIG. 3. Algorithm for the calculation of Ω_{ai}^{G} and Ω_{ai}^{H} contribution in the MO-SOS-RI-CC2 implementation.

5.2 Publication II: Scaled opposite-spin atomic-orbital based algebraic diagrammatic construction scheme for the polarization propagator with asymptotic linear-scaling effort: Theory and implementation

M. A. Ambroise, F. Sacchetta, D. Graf, C. Ochsenfeld, A. Dreuw
J. Chem. Phys. **158**, 124121 (2023).

Abstract

A novel local approach for the quantum-chemical computation of excited states is presented, where the concept of the atomic-orbital formulation of the second-order Møller–Plesset energy expression is extended to the second-order algebraic diagrammatic construction scheme by virtue of the Laplace transform. The scaled opposite-spin second-order algebraic diagrammatic construction method with Cholesky decomposed densities and density-fitting, or CDD-DF-SOS-ADC(2) for short, exploits the sparsity of the two-electron repulsion integrals, the atomic ground-state density matrix, and the atomic transition density matrix to drastically reduce the computational effort. By using a local density-fitting approximation, it is shown that asymptotically linear scaling can be achieved for linear carboxylic acids. For electron-dense systems, sub-cubic scaling can be achieved if the excitation is local, and hence the transition density is sparse. Furthermore, the memory footprint and accuracy of the CDD-DF-SOS-ADC(2) method are explored in detail.

Reprinted with permission from:

M. A. Ambroise, F. Sacchetta, D. Graf, C. Ochsenfeld, A. Dreuw
"Scaled opposite-spin atomic-orbital based algebraic diagrammatic construction scheme for the polarization propagator with asymptotic linear-scaling effort: Theory and implementation"
J. Chem. Phys. **158**, 124121 (2023).

https://doi.org/10.1063/5.0139894

The Journal of Chemical Physics ARTICLE scitation.org/journal/jcp

Scaled opposite-spin atomic-orbital based algebraic diagrammatic construction scheme for the polarization propagator with asymptotic linear-scaling effort: Theory and implementation

Cite as: J. Chem. Phys. 158, 124121 (2023); doi: 10.1063/5.0139894
Submitted: 24 December 2022 • Accepted: 9 March 2023 •
Published Online: 30 March 2023

M. A. Ambroise,[1] F. Sacchetta,[2] D. Graf,[2] C. Ochsenfeld,[2,3] and A. Dreuw[1,a)]

AFFILIATIONS

[1] Interdisciplinary Center for Scientific Computing, Ruprecht-Karls University, Im Neuenheimer Feld 205, 69120 Heidelberg, Germany
[2] Chair of Theoretical Chemistry, Department of Chemistry, University of Munich (LMU), D-81377 Munich, Germany
[3] Max Planck Institute for Solid State Research, 70569 Stuttgart, Germany

[a)] Author to whom correspondence should be addressed: dreuw@uni-heidelberg.de

ABSTRACT

A novel local approach for the quantum-chemical computation of excited states is presented, where the concept of the atomic-orbital formulation of the second-order Møller–Plesset energy expression is extended to the second-order algebraic diagrammatic construction scheme by virtue of the Laplace transform. The scaled opposite-spin second-order algebraic diagrammatic construction method with Cholesky decomposed densities and density-fitting, or CDD-DF-SOS-ADC(2) for short, exploits the sparsity of the two-electron repulsion integrals, the atomic ground-state density matrix, and the atomic transition density matrix to drastically reduce the computational effort. By using a local density-fitting approximation, it is shown that asymptotically linear scaling can be achieved for linear carboxylic acids. For electron-dense systems, sub-cubic scaling can be achieved if the excitation is local, and hence the transition density is sparse. Furthermore, the memory footprint and accuracy of the CDD-DF-SOS-ADC(2) method are explored in detail.

I. INTRODUCTION

The algebraic diagrammatic construction method (ADC),[1–3] along with the linear response (LR)[4–7] and equation-of-motion (EOM)[8–13] coupled cluster (CC) approaches are among the most accurate and reliable methods for computing excited states and their properties. However, increased accuracy usually comes at the price of a higher computational effort and memory demands. Even the most economical correlated methods, ADC(2)[3] and the approximate coupled-cluster scheme of second order (CC2),[14] scale with $\mathcal{O}(N^5)$ with increasing system size N, putting any molecule with more than 50 atoms or 2000 basis functions firmly out of reach of standard computers. The transformation of the two-electron repulsion integrals from the atomic-orbital (AO) to the molecular-orbital (MO) basis and the evaluation of intermediates involving these quantities are usually the main computational bottlenecks.

The first attempts to develop low-scaling excited-state methods were based on the local correlation treatment introduced by Saebo and Pulay.[15–17] As for ground-state Møller–Plesset and CC methods,[18,19] a compact representation of the virtual space is obtained by forming pair orbital domains, where each pair of local molecular orbitals (LMO) is assigned a domain $[ij]$, which includes only virtual molecular orbitals, in the form of projected atomic orbitals (PAOs) spatially close to ij. The resulting number of strong and weak electron pairs scales linearly.[18] It is important to notice that an electronic excitation can involve occupied and virtual orbitals that are far apart from each other (e.g., charge-transfer states), which would not be included in the orbital domains

of the ground-state (or other excitations). This deficiency can be addressed by extending the ground-state domains to the excitation domains $[ij]_{ex}$, which can be obtained by performing a Mulliken-like population analysis on transition densities of lower order methods like configuration interaction singles (CIS). This approach was first applied to EOM-coupled-cluster single double (CCSD)[20,21] and later to CC2.[22,23]

Closely related methods include the natural orbital (NO)[24–26] and pair-natural orbital approaches (PNOs).[27–30] The idea of NO methods is in the spirit of local correlation methods since again a compact (but not necessarily *localized*) representation of the orbital space is used that is smaller than the canonical space. In NO-CCSD,[24] a density matrix from a lower order method like MP2 is diagonalized to yield a smaller MO space in which the CCSD computation is performed. In the context of excited state methods, NO approaches encounter similar problems as LMOs: the optimal set of NOs for the ground state is not necessarily the best compact representation of the excitation space. The ground-state density generally needs to be augmented by adding excited state densities, e.g., the CIS, CIS with second-order perturbative corrections [CIS(D)][31] or CC2 density, or variations thereof. Natural orbital approaches to excited states have gained massively in popularity in recent years, and also incorporate ideas from local correlation methods.[32–34] Another type of natural orbitals often encountered in literature are natural transition orbitals (NTOs), which can be obtained by singular value decomposition (SVD) of transition densities.[35,36] Both LMO and NO excited state methods have one major disadvantage: to compute an excited state, they need prior information on that excited state. Moreover, they are often *state-specific*, i.e., the compact MO representation needs to be recomputed for each excited state, which may become the limiting factor for multi-state calculations, which are typically needed for the calculation of spectra.

So far, atomic-orbital (AO) formulations of excited states methods have been limited to CIS. Here, we present an efficient way to reduce the computational and memory scaling of the Laplace transform[37–39] (LT) density-fitting[40–43] (DF) scaled opposite-spin[44] (SOS) ADC(2) method[45,46] [DF-SOS-ADC(2)] by reformulating its intermediates in the AO basis and exploiting sparse linear algebra, as proposed in our recent work[47] for ground state DF-SOS-CC2. The intermediates in our AO-DF-SOS-ADC(2) method explicitly depend on the one-electron density (**P**) and its virtual counterpart (**Q**). For systems with non-zero HOMO–LUMO gaps, the number of significant elements in the density matrix scales linearly in the limit of large molecules. Therefore, we are able to reduce the scaling of DF-SOS-ADC(2) to quadratic by taking advantage of the sparsity of the AO-integrals and both ground-state and transition density matrices.[48] Furthermore, the scaling is reduced to asymptotically linear if short-range density fitting metrics are employed.[49,50] At last, the Cholesky decomposition of **P** provides local occupied orbitals inheriting the locality from the density matrix. The resulting CDD-DF-SOS-ADC(2) method has a lower prefactor and reduced memory demands with respect to AO-DF-SOS-CC2 and shows an early crossover with the MO formulation. The same approach is valid for the underlying MP2 ground-state calculations.[51–53]

This article is structured as follows: First, we discuss the ADC eigenvalue problem (Sec. II A), the SOS-ADC(2) equations[45] (Sec. II B), and the AO reformulation (Sec. II C). Section II D describes different density fitting metrics and the DF-based kernels employed in our method. The Cholesky decomposition of density matrices is introduced in Sec. II D, while the employed Davidson procedure is described in Sec. II E. After providing computational details in Sec. III A, we discuss the scaling behavior (Sec. III C) and the accuracy (Sec. III D) of our CDD-DF-SOS-ADC(2) method.

II. THEORY AND IMPLEMENTATION

In this section, we will first discuss the general eigenvalue problem encountered within the ADC(2) method. Then, we introduce the scaled opposite-spin approach and finally the intermediate atomic-orbital formulation for ADC(2).

A. The algebraic diagrammatic construction scheme

The ADC(2) matrix can be written in block-form as

$$\mathbf{A} = \begin{pmatrix} A_{\mu_1 \nu_1} & A_{\mu_1 \nu_2} \\ A_{\mu_2 \nu_1} & A_{\mu_2 \nu_2} \end{pmatrix}, \tag{1}$$

where μ_1, ν_1 and μ_2, ν_2 are single and double excitation manifolds, respectively. The lowest eigenvalues of the Jacobian **A** are obtained by matrix diagonalization using the iterative Davidson procedure.[54] The time determining step is the formation of matrix-vector products (MVPs) during the iterative procedure given by

$$\begin{aligned} r_{\mu_1} &= A_{\mu_1 \nu_1} u_{\nu_1} + A_{\mu_1 \nu_2} u_{\nu_2}, \\ r_{\mu_2} &= A_{\mu_2 \nu_1} u_{\nu_1} + A_{\mu_2 \nu_2} u_{\nu_2}, \end{aligned} \tag{2}$$

where **u** is the set of trial vectors in the current iteration of the Davidson procedure. Closed expressions for the MVPs have been derived, and thus, the full ADC matrix does not need to be computed.

In general, the trial-vector space expands with each iteration, with a memory requirement proportional to $N_{\mathrm{occ}}N_{\mathrm{vir}} + N_{\mathrm{occ}}^2 N_{\mathrm{vir}}^2$, with N_{occ} and N_{vir} being the number of occupied and virtual molecular orbitals, respectively, which becomes a limiting factor for larger molecules. Alternatively, the MVP may be reformulated only in terms of the singles component as

$$r_{\mu_1}(\omega_m) = A_{\mu_1 \nu_1} u_{\nu_1} + A_{\mu_1 \nu_2} \frac{A_{\nu_2 \lambda_1} u_{\lambda_1}}{\omega_m + \epsilon_{\nu_2}} = A^{\mathrm{eff}}_{\mu_1 \nu_1}(\omega_m) u_{\nu_1}, \tag{3}$$

where $\epsilon_{\nu_2} = \epsilon_i + \epsilon_j - \epsilon_a - \epsilon_b$, with ϵ_i, ϵ_j and ϵ_a, ϵ_b being the occupied and virtual molecular orbital energies. Equation (3) corresponds to multiplying an effective Jacobian matrix $\mathbf{A}^{\mathrm{eff}}(\omega_m)$ with the trial vector **u**. The doubles part is computed *on-the-fly* and does not need to be explicitly stored. This method, known as *doubles-folding*, only works when the $A_{\mu_2 \nu_2}$ block of the ADC matrix is diagonal, which is the case for *strict* ADC(2), but not for the extended ADC(2)-x[55] method or the higher order ADC(3)[56,57] method. Doubles-folding reduces the required disk space for the diagonalization procedure to $N_{\mathrm{occ}}N_{\mathrm{vir}}$. Due to the dependency of Eq. (3) on the eigenvalue ω_m, the standard Davidson method cannot be used for its solution. The Davidson algorithm used to solve this pseudo-eigenvalue problem will be discussed further below.

B. SOS-ADC(2)

In 2004, Jung *et al.*[44] proposed the scaled opposite-spin MP2 method (SOS-MP2), a variant of spin-component scaled MP2 (SCS-MP2) originally introduced by Grimme.[58] In SOS-MP2, same-spin contributions to the correlation energy are ignored, and opposite spin contributions are scaled up by a scaling factor c_{os}. The SOS method was later generalized to CC2,[59] CC2 linear response, and ADC(2).[45] For the latter two, an additional scaling factor has been introduced to scale the contributions of the $A_{\mu_1\nu_2}$ and $A_{\mu_2\nu_1}$ blocks. The SOS-ADC(2) method introduces the following modifications:

- The MP2 amplitudes $\mathbf{t}$ are substituted by their scaled opposite-spin analog,

$$t_{iajb}^{\mathrm{SOS}} = c_{\mathrm{os}} \frac{(ia|jb)}{\epsilon_a + \epsilon_b - \epsilon_i - \epsilon_j}, \tag{4}$$

  where $(ia|jb)$ are the two-electron integrals in the MO basis.

- All same-spin configurations $(\alpha\alpha\alpha\alpha)$ and $(\beta\beta\beta\beta)$ in the doubles manifold are deleted, while all remaining blocks are scaled up by a factor c_{osc}.

It should be noted that the matrix expressions for SOS-ADC(2) derived from SOS-CC2 are different from the ones obtained by applying the intermediate state representation (ISR) formalism to the SOS-MP2 ground state.[46] The ISR-SOS-ADC(2) scheme only ignores the same-spin contributions in the MP2 amplitudes but leaves the p-h/2p-2h and 2p-2h/p-h coupling blocks unmodified. In this work, we will focus on the standard SOS-ADC(2) scheme, as ISR-SOS-ADC(2) does not allow for a favorable factorization of terms when density fitting is used.

By applying the above modifications to the ADC(2) expressions of the MVP, the *restricted* SOS-ADC(2) working equations are given by

$$\begin{aligned} r_{ia}^{\mathrm{S,SOS}}(\omega) = {} & (\epsilon_a - \epsilon_i) u_{ia}^{\mathrm{S}} - \sum_{jb} [2(ia|jb) - (ij|ab)] u_{jb}^{\mathrm{S}} + \sum_b I_{ab}^{\mathrm{SOS}} u_{ib}^{\mathrm{S}} \\ & + \sum_j u_{ja}^{\mathrm{S}} I_{ij}^{\mathrm{SOS}} - \frac{1}{2} \sum_{jb} t_{iajb}^{\mathrm{SOS}} I_{jb}^{(1)\mathrm{S,SOS}} \\ & - \frac{1}{2} \sum_{jb} [2(ia|jb) - (ib|ja)] I_{jb}^{(2)\mathrm{S,SOS}} \\ & + c_{\mathrm{osc}} \left\{ \sum_{kcl} (ik|lc) u_{kalc}^{\mathrm{S,SOS}}(\omega) - \sum_{ckd} u_{ickd}^{\mathrm{S,SOS}}(\omega) (kd|ac) \right\}, \end{aligned} \tag{5}$$

$$\begin{aligned} r_{ia}^{\mathrm{T,SOS}}(\omega) = {} & (\epsilon_a - \epsilon_i) u_{ia}^{\mathrm{T}} - \sum_{jb} (ij|ab) u_{jb}^{\mathrm{T}} + \sum_b I_{ab}^{\mathrm{SOS}} u_{ib}^{\mathrm{T}} + \sum_j u_{ja}^{\mathrm{T}} I_{ij}^{\mathrm{SOS}} \\ & - \frac{1}{2} \sum_{jb} t_{iajb}^{\mathrm{SOS}} I_{jb}^{(1)\mathrm{T,SOS}} + \frac{1}{2} \sum_{jb} (ib|ja) I_{jb}^{(2)\mathrm{T,SOS}} \\ & + c_{\mathrm{osc}} \left\{ \sum_{kcl} (ik|lc) u_{kalc}^{\mathrm{T,SOS}}(\omega) - \sum_{ckd} u_{ickd}^{\mathrm{T,SOS}}(\omega) (kd|ac) \right\}, \end{aligned} \tag{6}$$

$$\begin{aligned} u_{iajb}^{\mathrm{S,SOS}}(\omega) = {} & \frac{c_{\mathrm{osc}}}{\omega - \epsilon_a - \epsilon_b + \epsilon_i + \epsilon_j} \left\{ \sum_k u_{ka}^{\mathrm{S}} (ki|bj) + \sum_k u_{kb}^{\mathrm{S}} (kj|ai) \right. \\ & \left. - \sum_c u_{ic}^{\mathrm{S}} (ac|bj) - \sum_c u_{jc}^{\mathrm{S}} (bc|ai) \right\}, \end{aligned} \tag{7}$$

$$\begin{aligned} u_{iajb}^{\mathrm{T,SOS}}(\omega) = {} & \frac{c_{\mathrm{osc}}}{\omega - \epsilon_a - \epsilon_b + \epsilon_i + \epsilon_j} \left\{ \sum_k u_{ka}^{\mathrm{T}} (ki|bj) - \sum_k u_{kb}^{\mathrm{T}} (kj|ai) \right. \\ & \left. - \sum_c u_{ic}^{\mathrm{T}} (ac|bj) + \sum_c u_{jc}^{\mathrm{T}} (bc|ai) \right\}, \end{aligned} \tag{8}$$

with the intermediates

$$I_{ab}^{\mathrm{SOS}} = \frac{1}{2} \left[\sum_{kcl} t_{kalc}^{\mathrm{SOS}} (kb|lc) \right]_{a \leftrightarrow b}, \tag{9}$$

$$I_{ij}^{\mathrm{SOS}} = \frac{1}{2} \left[\sum_{ckd} t_{ickd}^{\mathrm{SOS}} (jc|kd) \right]_{i \leftrightarrow j}, \tag{10}$$

$$I_{ia}^{(1)\mathrm{S,SOS}} = \sum_{jb} (2(ia|jb) - (ib|ja)) u_{jb}^{\mathrm{S}}, \tag{11}$$

$$I_{ia}^{(2)\mathrm{S,SOS}} = \sum_{jb} t_{iajb}^{\mathrm{SOS}} u_{jb}^{\mathrm{S}}, \tag{12}$$

$$I_{ia}^{(1)\mathrm{T,SOS}} = -\sum_{jb} (ib|ja) u_{jb}^{\mathrm{T}}, \tag{13}$$

$$I_{ia}^{(2)\mathrm{T,SOS}} = -\sum_{jb} t_{iajb}^{\mathrm{SOS}} u_{jb}^{\mathrm{T}}. \tag{14}$$

The superscripts S and T denote the singlet and triplet component, respectively, for each quantity.

To the best of our knowledge, the above expressions for restricted SOS-ADC(2) have not yet been explicitly presented in the literature.

The SOS method greatly reduces the prefactor of ADC(2) calculations but has no effect on the overall scaling. However, by applying the DF approximation[40–43] and the Laplace transform of the energy denominator[37–39,51] to the above expressions for the MVP, the computational scaling can be reduced to $\mathcal{O}(N^4)$ as described by Winter and Hättig.[45] In these algorithms, four-index intermediates are completely avoided and hence the scaling of memory requirements could be reduced to $N_{\mathrm{aux}} N_{\mathrm{bas}}^2$, where N_{bas} is the number of basis functions, and N_{aux} the number of auxiliary basis functions.

C. Atomic-orbital formulation of ADC(2)

For a detailed derivation of the working equations of SOS-ADC(2) in an atomic orbital representation, the reader is referred to the supplementary material. In this section, we will give a schematic outline of the method.

The low-scaling calculation of the MVPs in the AO basis depends on both the one-electron density matrices $\mathbf{P}$ and $\mathbf{Q}$,

$$P_{\mu\nu} = C_{\mu i} C_{\nu i}, \tag{15}$$

$$Q_{\mu\nu} = C_{\mu a} C_{\nu a}, \tag{16}$$

06 October 2023 13:44:43

as well as on the transition density matrix **U**,

$$U_{\mu\nu} = C_{\mu i} u_{ia} C_{\nu a}, \tag{17}$$

where **C** is the MO coefficient matrix and u_{ia} is the trial vector in the MO basis. The Einstein summation convention is used throughout. The transition density shows sparsity in the limit of large molecules and local excitations, as shown in Fig. 1 for $C_{79}H_{159}COOH$.

Here, we propose an approach to ADC(2), where some components of the MVP are computed in an intermediate AO basis before being transformed back to the MO basis for the Davidson procedure. We will demonstrate the procedure using an example. Consider the non-symmetrized SOS-ADC(2) intermediate matrix I_{ab}:

$$I_{ab}^{\mathrm{SOS,ns}} = \frac{1}{2}\sum_{kcl} \frac{(ka|lc)(kb|lc)}{\epsilon_b + \epsilon_c - \epsilon_k - \epsilon_l}. \tag{18}$$

The energy denominator in the t-amplitudes can be removed by virtue of the Laplace transform,

$$\frac{1}{\epsilon_a + \epsilon_b - \epsilon_i - \epsilon_j} = \int_0^\infty e^{-(\epsilon_a+\epsilon_b-\epsilon_i-\epsilon_j)t} dt. \tag{19}$$

The t-integration is then replaced by a finite summation using a functional approximation,

$$\frac{1}{\Delta_{iajb}} \approx \sum_{\alpha}^{N_{\mathrm{lap}}} |w^{(\alpha)}| e^{-\Delta_{iajb} t^{(\alpha)}} = \sum_{\alpha}^{N_{\mathrm{lap}}} |w^{(\alpha)}| e^{-\epsilon_a t^{(\alpha)}} e^{\epsilon_i t^{(\alpha)}} e^{-\epsilon_b t^{(\alpha)}} e^{\epsilon_j t^{(\alpha)}}, \tag{20}$$

where $w^{(\alpha)}$ and $t^{(\alpha)}$ are the Laplace weights and exponents at Laplace point α. Using a similar strategy as in AO-MP2 to factor out the coefficient matrices, the intermediates can be formulated as

$$I_{ab}^{\mathrm{SOS,ns}} = \frac{c_{\mathrm{os}}}{2}\sum_{kcl}\sum_{\alpha} |w^{(\alpha)}| e^{\Delta_{kalc} t^{(\alpha)}} (ka|lc)(kb|lc), \tag{21}$$

$$= \frac{c_{\mathrm{os}}}{2}\sum_{\lambda\sigma} C_{\lambda b} \sum_{\alpha} |w^{(\alpha)}|^{1/4} e^{-\epsilon_a t^{(\alpha)}} C_{\sigma a} \sum_{\kappa\gamma\tau} (\underline{\kappa}\sigma|\underline{\tau}\overline{\gamma})^{(\alpha)} (\kappa\lambda|\tau\gamma), \tag{22}$$

$$= \frac{c_{\mathrm{os}}}{2}\sum_{\lambda\sigma} C_{\lambda b} \sum_{\alpha} |w^{(\alpha)}|^{1/4} e^{-\epsilon_a t^{(\alpha)}} C_{\sigma a} I_{\sigma\lambda}^{(\alpha)\mathrm{AO-SOS}}, \tag{23}$$

with the pseudo-AO electron integrals and the occupied/virtual pseudo-density matrices,

$$(\underline{\kappa}\sigma|\underline{\tau}\overline{\gamma})^{(\alpha)} = P_{\kappa\kappa'}^{(\alpha)} (\kappa'\sigma|\tau'\gamma') P_{\tau\tau'}^{(\alpha)} Q_{\gamma\gamma'}^{(\alpha)}, \tag{24}$$

$$P_{\mu\mu'}^{(\alpha)} = \sum_i C_{\mu i} |w^{(\alpha)}|^{1/4} e^{\epsilon_i t^{(\alpha)}} C_{\mu' i}, \tag{25}$$

$$Q_{\nu\nu'}^{(\alpha)} = \sum_a C_{\nu a} |w^{(\alpha)}|^{1/4} e^{-\epsilon_a t^{(\alpha)}} C_{\nu' a}, \tag{26}$$

as well as the Laplace atomic-orbital intermediate,

$$I_{\mu\nu}^{(\alpha)\mathrm{AO-SOS}} = \sum_{\kappa\gamma\tau} (\underline{\kappa}\sigma|\underline{\tau}\overline{\gamma})^{(\alpha)} (\kappa\lambda|\tau\gamma). \tag{27}$$

A similar procedure is applied to all other components of the SOS-ADC(2) expression. We abbreviated the resulting method as AO-SOS-ADC(2), and the reader is referred to the supplementary material for the whole derivation.

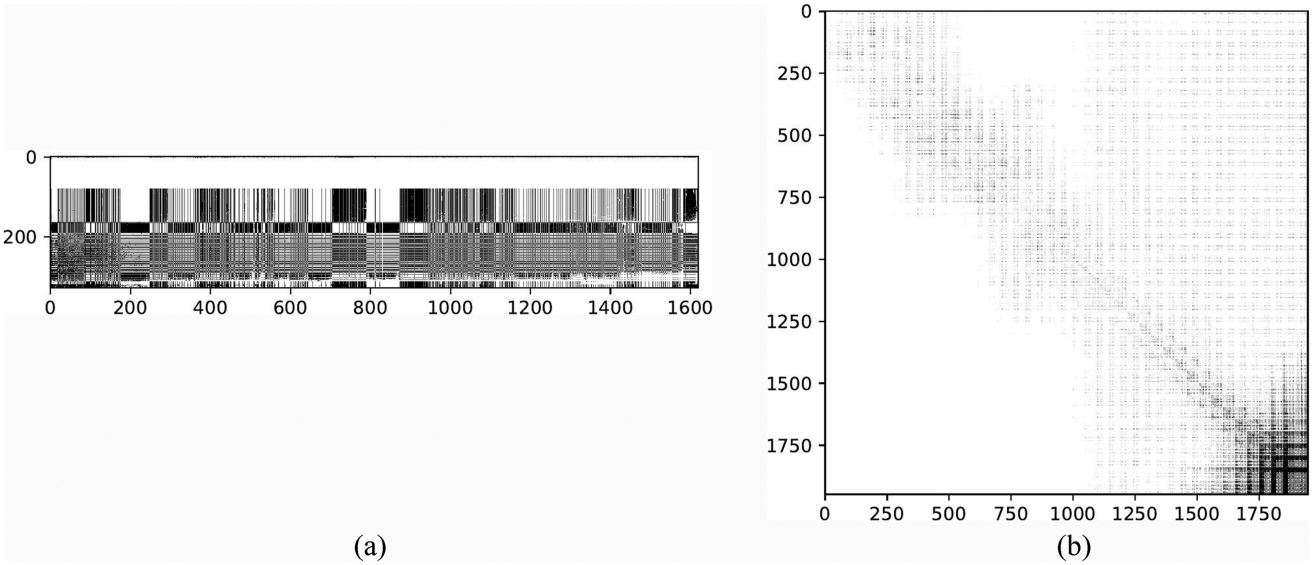

FIG. 1. Logarithm of the absolute values of the matrix elements in the transition densities for the lowest excited state for the carboxylic acid $C_{79}H_{159}COOH$, with the cc-pVDZ basis set: (a) in the MO basis and (b) in the AO basis. Black indicates significant elements, while white indicates values below the threshold (10^{-8}). The excitation domain is entirely localized on the carboxylic group. Using sparse matrix algebra, significant speed-ups can be obtained for CIS in the AO basis.

D. Local density fitting and Cholesky factorization

Even though the scaling of ADC(2) can be drastically reduced using an atomic-orbital formulation, the prefactor is very large due to the AO space being much larger than the particle–hole space. The four-index intermediates initially scale with N_{AO}^4, compared with $N_{\mathrm{occ}}^2 N_{\mathrm{vir}}^2$ for an MO formulation. To mitigate this problem, we introduce the density fitting (DF) approximation and the Cholesky decomposition of the density matrices.

The two-electron integrals over four atomic orbitals $\psi(\vec{r})$ can be expressed in terms of the one-electron charge densities,[60]

$$(\mu\nu|\lambda\sigma) = \int \psi_\mu(\vec{r_1})\psi_\nu(\vec{r_1})\frac{1}{r_{12}}\psi_\lambda(\vec{r_2})\psi_\sigma(\vec{r_2})d^3r_1 d^3r_2 = \int \rho_{\mu\nu}(\vec{r_1})\frac{1}{r_{12}}\rho_{\lambda\sigma}(\vec{r_2})d^3r_1 d^3r_2, \tag{28}$$

that in density fitting are approximated by fitting them to a set of auxiliary functions ψ_X,

$$\rho_{\mu\nu}(\vec{r}) = \sum_X C_{\mu\nu}^X \psi_X(\vec{r}), \tag{29}$$

where the fitting coefficients $C_{\mu\nu}^X$ are found by solving the set of linear equations,

$$C_{\mu\nu}^X = \sum_Y (Y|X)^{-1}(Y|\mu\nu), \tag{30}$$

with

$$B_{Y\mu\nu} = (Y|\mu\nu) = \int \psi_Y(\vec{r_1})\frac{1}{r_{12}}\psi_\mu(\vec{r_2})\psi_\nu(\vec{r_2})d^3r_1 d^3r_2, \tag{31}$$

$$(X|Y) = \int \psi_X(\vec{r_1})\frac{1}{r_{12}}\psi_Y(\vec{r_2})d^3r_1 d^3r_2. \tag{32}$$

The three-center integrals in Eq. (31) decay exponentially with the square of the distance between μ and ν, but decay only with r^{-1} as a function of the bra-ket distance. The number of non-negligible elements, therefore, scales with $\mathcal{O}(N^2)$. The two-center integrals, i.e., the Coulomb metric (CM) matrix, as well as its inverse are generally not sparse and scale with $\mathcal{O}(N^2)$, which also imposes at best a quadratic scaling for the number of non-negligible elements in the fitting coefficients. The density fitting procedure with the standard Coulomb metric is abbreviated to DFCM (density fitting in Coulomb metric) for simplicity.

Closely related to the idea of density fitting is the Cholesky decomposition of the two-electron integrals.[61] The resulting Cholesky vectors $L_{X\mu\nu}$ can be evaluated in $\mathcal{O}(N^2)$ time, and the number of significant elements scales quadratically as well. In this work, we will focus on the use of density fitting methods.

The fitting procedure given in Eq. (32) has the distinct disadvantage to introduce an unphysical long-range behavior between the charge density centers $(X|$ and $|\mu\nu)$, as it draws from all auxiliary functions ψ_X in the molecule. While introducing density fitting into existing quantum chemistry methods generally lowers computational overhead due to rank sparsity, it often does not lower the inherent scaling of the method itself due to the lack of element-wise sparsity. Introducing a short-range metric is one way to address this problem. The overlap metric is the most extreme case of short-range metrics, and the number of non-zero elements of $\mathbf{B}$ scales with $\mathcal{O}(N)$ in the limit of large molecules due to the exponential decay of the overlap metric. While it offers maximum element-wise sparsity, its decreased accuracy makes it impractical for most applications.[42,49,62]

TABLE I. Expressions for $\mathbf{B}$ and $\mathbf{M}$ for the kernels presented in this work. The subscript ω indicates that the Coulomb attenuated metric is used.

DF method	$B_{X\mu\nu}$	M_{XY}
DFCM	$(X\|\mu\nu)$	$(X\|Y)^{-1}$
DFCAM	$(X\|\mu\nu)_\omega$	$(X\|Y)_\omega^{-1}(Y\|R)(R\|S)_\omega^{-1}$
QRDF	$C_{\mu\nu}^X$	$(X\|Y)$

The Coulomb-attenuated metric (CAM) offers increased accuracy, however, at the cost of a reduction in element-wise sparsity.[49,62] The three- and two-electron integrals in this metric are given by

$$S_{XY} = \int \psi_X(\vec{r_1})\frac{\mathrm{erfc}(\omega r_{12})}{r_{12}}\psi_Y(\vec{r_2})d^3r_1 d^3r_2, \tag{33}$$

$$B_{X\mu\nu} = (X|\mu\nu)_\omega = \int \psi_X(\vec{r_1})\frac{\mathrm{erfc}(\omega r_{12})}{r_{12}}\psi_\mu(\vec{r_2})\psi_\nu(\vec{r_2})d^3r_1 d^3r_2, \tag{34}$$

where `erfc` is the complementary error function with a damping factor ω. When $\omega \to 0$ or $\omega \to \infty$, we recover the standard Coulomb metric or the overlap metric, respectively. The damping factor ω thus controls the degree of sparsity and numerical accuracy. A value of $\omega = 0.1$ was found to give high accuracy while still rendering only a linear number of elements significant.[47,62] The density fitting procedure with the Coulomb-attenuated metric is abbreviated to DFCAM (density fitting in Coulomb-attenuated metric) for simplicity.

As an alternative, a quasi-robust density-fitting (QRDF) formulation has been recently proposed,[50] which bears the advantages of increased element-wise sparsity while still keeping very high accuracy. The core idea consists in choosing a fitting domain $\{X\}$ close to the charge density $\rho_{\mu\nu}$ according to overlap criteria, but solving the linear least-squares problem in the Coulomb metric on a larger test domain $\{Y\}$. Although the number of fitting coefficients scales linearly in the asymptotic limit—with the set of functions chosen by overlap criteria—the quasi-robust DF method has a very large overhead due to the QR decomposition computed for each set of basis function pairs. Consequently, the computational time required to compute the fitting coefficients can surpass the time required to compute Hartree–Fock or MP2 energies in the case of electron-dense molecules or large basis sets. The information about the three different density fitting procedures is summarized in Table I.

Three- and two-center integrals will be used to rewrite the SOS-DF-ADC(2) equation proposed in Sec. II C, as well as within our *kernels* for the calculation of Coulomb and exchange-like matrices, abbreviated as J and K kernels, respectively.

$$\mathcal{J}[\mathbf{P},\mathbf{M}]\begin{cases} d_X = M_{XY}B_{Y\lambda\sigma}P_{\sigma\lambda}, \\ J_{\mu\nu} = B_{X\mu\nu}d_X, \end{cases} \tag{35}$$

$$\mathcal{K}[\mathbf{P},\mathbf{M}]\begin{cases} D_{\mu\nu}^X = M_{XY}B_{Y\mu\nu}, \\ K_{\mu\nu} = D_{X\mu\sigma}B_{X\nu\lambda}P_{\lambda\sigma}, \end{cases} \tag{36}$$

where the exact forms of $B_{X\mu\nu}$ and M_{XY} depend on the density fitting approximation that is used. Another kernel used is the Z-kernel encountered in CDD-SOS-MP2,[51,63]

$$\mathcal{Z}^{(\alpha)}\left[\mathbf{L}^{(\alpha)},\mathbf{Q}^{(\alpha)}\right]\begin{cases} D^{(\alpha)}_{X\mu\nu} = L^{(\alpha)}_{\mu i}\left[Q^{(\alpha)}_{\nu\nu'}\left[L^{(\alpha)}_{\mu' i}B_{X\mu'\nu'}\right]\right], \\ Z^{(\alpha)}_{XY} = B_{X\mu\nu}D^{(\alpha)}_{Y\mu\nu}, \end{cases} \tag{37}$$

where $\mathbf{L}^{(\alpha)}$ is obtained by the Cholesky decomposition[64,65] of the occupied pseudo-density $\mathbf{P}^{(\alpha)}$:

$$\mathbf{P}^{(\alpha)} = \underline{\mathbf{L}}^{(\alpha)}(\underline{\mathbf{L}}^{(\alpha)})^{T}. \tag{38}$$

The number of Cholesky orbitals (CO) is equal to or slightly less than the number of occupied canonical orbitals. Splitting the transformation of $\mathbf{B}$ with the occupied pseudo-density into two steps has the advantage of reduced overhead when multiplying the half-transformed tensor $B^{X}_{i\nu}$ with the virtual pseudo-density $\mathbf{Q}^{(\alpha)}$, as the summation runs only over N_{occ} orbitals instead of N_{AO}. The fully transformed tensor $\mathbf{D}$ can either be stored in-core, written to disk, or recomputed on-the-fly. Notice that the Z-kernel is specific to a certain Laplace point α and needs to be computed for each quadrature point.

The working equations for the resulting CDD-DF-SOS-ADC(2) method are given in Algorithms 1–4. Algorithm 1 shows the pre-iteration steps, that is, the computation of the Laplace parameters and the intermediates I_{ij} and I_{ab}. The construction of the intermediates can be formulated in terms of Z- and K-kernels. In the K-kernel, the metric matrix $\mathbf{M}$ is replaced by the Laplace matrix $\mathbf{G}$ formed by the Z-kernel. The contraction of $\mathbf{G}$ with $B_{X\mu\nu}$ in the K-kernel is the most expensive step in the pre-iteration procedure. The resulting tensor can be computed on-the-fly as it is not needed for any other contraction.

Algorithm 2 outlines the steps to form the singles part of the MVP. The steps are listed for both singlet and triplet. First, the Fock-like CIS matrix $\mathbf{F}^{\text{CIS}}$ is formed, as it represents an important intermediate for the subsequent steps. This is easily done using the J/K-kernels. Zeroth- and first-order contributions, as well as parts 2A and 2B of the second-order contributions, are trivially formed afterward using the intermediates. Part 2C is most conveniently computed using the J-kernel where the density matrix is replaced by a pseudo-density matrix $\tilde{\mathbf{F}}$ formed by contraction with a pseudo-AO CIS matrix. Part 2D is, however, a bit more involved. First, the matrix $\mathbf{T}$ is formed by looping over the Laplace points and using the J-kernel. Then, this matrix is used in a Fock-like construction scheme to get the final result.

Algorithm 3 shows the construction of the doubles part of the MVP, which is the computationally most expensive step of the SOS-ADC(2) calculation. First, the Laplace parameters are (re-)computed for the current excitation energy ω, and the occupied density matrix $\mathbf{P}$ is factorized using the Cholesky decomposition. The resulting Laplace parameters are different from the ones used in the previous steps. The algorithm then enters the Laplace loop. First, the intermediate tensors $B_{X\underline{\mu}\bar{\nu}}$ and $R_{X\underline{\mu}\underline{\nu}}$ are formed and stored. They are then used to form two intermediate matrices in the auxiliary basis. The final intermediate $D_{X\underline{\mu}\bar{\nu}}$ is formed and the contributions are added after two major contraction steps.

Alternatively, the virtual pseudo-Cholesky matrix may also be factorized to give virtual pseudo Cholesky orbitals (Algorithm 4). This further reduces the memory footprint from $N_{\text{aux}}N_{\text{occ}}N_{\text{AO}}$ to $N_{\text{aux}}N_{\text{occ}}N_{\text{vir}}$. The impact will be larger for smaller basis sets, where occupied and virtual spaces are of similar size. For larger basis sets with diffuse functions, which are often needed for ADC(2) calculations, the savings will be less pronounced as the virtual space increases with basis set size.

ALGORITHM 1. Pre-iterative steps for computing the ADC(2) intermediates.

Compute Laplace quadrature parameters $\{w^{(\alpha)}, t^{(\alpha)}\}$ for $(\epsilon_i + \epsilon_j - \epsilon_a - \epsilon_b)^{-1}$

If needed by the J,K or Z kernels, compute the Cholesky decompositions of the occupied and virtual pseudo-density matrix, and the intermediate matrices I_{ij} and I_{ab}

for $\alpha = 0$ **to** N_{lap} **do**

$G^{(\alpha)}_{XY} \leftarrow M_{XR}\mathcal{Z}\left\{\mathbf{P}^{(\alpha)},\mathbf{Q}^{(\alpha)}\right\}_{RS}M_{SY}$

$I_{ab} \leftarrow -\frac{c_{\text{os}}}{2}C_{\nu b}\sum_{\alpha}C_{\mu a} \mid w^{(\alpha)} \mid^{1/4} e^{-\epsilon_a t^{(\alpha)}}\mathcal{K}\left\{\mathbf{P}^{(\alpha)},\mathbf{G}^{(\alpha)}\right\}_{\mu\nu}$

$I_{ij} \leftarrow -\frac{c_{\text{os}}}{2}C_{\nu j}\sum_{\alpha}C_{\mu i} \mid w^{(\alpha)} \mid^{1/4} e^{\epsilon_i t^{(\alpha)}}\mathcal{K}\left\{\mathbf{Q}^{(\alpha)},\mathbf{G}^{(\alpha)}\right\}_{\mu\nu}$

Symmetrize matrices

$I_{ij} \leftarrow I_{ji}$

$I_{ab} \leftarrow I_{ba}$

ALGORITHM 2. Intermediates.

Compute the CIS Fock matrices

if singlet: $U_{\mu\nu} \leftarrow C_{\mu i} u_{ia}^{S} C_{\nu a}$

if triplet: $U_{\mu\nu} \leftarrow C_{\mu i} u_{ia}^{T} C_{\nu a}$

if singlet: $F_{\mu\nu}^{\mathrm{CIS}} \leftarrow 2 * \mathcal{J}\left\{\mathbf{U}, \mathbf{M}\right\}_{\mu\nu} - \mathcal{K}\left\{\mathbf{U}, \mathbf{M}\right\}_{\mu\nu}$

if triplet: $F_{\mu\nu}^{\mathrm{CIS}} \leftarrow -\mathcal{K}\left\{\mathbf{U}, \mathbf{M}\right\}_{\mu\nu}$

Add zero- and first-order terms

$r_{ia} \leftarrow (\epsilon_a - \epsilon_i) u_{ia}$

$r_{ia} \leftarrow C_{\mu i} F_{\mu\nu}^{\mathrm{CIS}} C_{\nu a}$

Compute part (A) and (B) of second-order term

$r_{ia} \leftarrow u_{ib} I_{ab}$

$r_{ia} \leftarrow u_{ja} I_{ij}$

Compute part (C) of second-order term

for $\theta = 0$ **to** N_{lap} **do**

if singlet: $\bar{F}_{\mu\nu}^{(\alpha)} \leftarrow P_{\mu'\mu}^{(\alpha)} Q_{\nu'\nu}^{(\alpha)} F_{\nu'\mu'}^{\mathrm{CIS}}$

if triplet: $\bar{F}_{\mu\nu}^{(\alpha)} \leftarrow -P_{\mu'\mu}^{(\alpha)} Q_{\nu'\nu}^{(\alpha)} F_{\nu'\mu'}^{\mathrm{CIS}}$

$r_{ia} \leftarrow \frac{-c_{\mathrm{os}}}{4} \mid w^{(\alpha)} \mid^{1/2} C_{\mu i} e^{\epsilon_i t^{(\alpha)}} C_{\nu a} e^{-\epsilon_a t^{(\alpha)}} \mathcal{J}\left\{\bar{\mathbf{F}}^{(\alpha)}, \mathbf{M}\right\}_{\mu\nu}$

Compute part (D) of second-order term

for $\alpha = 0$ **to** N_{lap} **do**

if singlet: $U_{\mu\nu}^{(\alpha)} \leftarrow \mid w^{(\alpha)} \mid^{1/2} C_{\mu i} e^{\epsilon_i t^{(\alpha)}} C_{\nu a} e^{-\epsilon_a t^{(\alpha)}} u_{ia}^{S}$

if triplet: $U_{\mu\nu}^{(\alpha)} \leftarrow -\mid w^{(\alpha)} \mid^{1/2} C_{\mu i} e^{\epsilon_i t^{(\alpha)}} C_{\nu a} e^{-\epsilon_a t^{(\alpha)}} u_{ia}^{T}$

$T_{\mu\nu} \leftarrow \frac{1}{2} \sum_{\alpha} P_{\mu\mu'}^{(\alpha)} Q_{\nu\nu'}^{(\alpha)} \mathcal{J}\left\{\mathbf{U}^{(\alpha)}, \mathbf{M}\right\}_{\nu\mu}$

$r_{ia} \leftarrow -\frac{c_{\mathrm{os}}}{2} C_{\mu i} C_{\nu a} \left[2\mathcal{J}\left\{\mathbf{T}, \mathbf{M}\right\}_{\mu\nu} - \mathcal{K}\left\{\mathbf{T}, \mathbf{M}\right\}_{\mu\nu}\right]$

E. Davidson diagonalization

As mentioned above, the standard Davidson procedure cannot be used to solve pseudo-eigenvalue problems of the form,

$$A_{\mathrm{eff}}(\omega_i)\mathbf{u}_i = \omega_i \mathbf{u}_i. \tag{39}$$

The modified version of the Davidson procedure used here is based on previous implementations for CC2.[23,45]

The starting guess for the eigenvectors and eigenvalues are taken as the CIS transition densities and excitation energies. For a given state n, a standard Davidson diagonalization is started with

ALGORITHM 3. Algorithm for singlet-excitations.

Compute Laplace quadrature parameters $\{w^{(\theta)}, t^{(\theta)}\}$ for $(-\omega + \epsilon_i + \epsilon_j - \epsilon_a - \epsilon_b)^{-1}$

for $\theta = 0$ **to** N_{lap} **do**

  Compute doubles pseudo-matrices $\mathbf{P}^{(\theta)}$ and $\mathbf{Q}^{(\theta)}$ and the Cholesky decomposition $L^{(\theta)}_{\mu\underline{i}}$

  $B^{(\theta)}_{X\underline{i}\overline{\sigma}} \leftarrow L^{(\theta)}_{\mu\underline{i}} B_{X\mu\nu} Q^{(\theta)}_{\nu\sigma}$

  $v^{(1)(\theta)}_{\underline{i}\overline{\sigma}} \leftarrow L^{(\theta)}_{\mu\underline{i}} S_{\mu\nu} u_{\nu\overline{\sigma}}$

  $v^{(2)(\theta)}_{\underline{\mu}\overline{\sigma}} \leftarrow u_{\mu\gamma} S_{\gamma\lambda} Q^{(\theta)}_{\lambda\sigma}$

  $R^{(\theta)}_{X\underline{i}\overline{\sigma}} \leftarrow L^{(\theta)}_{\mu\underline{i}} B_{X\mu\nu} v^{(2)(\theta)}_{\underline{\nu}\overline{\sigma}} - v^{(1)(\theta)}_{\underline{i}\overline{\gamma}} B_{X\gamma\nu} Q^{(\theta)}_{\nu\sigma}$

  $N^{(\theta)}_{PQ} \leftarrow L^{(\theta)}_{\mu\underline{i}} B^{(\theta)}_{P\underline{i}\overline{\sigma}} B_{Q\mu\sigma}$

  $G^{(\theta)}_{PQ} \leftarrow L^{(\theta)}_{\mu\underline{i}} R^{(\theta)}_{P\underline{i}\overline{\sigma}} B_{Q\mu\sigma}$

  $N^{(\theta)}_{XY} \leftarrow M_{XP} N^{(\theta)}_{PQ} M_{QY}$

  $G^{(\theta)}_{XY} \leftarrow M_{XP} G^{(\theta)}_{PQ} M_{QY}$

  $D^{(\theta)}_{X\underline{i}\overline{\sigma}} \leftarrow N^{(\theta)}_{XY} R^{(\theta)}_{Y\underline{i}\overline{\sigma}} + G^{(\theta)}_{XY} B^{(\theta)}_{Y\underline{i}\overline{\sigma}}$

  $r^{(A)}_{ia}(\theta,\omega) \leftarrow \overline{C}_{\lambda i} P_{\lambda\mu} \left[D^{(\theta)}_{X\underline{k}\overline{\sigma}} B_{X\nu\mu} L^{(\theta)}_{\nu\underline{k}} \right] \overline{C}_{\sigma a}$

  $r^{(B)}_{ia}(\theta,\omega) \leftarrow \overline{C}_{\mu i} L^{(\theta)}_{\mu\underline{i}} \left[D^{(\theta)}_{X\underline{i}\overline{\gamma}} B_{X\sigma\gamma} \right] Q_{\sigma\lambda} \overline{C}_{\lambda a}$

  $r_{ia} += c^2_{\text{osc}} e^{\omega t^{(\theta)}} \left[-r^{(A)}_{ia}(\theta,\omega) + r^{(B)}_{ia}(\theta,\omega) \right]$

fixed eigenvalue ω_n. The MVPs are computed as

$$\mathbf{v}_i(n) = \mathbf{A}_{\text{eff}}(\omega_n)\mathbf{u}_i(n), \tag{40}$$

where i runs over all vectors of the current Davidson subspace. Then the small Jacobian matrix is set up

$$A'_{ij}(n) = \mathbf{v}_i(n) \cdot \mathbf{u}_j(n). \tag{41}$$

Diagonalizing $\mathbf{A}'$ gives the eigenvalues ω' and eigenvectors $\mathbf{c}$ and the residual,

$$\mathbf{r}(n) = \sum_i c_{in}\mathbf{v}_i(n) - \omega'_i c_{in}\mathbf{u}_i(n). \tag{42}$$

New eigenvectors are computed as

$$\mathbf{b}(n) = \frac{\mathbf{r}(n)}{\mathbf{D}}, \tag{43}$$

where $\mathbf{D}$ is in this case, simply approximated by the MO energy differences $\epsilon_i - \epsilon_a$. The eigenvector $\mathbf{b}$ is normalized and orthogonalized against the other eigenvectors $\mathbf{u}$. These *micro-iterations* are repeated until the total change of the eigenvalue $\omega'(n)$ since the first iteration is smaller than the difference $|\,\omega'(n) - \omega\,|$. Then $\omega(n)$ is set to $\omega'(n)$ and a new Davidson procedure or *macro-iteration* commences. The whole procedure is converged if the norm of the residual vector $\mathbf{r}$ falls below 1×10^{-3}.

The roots are then further converged using the direct inversion of the iterative subspace (DIIS).[66] At each DIIS iteration, a new MVP $\mathbf{v}(n)$ is computed according to Eq. (40) using the current guess for the eigenvector $\mathbf{u}(n)$ and eigenvalue ω. The new excitation energy is then computed as

$$\omega' = \frac{\mathbf{u} \cdot \mathbf{v}(n)}{\|\mathbf{u}\|}. \tag{44}$$

The residual is computed according to Eq. (42) and added to the current guess vector $\mathbf{u}$ and a new guess $\mathbf{u}'$ is obtained by extrapolation of the $\mathbf{u}$-vectors of the previous iterations. The DIIS iterations

ALGORITHM 4. Algorithm for singlet-excitations.

Compute Laplace quadrature parameters $\{w^{(\theta)}, t^{(\theta)}\}$ for $(-\omega + \epsilon_i + \epsilon_j - \epsilon_a - \epsilon_b)^{-1}$

for $\theta = 0$ **to** N_{lap} **do**

  Compute doubles pseudo-matrices $\mathbf{P}^{(\theta)}$ and $\mathbf{Q}^{(\theta)}$ and their Cholesky decompositions $L^{(\theta)}_{\mu\underline{i}}$ and $L^{(\theta)}_{\sigma\overline{a}}$

  $B^{(\theta)}_{X\underline{i}\overline{a}} \leftarrow L^{(\theta)}_{\mu\underline{i}} B_{X\mu\nu} L^{(\theta)}_{\nu\overline{a}}$

  $v^{(1)(\theta)}_{\underline{i}\overline{\sigma}} \leftarrow L^{(\theta)}_{\mu\underline{i}} S_{\mu\nu} u_{\underline{\nu}\overline{\sigma}}$

  $v^{(2)(\theta)}_{\underline{\mu}\overline{a}} \leftarrow u_{\underline{\mu}\overline{\gamma}} S_{\gamma\lambda} L^{(\theta)}_{\lambda\overline{a}}$

  $R^{(\theta)}_{X\underline{i}\overline{a}} \leftarrow L^{(\theta)}_{\mu\underline{i}} B_{X\mu\nu} v^{(2)(\theta)}_{\underline{\nu}\overline{a}} - v^{(1)(\theta)}_{\underline{i}\overline{\gamma}} B_{X\gamma\nu} L^{(\theta)}_{\nu\overline{a}}$

  $N^{(\theta)}_{PQ} \leftarrow B^{(\theta)}_{P\underline{i}\overline{a}} B^{(\theta)}_{Q\underline{i}\overline{a}}$

  $G^{(\theta)}_{PQ} \leftarrow R^{(\theta)}_{P\underline{i}\overline{a}} B^{(\theta)}_{Q\underline{i}\overline{a}}$

  $N^{(\theta)}_{XY} \leftarrow M_{XP} N^{(\theta)}_{PQ} M_{QY}$

  $G^{(\theta)}_{XY} \leftarrow M_{XP} G^{(\theta)}_{PQ} M_{QY}$

  $D^{(\theta)}_{X\underline{i}\overline{a}} \leftarrow N^{(\theta)}_{XY} R^{(\theta)}_{Y\underline{i}\overline{a}} + G^{(\theta)}_{XY} B^{(\theta)}_{Y\underline{i}\overline{a}}$

  $r^{(A)}_{ia}(\theta,\omega) \leftarrow \overline{C}_{\lambda i} P_{\lambda\mu} \left[D^{(\theta)}_{X\underline{k}\overline{a}} B_{X\nu\mu} L^{(\theta)}_{\nu\underline{k}} \right] L^{(\theta)}_{\sigma\overline{a}} \overline{C}_{\sigma a}$

  $r^{(B)}_{ia}(\theta,\omega) \leftarrow \overline{C}_{\mu i} L^{(\theta)}_{\mu\underline{i}} \left[D^{(\theta)}_{X\underline{i}\overline{b}} B_{X\gamma\sigma} L^{(\theta)}_{\sigma\overline{b}} \right] Q_{\gamma\lambda} \overline{C}_{\lambda a}$

  $r_{ia} += c^2_{\text{osc}} e^{\omega t^{(\theta)}} \left[-r^{(A)}_{ia}(\theta,\omega) + r^{(B)}_{ia}(\theta,\omega) \right]$

are repeated until the norm of the residual is below the desired threshold.

III. RESULTS AND DISCUSSION

In this section, we will discuss the performance of the CDD-DF-SOS-ADC(2) method in terms of scaling, memory footprint, and accuracy.

A. Computational details

All algorithms presented in this article are implemented in a developmental quantum chemistry package called `MEGALOchem`. The main goal of `MEGALOchem` is to offer a set of modular sparse tensor kernels for various use in LCAO methods for ground and excited state calculations. The electron integrals are computed using the libcint library,[67] and matrix algebra operations, such as matrix diagonalization, QR, SVD, etc., are performed using LAPACK, ScaLAPACK, and Eigen.[68] `MEGALOchem` is open-source and for further details, the reader is referred to the GitHub repository at https://github.com/ambmax00/megalochem. Sparse tensor contractions are computed using the DBCSR library.[69,70]

Reference excitation energies for SOS-ADC(2) are computed using Q-Chem. All calculations have been performed using two nodes with two Intel E5-2690v3 Haswell CPUs and 512 GB RAM each.

B. Molecular systems

We choose two different types of systems, which represent the "optimal" and "non-optimal" cases for our method. For excited states, sparsity can both arise in the ground-state density matrix and the transition density matrix. The best-case scenario is represented by linear carboxylic acids (LCAs), shown in Fig. 2(a).

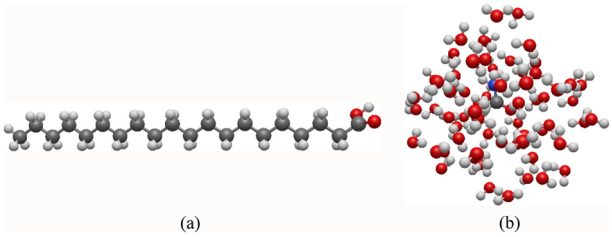

FIG. 2. (a) Structure of a linear carboxylic acid with 20 C atoms. (b) Structure of water solvated formamide.

TABLE II. Total number of basis functions for linear carboxlyic acids (LCA) and solvated formamide (FW) with the cc-pVDZ basis set.

Abbr.	Formula	N_{AO}	Abbr.	Formula	N_{AO}
LCA20	$H_{41}C_{20}O$	508	FW15	$H_{33}CNO_{16}$	417
LCA40	$H_{81}C_{40}O$	988	FW30	$H_{63}CNO_{31}$	777
LCA80	$H_{161}C_{80}O$	1948	FW63	$H_{129}CNO_{64}$	1569
LCA160	$H_{321}C_{160}O$	3868	FW144	$H_{291}CNO_{145}$	3513

They are ideal for quickly testing the performance of low-scaling excited state methods as the elements of both the atomic density matrix and the atomic transition-density matrix for the first excited state rapidly decay with increasing distance between atomic orbitals. The excited state is a $n \rightarrow \pi^*$ transition localized on the COOH group.

The second group of molecules considered here are formamides with differently sized water solvation shells [Fig. 2(b)], with the first singlet excitation localized on the formamide molecule.[36] In a sense, these systems are intermediate between best and worst-case scenario: the ground-state density matrix is dense, but the transition-density matrix of the lowest excited state is sparse due to the local character of the transition. They will demonstrate whether the CDD-DF-SOS-ADC(2) can be competitive with canonical SOS-ADC(2) for mixed sparsity scenarios. Only the lowest singlet excited states will be investigated in this article.

C. Scaling behavior

The scaling behavior is discussed by considering the time needed to construct a single matrix-vector product as a function of the number of basis functions for linear carboxylic acids of increasing size, using the cc-pVDZ basis set (Table II).[71] We take as trial vector **u** the CIS optimized transition density. It should be noted that it is crucial to use CIS for generating the initial guess because a guess based on molecular orbital energy differences alone can be very dense and negatively impact scaling. Algorithm 4 is used to evaluate the doubles part of the MVP and the timings are plotted in Fig. 3(a) for three different density fitting procedures: the DFCM method, the DFCAM method with the attenuation parameter $\omega = 0.1$, and the QRDF method with $\theta = 1 \times 10^{-5}$ and $R = 40$. The timings for the QRDF procedure are not included because the aim of this section is to demonstrate that both local density fitting approximations (DFCAM and QRDF) allow for scaling reduction, without comparing the performance of the density fitting procedure. We want to note that, at the current stage, the QRDF procedure comes with a large prefactor due to the QR decompositions. Therefore, we generally recommend the use of the DFCAM procedure for calculations on large systems with large basis sets.

Table III lists the corresponding scaling factors. The evaluation of the MVP scales as $\mathcal{O}(N^2)$ with the Coulomb metric, while linear scaling is obtained with the attenuated metric and the QRDF method. The cross-over to the low-scaling regime is quick and can already be observed for LCA40 for DFCAM. The same is true for timings with the QRDF method, however, only if the time needed to compute the QRDF coefficients is excluded. Figure 3(b) shows the total wall time for each individual component of the MVP calculation. The evaluation of the intermediate matrices (intermeds) and lines 13–14 of Algorithm 3 are the most expensive steps. The computational timings for computing parts 2C, 2D, and the CIS Fock matrices (jk) are one order of magnitude lower. Part 2A and 2B only involve a single matrix multiplication of the MO transition

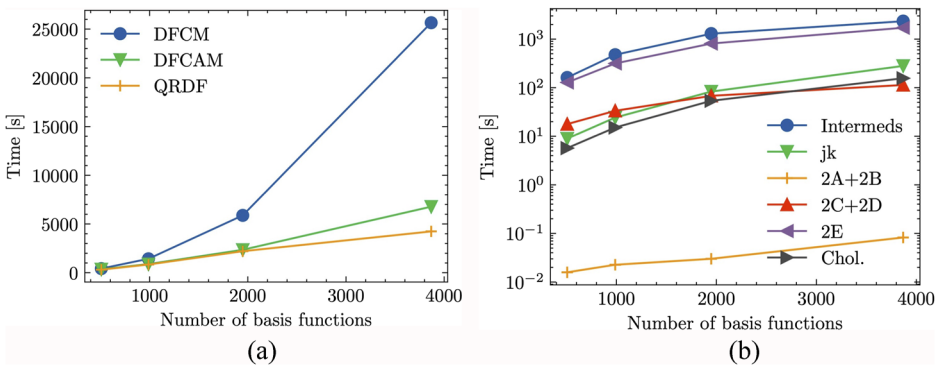

FIG. 3. (a) Total time needed to construct an ADC(2) MVP as function of the number of basis functions using different density fitting approximations (LCA). (b) Total time needed to evaluate each separate component of the MVP using quasi-robust density fitting (LCA). Important to note: timings for QRDF are not taken into account.

TABLE III. (Upper part) Scaling factors for the construction of the MVP for linear carboxylic acids. (Bottom part) Scaling factors for the construction of the MVP for solvated formamide.

N_{AO}	DFCM	DFCAM	QRDF
508	...	...	...
988	1.8	1.4	1.5
1948	2.1	1.5	1.4
3868	2.2	1.5	1.0

N_{AO}	DFCM	DFCAM
417	...	...
777	2.3	2.3
1569	2.1	2.0
3513	2.74	...

matrix with the intermediate matrices and are, therefore, evaluated very quickly. The Cholesky decompositions also do not considerably influence the total scaling.

Concerning the memory foot print of CDD-DF-SOS-ADC(2), it is important to consider that tensors are kept in memory at which step of the MVP calculation. All tensors scale at most quadratically with memory for any density fitting method. In the current implementation, the tensors $B_{X\mu\nu}$ and $C_{X\mu\nu}$ (which corresponds to $M_{XY}B_{Y\mu\nu}$) are kept in memory at all times. Tensors that depend on the Laplace quadrature parameters are computed prior to the step in which they are needed before being immediately discarded. These include $C'_{X\mu\nu}$ ($G_{XY}B_{Y\mu\nu}$ in the K kernel during the evaluation of the intermediates, see Algorithm 2), and the intermediate Laplace tensors in the Cholesky orbital (CO) basis ($B^{(\theta)}_{X\bar{i}\bar{a}}$, $R^{(\theta)}_{X\bar{i}\bar{a}}$, $D^{(\theta)}_{X\bar{i}\bar{a}}$), as defined in Algorithm 4. The tensors will be abbreviated as $\mathbf{C}'$, $\mathbf{B}_{CO}$, $\mathbf{R}_{CO}$, and $\mathbf{D}_{CO}$ for this discussion, and $\mathbf{B}_{AO}$ is used for $B_{X\mu\nu}$.

Figure 4(a) shows the block sparsity of these tensors for LCA + QRDF, with $\mathbf{B}_{AO}$ as a reference. Block sparsity is defined as the number of significant blocks divided by the total number of blocks in the dense tensor. $\mathbf{C}'$ and $\mathbf{B}_{CO}$ are quite dense, with a block sparsity slightly below 10%. The intermediate Laplace tensors $\mathbf{D}_{CO}$ and $\mathbf{R}_{CO}$ decay much faster than $\mathbf{B}_{AO}$, which was shown to scale with $\mathcal{O}(N)$; for LCA160, e.g., $\mathbf{D}_{CO}$ and $\mathbf{R}_{CO}$ are an order of magnitude sparser (≈0.1%) than $\mathbf{B}_{AO}$. The difference to the other Laplace tensor $\mathbf{B}_{CO}$ is that $\mathbf{D}_{CO}$ and $\mathbf{R}_{CO}$ are formed by the multiplication of $\mathbf{B}_{AO}$ with both the AO ground-state density $\mathbf{P}$ $[\mathcal{O}(N)]$ and the AO transition-density matrix $\mathbf{U}$, whose number of relevant blocks becomes constant for large LCA. This property of the $\mathbf{U}$ matrix explains the increased sparsity of $\mathbf{D}_{CO}$ and $\mathbf{R}_{CO}$ compared with $\mathbf{B}_{CO}$, which is formed using the AO ground state densities only. Moreover, the number of relevant blocks within $\mathbf{R}_{CO}$ becomes constant for large systems resulting in the $\mathcal{O}(N)$ scaling shown in Table III.

It is interesting to notice that the intermediate tensor $\mathbf{D}_{CO}$, which is formed from $\mathbf{B}_{CO}$ and $\mathbf{R}_{CO}$, is sparser than both of its input tensors. This indicates a potentially faster route to evaluate $\mathbf{D}_{CO}$ by imposing sparsity criteria on $\mathbf{B}_{CO}$ and $\mathbf{R}_{CO}$. How these criteria exactly would need to be defined is the subject of future investigation. The most plausible route is via a sparsity analysis of the trial vector $\mathbf{u}$, similar to how LMO or NO excited state methods generate a compact virtual orbital space. Similarly, the evaluation of the intermediate tensors can be sped up by only taking into account the AOs which are near or within the excitation space. This would, however, lead to a state specificity of the CDD-DF-SOS-ADC(2) method.

Table III shows the performance of CDD-DF-SOS-ADC(2) for solvated formamide with up to 144 water molecules. Due to the dense electronic structure of these systems, both performance and scaling are negatively affected compared with the LCAs. Nonetheless, our CDD-DF-SOS-ADC(2) method shows sub-cubic scaling behavior indicating that our CDD-DF-SOS-ADC(2) method can always reduce the computational scaling of excited states calculations if the excitation space is small and localized. Although Table III shows sub-cubic scaling, we want to stress that, even for solvated formamide, the scaling is asymptotically linear if a local density fitting procedure is used. Please note that the value for FW144 is missing in Table III due to numerical issues that were encountered during the inversion of the two-center-two-electron integral matrix in the Coulomb attenuated metric.

D. Accuracy

To get an impression of the accuracy that can be achieved with CDD-DF-SOS-ADC(2), the lowest-lying singlet excitation energies for a small set of molecules are compared with the results obtained with exact/canonical SOS-ADC(2), as implemented in Q-Chem.[72]

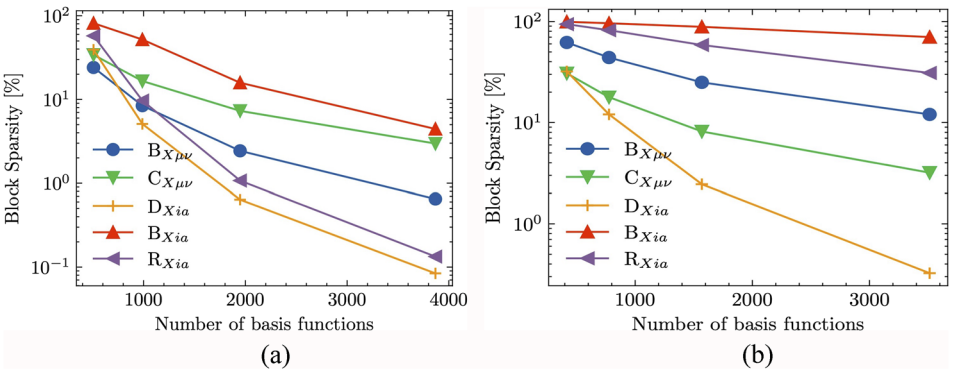

FIG. 4. (a) Block sparsity for the major 3-index tensors appearing in the evaluation of the MVP (LCA, DFCM). (b) Block sparsity for the major 3-index tensors appearing in the evaluation of the MVP (FW, DFCM).

The Hartree–Fock wave function taken as reference for CDD-DF-SOS-ADC(2) is optimized using density fitting in the Coulomb metric, while the exact HF ground state is used for the canonical calculations. The aug-cc-pVDZ basis set,[71,73] and the auxiliary basis sets cc-pVTZ-jkfit[74] and aug-cc-pVDZ-ri[75] are used for Hartree–Fock and CDD-DF-SOS-ADC(2), respectively. The test systems include linear alkanes and carboxylic acids, solvated formamide, as well as the boron-dipyrromethene-flavin dyad (FLVA)[76] and the phenothiazine-isoalloxazine dyad (DYAP).[20]

Before considering the results, it is important to note that convergence issues were commonly encountered in the Davidson procedure when using local density fitting approximations. This is due to linear dependencies in the auxiliary basis set space, which then leads to numerical issues in the fitting procedure. The error propagates through the Davidson iterations and causes convergence issues in the form of negative excitation energies. Fortunately, the problem can often be solved by filtering out all eigenvectors with an associated eigenvalue below a certain threshold (typically around 1×10^{-6}–1×10^{-4}). Alternatively, the problem can be solved by removing the linear dependencies from the basis set itself, e.g., by means of a Cholesky decomposition of the auxiliary overlap matrix.[77–79]

Similar problems were encountered in our original implementation of QRDF. For each block of fitting functions X, the test functions Y are chosen by considering only the overlap of basis functions with the smallest exponent in each block. This screening method, however, leads to many near-zero overlap values between tighter basis functions in the same block, which in turn cause numerical issues in the QR decomposition when solving the linear least-squares problem. Here, an alternative QRDF algorithm is used, where the test functions are chosen by weighted average criteria using the auxiliary overlap matrix to avoid near-zero values in the rectangular matrix $(X|Y)$.

Table IV shows the SOS-ADC(2) excitation energy differences in meV. Values are given for DFCM, DFCAM with attenuation factors 0.1, and the improved QRDF algorithm. DFCM shows errors on the order of several meV for the linear systems LCA12, LCA20, and LA20, and lower for the other test systems. As expected, DFCAM introduces much larger errors. The iterative nature of the Davidson procedure, therefore, has a significant impact on the accuracy for DFCAM. Errors are much smaller for QRDF, and even problematic systems like LA20 have similar accuracy to DFCM. It should be noted, however, that the total errors for all metrics and systems are well below the experimental accuracy of 0.1 eV for SOS-ADC(2).

TABLE IV. Differences for the lowest lying singlet excitation energies between canonical SOS-ADC(2) and CDD-DF-SOS-ADC(2), in meV, for different density fitting approximations. LA = linear alkane, LCA = linear carboxylic acid, FW = solvated formamide, flva(a) = borondipyrromethene-flavin dyad, dyap = phenothiazine-isoalloxazine dyad.

System	DFCM	DFCAM(0.1)	QRDF
LCA12	5.3	0.2	4.1
LCA20	3.6	9.6	3.2
LA20	1.5	10.6	0.8
FW10	0.2	15.1	0.5
FW15	1.6	2.1	0.3
FLVA	0.9	0.1[a]	0.9
DYAP	5.8	89.7	5.8

[a]The cc-pVTZ-ri[75] auxiliary basis set was used instead of aug-cc-pVDZ-ri due to convergence problems.

Furthermore, it should be noted that the accuracy of the excitation energies is also affected by the quality of the HF wave function. In fact, we used a different HF wave function (with no RI-J approximation) in the reference calculations, which possibly introduces some errors in the CDD-DF-SOS-ADC(2) calculations. However, all CDD-DF-SOS-ADC(2) calculations employed a RI-HF reference ground-state allowing a consistent comparison.

IV. CONCLUSION

We have successfully demonstrated how an atomic-orbital formulation of the scaled opposite-spin ADC(2) scheme can drastically reduce its scaling by several orders of magnitude, using sparse matrix algebra and local density fitting. Our method can exploit both localities in the electronic structure via the sparsity of the ground-state density matrix, and the locality of the excitation via the sparsity of the transition-density matrix. In the ideal case, linear scaling can be achieved if DFCAM is used. For electron-dense systems, subcubic scaling is possible if the excitation is localized. As opposed to local molecular orbital or natural orbital approaches to excited-state calculations, the proposed method does not need any *a priori* information on the excited state and is not state-specific.

SUPPLEMENTARY MATERIAL

See the supplementary material for details about the derivation of the MVP equations in the AO basis with doubles-folding and information about molecular structures.

ACKNOWLEDGMENTS

Numerical results were obtained at the PDC Center for High Performance Computing at the KTH Royal Institute of Technology in Stockholm. We would like to thank Professor Patrick Norman for arranging access to the computing resources. The authors acknowledge the support from the Marie Skłodowska-Curie European Training Network "COSINE - COmputational Spectroscopy In Natural sciences and Engineering," Grant Agreement No. 765739. C.O. further acknowledges financial support as Max-Planck-Fellow at the MPI-FKF Stuttgart.

AUTHOR DECLARATIONS

Conflict of Interest

The authors have no conflicts to disclose.

Author Contributions

M. A. Ambroise: Conceptualization (equal); Data curation (equal); Formal analysis (equal); Investigation (equal); Software (equal);

Validation (equal); Writing – original draft (lead). **F. Sacchetta**: Conceptualization (equal); Data curation (equal); Formal analysis (equal); Methodology (equal); Software (equal); Validation (equal); Writing – original draft (lead). **D. Graf**: Conceptualization (equal); Data curation (equal); Formal analysis (equal); Supervision (equal); Writing – original draft (equal); Writing – review & editing (equal). **C. Ochsenfeld**: Conceptualization (lead); Formal analysis (equal); Funding acquisition (lead); Methodology (equal); Resources (equal); Supervision (lead); Writing – review & editing (equal). **A. Dreuw**: Conceptualization (lead); Funding acquisition (lead); Project administration (lead); Resources (equal); Supervision (lead); Writing – review & editing (equal).

DATA AVAILABILITY

The data that support the findings of this study are available within the article and its supplementary material.

REFERENCES

[1] J. Schirmer, "Beyond the random-phase approximation: A new approximation scheme for the polarization propagator," Phys. Rev. A **26**, 2395–2416 (1982).
[2] J. Schirmer and A. B. Trofimov, "Intermediate state representation approach to physical properties of electronically excited molecules," J. Chem. Phys. **120**, 11449–11464 (2004).
[3] A. Dreuw and M. Wormit, "The algebraic diagrammatic construction scheme for the polarization propagator for the calculation of excited states," Wiley Interdiscip. Rev.: Comput. Mol. Sci. **5**, 82–95 (2015).
[4] H. Sekino and R. J. Bartlett, "A linear response, coupled-cluster theory for excitation energy," Int. J. Quantum Chem. **26**, 255–265 (1984).
[5] H. Koch and P. Jørgensen, "Coupled cluster response functions," J. Chem. Phys. **93**, 3333–3344 (1990).
[6] H. Koch, H. J. A. Jensen, P. Jørgensen, and T. Helgaker, "Excitation energies from the coupled cluster singles and doubles linear response function (CCSDLR). Applications to Be, CH^+, CO, and H_2O," J. Chem. Phys. **93**, 3345–3350 (1990).
[7] K. Sneskov and O. Christiansen, "Excited state coupled cluster methods," Wiley Interdiscip. Rev.: Comput. Mol. Sci. **2**, 566–584 (2012).
[8] J. Geertsen, M. Rittby, and R. J. Bartlett, "The equation-of-motion coupled-cluster method: Excitation energies of Be and CO," Chem. Phys. Lett. **164**, 57–62 (1989).
[9] K. Emrich, "An extension of the coupled cluster formalism to excited states (I)," Nucl. Phys. A **351**, 379–396 (1981).
[10] J. F. Stanton and R. J. Bartlett, "The equation of motion coupled-cluster method. A systematic biorthogonal approach to molecular excitation energies, transition probabilities, and excited state properties," J. Chem. Phys. **98**, 7029–7039 (1993).
[11] J. F. Stanton and J. Gauss, "Analytic energy derivatives for ionized states described by the equation-of-motion coupled cluster method," J. Chem. Phys. **101**, 8938–8944 (1994).
[12] A. I. Krylov, "Equation-of-motion coupled-cluster methods for open-shell and electronically excited species: The Hitchhiker's guide to Fock space," Annu. Rev. Phys. Chem. **59**, 433–462 (2008).
[13] R. J. Bartlett, "Coupled-cluster theory and its equation-of-motion extensions," Wiley Interdiscip. Rev.: Comput. Mol. Sci. **2**, 126–138 (2012).
[14] O. Christiansen, H. Koch, and P. Jørgensen, "The second-order approximate coupled cluster singles and doubles model CC2," Chem. Phys. Lett. **243**, 409–418 (1995).
[15] P. Pulay, "Localizability of dynamic electron correlation," Chem. Phys. Lett. **100**, 151–154 (1983).
[16] S. Sæbø and P. Pulay, "Local configuration interaction: An efficient approach for larger molecules," Chem. Phys. Lett. **113**, 13–18 (1985).
[17] S. Saebo and P. Pulay, "Local treatment of electron correlation," Annu. Rev. Phys. Chem. **44**, 213–236 (1993).
[18] M. Schütz, G. Hetzer, and H.-J. Werner, "Low-order scaling local electron correlation methods. I. Linear scaling local MP2," J. Chem. Phys. **111**, 5691–5705 (1999).
[19] M. Schütz and H.-J. Werner, "Low-order scaling local electron correlation methods. IV. Linear scaling local coupled-cluster (LCCSD)," J. Chem. Phys. **114**, 661–681 (2001).
[20] T. D. Crawford and R. A. King, "Locally correlated equation-of-motion coupled cluster theory for the excited states of large molecules," Chem. Phys. Lett. **366**, 611–622 (2002).
[21] T. Korona and H.-J. Werner, "Local treatment of electron excitations in the EOM-CCSD method," J. Chem. Phys. **118**, 3006–3019 (2003).
[22] D. Kats, T. Korona, and M. Schütz, "Local CC2 electronic excitation energies for large molecules with density fitting," J. Chem. Phys. **125**, 104106 (2006).
[23] D. Kats and M. Schütz, "A multistate local coupled cluster CC2 response method based on the Laplace transform," J. Chem. Phys. **131**, 124117 (2009).
[24] A. G. Taube and R. J. Bartlett, "Frozen natural orbital coupled-cluster theory: Forces and application to decomposition of nitroethane," J. Chem. Phys. **128**, 164101 (2008).
[25] P. R. Nagy, G. Samu, and M. Kállay, "Optimization of the linear-scaling local natural orbital CCSD(T) method: Improved algorithm and benchmark applications," J. Chem. Theory Comput. **14**, 4193–4215 (2018).
[26] Z. Rolik, L. Szegedy, I. Ladjánszki, B. Ladóczki, and M. Kállay, "An efficient linear-scaling CCSD(T) method based on local natural orbitals," J. Chem. Phys. **139**, 094105 (2013).
[27] C. Edmiston and M. Krauss, "Configuration-interaction calculation of H_3 and H_2," J. Chem. Phys. **42**, 1119–1120 (1965).
[28] F. Neese, A. Hansen, and D. G. Liakos, "Efficient and accurate approximations to the local coupled cluster singles doubles method using a truncated pair natural orbital basis," J. Chem. Phys. **131**, 064103 (2009).
[29] F. Neese, F. Wennmohs, and A. Hansen, "Efficient and accurate local approximations to coupled-electron pair approaches: An attempt to revive the pair natural orbital method," J. Chem. Phys. **130**, 114108 (2009).
[30] A. Hansen, D. G. Liakos, and F. Neese, "Efficient and accurate local single reference correlation methods for high-spin open-shell molecules using pair natural orbitals," J. Chem. Phys. **135**, 214102 (2011).
[31] M. Head-Gordon, R. J. Rico, M. Oumi, and T. J. Lee, "A doubles correction to electronic excited states from configuration interaction in the space of single substitutions," Chem. Phys. Lett. **219**, 21–29 (1994).
[32] D. Mester, P. R. Nagy, and M. Kállay, "Reduced-cost linear-response CC2 method based on natural orbitals and natural auxiliary functions," J. Chem. Phys. **146**, 194102 (2017).
[33] D. Mester, P. R. Nagy, and M. Kállay, "Reduced-cost second-order algebraic-diagrammatic construction method for excitation energies and transition moments," J. Chem. Phys. **148**, 094111 (2018).
[34] D. Mester, P. R. Nagy, and M. Kállay, "Reduced-scaling correlation methods for the excited states of large molecules: Implementation and benchmarks for the second-order algebraic-diagrammatic construction approach," J. Chem. Theory Comput. **15**, 6111–6126 (2019).
[35] P. Baudin and K. Kristensen, "LoFEx—A local framework for calculating excitation energies: Illustrations using RI-CC2 linear response theory," J. Chem. Phys. **144**, 224106 (2016).
[36] P. Baudin and K. Kristensen, "Correlated natural transition orbital framework for low-scaling excitation energy calculations (CorNFLEx)," J. Chem. Phys. **146**, 214114 (2017).
[37] M. Häser and J. Almlöf, "Laplace transform techniques in Møller–Plesset perturbation theory," J. Chem. Phys. **96**, 489–494 (1992).
[38] A. Takatsuka, S. Ten-no, and W. Hackbusch, "Minimax approximation for the decomposition of energy denominators in Laplace-transformed Møller–Plesset perturbation theories," J. Chem. Phys. **129**, 044112 (2008).

[39]B. Helmich-Paris and L. Visscher, "Improvements on the minimax algorithm for the Laplace transformation of orbital energy denominators," J. Comput. Phys. **321**, 927–931 (2016).
[40]J. L. Whitten, "Coulombic potential energy integrals and approximations," J. Chem. Phys. **58**, 4496–4501 (1973).
[41]E. J. Baerends, D. E. Ellis, and P. Ros, "Self-consistent molecular Hartree—Fock—Slater calculations I. The computational procedure," Chem. Phys. **2**, 41–51 (1973).
[42]O. Vahtras, J. Almlöf, and M. W. Feyereisen, "Integral approximations for LCAO-SCF calculations," Chem. Phys. Lett. **213**, 514–518 (1993).
[43]C.-K. Skylaris, L. Gagliardi, N. C. Handy, A. G. Ioannou, S. Spencer, and A. Willetts, "On the resolution of identity Coulomb energy approximation in density functional theory," J. Mol. Struct.: THEOCHEM **501–502**, 229–239 (2000).
[44]Y. Jung, R. C. Lochan, A. D. Dutoi, and M. Head-Gordon, "Scaled opposite-spin second order Møller–Plesset correlation energy: An economical electronic structure method," J. Chem. Phys. **121**, 9793–9802 (2004).
[45]N. O. C. Winter and C. Hättig, "Scaled opposite-spin CC2 for ground and excited states with fourth order scaling computational costs," J. Chem. Phys. **134**, 184101 (2011).
[46]C. M. Krauter, M. Pernpointner, and A. Dreuw, "Application of the scaled-opposite-spin approximation to algebraic diagrammatic construction schemes of second order," J. Chem. Phys. **138**, 044107 (2013).
[47]F. Sacchetta, D. Graf, H. Laqua, M. A. Ambroise, J. Kussmann, A. Dreuw, and C. Ochsenfeld, "An effective sub-quadratic scaling atomic-orbital reformulation of the scaled opposite-spin RI-CC2 ground-state model using Cholesky-decomposed densities and an attenuated Coulomb metric," J. Chem. Phys. **157**, 104104 (2022).
[48]F. Aquilante, T. B. Pedersen, A. Sánchez de Merás, and H. Koch, "Fast non-iterative orbital localization for large molecules," J. Chem. Phys. **125**, 174101 (2006).
[49]Y. Jung, A. Sodt, P. M. W. Gill, and M. Head-Gordon, "Auxiliary basis expansions for large-scale electronic structure calculations," Proc. Natl. Acad. Sci. U. S. A. **102**, 6692–6697 (2005).
[50]D. P. Tew, "Communication: Quasi-robust local density fitting," J. Chem. Phys. **148**, 011102 (2018).
[51]S. A. Maurer, L. Clin, and C. Ochsenfeld, "Cholesky-decomposed density MP2 with density fitting: Accurate MP2 and double-hybrid DFT energies for large systems," J. Chem. Phys. **140**, 224112 (2014).
[52]M. Glasbrenner, D. Graf, and C. Ochsenfeld, "Efficient reduced-scaling second-order Møller–Plesset perturbation theory with Cholesky-decomposed densities and an attenuated Coulomb metric," J. Chem. Theory Comput. **16**, 6856–6868 (2020).
[53]J. Zienau, L. Clin, B. Doser, and C. Ochsenfeld, "Cholesky-decomposed densities in Laplace-based second-order Møller–Plesset Perturbation theory," J. Chem. Phys. **130**, 204112 (2009).
[54]E. R. Davidson, "The iterative calculation of a few of the lowest eigenvalues and corresponding eigenvectors of large real-symmetric matrices," J. Comput. Phys. **17**, 87–94 (1975).
[55]A. B. Trofimov and J. Schirmer, "An efficient polarization propagator approach to valence electron excitation spectra," J. Phys. B: At., Mol. Opt. Phys. **28**, 2299–2324 (1995).
[56]A. B. Trofimov, G. Stelter, and J. Schirmer, "A consistent third-order propagator method for electronic excitation," J. Chem. Phys. **111**, 9982–9999 (1999).
[57]P. H. P. Harbach, M. Wormit, and A. Dreuw, "The third-order algebraic diagrammatic construction method (ADC(3)) for the polarization propagator for closed-shell molecules: Efficient implementation and benchmarking," J. Chem. Phys. **141**, 064113 (2014).
[58]S. Grimme, "Improved second-order Møller–Plesset perturbation theory by separate scaling of parallel- and antiparallel-spin pair correlation energies," J. Chem. Phys. **118**, 9095–9102 (2003).
[59]A. Hellweg, S. A. Grün, and C. Hättig, "Benchmarking the performance of spin-component scaled CC2 in ground and electronically excited states," Phys. Chem. Chem. Phys. **10**, 4119–4127 (2008).
[60]H.-J. Werner, F. R. Manby, and P. J. Knowles, "Fast linear scaling second-order Møller-Plesset perturbation theory (MP2) using local and density fitting approximations," J. Chem. Phys. **118**, 8149–8160 (2003).
[61]H. Koch, A. Sánchez de Merás, and T. B. Pedersen, "Reduced scaling in electronic structure calculations using Cholesky decompositions," J. Chem. Phys. **118**, 9481 (2003).
[62]A. Luenser, H. F. Schurkus, and C. Ochsenfeld, "Vanishing-overhead linear-scaling random phase approximation by Cholesky decomposition and an attenuated coulomb-metric," J. Chem. Theory Comput. **13**, 1647–1655 (2017).
[63]S. A. Maurer, J. Kussmann, and C. Ochsenfeld, "Communication: A reduced scaling J-engine based reformulation of SOS-MP2 using graphics processing units," J. Chem. Phys. **141**, 051106 (2014).
[64]N. J. Higham, "Cholesky factorization," Wiley Interdiscip. Rev.: Comput. Stat. **1**, 251–254 (2009).
[65]H. Harbrecht, M. Peters, and R. Schneider, "On the low-rank approximation by the pivoted Cholesky decomposition," Appl. Numer. Math. **62**, 428–440 (2012).
[66]P. Pulay, "Convergence acceleration of iterative sequences. The case of SCF iteration," Chem. Phys. Lett. **73**, 393–398 (1980).
[67]Q. Sun, "Libcint: An efficient general integral library for Gaussian basis functions," J. Comput. Chem. **36**, 1664–1671 (2015).
[68]G. Guennebaud, B. Jacob *et al.*, "Eigen v3," http://eigen.tuxfamily.org, 2010.
[69]U. Borštnik, J. VandeVondele, V. Weber, and J. Hutter, "Sparse matrix multiplication: The distributed block-compressed sparse row library," Parallel Comput. **40**, 47–58 (2014).
[70]TCD Group, DBCSR: Distributed Block Compressed Sparse Row matrix library, 2020.
[71]T. H. Dunning, "Gaussian basis sets for use in correlated molecular calculations. I. The atoms boron through neon and hydrogen," J. Chem. Phys. **90**, 1007–1023 (1989).
[72]Y. Shao, Z. Gan, E. Epifanovsky, A. T. B. Gilbert, M. Wormit, J. Kussmann, A. W. Lange, A. Behn, J. Deng, X. Feng, D. Ghosh, M. Goldey, P. R. Horn, L. D. Jacobson, I. Kaliman, R. Z. Khaliullin, T. Kuś, A. Landau, J. Liu, E. I. Proynov, Y. M. Rhee, R. M. Richard, M. A. Rohrdanz, R. P. Steele, E. J. Sundstrom, H. L. Woodcock, P. M. Zimmerman, D. Zuev, B. Albrecht, E. Alguire, B. Austin, G. J. O. Beran, Y. A. Bernard, E. Berquist, K. Brandhorst, K. B. Bravaya, S. T. Brown, D. Casanova, C.-M. Chang, Y. Chen, S. H. Chien, K. D. Closser, D. L. Crittenden, M. Diedenhofen, R. A. DiStasio, H. Do, A. D. Dutoi, R. G. Edgar, S. Fatehi, L. Fusti-Molnar, A. Ghysels, A. Golubeva-Zadorozhnaya, J. Gomes, M. W. D. Hanson-Heine, P. H. P. Harbach, A. W. Hauser, E. G. Hohenstein, Z. C. Holden, T.-C. Jagau, H. Ji, B. Kaduk, K. Khistyaev, J. Kim, J. Kim, R. A. King, P. Klunzinger, D. Kosenkov, T. Kowalczyk, C. M. Krauter, K. U. Lao, A. D. Laurent, K. V. Lawler, S. V. Levchenko, C. Y. Lin, F. Liu, E. Livshits, R. C. Lochan, A. Luenser, P. Manohar, S. F. Manzer, S.-P. Mao, N. Mardirossian, A. V. Marenich, S. A. Maurer, N. J. Mayhall, E. Neuscamman, C. M. Oana, R. Olivares-Amaya, D. P. O'Neill, J. A. Parkhill, T. M. Perrine, R. Peverati, A. Prociuk, D. R. Rehn, E. Rosta, N. J. Russ, S. M. Sharada, S. Sharma, D. W. Small, A. Sodt, T. Stein, D. Stück, Y.-C. Su, A. J. W. Thom, T. Tsuchimochi, V. Vanovschi, L. Vogt, O. Vydrov, T. Wang, M. A. Watson, J. Wenzel, A. White, C. F. Williams, J. Yang, S. Yeganeh, S. R. Yost, Z.-Q. You, I. Y. Zhang, X. Zhang, Y. Zhao, B. R. Brooks, G. K. L. Chan, D. M. Chipman, C. J. Cramer, W. A. Goddard, M. S. Gordon, W. J. Hehre, A. Klamt, H. F. Schaefer, M. W. Schmidt, C. D. Sherrill, D. G. Truhlar, A. Warshel, X. Xu, A. Aspuru-Guzik, R. Baer, A. T. Bell, N. A. Besley, J.-D. Chai, A. Dreuw, B. D. Dunietz, T. R. Furlani, S. R. Gwaltney, C.-P. Hsu, Y. Jung, J. Kong, D. S. Lambrecht, W. Liang, C. Ochsenfeld, V. A. Rassolov, L. V. Slipchenko, J. E. Subotnik, T. Van Voorhis, J. M. Herbert, A. I. Krylov, P. M. W. Gill, and M. Head-Gordon, "Advances in molecular quantum chemistry contained in the Q-Chem 4 program package," Mol. Phys. **113**, 184–215 (2015).
[73]R. A. Kendall, T. H. Dunning, and R. J. Harrison, "Electron affinities of the first-row atoms revisited. Systematic basis sets and wave functions," J. Chem. Phys. **96**, 6796–6806 (1992).

[74]F. Weigend, "A fully direct RI-HF algorithm: Implementation, optimised auxiliary basis sets, demonstration of accuracy and efficiency," Phys. Chem. Chem. Phys. **4**, 4285–4291 (2002).
[75]F. Weigend, A. Köhn, and C. Hättig, "Efficient use of the correlation consistent basis sets in resolution of the identity MP2 calculations," J. Chem. Phys. **116**, 3175–3183 (2002).
[76]D. Kats, T. Korona, and M. Schütz, "Transition strengths and first-order properties of excited states from local coupled cluster CC2 response theory with density fitting," J. Chem. Phys. **127**, 064107 (2007).
[77]F. Aquilante, L. Boman, J. Boström, H. Koch, R. Lindh, A. S. de Merás, and T. B. Pedersen, "Cholesky decomposition techniques in electronic structure theory, " in *Linear-Scaling Techniques in Computational Chemistry and Physics: Methods and Applications* (Springer, 2011), pp. 301–343.
[78]N. H. F. Beebe and J. Linderberg, "Simplifications in the generation and transformation of two-electron integrals in molecular calculations," Int. J. Quantum Chem. **12**, 683–705 (1977).
[79]S. Lehtola, "Curing basis set overcompleteness with pivoted Cholesky decompositions," J. Chem. Phys. **151**, 241102 (2019).

Supplementary Information

1 Derivation of AO-SOS-ADC(2)

In this section, we outline each step in detail to derive AO-SOS-ADC(2) starting from canonical SOS-ADC(2).

1.1 Restricted SOS-ADC(2) with Doubles-Folding

The working equations for restricted SOS-ADC(2) with doubles folding are given by

$$\begin{aligned} r_{ia}^{S,SOS}(\omega) = (\epsilon_a - \epsilon_i)u_{ia}^S - \sum_{jb} \left[2\,(ia \mid jb) - (ij \mid ab)\right] u_{jb}^S + \sum_b I_{ab}^{SOS} u_{ib} + \sum_j u_{ja}^S I_{ij}^{SOS} \\ - \frac{1}{2}\sum_{jb} t_{iajb}^{SOS} I_{jb}^{(1)S,SOS} - \frac{1}{2}\sum_{jb} \left[2\,(ia \mid jb) - (ib \mid ja)\right] I_{jb}^{(2)S,SOS} \\ + c_{osc}\left\{\sum_{kcl} (ik \mid lc)\, u_{kalc}^{S,SOS}(\omega) - \sum_{ckd} u_{ickd}^{S,SOS}(\omega)\,(kd \mid ac)\right\} \end{aligned} \tag{1}$$

$$\begin{aligned} r_{ia}^{T,SOS}(\omega) = (\epsilon_a - \epsilon_i)u_{ia}^S - \sum_{jb} (ij \mid ab)\, u_{jb}^T + \sum_b I_{ab}^{SOS} u_{ib} + \sum_j u_{ja}^S I_{ij}^{SOS} \\ - \frac{1}{2}\sum_{jb} t_{iajb}^{SOS} I_{jb}^{(1)T,SOS} + \frac{1}{2}\sum_{jb} (ib \mid ja)\, I_{jb}^{(2)T,SOS} \\ + c_{osc}\left\{\sum_{kcl} (ik \mid lc)\, u_{kalc}^{T,SOS}(\omega) - \sum_{ckd} u_{ickd}^{T,SOS}(\omega)\,(kd \mid ac)\right\} \end{aligned} \tag{2}$$

with the on-the-fly doubles

$$\begin{aligned} u_{iajb}^{S,SOS}(\omega) = \frac{c_{osc}}{\omega - \epsilon_a - \epsilon_b + \epsilon_i + \epsilon_j}\left\{\sum_k u_{ka}\,(ki \mid bj) + \sum_k u_{kb}\,(kj \mid ai)\right. \\ \left. - \sum_c u_i c\,(ac \mid bj) - \sum_c u_{jc}\,(bc \mid ai)\right\} \end{aligned} \tag{3}$$

$$\begin{aligned} u_{iajb}^{T,SOS}(\omega) = \frac{c_{osc}}{\omega - \epsilon_a - \epsilon_b + \epsilon_i + \epsilon_j}\left\{\sum_k u_{ka}\,(ki \mid bj) - \sum_k u_{kb}\,(kj \mid ai)\right. \\ \left. - \sum_c u_i c\,(ac \mid bj) + \sum_c u_{jc}\,(bc \mid ai)\right\} \end{aligned} \tag{4}$$

and the intermediates

$$I_{ab}^{SOS} = \frac{c_{os}}{2}\left[\sum_{kcl} t_{kalc}\,(kb \mid lc)\right]_{a\leftrightarrow b} \tag{5}$$

$$I_{ij}^{SOS} = \frac{c_{os}}{2}\left[\sum_{ckd} t_{ickd}\,(jc \mid kd)\right]_{i\leftrightarrow j} \tag{6}$$

$$I_{ia}^{(1)S,SOS} = \sum_{jb}\left(2\,(ia \mid jb) - (ib \mid ja)\right) u_{jb}^{S} \tag{7}$$

$$I_{ia}^{(2)S,SOS} = c_{os}\sum_{jb} t_{iajb} u_{jb}^{S} \tag{8}$$

$$I_{ia}^{(1)T,SOS} = -\sum_{jb}\left(ib \mid ja\right) u_{jb}^{T} \tag{9}$$

$$I_{ia}^{(2)T,SOS} = -c_{os}\sum_{jb} t_{iajb} u_{jb}^{T} \tag{10}$$

1.2 Restricted SOS-ADC(2) with Doubles-Folding in an Atomic Orbital Basis

The goal of an atomic orbital based formulation of ADC(2) is to compute the matrix-vector product in an intermediate AO basis and transform it back to the MO basis (or alternatively an LMO basis) for the Davidson procedure, similarly to how it is done for CIS:

$$r_{ia} = C_{\mu i} r_{\underline{\mu}\overline{\nu}} C_{\nu a} \tag{11}$$

Furthermore, it is convenient to split the MVP into six components which are evaluated individually

$$r_{ia}(\omega) = r_{ia}^{CIS} + r_{ia}^{2A} + r_{ia}^{2B} + r_{ia}^{2C} + r_{ia}^{2D} + r_{ia}^{2E}(\omega) \tag{12}$$

In the next sections, using Equations 1 and 2 as starting points, the working equations for restricted AO-SOS-ADC(2) will be derived and discussed in detail.

1.2.1 First Order

The first order part of the MVP is identical in both ADC(2) and SOS-ADC(2)

$$r_{ia}^{S,CIS} = (\epsilon_a - \epsilon_i) u_{ia}^{S} + \sum_{jb}\left[2\,(ia \mid jb) - (ij \mid ab)\right] u_{jb}^{S} \tag{13}$$

$$r_{ia}^{T,CIS} = (\epsilon_a - \epsilon_i) u_{ia}^{T} - \sum_{jb}\left(ij \mid ab\right) u_{jb}^{T} \tag{14}$$

An AO formulation is obtained in an identical manner to AO-CIS by factoring out the coefficient matrices to obtain Hartree-Fock-like expressions:

$$\begin{aligned} r_{ia}^{S,CIS,AO} &= (\epsilon_a - \epsilon_i)u_{ia}^S + \sum_{ia} C_{\mu i} C_{\sigma a} \left[\left(2\left(\mu\sigma \mid \nu\lambda\right) - \left(\mu\nu \mid \sigma\lambda\right)\right) u_{\underline{\nu\lambda}}^S \right] \\ &= (\epsilon_a - \epsilon_i)u_{ia}^S + \sum_{ia} C_{\mu i} C_{\sigma a} \left[2\tilde{J}_{\mu\sigma}^S - \tilde{K}_{\mu\sigma}^S \right] \end{aligned} \tag{15}$$

$$\begin{aligned} r_{ia}^{T,CIS,AO} &= (\epsilon_a - \epsilon_i)u_{ia}^T - \sum_{ia} C_{\mu i} C_{\sigma a} \left[\left(\mu\nu \mid \sigma\lambda\right) u_{\underline{\nu\lambda}}^T \right] \\ &= (\epsilon_a - \epsilon_i)u_{ia}^T - \sum_{ia} C_{\mu i} C_{\sigma a} \tilde{K}_{\mu\sigma}^T \end{aligned} \tag{16}$$

where $\tilde{\mathbf{J}}$ and $\tilde{\mathbf{K}}$ are the Coulomb and exchange kernels, and $u_{\underline{\mu\sigma}}$ is the transition density in the AO basis

$$u_{\underline{\mu\sigma}} = C_{\mu i} u_{ia} C_{\overline{\sigma} a} \tag{17}$$

The zero order terms (i.e. the molecular orbital energy differences) do not need to be formulated in an AO basis, because the computation time is negligible. Similarly, transforming $\tilde{\mathbf{J}}$ and $\tilde{\mathbf{K}}$ to the MO basis formerly scales as $\mathcal{O}(N^3)$ but has very low overhead and does not influence the overall scaling of AO-SOS-ADC(2). The time-determining steps are the computation of the J-kernel, which scales as $\mathcal{O}(N^2)$ and the K-kernel, which scales as $\mathcal{O}(N)$ in the limit of large systems. For triplet excitations, the scaling is reduced to linear due to the absence of coulomb contributions.

1.2.2 Second Order: Part 2A and 2B

The expressions for component 2A and 2B read

$$r_{ia}^{S,SOS,2A} = \sum_b I_{ab}^{SOS} u_{ib}^S + \sum_j I_{ij}^{SOS} u_{ja}^S \tag{18}$$

$$r_{ia}^{T,SOS,2A} = \sum_b I_{ab}^{SOS} u_{ia}^T + \sum_j I_{ij}^{SOS} u_{ja}^T \tag{19}$$

with the intermediates as defined in the previous section. Rather than casting the whole expression into the AO basis, it is more convenient to evaluate only the non-symmetrized intermediates $I_{ab}^{SOS,ns}$ and $I_{ij}^{SOS,ns}$ in the AO basis. The expressions for the intermediates involve the t-amplitudes, and to obtain an orbital-invariant formulation, it is necessary to use the Laplace transform

$$\frac{1}{\epsilon_a - \epsilon_i + \epsilon_b - \epsilon_j} = \sum_\alpha^{nlap} |w^{(\alpha)}| e^{-\epsilon_a t^{(\alpha)}} e^{\epsilon_i t^{(\alpha)}} e^{-\epsilon_b t^{(\alpha)}} e^{\epsilon_j t^{(\alpha)}} \tag{20}$$

Using a similar strategy to AO-MP2 to factor out the coefficient matrices, the intermediates can be formulated as

$$I_{ab}^{AO-SOS,ns} = \frac{c_{os}}{2} \sum_{kcl} \sum_{\alpha} |w^{(\alpha)}| e^{\Delta_{kalc} t^{(\alpha)}} \left(ka \mid lc\right) \left(kb \mid lc\right) \tag{21}$$

$$= \frac{c_{os}}{2} \sum_{b} C_{\lambda b} \sum_{\alpha} \mid w^{(\alpha)} \mid^{1/4} e^{-\epsilon_a t^{(\alpha)}} C_{\sigma a} \sum_{\kappa\gamma\tau} \left(\underline{\kappa}\sigma \mid \underline{\tau}\overline{\gamma}\right)^{(\alpha)} \left(\kappa\lambda \mid \tau\gamma\right) \tag{22}$$

$$= \frac{c_{os}}{2} \sum_{b} C_{\lambda b} \sum_{\alpha} \mid w^{(\alpha)} \mid^{1/4} e^{-\epsilon_a t^{(\alpha)}} C_{\sigma a} A_{\sigma\lambda}^{(\alpha)} \tag{23}$$

with the pseudo-AO electron integrals and the occupied/virtual pseudo density matrices

$$\left(\underline{\kappa}\sigma \mid \underline{\tau}\overline{\gamma}\right)^{(\alpha)} = P_{\kappa\kappa'}^{(\alpha)} \left(\kappa'\sigma \mid \tau'\gamma'\right) P_{\tau\tau'}^{(\alpha)} Q_{\gamma\gamma'}^{(\alpha)} \tag{24}$$

$$P_{\mu\mu'}^{(\alpha)} = \sum_{i} C_{\mu i} e^{0.25 ln \left|w^{(\alpha)}\right| + \epsilon_i t^{(\alpha)}} C_{\mu' i} \tag{25}$$

$$Q_{\nu\nu'}^{(\alpha)} = \sum_{a} C_{\nu a} e^{0.25 ln \left|w^{(\alpha)}\right| - \epsilon_a t^{(\alpha)}} C_{\nu' a} \tag{26}$$

Similarly

$$I_{ij}^{AO-SOS,ns} = \frac{c_{os}}{2} \sum_{\alpha} \sum_{ckd} \left|w^{(\alpha)}\right| e^{\Delta_{ickd} t^{(\alpha)}} \left(ic \mid kd\right) \left(jc \mid kd\right) \tag{27}$$

$$= \frac{c_{os}}{2} \sum_{j} C_{\nu j} \sum_{i} \left|w^{(\alpha)}\right|^{1/4} C_{\mu i} e^{\epsilon_i t^{(\alpha)}} \sum_{\gamma\kappa\delta} \left(\mu\overline{\gamma} \mid \underline{\kappa}\overline{\delta}\right) \left(\nu\gamma \mid \kappa\delta\right) \tag{28}$$

$$= \frac{c_{os}}{2} \sum_{j} C_{\nu j} \sum_{i} \left|w^{(\alpha)}\right|^{1/4} C_{\mu i} e^{\epsilon_i t^{(\alpha)}} B_{\mu\nu}^{(\alpha)} \tag{29}$$

Finally, the intermediates are symmetrized

$$I_{ab}^{AO-SOS} = I_{ab}^{AO-SOS,ns} + I_{ba}^{AO-SOS,ns} \tag{30}$$

$$I_{ij}^{AO-SOS} = I_{ij}^{AO-SOS,ns} + I_{ji}^{AO-SOS,ns} \tag{31}$$

The time-determining step for both intermediates is the computation of the Laplace intermediates $\mathbf{A}^{(\alpha)}$ and $\mathbf{B}^{(\alpha)}$. The subsequent multiplication with the coefficient matrices is again negligible.

1.2.3 Second Order: Part 2C

Component 2C is computed as

$$r_{ia}^{S,SOS,2C} = -\frac{c_{os}}{2} \sum_{jb} t_{iajb} I_{jb}^{(1)S,SOS} \tag{32}$$

$$r_{ia}^{T,SOS,2C} = -\frac{c_{os}}{2} \sum_{jb} t_{iajb} I_{jb}^{(1)T,SOS} \tag{33}$$

Applying the Laplace transform, this then gives

$$\begin{aligned} r_{ia}^{S,AO-SOS,2C} &= -\frac{c_{os}}{2}\sum_{jb}\sum_{\alpha}\left|w^{(\alpha)}\right| e^{\Delta_{iajb}t^{(\alpha)}}\left(ia \mid jb\right)\left[\sum_{kc}\left(2\left(jb \mid kc\right)-\left(jc \mid kb\right)\right)u_{kc}^{S}\right] \\ &= -\frac{c_{os}}{2}\sum_{\alpha}\sum_{ia}\left|w^{(\alpha)}\right|^{1/2} C_{\mu i}e^{\epsilon_i t^{(\alpha)}} C_{\sigma a}e^{-\epsilon_a t^{(\alpha)}} \\ &\times\left\{\sum_{\nu\lambda}\left(\mu\alpha \mid \underline{\nu\lambda}\right)^{(\alpha)}\left[\sum_{\kappa\gamma}\left(2\left(\nu\lambda \mid \kappa\gamma\right)-\left(\nu\gamma \mid \kappa\lambda\right)\right)u_{\underline{\kappa\gamma}}^{S}\right]\right\} \\ &= -\frac{c_{os}}{2}\sum_{\alpha}\sum_{ia}\left|w^{(\alpha)}\right|^{1/2} C_{\mu i}e^{\epsilon_i t^{(\alpha)}} C_{\sigma a}e^{-\epsilon_a t^{(\alpha)}} \\ &\times\left\{\sum_{\nu\lambda}\left(\mu\alpha \mid \underline{\nu\lambda}\right)^{(\alpha)}\left[2\tilde{J}_{\lambda\nu}-\tilde{K}_{\lambda\nu}\right]\right\} \\ &= -\frac{c_{os}}{2}\sum_{\alpha}\sum_{ia}\left|w^{(\alpha)}\right|^{1/2} C_{\mu i}e^{\epsilon_i t^{(\alpha)}} C_{\sigma a}e^{-\epsilon_a t^{(\alpha)}} I_{\mu\sigma}^{(1)(\alpha)S,AO-SOS} \end{aligned} \tag{34}$$

Similarly, triplet contributions are given by

$$\begin{aligned} r_{ia}^{T,AO-SOS,2C} &= \frac{c_{os}}{2}\sum_{alpha}\sum_{ia}\left|w^{(\alpha)}\right|^{1/2} C_{\mu i}e^{\epsilon_i t^{(\alpha)}} C_{\sigma a}e^{-\epsilon_a t^{(\alpha)}}\left\{\sum_{\nu\lambda}\left(\mu\alpha \mid \underline{\nu\lambda}\right)^{(\alpha)}\tilde{K}_{\lambda\nu}\right\} \\ &= \frac{c_{os}}{2}\sum_{alpha}\sum_{ia}\left|w^{(\alpha)}\right|^{1/2} C_{\mu i}e^{\epsilon_i t^{(\alpha)}} C_{\sigma a}e^{-\epsilon_a t^{(\alpha)}} I_{\mu\sigma}^{(1)(\alpha)T,AO-SOS} \end{aligned} \tag{35}$$

where $\tilde{\mathbf{J}}$ and $\tilde{\mathbf{K}}$ are the same matrices needed for the CIS contributions. Note that the matrices are *transposed*, i.e. the index order is $\lambda\nu$, and not $\nu\lambda$. The time-determining step is the formation of the Laplace AO intermediates $I_{\mu\nu}^{\alpha(1)}$.

1.2.4 Second Order: Part 2D

Now consider part 2D

$$\begin{aligned} r_{ia}^{S,SOS,2D} &= -\frac{1}{2}\sum_{jb}\left[2\left(ia \mid jb\right)-\left(ib \mid ja\right)\right] I_{jb}^{(2)S,SOS} \\ &= -\frac{1}{2}\sum_{jb} K_{iajb} I_{jb}^{(2)S,SOS} \end{aligned} \tag{36}$$

$$r_{ia}^{T,SOS,2D} = \frac{1}{2}\sum_{jb}\left(ib \mid ja\right) I_{jb}^{(2)T,SOS} \tag{37}$$

Applying the Laplace transform gives the singlet expression

$$\begin{aligned} r_{ia}^{S,AO-SOS,2D} &= -\frac{c_{os}}{2}\sum_{jb} K_{iajb} \sum_{kc}\sum_{\alpha} \left|w^{(\alpha)}\right| e^{\Delta_{iajb}t^{(\alpha)}} (jb \mid kc)\, u_{kc}^{S} \\ &= -\frac{c_{os}}{2}\sum_{ia} C_{\mu i} C_{\sigma a} \left[K_{\mu\sigma\nu\lambda} \left(\sum_{\alpha} \left(\underline{\nu\overline{\lambda}} \mid \kappa\gamma\right)^{(\alpha)} u_{\underline{\kappa}\overline{\gamma}}^{(\alpha)S} \right) \right] \\ &= -\frac{c_{os}}{2}\sum_{ia} C_{\mu i} C_{\sigma a} I_{\mu\sigma}^{(2)S,AO-SOS} \end{aligned} \tag{38}$$

Similarly, the triplet expressions

$$\begin{aligned} r_{ia}^{T,AO-SOS,2D} &= \frac{c_{os}}{2}\sum_{jb} (ia \mid jb) \sum_{kc}\sum_{\alpha} \left|w^{(\alpha)}\right| e^{\Delta_{iajb}t^{(\alpha)}} (jb \mid kc)\, u_{kc}^{T} \\ &= \frac{c_{os}}{2}\sum_{ia} C_{\mu i} C_{\sigma a} \left[(\mu\sigma \mid \nu\lambda) \left(\sum_{\alpha} \left(\underline{\nu\overline{\lambda}} \mid \kappa\gamma\right)^{(\alpha)} u_{\underline{\kappa}\overline{\gamma}}^{(\alpha)T} \right) \right] \\ &= \frac{c_{os}}{2}\sum_{ia} C_{\mu i} C_{\sigma a} I_{\mu\sigma}^{(2)T,AO-SOS} \end{aligned} \tag{39}$$

With the transition density in the pseudo atomic orbital basis

$$u_{\underline{\mu}\overline{\sigma}}^{(\alpha)} = \left|w^{(\alpha)}\right|^{1/2} C_{\mu i} e^{\epsilon_i t^{(\alpha)}} u_{ia} C_{\sigma a} e^{-\epsilon_a t^{(\alpha)}} \tag{40}$$

The computation of the AO intermediates $I^{(2)SOS-AO}$ is the time-determining step, and is best evaluated as

$$\tilde{J}_{\mu\sigma}^{(\alpha)} = (\mu\sigma \mid \nu\lambda)\, u_{\underline{\nu}\overline{\lambda}}^{(\alpha)} \tag{41}$$

$$\tilde{J}_{\underline{\mu}\overline{\sigma}}^{(\alpha)} = P_{\mu\mu'}^{(\alpha)} \tilde{J}_{\mu\nu}^{(\alpha)} Q_{\nu\nu'}^{(\alpha)} \tag{42}$$

$$I_{\mu\sigma}^{(2)SOS-AO} = \sum_{\alpha} \left[2\,(\mu\sigma \mid \nu\lambda) - (\mu\lambda \mid \nu\sigma)\right] \tilde{J}_{\underline{\nu}\overline{\lambda}}^{(\alpha)} \tag{43}$$

1.2.5 Second Order: Part 2E

The final part is given by

$$r_{ia}^{S,SOS,2E}(\omega) = c_{osc} \left\{ \sum_{kcl} (ik \mid lc)\, u_{kalc}^{S,SOS}(\omega) - \sum_{ckd} u_{ickd}^{S,SOS}(\omega)\, (kd \mid ac) \right\} \tag{44}$$

$$r_{ia}^{T,SOS,2E}(\omega) = c_{osc} \left\{ \sum_{kcl} (ik \mid lc)\, u_{kalc}^{T,SOS}(\omega) - \sum_{ckd} u_{ickd}^{T,SOS}(\omega)\, (kd \mid ac) \right\} \tag{45}$$

With the doubles intermediates as given in Equation 3 and 4. The Laplace transform needs to be applied to the energy denominator present in these intermediates. The optimal Laplace parameters are however different from the ones used for the t-amplitudes, due to the additional factor of the excitation energy ω. For each different excitation energy ω, a new Laplace quadrature needs to be computed, alongside a new set of pseudo-density

matrices $\mathbf{P}$ and $\mathbf{Q}$. The additional time is however negligible for the standard number of quadrature points ($n_{lap} < 10$). The symbol θ is used to designate the Laplace quadrature for the doubles denominator to differentiate them from the ones for the t-amplitudes.

First, an AO formulation of the doubles amplitudes will be derived such that

$$u_{iajb}(\omega) = C_{\mu i} C_{\sigma a} u_{\mu\sigma\nu\lambda} C_{\nu j} C_{\lambda b} \tag{46}$$

For quantities like the MO integrals $(ia \mid jb)$, this is straight forwardly done by factoring out the coefficient matrices. However, the situation is more complex in the doubles intermediates, due to the presence of terms like $u_{ka}\,(ki \mid bj)$. For the MO transition densities, the non-orthogonality of the AO basis needs to be taken into consideration. The MO coefficient matrices are factored out by a PAO backtransform:

$$u_{ia} = C_{\mu i} S_{\mu\mu'} u_{\underline{\mu}'\overline{\sigma}'} S_{\sigma'\sigma} C_{\sigma a} \tag{47}$$

The doubles intermediates can then be expressed as

$$\begin{aligned}
u^{S/T}_{iajb}(\omega) = -c_{osc} \sum_{\theta} \sum_{\mu\sigma\nu\lambda} |w^{(\theta)}| e^{(\omega - \epsilon_a - \epsilon_b + \epsilon_i + \epsilon_j) t^{(\theta)}} C_{\mu i} C_{\sigma a} C_{\nu j} C_{\lambda b} \Bigg\{ \\
\sum_{\kappa} \left[u^{S/T}_{\underline{\kappa}\overline{\sigma}'} S_{\sigma'\sigma} \left(\kappa\mu \mid \nu\lambda\right) \pm u^{S/T}_{\underline{\kappa}\overline{\lambda}'} S_{\lambda'\lambda} \left(\nu\kappa \mid \mu\sigma\right) \right] \\
- \sum_{\gamma} \left[S_{\mu\mu'} u^{S/T}_{\underline{\mu}'\overline{\sigma}} \left(\nu\lambda \mid \sigma\gamma\right) \pm S_{\nu\nu'} u^{S/T}_{\underline{\nu}'\overline{\gamma}} \left(\mu\sigma \mid \gamma\lambda\right) \right] \Bigg\} \\
= - \sum_{\theta} \sum_{\mu\sigma\nu\lambda} |w^{(\theta)}| e^{(\omega - \epsilon_a - \epsilon_b + \epsilon_i + \epsilon_j) t^{(\theta)}} C_{\mu i} C_{\sigma a} u^{S/T}_{\mu\sigma\nu\lambda} C_{\nu j} C_{\lambda b}
\end{aligned} \tag{48}$$

Note the additional minus sign in front of the Laplace summation. After the Laplace transform, the sign of the denominator is swapped, i.e. $\frac{1}{\pm x} \rightarrow exp(\mp x t^{(\theta)})$. For large negative occupied molecular orbital energies ϵ_i or large positive virtual molecular orbital energies ϵ_a, this would lead to very large values and numerical instabilities. For this reason, the minus sign is factored out to reverse the sign in the exponent.

Inserting 48 into Equations 44 and 45 gives the expression for part 2E constructed via AO intermediates:

$$\begin{aligned}
r^{S/T,AO-SOS,2E}_{ia}(\omega) = -c^2_{osc} \sum_{\theta} e^{\omega t^{(\theta)}} \Bigg\{ C_{\mu i} |w^{(\theta)}|^{1/4} C_{\sigma a} e^{-\epsilon_a t^{(\theta)}} \left[\sum_{\kappa\gamma\tau} \left(\mu\underline{\kappa} \mid \underline{\tau}\overline{\gamma}\right)^{(\theta)} u^{S/T}_{\kappa\sigma\tau\gamma} \right] \\
- |w^{(\theta)}|^{1/4} C_{\mu i} e^{\epsilon_i t^{(\theta)}} C_{\sigma a} \left[\sum_{\gamma\kappa\delta} u^{S/T}_{\mu\gamma\kappa\delta} \left(\underline{\kappa}\overline{\delta} \mid \sigma\overline{\gamma}\right)^{(\theta)} \right] \Bigg\} \\
= -c^2_{osc} \sum_{\theta} e^{\omega t^{(\theta)}} \Big\{ C_{\mu i} |w^{(\theta)}|^{1/4} C_{\sigma a} e^{-\epsilon_a t^{(\theta)}} R^{(\theta)(1)S/T}_{\mu\overline{\sigma}} \\
- |w^{(\theta)}|^{1/4} C_{\mu i} e^{\epsilon_i t^{(\theta)}} C_{\sigma a} R^{(\theta)(2)S/T}_{\underline{\mu}\sigma} \Big\}
\end{aligned} \tag{49}$$

Similarly to previous expressions, the AO electron repulsion integrals are not completely transformed into the pseudo-AO basis, but only three-quarter transformed integrals are

obtained. To obtain fully-transformed integrals, it is beneficial to perform the following transformation:

$$r_{ia} = \bar{C}_{\mu i'} r_{\mu\sigma} \bar{C}_{\sigma a'} = \bar{C}_{\mu i'} C_{\mu i} r_{ia} C_{\sigma a} \bar{C}_{\sigma a'} \tag{50}$$

Inserting this expression into Equation 49 yields

$$\begin{aligned} r_{ia}^{S/T,AO-SOS,2E}(\omega) = -c_{osc}^2 \sum_{\theta} e^{\omega t^{(\theta)}} \Bigg\{ & \bar{C}_{\mu i} P_{\mu\nu} \bar{C}_{\sigma a} \left[\sum_{\kappa\gamma\tau} \left(\underline{\nu\kappa} \mid \underline{\tau}\overline{\gamma} \right)^{(\theta)} u_{\kappa\sigma\tau\gamma}^{S/T} \right] \\ & - \bar{C}_{\mu i} \bar{C}_{\sigma a} Q_{\sigma\nu} \left[\sum_{\gamma\kappa\delta} u_{\mu\gamma\kappa\delta}^{S/T} \left(\underline{\kappa}\overline{\delta} \mid \overline{\nu\gamma} \right)^{(\theta)} \right] \Bigg\} \\ = -c_{osc}^2 \sum_{\theta} e^{\omega t^{(\theta)}} & \left\{ \bar{C}_{\mu i} \bar{C}_{\sigma a} R_{\underline{\mu}\overline{\sigma}}^{(\theta)(1)S/T} - \bar{C}_{\mu i} \bar{C}_{\sigma a} R_{\underline{\mu}\overline{\sigma}}^{(\theta)(2)S/T} \right\} \end{aligned} \tag{51}$$

which gives fully transformed integrals. This step is necessary to obtain a better factorization for part 2E in the density fitting approximation. Note that there are other cases of non-fully transformed integrals in the previous parts - however a full transformation does not give any significant advantage over a DF formulation, so they are left unchanged.

The time-determining step is the formation of the **R** intermediates, which in turn depend on the AO doubles intermediates.

1.3 Summary

The AO-SOS-ADC(2) matrix-vector product is finally computed as

$$\begin{aligned} r_{ia}^{S,AO-DF-SOS}(\omega) = & (\epsilon_a - \epsilon_i) u_{ia}^S + \sum_{\mu\nu} C_{\mu i} C_{\nu a} \left(2\tilde{J}_{\mu\nu}^S - \tilde{K}_{\mu\nu}^S \right) \\ & + \sum_b I_{ab}^{AO-DF-SOS} u_{ib}^S + \sum_j I_{ij}^{AO-DF-SOS} u_{ja}^S \\ & - \frac{c_{os}}{2} \sum_{\alpha} \sum_{ia} \left| w^{(\alpha)} \right|^{1/2} C_{\mu i}^{(\alpha)} C_{\sigma a}^{(\alpha)} I_{\mu\sigma}^{(1)(\alpha)S,AO-DF-SOS} \\ & - \frac{c_{os}}{2} \sum_{ia} C_{\mu i} C_{\sigma a} I_{\mu\sigma}^{(2)S,AO-DF-SOS} \\ & - c_{osc}^2 \sum_{\theta} e^{\omega t^{(\theta)}} \left\{ \bar{C}_{\mu i} \bar{C}_{\sigma a} R_{\underline{\mu}\overline{\sigma}}^{(\theta)(1)S} - \bar{C}_{\mu i} \bar{C}_{\sigma a} R_{\underline{\mu}\overline{\sigma}}^{(\theta)(2)S} \right\} \end{aligned} \tag{52}$$

$$\begin{aligned} r_{ia}^{T,AO-DF-SOS}(\omega) = & (\epsilon_a - \epsilon_i) u_{ia}^T + \sum_{\mu\nu} C_{\mu i} C_{\nu a} \tilde{K}_{\mu\nu}^T \\ & + \sum_b I_{ab}^{AO-DF-SOS} u_{ib}^T + \sum_j I_{ij}^{AO-DF-SOS} u_{ja}^T \\ & - \frac{c_{os}}{2} \sum_{\alpha} \sum_{ia} \left| w^{(\alpha)} \right|^{1/2} C_{\mu i}^{(\alpha)} C_{\sigma a}^{(\alpha)} I_{\mu\sigma}^{(1)(\alpha)T,AO-DF-SOS} \\ & - \frac{c_{os}}{2} \sum_{ia} C_{\mu i} C_{\sigma a} I_{\mu\sigma}^{(2)T,AO-DF-SOS} \\ & - c_{osc}^2 \sum_{\theta} e^{\omega t^{(\theta)}} \left\{ \bar{C}_{\mu i} \bar{C}_{\sigma a} R_{\underline{\mu}\overline{\sigma}}^{(\theta)(1)T} - \bar{C}_{\mu i} \bar{C}_{\sigma a} R_{\underline{\mu}\overline{\sigma}}^{(\theta)(2)T} \right\} \end{aligned} \tag{53}$$

where the intermediates are evaluated as presented in the previous sections. The 2-index intermediates still need to be transformed back to the canonical MO basis for the Davidson procedure, but the computational effort required is negligible.

1.4 Restricted DF-SOS-ADC(2) with Doubles-Folding in the AO Basis

To lower the prefactor of AO-SOS-ADC(2), the density fitting approximation is introduced. The two-electron repulsion integrals are approximated using the generalized form

$$(\mu\sigma \mid \nu\lambda) = B_{\mu\sigma X} M_{XY} B_{Y\nu\lambda} \tag{54}$$

where the quantities $\mathbf{B}$ and $\mathbf{M}$ depend on the density fitting method. By inserting the relation 54 into the working equations for AO-SOS-ADC(2) derived in the previous section, we obtain the MVP expressions for AO-DF-SOS-ADC(2) as outlined in Algorithm 1-3 in the article.

2 Molecular Structures

The xyz files for the linear carboxylic acids for C20 to C160 can be found under `https://github.com/ambmax00/dissertation/tree/main/Structures`. Their geometries were optimized using DFT/B3LYP with the 6-31G* basis set.

All other structures used for benchmarking can be found within the references indicated in the article.

5.3 Publication III: Efficient Low-scaling Calculation of THC-SOS-LR-CC2 and THC-SOS-ADC(2) Excitation Energies Through Density-based Integral-direct Tensor Hypercontraction

F. Sacchetta, F. H. Bangerter, H. Laqua, C. Ochsenfeld
To be submitted (2023).

Abstract

In recent years, rapid improvements in computer hardware, as well as theoretical and algorithmic advances have enabled the calculation of ever larger systems in computational chemistry. In this avenue, we present efficient implementations of the scaled opposite-spin (SOS) second-order approximate coupled cluster (CC2) method and the closely related second-order algebraic diagrammatic construction (ADC(2)) method. The implementations leverage the least-squares tensor hypercontraction approximation, for which a new density-based integral-direct reformulation of the grid-projection of the electron integral tensor is presented. Together with screening based on local Cholesky orbitals stemming from the decomposition of the one-particle densities (CDD) in the Laplace integration and optimized block-sparse linear algebra, effectively $\mathcal{O}(N^2)$ scaling variants of linear-response SOS-CC2 and SOS-ADC(2) are obtained. The derived CDD-THC-SOS-LR-CC2/ADC(2) methods are shown to be capable of targeting excitation energies of systems up to $\sim$1000 atoms and $\sim$12000 basis functions on a single compute node.

F. Sacchetta, F. H. Bangerter, H. Laqua, C. Ochsenfeld
To be submitted (2023).

Efficient Low-scaling Calculation of THC-SOS-LR-CC2 and THC-SOS-ADC(2) Excitation Energies Through Density-based Integral-direct Tensor Hypercontraction

Filippo Sacchetta,[†,¶] Felix H. Bangerter,[†,¶] Henryk Laqua,[†] and Christian Ochsenfeld[*,†,‡]

†*Chair of Theoretical Chemistry, Department of Chemistry, University of Munich (LMU), D-81377 Munich, Germany*

‡*Max Planck Institute for Solid State Research, D-70569 Stuttgart, Germany*

¶*These authors contributed equally to this work.*

E-mail: christian.ochsenfeld@cup.uni-muenchen.de

Abstract

In recent years, rapid improvements in computer hardware, as well as theoretical and algorithmic advances have enabled the calculation of ever larger systems in computational chemistry. In this avenue, we present efficient implementations of the scaled opposite-spin (SOS) second-order approximate coupled cluster (CC2) method and the closely related second-order algebraic diagrammatic construction (ADC(2)) method. The implementations leverage the least-squares tensor hypercontraction approximation, for which a new density-based integral-direct reformulation of the grid-projection of the electron integral tensor is presented. Together with screening based on local Cholesky orbitals stemming from the decomposition of the one-particle densities (CDD) in the

Laplace integration and optimized block-sparse linear algebra, effectively $\mathcal{O}(N^2)$ scaling variants of linear-response SOS-CC2 and SOS-ADC(2) are obtained. The derived CDD-THC-SOS-LR-CC2/ADC(2) methods are shown to be capable of targeting excitation energies of systems up to ∼1000 atoms and ∼12000 basis functions on a single compute node.

1 Introduction

An accurate description of the electronic excited states of chemical systems is crucial for the useful interplay of theory and experiment,[1] where spectroscopy measures transitions between particular states, such as those that are electronically, vibronically, and/or rotationally excited. Amongst the spectroscopic methods probing transitions between the ground and electronically excited states, UV-vis spectroscopy (UV-vis), which involves the absorption and emission of photons in the ultraviolet (UV) and visible (vis) regions, and X-ray absorption spectroscopy (XAS), which involves the excitation of core electrons, are two of the most widely used methods.[2–4] Thus, in order to relate the experimentally observed absorption/emission bands to electronic transitions, accurate methods to compute vertical excitation energies are required. Additionally, calculating transition dipole moments directly relates to the observed intensities of the transitions through Fermis Golden Rule relating it to the oscillator strength

While exact excitation energies can – in the limit of the Born–Oppenheimer approximation and a finite basis set – be obtained through the full configuration interaction (FCI) method,[5,6] its exponentially scaling cost renders it inapplicable for all but the smallest systems. Therefore, considerable effort has been put into the formulation of approximate methods, also in combination with reduced scaling methods to reach ever larger system sizes, preferably without sacrificing accuracy. Here, considerable theoretical as well as algorithmic advances have been made in the past decades.[6–8] The former include reformulations of many of the commonly encountered methods in quantum chemistry under the paradigm of response

theory, i.e., the quasidegenerate second-order perturbation corrected CIS (CIS(D_∞)),[9] time-dependent density functional theory (TDDFT),[10–12] the family of complete active space self-consistent field (CASSCF)[13–15] methods, algebraic diagrammatic construction (ADC)[7,16–19] methods, as well as linear-response coupled cluster (CC)[20–24] theory. Here also approximate CC models were introduced, such as the commonly used approximate CC singles and doubles (CC2).[25] Without further approximations, CC2 and the closely related second-order ADC (ADC(2)) method exhibit quintic scaling, which necessitates additional algorithmic improvements in order for the methods to be applicable to larger systems. While conceptually simple, the opposite-spin (SOS)[26–28] approximation by Jung *et al.* achieves a significant reduction of the scaling prefactor by complete neglect of the expensive same-spin terms, while at the same time largely retaining the accuracy.[29,30] Due to the required transformation of the electron repulsion integral (ERI) tensor into the molecular orbital (MO) basis, the scaling remains $\mathcal{O}(N^5)$. However, a reduction of the scaling exponent can be achieved by using a factorized form of the ERI tensor, such as the resolution-of-the-identity (RI)[29,31–34] approximation or the Cholesky decomposition[35] in conjunction with the Laplace transformation[29,36,37] to obtain a separable form of the orbital energy denominator. Recently, Ochsenfeld, Dreuw, and coworkers[38,39] put forth atomic orbital (AO) based formulations of SOS-CC2 and SOS-ADC(2), which achieve sub-quadratic to linear scaling through a combination of the RI approximation with an attenuated Coulomb metric (ω-RI)[40] and Cholesky decomposed densities (CDD).[40–42,42–45] To achieve even further reduction of both the memory requirements and the number of required floating point operations (FLOP), tensor hypercontraction (THC) by Martínez and coworkers[46–49] can be applied, which circumvents the necessity to store and contract third- (or higher-) order tensors completely. THC variants of CC methods have previously been reported for CC2,[50] CCSD,[51–53] and CCSD(T)[54] ground-state energies as well as for excitation energies based on EOM-CC2.[55]

In this work, we propose a density-matrix-based and integral-direct approach for obtaining the THC-factorized ERI tensor, which adds only a marginal overhead when applied to an

electron correlation method. In this regard, SOS-LR-CC2 and SOS-ADC(2) are ideal methods for the application of THC, since they 1) require the AO-ERI tensor to be repeatedly transformed into different MO subspaces, which can efficiently be done by matrix-matrix multiplications, and 2) only include OS contributions, for which THC allows to reformulate the expressions to only use matrix linear algebra without the occurrence of higher than second-order tensors. By combining THC with local Cholesky pseudo-MOs from the CDD approach in the Laplace integration and block-sparse linear algebra, effectively $\mathcal{O}(N^2)$ scaling formulations of SOS-LR-CC2 and SOS-ADC(2) are obtained. The proposed methods are benchmarked using a set of medium- to large-size systems to assess the behavior of the error for increasingly large molecules. The accuracy of the ground state energies is analyzed by considering an additional set previously used by DiStasio *et al.*[56] for relative energies. Finally, the efficiency of the proposed methods is demonstrated for nucleic acid double helices up to ∼1000 atoms and ∼12000 basis functions, which reveals overall $\mathcal{O}(N^2)$ scaling.

2 Theory

2.1 Notation

Throughout this work, we employ the following notation:

- $\mu, \nu, \lambda, \sigma$: atomic orbital indices belonging to the AO basis $\{\chi_\mu\}$ of size N_{bf}.
- $\alpha, \beta, \gamma, \delta$: auxiliary function basis indices belonging to the density fitting basis $\{\chi_\alpha\}$ of size N_{aux} (usually $N_{\text{aux}} \approx 3 \cdot N_{\text{bf}}$).
- P, Q, R, S: auxiliary function basis indices belonging to the THC basis of size $N_{\text{aux-THC}}$; in the context of LS-THC gridpoint indices belonging to the LS-THC grid of size N_{grid} (usually $N_{\text{grid}} \approx 3 \cdot N_{\text{aux}}$).
- i, j, k: occupied molecular orbital indices belonging to the MO basis $\{\phi_i\}$ of size N_{occ}.

- a, b, c: virtual molecular orbital indices belonging to the MO basis $\{\phi_a\}$ of size N_{virt} ($N_{\text{virt}} \gg N_{\text{occ}}$).
- $\underline{i}, \underline{k}, \underline{j}$: occupied local Cholesky orbitals basis $\{\phi_{\underline{i}}\}$ of size N_{occ}; obtained via pivoted Cholesky decomposition of the occupied one-electron density.
- p, q, r, s: general orbital indices.
- τ: Laplace quadrature point of size N_τ (usually $5 \leq N_\tau \leq 10$ is sufficiently accurate).

2.2 Integral-direct Tensor Hypercontraction

2.2.1 Review of Tensor Hypercontraction

In its most general form, tensor hypercontraction (THC) is a low-dimensional representation of a multi-dimensional tensor, which – in the context of quantum mechanics – represents the interactions between particles in a system. For a two-body potential $\hat{V} = 1/r_{12}$, said representation of the electron-electron interactions in a real one-particle basis is the integral tensor, the elements of which are given by

$$(pq|rs) = \iint d\mathbf{r}_1 d\mathbf{r}_2 \, \varphi_p(\mathbf{r}_1)\varphi_p(\mathbf{r}_1)\frac{1}{r_{12}}\varphi_r(\mathbf{r}_2)\varphi_s(\mathbf{r}_2) \tag{1}$$

However, in practical quantum chemistry calculations, the manipulation and storage of such a high-dimensional tensor quickly becomes computationally intractable as the system or the basis set size grows. To alleviate this issue, THC provides the means to formally compress the fourth-order integral tensor into five second-order tensors as

$$(pq|rs) = \sum_{PQ} X_p^P X_q^P Z^{PQ} X_r^Q X_s^Q \tag{2}$$

The factorization is exact if the number of THC auxiliary functions $N_{\text{aux-THC}}$ is at least N_{bf}^2, but only reduces computational demands and storage requirements if $N_{\text{aux-THC}} < N_{\text{bf}}^2$. If sufficient accuracy is reached with significantly less than N_{bf}^2 THC auxiliary functions, the THC factorization enables efficient storage and manipulation of the ERI tensor, making complex calculations feasible for larger systems.

In the least-squares variant of THC (LS-THC),[47] the THC auxiliary indices are taken to be grid points of a molecular grid similar to the ones commonly used in density function theory. For LS-THC the time-determining step of factorizing the ERI tensor into the THC format is the quintic scaling grid-projection of the electron repulsion integral (ERI) tensor, which in the atomic orbital (AO) basis is given by

$$E^{PQ} = \sum_{\mu\nu\lambda\sigma} X_\mu^P X_\nu^P (\mu\nu|\lambda\sigma) X_\lambda^Q X_\sigma^Q \tag{3}$$

where the so-called collocation matrices $\mathbf{X}$ are simply the AO basis functions evaluated at the THC grid nodes scaled by the node's weight, given as

$$X_\mu^P = \sqrt[4]{w_P}\, \chi_\mu(\mathbf{r}_P) \tag{4}$$

In the general molecular orbital (MO) formulation the above equation becomes

$$E^{PQ} = \sum_{pqrs} X_p^P X_q^P (pq|rs) X_r^Q X_s^Q \tag{5}$$

which requires a transformation of the AO ERI tensor into the MO basis. From $\mathbf{E}$, the final $\mathbf{Z}$ tensor in eq. 2 is obtained as

$$Z^{PQ} = \sum_{P'Q'} [\mathbf{S}^{-1}]^{PP'} E^{P'Q'} [\mathbf{S}^{-1}]^{QQ'} \tag{6}$$

where $\mathbf{S}^{-1}$ is the inverse of the THC grid metric, which is given as the inverse of

$$S^{PP'} = \sum_{pq} X_p^P X_p^{P'} X_q^P X_q^{P'} \tag{7}$$

Note, that eq. 6 can be solved either by direct inversion of the grid metric,[47] which generally requires pseudoinversion due to its rank-deficiency, or by solving the associated system of linear equations.[57,58]

2.2.2 Density-based Integral-direct Tensor Hypercontraction

By undoing the AO-to-MO transformations in eq. 5, i.e.,

$$E^{PQ} = \sum_{pqrs} \sum_{\mu\nu\lambda\sigma} \sum_{\mu'\nu'\lambda'\sigma'} X_\mu^P C_{\mu p} \cdot X_\nu^P C_{\nu q} \cdot C_{\mu' p} C_{\nu' q} (\mu'\nu'|\lambda'\sigma') C_{\lambda' r} C_{\sigma' s} \cdot X_\lambda^Q C_{\lambda r} \cdot X_\sigma^Q C_{\sigma s} \tag{8}$$

and by carrying out the summation over the MO indices first, the expression can be reformulated in terms of densities as

$$E^{PQ} = \sum_{\mu\nu\lambda\sigma} \sum_{\mu'\nu'\lambda'\sigma'} X_\mu^P X_\nu^P P_{\mu\mu'} P_{\nu\nu'} (\mu'\nu'|\lambda'\sigma') P_{\lambda\lambda'} P_{\sigma\sigma'} X_\lambda^Q X_\sigma^Q \tag{9}$$

which – when contracting the densities with the THC $\mathbf{X}$ matrices – becomes

$$E^{PQ} = \sum_{\mu'\nu'\lambda'\sigma'} X_{\mu'}^P X_{\nu'}^P (\mu'\nu'|\lambda'\sigma') X_{\lambda'}^Q X_{\sigma'}^Q \tag{10}$$

To highlight the universality of this approach, we will use intermediate $X_{\mu'}^P$ with the primed basis function index as a proxy for both the collocation matrix in the AO basis and when transformed with a general density matrix, i.e.,

$$X^P_{\mu'} = \sum_{\mu} X^P_{\mu} P_{\mu\mu'} \tag{11}$$

Therefore, the expressions for the AO-THC and the MO-THC variant only differ in an additional contraction of the THC $\mathbf{X}$ matrices with a density. Consequently, the same routines can be used for the construction of intermediate $\mathbf{E}$ in both the AO and an arbitrary MO basis. The latter is particularly convenient since for many correlation methods different kinds of integrals, e.g., (oo|vo), (vo|vo), and (vv|vo) are required. Furthermore, the above expression permits an integral-direct formulation, as outlined in the following, which avoids the prohibitive storage requirements of the full ERI tensor before the transformation into the grid basis. The key idea is that the contraction of the ket side of the ERI tensor can be viewed as N_{grid} Coulomb matrix builds with slices of the joint collocation tensor $\mathbf{R}$, defined as $R^Q_{\lambda\sigma} = X^Q_{\lambda} X^Q_{\sigma}$, acting as the density matrix. Intermediate $\mathbf{E}$ in the AO basis from eq. 3 can then exemplarily be formed according to algorithm 1.

Algorithm 1 Coulomb Matrix Build-based Integral-direct Formation of $\mathbf{E}$ in the AO Basis

$R^P_{\mu\nu} \leftarrow X^P_{\mu} X^P_{\nu}$
$R^Q_{\lambda\sigma} \leftarrow X^Q_{\lambda} X^Q_{\sigma}$
for all Q **do**
    $\mathbf{J} \leftarrow \texttt{MakeJ}(\mathbf{R}^{(Q)})$ ▷ $R^{(Q)}_{\lambda\sigma}$ replaces $P_{\lambda\sigma}$ in the $\mathbf{J}$ build ▷ $\mathcal{O}(N^5)$
    for all P **do**
        $E^{PQ} \leftarrow \sum_{\mu\nu} R^{(P)}_{\mu\nu} J_{\mu\nu}$ ▷ $\mathcal{O}(N^4)$
    end for
end for

We note here, that for a memory efficient implementation the joint collocation tensor $\mathbf{R}$ should not be constructed explicitly. Instead, the required tensor slices $\mathbf{R}^{(Q)}$ can be constructed on-the-fly as a vector outer product of all elements of the $\mathbf{X}$ tensor belonging to that grid point, i.e., $\mathbf{R}^{(Q)} = \mathbf{X}^Q_{:} \bigotimes (\mathbf{X}^Q_{:})^{\mathrm{T}}$.

Together with the idea to reformulate the MO-THC equations in a density-based manner, the Coulomb matrix-based approach permits an efficient and simultaneous formation of all intermediates required for the integrals occurring in CC2/ADC(2) (see Section 2.3.1)

according to algorithm 2.

Algorithm 2 Coulomb Matrix Build-based Integral-direct Formation of $\mathbf{E}^{(\mathrm{oovo})}$, $\mathbf{E}^{(\mathrm{vovo})}$, and $\mathbf{E}^{(\mathrm{vvvo})}$

1: $\mathbf{X}^{(\mathrm{o})} \leftarrow \mathbf{XP}$ ▷ $\mathbf{P} \mathrel{\widehat{=}}$ occupied one-particle density matrix
2: $\mathbf{X}^{(\mathrm{v})} \leftarrow \mathbf{XQ}$ ▷ $\mathbf{Q} \mathrel{\widehat{=}}$ virtual one-particle density matrix
3: $\mathbf{R}^{(\mathrm{oo})} \leftarrow \mathbf{X}^{(\mathrm{o})} \otimes_c \mathbf{X}^{(\mathrm{o})}$ ▷ $\otimes_c$ denotes the column-wise Kronecker product
4: $\mathbf{R}^{(\mathrm{vo})} \leftarrow \mathbf{X}^{(\mathrm{v})} \otimes_c \mathbf{X}^{(\mathrm{o})}$
5: $\mathbf{R}^{(\mathrm{vv})} \leftarrow \mathbf{X}^{(\mathrm{v})} \otimes_c \mathbf{X}^{(\mathrm{v})}$
6: **for all** Q **do**
7: $\quad \mathbf{P}^{(\mathrm{vo})} \leftarrow \mathbf{R}^{(Q),(\mathrm{vo})} + (\mathbf{R}^{(Q),(\mathrm{vo})})^{\mathrm{T}}$
8: $\quad \mathbf{J}^{(\mathrm{vo})} \leftarrow \frac{1}{2} \times \texttt{MakeJ}(\mathbf{P}^{(\mathrm{vo})})$ ▷ $\mathcal{O}(N^5)$
9: $\quad$ **for all** P **do**
10: $\quad\quad E^{PQ,(\mathrm{oovo})} \leftarrow \sum_{\mu\nu} R_{\mu\nu}^{(P),(\mathrm{oo})} J_{\mu\nu}^{(\mathrm{vo})}$ ▷ $\mathcal{O}(N^4)$
11: $\quad\quad E^{PQ,(\mathrm{vovo})} \leftarrow \sum_{\mu\nu} R_{\mu\nu}^{(P),(\mathrm{vo})} J_{\mu\nu}^{(\mathrm{vo})}$ ▷ $\mathcal{O}(N^4)$
12: $\quad\quad E^{PQ,(\mathrm{vvvo})} \leftarrow \sum_{\mu\nu} R_{\mu\nu}^{(P),(\mathrm{vv})} J_{\mu\nu}^{(\mathrm{vo})}$ ▷ $\mathcal{O}(N^4)$
13: $\quad$ **end for**
14: **end for**

The key idea for an efficient implementation is to do the expensive formation of the **J** intermediate once in the ov space, since all integral types, i.e., (oo|vo), (vo|vo), and (vv|vo), share this as a common ket. We note here, that most routines for the construction of Coulomb-type matrices assume the density to be symmetric. This is not the case for slices of the joint collocation tensor $\mathbf{R}^{(\mathrm{vo})}$, which is why the transpose is added in line 7 and the resulting matrix is scaled by a factor of 1/2. Based on the resulting **J** intermediate, the final intermediates **E** for all integral types can be formed simultaneously without further integral evaluations. We also note, that the frozen-core approximation can easily be included in this formulation by simply using the frozen-core density matrix for the occupied space.

To lower the formal scaling behavior, the resolution-of-the-identity approximation (RI)[31–34] can be inserted into eq. 10, which allows to perform the grid-projection of the bra and the ket side of the ERI tensor separately at reduced scaling. Inserting the RI approximation into eq. 10 leads to

$$E^{PQ} = \sum_{\alpha\beta\gamma} Y_\beta^P \, [\mathbf{V}^{-\frac{1}{2}}]_{\beta\alpha} [\mathbf{V}^{-\frac{1}{2}}]_{\alpha\gamma} \, Y_\gamma^Q = \sum_{\mu'\nu'\lambda'\sigma'} X_{\mu'}^P X_{\nu'}^P (\mu'\nu'|\beta) [\mathbf{V}^{-\frac{1}{2}}]_{\beta\alpha} [\mathbf{V}^{-\frac{1}{2}}]_{\alpha\gamma} (\gamma|\lambda'\sigma') X_{\lambda'}^Q X_{\sigma'}^Q \tag{12}$$

where $\mathbf{V}$ is the two-center RI integral tensor. Intermediate $\mathbf{Y}$ is given by

$$Y_\beta^P = \sum_{\mu'\nu'} X_{\mu'}^P X_{\nu'}^P (\mu'\nu'|\beta) \tag{13}$$

and represents one side of the grid-projected ERI tensor. Like for the $\mathbf{E}$ intermediate, the formally quartic scaling formation of the $\mathbf{Y}$ intermediate can be done in an integral-direct fashion. The final factorization then becomes

$$(pq|rs) = \sum_{PQ} \sum_{\gamma} X_p^P X_q^P \Gamma_\alpha^P \Gamma_\alpha^Q X_r^Q X_s^Q \tag{14}$$

with $\mathbf{\Gamma}$, representing one half of the $\mathbf{Z}$ tensor, defined as

$$\Gamma_\alpha^P = \sum_{P'} \sum_{\beta} [\mathbf{S}^{-1}]^{PP'} Y_\beta^{P'} [\mathbf{V}^{-\frac{1}{2}}]_{\beta\alpha} \tag{15}$$

Instead of employing routines for the construction of Coulomb matrices, for the $\mathbf{Y}$ intermediate existing routines for the contraction of density matrices with three-center RI integrals can be used. Amongst these routines, variants optimized for the contraction of multiple densities, such as the J-engine approach to SOS-RI-MP2 by Maurer *et al.*[59] or the RI-J implementation by Kussmann *et al.*[60] are employed since N_{grid} Coulomb matrix builds need to be performed for each $\mathbf{Y}$ intermediate. While these algorithms provide performance improvements over a naïve implementation, in which the Coulomb matrix kernel is simply invoked N_{grid} times, an optimized integral kernel for this kind of contraction is certainly favorable.

2.2.3 Efficient Integral-direct Algorithm for the Y Intermediate

Instead of relying on repetitive J-engine or RI-J based evaluations of the Coulomb potential for many density-like matrices, a more efficient algorithm is proposed inspired by our previous optimal-batching scheme[61] for evaluating correlation energies on the random phase approximation (RPA) level of theory. In the integral-direct variant (algorithm 3) the necessary 3-center-2-electron (3c2e) integrals $(\mu'\nu'|\alpha)$ and the vector outer products $\mathbf{R}$ are computed on-the-fly during the formation of the $\mathbf{Y}$-intermediate removing the unfavorable $\mathcal{O}(N^3)$ memory complexity associated with storing the full third-order tensors. The following discussion is exemplariliy carried out for the virtual-occupied subspace but is applicable to all required $\mathbf{\Gamma}$ intermediates.

Algorithm 3 Integral-direct formation of $\mathbf{Y}$

Pre-process $\mathbf{X}^{(o)}$, $\mathbf{X}^{(v)}$ (Pure $\rightarrow$ Cartesian) ▷ $\mathcal{O}(N^2)$
for all P-batches **do** ▷ OpenMP parallel
  for all $\mu'\nu'$-batches **do** ▷ only sign. function-pairs; OpenMP parallel
    for all $\mu'\nu'$ in batch **do**
      for all P in batch **do**
        $R^{P,(\mathrm{vo})}_{\mu'\nu'} \leftarrow X^{P,(\mathrm{v})}_{\mu'} X^{P,(\mathrm{o})}_{\nu'} + \mathrm{transpose}$ ▷ $\mathcal{O}(N^3)$
      end for
    end for
    for all α-batches **do**
      for all $\mu'\nu'$-shell-pairs in batch **do**
        for all α-shells in batch **do**
          Compute 3c2e integrals $(\mu'\nu'|\alpha)$ ▷ shell-triplet wise; $\mathcal{O}(N^3)$
        end for
      end for
      for all α in batch **do**
        for all P in batch **do**
          $Y^P_\alpha \mathrel{+}= \sum_{\mu'\nu'} R^{P,(\mathrm{vo})}_{\mu'\nu'} (\mu'\nu'|\alpha)$ ▷ BLAS-3; $\mathcal{O}(N^4)$
        end for
      end for
    end for
  end for
end for
Post-process $\mathbf{Y}$ (Cartesian $\rightarrow$ Pure, reordering, scale by $\frac{1}{2}$) ▷ $\mathcal{O}(N^2)$

The naïve application of the optimization scheme of Ref. 61 would predict minimal batch-

sizes for the function-pair index $\mu'\nu'$ and the auxiliary basis function index α but maximal batch-sizes for the quadrature point index P, since the more points P are included per batch, the more often any computed given 3c2e integral $(\mu'\nu'|\alpha)$ can be reused for the computation of $\mathbf{Y}$. In practice, however, there are diminishing returns beyond 1000 P points per batch, so we decided to round to the nearest power of 2, i.e., employing 1024 P points per batch. The batch sizes for α and $\mu'\nu'$ are be chosen as 96, which is as small as possible, while still allowing for an efficient execution of the BLAS-3 linear algebra routines, here matrix-matrix multiplications, within the formation of $\mathbf{Y}$ in line 17. In practice, the precise batch sizes of each batch slightly deviate from 96 to match a multiple of the number of functions/function-pairs for the respective l-quantum numbers of the shells/shell-pairs within a batch, because the 3c2e integral evaluation is most efficient if operating on full shell-triplets. This approach leads to batches with ∼10000 elements for $(\mu'\nu'|\alpha)$ and ∼100000 elements for $R^{P,(\mathrm{ov})}_{\mu'\nu'}$, making the algorithm cache-friendly, i.e., all necessary quantities can be stored in temporary static random access memory (SRAM) storage (cache) close to the processing units, even for large systems. Moreover, we always aim for multiples of 16 for the innermost loops and order each participating tensor such that the leading index matches the innermost loop. Both design decisions improve the efficiency of memory accesses (cache-lines) and are very favorable for single instruction multiple data (SIMD) vector execution.

In particular, the 3c2e integrals are stored with the auxiliary-shell index as the leading index, so that the 3c2e integral evaluation can make optimal use of SIMD vector routines parallelizing over shell-triplets, i.e., each SIMD-thread handles a separate shell-triplet. For the most efficient use of SIMD-vector routines, the auxiliary basis set is considered fully uncontracted, since varying numbers of primitive Gaussian basis functions per shell would otherwise interfere with vectorization, which requires an identical workload for each thread to be efficient. In practice, this is of little concern, since the auxiliary basis sets used for RI-fitting of electron-correlation energies (e.g., the Dunning RI basis sets[62–64] employed in Section 4) are usually completely – or at least mostly – uncontracted already. In addition, the

transformation from Cartesian to pure (spherical harmonics) basis functions is not performed at the 3-center integral level, instead the whole $\mathbf{Y}$-build is carried out in the Cartesian basis so that only input and output need to be transformed, avoiding any transformations of third-order tensors.

The 3c2e integrals are evaluated using symbolically optimized Obara-Saika[65,66] recursion relations, similar to the integral kernels used for the 3-center-1-electron (3c1e) integrals within our seminumerical exchange method (sn-LinK),[67–69] but adjusted for 2-electron integrals, i.e., by including recurrence relations for both the AO shell-pair and the auxiliary shell. That is, for any given l-quantum number combination the recursion relations are fully expanded symbolically for each final primitive Cartesian integral within the shell-triplet until each integral is solely expressed in terms of primitive Boys integrals. Subsequently the entire set of equations is optimized by removing redundant sub-expressions within the shell-triplet using common-sub-expression-elimination (CSE) as provided by the SymPy[70] package.

Overall, algorithm 3 formally scales as $\mathcal{O}(N^4)$ and the matrix-matrix-multiplication for the formation of $\mathbf{Y}$ in line 17 is by far the slowest step. This formal scaling is easily reduced to asymptotically $\mathcal{O}(N^3)$ by exploiting the sparsity of the function-pairs $\mu'\nu'$, i.e., only function-pairs belonging to significantly overlapping shell-pairs according to the Schwarz integral are considered. In addition, the batch-wise nature of the algorithm is also straightforward to OpenMP parallelize over multiple CPU cores using both the P-batch as well as the $\mu'\nu'$ batch index for parallelization. While P-batch execution is already embarrassingly parallel, parallelization over $\mu'\nu'$ requires special treatment of the race-condition associated with accumulation over that index. In practice, the workload is organized such that each thread accumulates as many $\mu'\nu'$-batches as possible in a thread-private buffer, so the serial (OpenMP critical section; mutually exclusive between threads) accumulation to the global $\mathbf{Y}$ needs to be performed as rarely as possible.

2.3 THC-CC2 and THC-ADC(2) for Ground and Excited States

2.3.1 Review of CC2 and ADC(2)

The scaled opposite-spin CC2 ground state energy in the THC approximation defined as

$$\begin{aligned} E^{\text{SOS-CC2}} &= \langle \text{HF}|\hat{H} + c_{\text{os}}[\hat{H}, T_2^{\text{os}}]|\text{HF}\rangle \\ &= E_{\text{HF}} + c_{\text{os}} \sum_{aibj} \sum_{\beta} \sum_{RS} t_{ai} t_{bj} \left[X_a^{R,(\text{vo})} X_i^{R,(\text{vo})} \Gamma_\beta^{R,(\text{vo})} \Gamma_\beta^{S,(\text{vo})} X_b^{S,(\text{vo})} X_j^{S,(\text{vo})} \right] \\ &- c_{\text{os}} \sum_{aibj} \hat{t}_{aibj}^{\text{os}} \left[\sum_{\beta} \sum_{RS} X_a^{R,(\text{vo})} X_i^{R,(\text{vo})} \Gamma_\beta^{R,(\text{vo})} \Gamma_\beta^{S,(\text{vo})} X_b^{S,(\text{vo})} X_j^{S,(\text{vo})} \right] \end{aligned} \tag{16}$$

where $\hat{H}$ is the similarity-transformed Hamiltonian and T_2^{os} is the two-electron excitation operator acting on two electrons with different spins.[27,29] The cluster amplitudes are determined by solving the coupled cluster equations, defined by

$$\begin{aligned} 0 = \Omega_{\mu_1} &= \langle \mu_1|\hat{H} + c_{\text{os}}[\hat{H}, T_2^{\text{os}}]|\text{HF}\rangle = (\epsilon_a - \epsilon_i) t_{ai} + \Omega_{ai}^{\text{G}} + \Omega_{ai}^{\text{H}} + \Omega_{ai}^{\text{I}} + \Omega_{ai}^{\text{J}} \\ &= (\epsilon_a - \epsilon_i) t_{ai} + c_{\text{os}} \sum_{cbj} \hat{t}_{cibj}^{\text{os}} \left[\sum_{\beta} \sum_{RS} X_j^{R,(\text{vo})} X_b^{R,(\text{vo})} \Gamma_\beta^{R,(\text{vo})} \Gamma_\beta^{S,(\text{vv})} \hat{X}_a^{S,(\text{vv}} X_c^{S,(\text{vv})} \right] \\ &- c_{\text{os}} \sum_{kbj} \hat{t}_{akbj}^{\text{os}} \left[\sum_{\beta} \sum_{RS} X_j^{R,(\text{vo})} X_b^{R,(\text{vo})} \Gamma_\beta^{R,(\text{vo})} \Gamma_\beta^{S,(\text{oo})} X_k^{S,(\text{vo})} \hat{X}_i^{S,(\text{vo})} \right] + c_{\text{os}} \sum_{bj} \hat{t}_{aibj}^{\text{os}} \hat{F}_{jb} + \hat{F}_{ai} \end{aligned} \tag{17}$$

$$\begin{aligned} 0 = \Omega_{\mu_2} &= \langle \mu_2^{\text{os}}|\hat{H} + [F, T_2^{\text{os}}]|\text{HF}\rangle = \Omega_{aibj}^{E} + \Omega_{aibj}^{F} \\ &= (\epsilon_a - \epsilon_i + \epsilon_b - \epsilon_j) \hat{t}_{aibj}^{\text{os}} + \left[\sum_{\alpha} \sum_{PQ} \hat{X}_a^{P,(\text{vo})} \hat{X}_i^{P,(\text{vo})} \Gamma_\alpha^{P,(\text{vo})} \Gamma_\alpha^{Q,(\text{vo})} \hat{X}_b^{Q,(\text{vo})} \hat{X}_j^{Q,(\text{vo})} \right] \end{aligned} \tag{18}$$

The Fock matrices $\hat{\mathbf{F}}$ are computed using the integral-direct RI-J[71] and sn-LinK[67–69] kernels to form the Coulomb and exchange terms with high efficiency. The explicit expressions are provided in the literature.[29,72]

The opposite-spin scaling factor is set to $c_{\text{os}} = 1.3$, as for SOS-MP2.[27,29] The solution of

equations 16-18 scales as $\mathcal{O}(N^3)$ for the MO-based THC-SOS-CC2 formulation.[55] The MO energies in the denominator of the double amplitudes can be decoupled using the Laplace technique

$$\frac{1}{\epsilon_{aibj}} = \int_0^\infty e^{-\epsilon_{aibj}} dt = \sum_\tau^n w_\tau e^{-\epsilon_{aibj} t_\tau} \tag{19}$$

to rewrite eq. 18 as

$$\begin{aligned} \hat{t}^{\mathrm{os}}_{aibj} &= -\sum_\tau w_\tau \sum_\alpha \sum_{PQ} \hat{X}^{P,(\mathrm{vo})}_a \hat{X}^{P,(\mathrm{vo})}_i \Gamma^{P,(\mathrm{vo})}_\alpha \Gamma^{Q,(\mathrm{vo})}_\alpha \hat{X}^{Q,(\mathrm{vo})}_b \hat{X}^{Q,(\mathrm{vo})}_j e^{-\epsilon_{ai} t_\tau} e^{-\epsilon_{bj} t_\tau} \\ &= -\sum_\tau \sum_\alpha \sum_{PQ} \hat{X}^{P,(\mathrm{vo})}_{a,\tau} \hat{X}^{P,(\mathrm{vo})}_{i,\tau} \Gamma^{P,(\mathrm{vo})}_\alpha \Gamma^{Q,(\mathrm{vo})}_\alpha \hat{X}^{Q,(\mathrm{vo})}_{b,\tau} \hat{X}^{Q,(\mathrm{vo})}_{j,\tau} \end{aligned} \tag{20}$$

The THC $\mathbf{X}$ matrices in eq. 16-20 are transformed using the transformation matrices

$$\Lambda^p_{\mu a} = C_{\mu a} - \sum_i C_{\mu i} t_{ai} \qquad\qquad \Lambda^h_{\mu i} = C_{\mu i} + \sum_a C_{\mu a} t_{ai} \tag{21}$$

according to

$$\hat{X}^P_{a,\tau} = w_\tau^{\frac{1}{4}} \hat{X}^P_a e^{-\epsilon_a t_\tau} \qquad\qquad \hat{X}^P_a = \sum_\mu \Lambda^p_{\mu a} X^P_\mu \tag{22}$$

$$\hat{X}^P_{i,\tau} = w_\tau^{\frac{1}{4}} \hat{X}^P_i e^{\epsilon_i t_\tau} \qquad\qquad \hat{X}^P_i = \sum_\nu \Lambda^h_{\nu i} X^P_\nu \tag{23}$$

The singles amplitudes are obtained by inserting eq. 20 into eq. 17

$$-(\epsilon_a - \epsilon_i)t_{ai} = \Omega^{\mathrm{G}}_{ai} + \Omega^{\mathrm{H}}_{ai} + \Omega^{\mathrm{I}}_{ai} + \Omega^{\mathrm{J}}_{ai} \tag{24}$$

$$\Omega^{\mathrm{G}}_{ai} = -c_{\mathrm{os}} \sum_{\tau} \sum_{PS} \hat{X}^{P,(\mathrm{vo})}_{i,\tau} \hat{M}^{PS,(\mathrm{ovvv})}_{\tau} \hat{X}^{S,(\mathrm{vv})}_{a} \tag{25}$$

$$\Omega^{\mathrm{H}}_{ai} = c_{\mathrm{os}} \sum_{\tau} \sum_{PS} \hat{X}^{P,(\mathrm{vo})}_{a,\tau} \hat{N}^{PS,(\mathrm{vooo})}_{\tau} \hat{X}^{S,(\mathrm{oo})}_{i} \tag{26}$$

$$\Omega^{\mathrm{I}}_{ai} = -c_{\mathrm{os}} \sum_{\tau} \sum_{P} \hat{X}^{P,(\mathrm{vo})}_{a,\tau} \hat{X}^{P,(\mathrm{vo})}_{i,\tau} \hat{n}^{P,(\mathrm{vo})}_{\tau} \tag{27}$$

$$\Omega^{\mathrm{J}}_{ai} = \hat{F}_{ai} \tag{28}$$

The working equations of the intermediates in eq. 25-27 are provided in the SI. The evaluation of the MO-THC-SOS-CC2 correction to the ground state energy is then achieved with negligible computational cost as

$$E^{\text{SOS-CC2}} = c_{\mathrm{os}} \sum_{aibj} \sum_{\beta} \sum_{PQ} t_{ai} t_{bj} X^{R,(\mathrm{vo})}_{a} X^{R,(\mathrm{vo})}_{i} \Gamma^{R,(\mathrm{vo})}_{\beta} \Gamma^{S,(\mathrm{vo})}_{\beta} X^{S,(\mathrm{vo})}_{b} X^{S,(\mathrm{vo})}_{j} - c_{\mathrm{os}} \sum_{\alpha\beta} \hat{D}^{\alpha\beta}_{\tau} \hat{D}^{\alpha\beta}_{\tau} \tag{29}$$

which can also be used to get the simpler MO-THC-SOS-MP2 energy correction by simply setting $\mathbf{t}_{\mu_1}$ to zero.

The SOS-LR-CC2 excitation energies are obtained as eigenvalues of the Jacobian matrix, which is defined as the derivative of the vector functions (eq. 17 and 18) with respect to the cluster amplitudes[25] and is given by

$$\mathbf{A}^{\text{SOS-CC2}} = \begin{pmatrix} A_{\mu_1\nu_1} & A_{\mu_1\nu_2} \\ A_{\mu_2\nu_1} & A_{\mu_2\nu_2} \end{pmatrix} = \begin{pmatrix} \langle \mu_1 | [(\hat{H} + c_{\mathrm{os}}[\hat{H}, T^{\mathrm{os}}_2]), \tau_{\nu_1}] | HF \rangle & \langle \mu_1 | c_{\mathrm{os}}[\hat{H}, \tau^{\mathrm{os}}_{\nu_2}] | HF \rangle \\ \langle \mu^{\mathrm{os}}_2 | [\hat{H}, \tau_{\nu_1}] | HF \rangle & \delta_{\mu_2\nu_2}\epsilon_{\mu_2} \end{pmatrix} \tag{30}$$

where the diagonal double-double block ($A_{\mu_2\nu_2}$) is equal to $\epsilon_{aibj} = \epsilon_a - \epsilon_i + \epsilon_b - \epsilon_j$. From

eq. 30, secular matrices of simpler excited states methods are derived. The SOS-CIS(D_∞) approach introduced by Head-Gordon *et al.*[9] can be derived from the SOS-LR-CC2 theory by setting the singles part of the ground-state cluster amplitudes t_1 equal to zero, that is the similarity transformation of the Hamiltonian vanishes. The SOS-CIS(D_∞) Jacobi matrix is given by

$$\mathbf{A}^{\text{SOS-CIS}(D_\infty)} = \begin{pmatrix} \langle \mu_1 | [(H + c_{\text{os}}[H, T_2^{\text{os}}]), \tau_{\nu_1}] | HF \rangle & \langle \mu_1 | c_{\text{os}}[H, \tau_{\nu_2}^{\text{os}}] | HF \rangle \\ \langle \mu_2^{\text{os}} | [H, \tau_{\nu_1}] | HF \rangle & \delta_{\mu_2\nu_2}\epsilon_{\mu_2} \end{pmatrix} \tag{31}$$

where T_2^{os} are the MP2 double amplitudes. In addition, the secular matrix for the SOS-ADC(2) method is related to eq. 31 by the symmetrization[29,30,73]

$$\mathbf{A}^{\text{SOS-ADC(2)}} = \frac{1}{2}\left[\mathbf{A}^{\text{SOS-CIS}(D_\infty)} + (\mathbf{A}^{\text{SOS-CIS}(D_\infty)})^{\text{T}}\right] \tag{32}$$

As discussed by Krauter *et al.*,[30] it is important to derive the SOS-ADC(2) secular matrix from the SOS-CC2 Jabobian in order to reduce the dimension of the doubles-doubles block $A_{\mu_2\nu_2}$. In this work, we do not symmetrize the full CISD(D_∞) matrix but only the $A_{\mu_1\nu_1}$ block. That is we retain the non-hermiticity of the coupling blocks and only scale the $A_{\mu_1\nu_2}$ block by the c_{os} factor.[29] Using the diagonal form of the double-double block, we can obtain the doubles part of the excitation vector

$$R_{\mu_2}^m = -\frac{A_{\mu_2\nu_1}R_{\nu_1}}{\epsilon_{\gamma_2} - \bar{\omega}^m} \tag{33}$$

and solve the eigenvalue problem of SOS-LR-CC2 and SOS-ADC(2) in the single excitations manifold[29,72] given by

$$\left[A_{\mu_1\nu_1} - \frac{A_{\mu_1\gamma_2}A_{\gamma_2\nu_1}}{\epsilon_{\gamma_2} - \bar{\omega}}\right] R_{\nu_1} = A_{\mu_1\nu_1}^{\text{eff}}(\bar{\omega})R_{\nu_1} = \sigma_{\mu_1}(\bar{\omega}, R_{\nu_1}) = \bar{\omega}R_{\mu_1} \tag{34}$$

Notice that the effective $\mathbf{A}$ matrix is hermitian for ADC(2) and σ is the matrix-vector

product. In order to solve the nonlinear eq. 34, the solutions, i.e., the excitation energy $\bar{\omega}$ and eigenvector R_{μ_1} have to be found until self-consistency is reached. If the initial guess of the eigenvector and eigenvalue is close enough to the final results, a common choice for the solution of the nonlinear problem is an algorithm based on the direct inversion in the iterative subspace (DIIS) technique,[35,72,74] which was shown to be stable and rapidly convergent.[29,35] In addition, it has the advantage of being a single root algorithm, thus allowing to aim for high-lying excited states without converging all lower-lying states. On the contrary, if the initial guess is far from the converged CC2 or ADC(2) result, the eigenvalue and the eigenvector must be pre-optimized using an alternative algorithm. For this purpose, we use a modification of the Davidson algorithm,[72,75] leveraging the fact that a set of converged eigenvalues and eigenvectors will fulfill the linear generalized eigenproblem

$$\sum_{\mu_1\nu_1} R_{\mu_1} A^{\text{eff}}_{\mu_1\nu_1}(\bar{\omega}) R_{\nu_1} = \sum_{\mu_1} R_{\mu_1} \sigma_{\mu_1}(\bar{\omega}, R_{\nu_1}) = \sum_{\mu_1} \bar{\omega} R_{\mu_1} R_{\mu_1} \tag{35}$$

Both DIIS and Davidson procedures for CC2 and ADC(2) are described in literature[29,35,72,75] and will not be discussed here further. The time-determining step for the solution of the eigenvalue problem is the formation of the matrix-vector product:

$$\begin{aligned}\sigma_{ai}^{\text{SOS-CC2}} &= \sum_b \hat{F}_{ab} R_{bi} - \sum_j R_{aj} \hat{F}_{ji} + \bar{F}_{ai} - c_{\text{os}} \sum_b E_{ab} R_{bi} - c_{\text{os}} \sum_j R_{aj} E_{ji} \\ &\quad + \sigma_{ai}^{\text{G, (1)}}(R_{\mu_2}) + \sigma_{ai}^{\text{H, (1)}}(R_{\mu_2}) + \sigma_{ai}^{\text{I, (1)}}(R_{\mu_2}) \end{aligned} \tag{36}$$

$$\begin{aligned}\sigma_{ai}^{\text{SOS-ADC(2)}} &= (\epsilon_a - \epsilon_i) R_{ai} + \bar{F}_{ai} - c_{\text{os}} \sum_b E'_{ab} R_{bi} - c_{\text{os}} \sum_j R_{aj} E'_{ji} \\ &\quad + \sigma_{ai}^{\text{G, (2)}}(R_{\mu_2}) + \sigma_{ai}^{\text{H, (2)}}(R_{\mu_2}) + \sigma_{ai}^{\text{I, (2)}} \end{aligned} \tag{37}$$

Making use of the Laplace transformation of the energy denominator, the double part of the

singlet excitation vector can be rewritten as

$$R_{ij}^{ab}(\bar{\omega}) = -\sum_{\tau} e^{\bar{\omega} t_\tau} \sum_{PQ} \sum_{\alpha} \Bigg\{ \Big[\bar{X}_{a,\tau}^{P} \hat{X}_{i,\tau}^{P} + \hat{X}_{a,\tau}^{P} \bar{X}_{i,\tau}^{P} \Big] \Gamma_{\alpha}^{P} \Gamma_{\alpha}^{Q} \hat{X}_{b,\tau}^{Q} \hat{X}_{j,\tau}^{Q} + \Big[\bar{X}_{b,\tau}^{P} \hat{X}_{j,\tau}^{P} + \hat{X}_{b,\tau}^{P} \bar{X}_{j,\tau}^{P} \Big] \Gamma_{\alpha}^{P} \Gamma_{\alpha}^{Q} \hat{X}_{a,\tau}^{Q} \hat{X}_{i,\tau}^{Q} \Bigg\} \tag{38}$$

for which the state-specific THC $\bar{\mathbf{X}}$ matrices using the transformation matrices $\bar{\mathbf{\Lambda}}$

$$\bar{\Lambda}_{\mu a}^{p} = \sum_{i} C_{\mu i} R_{a i} \qquad\qquad \bar{\Lambda}_{\mu i}^{h} = \sum_{a} C_{\mu a} R_{a i} \tag{39}$$

are given according to

$$\bar{X}_{a,\tau}^{P} = w^{\frac{1}{4}} \bar{X}_{a}^{P} e^{-\epsilon_a t_\tau} \qquad\qquad \bar{X}_{a}^{P} = \sum_{\mu} X_{\mu}^{P} \bar{\Lambda}_{\mu a}^{p} \tag{40}$$

$$\bar{X}_{i,\tau}^{P} = w^{\frac{1}{4}} \bar{X}_{i}^{P} e^{\epsilon_i t_\tau} \qquad\qquad \bar{X}_{i}^{P} = \sum_{\mu} X_{\mu}^{P} \bar{\Lambda}_{\mu i}^{h} \tag{41}$$

Inserting eq. 38 into 36, reduced scaling expressions for the most time-consuming contributions can be formulated as

$$\begin{aligned} \sigma_{ai}^{\mathrm{G,\,(1)}} &= +c_{\mathrm{os}} \sum_{jbc} R_{ij}^{cb}(\bar{\omega}) \Bigg[\sum_{\beta} \sum_{RS} X_{j}^{R,(\mathrm{vo})} X_{b}^{R,(\mathrm{vo})} \Gamma_{\beta}^{R,(\mathrm{vo})} \Gamma_{\beta}^{S,(\mathrm{vv})} \hat{X}_{a}^{S,(\mathrm{vv})} X_{c}^{S,(\mathrm{vv})} \Bigg] \\ &= -c_{\mathrm{os}} \sum_{\tau} e^{\bar{\omega} t_\tau} \sum_{PS} \Big[\hat{X}_{i,\tau}^{P,(\mathrm{vo})} \bar{M}_{\tau}^{PS,(\mathrm{ovvv})} + \bar{X}_{i,\tau}^{P,(\mathrm{vo})} \hat{M}_{\tau}^{PS,(\mathrm{ovvv})} \Big] \hat{X}_{a}^{S,(\mathrm{vv})} = \sum_{S} \bar{Y}_{i}^{S,(\mathrm{vv})} \hat{X}_{a}^{S,(\mathrm{vv})} \end{aligned} \tag{42}$$

$$\begin{aligned} \sigma_{ai}^{\mathrm{H,\,(1)}} &= -c_{\mathrm{os}} \sum_{jbk} R_{kj}^{ab}(\bar{\omega}) \Bigg[\sum_{\beta} \sum_{RS} X_{j}^{R,(\mathrm{vo})} X_{b}^{R,(\mathrm{vo})} \Gamma_{\beta}^{R,(\mathrm{vo})} \Gamma_{\beta}^{S,(\mathrm{oo})} X_{k}^{S,(\mathrm{vv})} X_{i}^{S,(\mathrm{oo})} \Bigg] \\ &= +c_{\mathrm{os}} \sum_{\tau} e^{\bar{\omega} t_\tau} \sum_{PS} \Big[\bar{X}_{a,\tau}^{P,(\mathrm{vo})} \hat{N}_{\tau}^{PS,(\mathrm{vooo})} + \hat{X}_{a,\tau}^{P,(\mathrm{vo})} \bar{N}_{\tau}^{PS,(\mathrm{vooo})} \Big] \hat{X}_{i}^{S,(\mathrm{oo})} = \sum_{S} \bar{Y}_{a}^{S,(\mathrm{oo})} \hat{X}_{i}^{S,(\mathrm{oo})} \end{aligned} \tag{43}$$

where the contained intermediates are given by

$$\begin{aligned}
\bar{M}_{\tau}^{PS,(\mathrm{ovvv})} &= \bar{M}_{\tau,(1)}^{PS,(\mathrm{ovvv})} + \bar{M}_{\tau,(2)}^{PS,(\mathrm{ovvv})} \\
&= \hat{B}_{\tau}^{PS,(\mathrm{ovvv})}\bar{D}_{\tau}^{PS,(\mathrm{ovvv})} + \bar{B}_{\tau}^{PS,(\mathrm{ovvv})}\hat{D}_{\tau}^{PS,(\mathrm{ovvv})} \qquad (44) \\
\bar{N}_{\tau}^{PS,(\mathrm{vooo})} &= \bar{N}_{\tau,(1)}^{PS,(\mathrm{vooo})} + \bar{N}_{\tau,(2)}^{PS,(\mathrm{vooo})} \\
&= \hat{A}_{\tau}^{PS,(\mathrm{vooo})}\bar{D}_{\tau}^{PS,(\mathrm{vooo})} + \bar{A}_{\tau}^{PS,(\mathrm{vooo})}\hat{D}_{\tau}^{PS,(\mathrm{vooo})} \qquad (45) \\
\bar{Y}_{i}^{S,(\mathrm{vv})} &= -c_{\mathrm{os}}\sum_{\tau} e^{\bar{\omega}t_{\tau}} \sum_{P}\left[\hat{X}_{i,\tau}^{P,(\mathrm{vo})}\bar{M}_{\tau}^{PS,(\mathrm{ovvv})} + \bar{X}_{i,\tau}^{P,(\mathrm{vo})}\hat{M}_{\tau}^{PS,(\mathrm{ovvv})}\right] \qquad (46) \\
\bar{Y}_{a}^{S,(\mathrm{oo})} &= +c_{\mathrm{os}}\sum_{\tau} e^{\bar{\omega}t_{\tau}} \sum_{P}\left[\bar{X}_{a,\tau}^{P,(\mathrm{vo})}\hat{N}_{\tau}^{PS,(\mathrm{vooo})} + \hat{X}_{a,\tau}^{P,(\mathrm{vo})}\bar{N}_{\tau}^{PS,(\mathrm{vooo})}\right] \qquad (47)
\end{aligned}$$

The contribution $\sigma^{\mathrm{I},\,(1)}$ is computed as:

$$\begin{aligned}
\sigma_{ai}^{\mathrm{I},\,(1)} &= +c_{\mathrm{os}}\sum_{bj} t_{aibj}^{(os)}\bar{F}_{jb} + \sum_{bj} c_{\mathrm{os}} R_{ij}^{ab}(\bar{\omega})\hat{F}_{jb} \\
&= -c_{\mathrm{os}}\sum_{\tau} e^{\bar{\omega}t_{\tau}} \sum_{P}\left[\bar{X}_{a,\tau}^{P,(\mathrm{vo})}\hat{X}_{i,\tau}^{P,(\mathrm{vo})} + \hat{X}_{a,\tau}^{P,(\mathrm{vo})}\bar{X}_{i,\tau}^{P,(\mathrm{vo})}\right]\hat{I}_{\tau}^{P,(\mathrm{vo})} - c_{\mathrm{os}}\sum_{\tau}\sum_{P}\hat{X}_{a}^{P,\tau}\hat{X}_{i}^{P,\tau}\bar{I}_{\tau,(1)}^{P,(\mathrm{vo})}
\end{aligned} \qquad (48)$$

with

$$\bar{I}_{\tau,(1)}^{P,(\mathrm{vo})} = \sum_{bj}\hat{X}_{b,\tau}^{P}\hat{X}_{j,\tau}^{P}\bar{F}_{jb} \qquad (49)$$

As for the ground state, the Fock-like terms

$$\bar{F}_{ai} = \sum_{ck}[2(ai\hat{|}kc) - (ac\hat{|}ki)]R_{ck} \qquad \bar{F}_{ld} = \sum_{ck}[2(ld\hat{|}kc) - (lc\hat{|}kd)]R_{ck} \qquad (50)$$

are not reformulated using the THC factorization. Notice that, by applying the THC decomposition to eq. 37, a similar expressions for the SOS-ADC(2) term is obtained. In fact, the contributions $\boldsymbol{\sigma}^{\mathrm{G},(2)}$ and $\boldsymbol{\sigma}^{\mathrm{H},(2)}$ are obtained from eq. 42 and 43, respectively, by simply

setting $\mathbf{t}_{\mu_1}$ amplitudes to zero. The contribution $\boldsymbol{\sigma}^{\mathrm{I},(2)}$ is computed according to

$$\begin{aligned}\sigma_{ai}^{\mathrm{I},\,(2)} &= +\frac{c_{\mathrm{os}}}{2}\sum_{bj} t_{aibj}^{(os)}\bar{F}_{jb} + \frac{c_{\mathrm{os}}}{2}\sum_{bj}[2(ia\hat{|}jb) - (ib\hat{|}ja)]\Big[\sum_{ck} t_{ckbj}^{(os)} R_{ck}\Big] \\ &= -\frac{c_{\mathrm{os}}}{2}\sum_{\tau}\sum_{P} X_a^{P,\tau} X_i^{P,\tau}\bar{I}_{\tau,(1)}^{P,(\mathrm{vo})} - \frac{c_{\mathrm{os}}}{2}\sum_{bj}[2(ia|jb) - (ib|ja)]\bar{I}_{bj} \end{aligned} \tag{51}$$

where

$$\bar{I}_{bj} = \sum_{P}\sum_{\tau} X_{b,\tau}^{P} X_{j,\tau}^{P}\bar{I}_{\tau,(2)}^{P,(\mathrm{vo})} \tag{52}$$

$$\bar{I}_{\tau,(2)}^{P,(\mathrm{vo})} = \sum_{bj} X_{c,\tau}^{P} X_{k,\tau}^{P} R_{ck} \tag{53}$$

and $\bar{I}_{\tau,(1)}^{P,(\mathrm{vo})}$ is computed as in eq. 49 by setting $\hat{X}_a^P = X_a^P$ and $\hat{X}_i^P = X_i^P$. The explicit expressions for $\mathbf{E}$ and $\mathbf{E}' = \frac{1}{2}(\mathbf{E} + \mathbf{E}^\dagger)$ in eq. 36 and 37, as well as the programmable equations for the MO-based matrix-vector product are provided in the SI.

2.3.2 Reformulation of the Ground State Equations

As demonstrated in our previous work on RI-SOS-CC2,[38] the equations for the ground state energy can be reformulated in a local basis and hence the intermediates can be expressed in terms of the occupied and virtual one-electron densities

$$P_{\mu\nu} = \sum_{i} C_{\mu i} C_{\nu i} \qquad\qquad Q_{\mu\nu} = \sum_{a} C_{\mu a} C_{\nu a} \tag{54}$$

in order to benefit from the locality of the electronic structure. Despite decreasing the scaling with the system size for the evaluation of most intermediates, the use of the AO basis increases the scaling with the basis set size for a given system. To counteract this, the Cholesky decomposition of the occupied ground state density matrix with complete

pivoting[76,77] is be applied

$$P_{\mu\nu} = \sum_{\underline{i}} L_{\mu\underline{i}} L_{\nu\underline{i}} \tag{55}$$

as well as the idempotency relation of the occupied and virtual pseudo-density matrices $\mathbf{P}^\tau$ and $\mathbf{Q}^\tau$

$$P^\tau_{\mu\nu} = w^{\frac{1}{4}} \sum_i C_{\mu i} C_{\nu i} e^{\epsilon_i t_\tau} \tag{56}$$

$$Q^\tau_{\mu\nu} = w^{\frac{1}{4}} \sum_a C_{\mu a} C_{\nu a} e^{-\epsilon_a t_\tau} \tag{57}$$

$$P^\tau_{\mu\nu} = \sum_{\sigma\lambda} P^\tau_{\mu\sigma} S_{\sigma\lambda} P_{\lambda\nu} = \sum_{\sigma\lambda\underline{i}} P^\tau_{\mu\sigma} S_{\sigma\lambda} L_{\lambda\underline{i}} L_{\nu\underline{i}} \tag{58}$$

$$Q^\tau_{\mu\nu} = \sum_{\sigma\lambda} Q^\tau_{\mu\sigma} S_{\sigma\lambda} Q_{\lambda\nu} \tag{59}$$

For the solution of the SOS-CC2 equations, another set of asymmetric one-electron density matrices is generated from the T1-transformed coefficients:

$$\hat{Q}_{\mu\nu} = \sum_d C_{\mu d} \Lambda^p_{\nu d} = Q_{\mu\nu} - \sum_{\mu'\sigma\lambda\nu'} Q_{\mu\mu'} S_{\mu'\sigma} t_{\sigma\lambda} S_{\lambda\nu'} P_{\nu'\nu} \tag{60}$$

$$\hat{Q}^\tau_{\mu\nu} = \sum_d w^{\frac{1}{4}}_\tau C_{\mu d} e^{-\epsilon_d t_\tau} \Lambda^p_{\nu d} = Q^\tau_{\mu\nu} - \sum_{\mu'\sigma\lambda\nu'} Q^\tau_{\mu\mu'} S_{\mu'\sigma} t_{\sigma\lambda} S_{\lambda\nu'} P_{\nu'\nu} \tag{61}$$

$$\begin{aligned} \hat{P}_{\mu\nu} &= \sum_l \Lambda^h_{\mu l} C_{\nu l} = P_{\mu\nu} + \sum_{\mu'\sigma\lambda\nu'} Q_{\mu\mu'} S_{\mu'\sigma} t_{\sigma\lambda} S_{\lambda\nu'} P_{\nu'\nu} \\ &= \sum_{\underline{l}} \left(L_{\mu\underline{l}} + \sum_{\mu'\sigma\lambda\nu'} Q_{\mu\mu'} S_{\mu'\sigma} t_{\sigma\lambda} S_{\lambda\nu'} L_{\nu'\underline{l}} \right) L_{\nu\underline{l}} = \hat{P}_{\mu\underline{l}} L_{\nu\underline{l}} \end{aligned} \tag{62}$$

$$\begin{aligned} \hat{P}^\tau_{\mu\nu} &= \sum_i w^{\frac{1}{4}}_\tau \Lambda^h_{\mu i} e^{(\epsilon_i) t_\tau} C_{\nu i} \\ &= \sum_{\underline{i}} \left[\sum_{\sigma'\lambda'} \sum_{\underline{j}} \left(L_{\mu\underline{j}} + \sum_{\nu'\sigma\lambda\nu''} Q_{\mu\nu'} S_{\nu'\sigma} t_{\sigma\lambda} S_{\lambda\nu''} L_{\nu''\underline{j}} \right) L_{\sigma'\underline{j}} S_{\sigma'\lambda'} P^\tau_{\lambda'\underline{i}} \right] L_{\nu\underline{i}} \end{aligned} \tag{63}$$

To obtain an expression for the singles amplitudes in the AO basis, eq. 17 in the MO basis is back-transformed to the AO basis according to

$$\Omega_{\mu\nu} = \sum_{ai} C_{\mu a}(\Omega^{\mathrm{G}}_{ai} + \Omega^{\mathrm{H}}_{ai} + \Omega^{\mathrm{I}}_{ai} + \Omega^{\mathrm{J}}_{ai})C_{\nu i} = \Omega^{\mathrm{G}}_{\mu\nu} + \Omega^{\mathrm{H}}_{\mu\nu} + \Omega^{\mathrm{I}}_{\mu\nu} + \Omega^{\mathrm{J}}_{\mu\nu} \tag{64}$$

for which the one-electron density matrices in eq. 54-63 permit to rewrite Ω_{μ_1} as

$$\begin{aligned}
\Omega^{\mathrm{G}}_{\mu\nu} &= \sum_{\underline{i}} \Omega^{\mathrm{G}}_{\mu\underline{i}} L_{\nu\underline{i}} = \sum_{\underline{i}} \left[-c_{\mathrm{os}} \sum_{\tau} \sum_{PS} \sum_{\mu'} \hat{X}^{P,(\mathrm{vo})}_{\underline{i},\tau} \hat{M}^{PS,(\mathrm{ovvv})}_{\tau} X^{S,(\mathrm{vv})}_{\mu'} \hat{Q}_{\mu\mu'} \right] L_{\nu\underline{i}} = \\
&= \sum_{\underline{i}} \left[-c_{\mathrm{os}} \sum_{S} \hat{Q}_{\mu\mu'} X^{S,(\mathrm{vv})}_{\mu'} \hat{Y}^{S,(\mathrm{vv})}_{\underline{i}} \right] L_{\nu\underline{i}} \qquad (65) \\
\Omega^{\mathrm{H}}_{\mu\nu} &= \sum_{\underline{i}} \Omega^{\mathrm{H}}_{\mu\underline{i}} L_{\nu\underline{i}} = \sum_{\underline{i}} \left[c_{\mathrm{os}} \sum_{\tau} \sum_{PS} \hat{X}^{P,(\mathrm{vo})}_{\mu,\tau} \hat{N}^{PS,(\mathrm{vooo})}_{\tau} \hat{X}^{S,(\mathrm{oo})}_{\underline{i}} \right] L_{\nu\underline{i}} \\
&= \sum_{\underline{i}} \left[c_{\mathrm{os}} \sum_{S} \hat{Y}^{Q,(\mathrm{oo})}_{\mu} \hat{X}^{S,(\mathrm{oo})}_{\underline{i}} \right] L_{\nu\underline{i}} \qquad (66) \\
\Omega^{\mathrm{I}}_{\mu\nu} &= \sum_{\underline{i}} \Omega^{\mathrm{I}}_{\mu\underline{i}} L_{\nu\underline{i}} = \sum_{\underline{i}} \left[-c_{\mathrm{os}} \sum_{\tau} \sum_{P} \hat{X}^{P,(\mathrm{vo})}_{\mu,\tau} \hat{X}^{P,(\mathrm{vo})}_{\underline{i},\tau} \hat{n}^{P,(\mathrm{vo})}_{\tau} \right] L_{\nu\underline{i}} \qquad (67) \\
\Omega^{\mathrm{J}}_{\mu\nu} &= \sum_{\underline{i}} \Omega^{\mathrm{J}}_{\mu\underline{i}} L_{\nu\underline{i}} = \sum_{\underline{i}} \left[\hat{Q}_{\mu\mu'} \hat{F}_{\mu'\nu'} \hat{P}_{\nu'\underline{i}} \right] L_{\nu\underline{i}} \qquad (68)
\end{aligned}$$

The $\mathbf{X}$ matrices are transformed with a computational effort scaling as $\mathcal{O}(N)$, by contraction with the T1-transformed one-electron densities:

$$\hat{X}^{P}_{\underline{i}} = \sum_{\mu'} X^{P}_{\mu'} \hat{P}_{\mu'\underline{i}} \tag{69}$$

$$\hat{X}^{P}_{\mu,\tau} = \sum_{\mu'} \hat{Q}^{\tau}_{\mu\mu'} X^{P}_{\mu'} \tag{70}$$

$$\hat{X}^{P}_{\underline{i},\tau} = \sum_{\mu'} X^{P}_{\mu'} \hat{P}^{\tau}_{\mu'\underline{i}} \tag{71}$$

The working equations in the Cholesky basis are provided in Table 1 together with the

asymptotic computational scaling of each step.

Table 1: Programmable equations of the intermediates for the solution of the CDD-THC-SOS-CC2/MP2 equations. Throughout this table Einstein's summation convention is used.

	Intermediates	Asymptotic Scaling
(a)	$\hat{A}_{\tau}^{QR,(\mathrm{vovo})} = \hat{X}_{\underline{i},\tau}^{Q,(\mathrm{vo})} X_{\underline{i}}^{R,(\mathrm{vo})}$	$\mathcal{O}(N)$
(b)	$\hat{B}_{\tau}^{QR,(\mathrm{vovo})} = \hat{X}_{\mu,\tau}^{Q,(\mathrm{vo})} X_{\mu}^{R,(\mathrm{vo})}$	$\mathcal{O}(N)$
(c)	$\hat{C}_{\tau}^{QR,(\mathrm{vovo})} = \hat{A}^{QR,(\mathrm{vovo})} \hat{B}^{QR,(\mathrm{vovo})}$	$\mathcal{O}(N)$
(d)	$\hat{D}_{\tau}^{\alpha\beta} = \Gamma_{\alpha}^{Q,(\mathrm{vo})} \hat{C}_{\tau}^{QR,(\mathrm{vovo})} \Gamma_{\beta}^{R,(\mathrm{vo})}$	$\mathcal{O}(N^3)$
(e)	$\hat{D}_{\tau}^{PS,(\mathrm{ovvv})} = \Gamma_{\alpha}^{P,(\mathrm{vo})} \hat{D}_{\tau}^{\alpha\beta} \Gamma_{\beta}^{S,(\mathrm{vv})}$	$\mathcal{O}(N^3)$
(f)	$\hat{D}_{\tau}^{PS,(\mathrm{vooo})} = \Gamma_{\alpha}^{P,(\mathrm{vo})} \hat{D}_{\tau}^{\alpha\beta} \Gamma_{\beta}^{S,(\mathrm{oo})}$	$\mathcal{O}(N^3)$
(e')	$\hat{D}_{\tau}^{PS,(\mathrm{ovvv})} = Z^{PQ,(\mathrm{vovo})} \hat{C}_{\tau}^{QR,(\mathrm{vovo})} Z^{RS,(\mathrm{ovvv})}$	$\mathcal{O}(N^2)$
(f')	$\hat{D}_{\tau}^{PS,(\mathrm{vooo})} = Z^{PQ,(\mathrm{vovo})} \hat{C}_{\tau}^{QR,(\mathrm{vovo})} Z^{RS,(\mathrm{vooo})}$	$\mathcal{O}(N^2)$
(g)	$\hat{A}_{\tau}^{PS,(\mathrm{vooo})} = \hat{X}_{\underline{i},\tau}^{P,(\mathrm{vo})} X_{\underline{i}}^{S,(\mathrm{oo})}$	$\mathcal{O}(N)$
(h)	$\hat{B}_{\tau}^{PS,(\mathrm{ovvv})} = \hat{X}_{\mu,\tau}^{P,(\mathrm{vo})} X_{\mu}^{S,(\mathrm{vv})}$	$\mathcal{O}(N)$
(i)	$\hat{M}_{\tau}^{PS,(\mathrm{ovvv})} = \hat{D}_{\tau}^{PS,(\mathrm{ovvv})} \hat{B}_{\tau}^{PS,(\mathrm{ovvv})}$	$\mathcal{O}(N)$
(j)	$\hat{N}_{\tau}^{PS,(\mathrm{vooo})} = \hat{D}_{\tau}^{PS,(\mathrm{vooo})} \hat{A}_{\tau}^{PS,(\mathrm{vooo})}$	$\mathcal{O}(N)$
(k)	$\hat{Y}_{\mu}^{S,(\mathrm{oo})} = \hat{X}_{\mu,\tau}^{P,(\mathrm{vo})} \hat{N}_{\tau}^{PS,(\mathrm{vooo})}$	$\mathcal{O}(N)$
(l)	$\hat{Y}_{\underline{i}}^{S,(\mathrm{vv})} = \hat{X}_{i,\tau}^{P,(\mathrm{vo})} \hat{M}_{\tau}^{PS,(\mathrm{ovvv})}$	$\mathcal{O}(N)$
(m)	$\hat{I}_{j,\tau}^{P,(\mathrm{ov})} = \hat{X}_{\mu,\tau}^{P,(\mathrm{vo})} \hat{F}_{\underline{j}\mu}$	$\mathcal{O}(N^2)$
(n)	$\hat{n}_{\tau}^{P,(\mathrm{ov})} = \hat{X}_{\underline{j},\tau}^{P,(\mathrm{vo})} \hat{I}_{\underline{j},\tau}^{P,(\mathrm{ov})}$	$\mathcal{O}(N^2)$

The order of contractions follows the general ideas presented in Ref. 78. Naturally, to minimize the number of FLOP, common intermediates, such as $\hat{\mathbf{A}}$, $\hat{\mathbf{B}}$, and $\hat{\mathbf{D}}$ should be reused as much as possible. For this, first all possible $\mathbf{X}$ tensors are contracted over the orbital index. For the subsequent formation of the $\hat{\mathbf{D}}$ intermediates two possible routes have to be considered. In order to minimize the number of FLOP, the $\mathbf{\Gamma}$-factorized form of the THC $\mathbf{Z}$ tensor should be used and contracted in a total of four matrix-matrix multiplications in steps (d)-(e). However, the fact that the one-electron density becomes sparse for sufficiently large systems with a significant HOMO-LUMO gap can be used here to perform the step in

$\mathcal{O}(N^2)$ operations. The first contraction in step (e')-(f') with one of the $\mathbf{Z}$ matrices scales quadratically as the $\mathbf{C}$ matrix is sparse, whereas $\mathbf{Z}$ itself is not. For the multiplication with the second $\mathbf{Z}$ matrix the fact that the resulting $\hat{\mathbf{D}}$ matrix is Schur multiplied with either the $\hat{\mathbf{A}}$ or the $\hat{\mathbf{B}}$ matrices in steps (i)-(j) can be leveraged. Since intermediates $\hat{\mathbf{A}}$ and $\hat{\mathbf{B}}$ are sparse and the Schur product will only contain elements – or blocks when using block-sparse algebra – which are significant in both $\hat{\mathbf{A}}/\hat{\mathbf{B}}$ and $\hat{\mathbf{D}}$, only elements in $\hat{\mathbf{D}}$ which are significant in $\hat{\mathbf{A}}/\hat{\mathbf{B}}$ need to be computed in steps (e')-(f'). In total, this enables the formation of the expensive $\hat{\mathbf{D}}$ intermediates in $\mathcal{O}(N^2)$ time. All final contractions in steps (k)-(n) are at most quadratically scaling, which results in overall quadratic scaling for the entire CDD-THC-SOS-CC2 method.

2.3.3 Reformulation of the Excited State Equations

The strategy displayed in the previous section can be applied to the matrix-vector products of SOS-LR-CC2 and SOS-ADC(2). For simplicity, we will only discuss the reformulation of eq. 36, according to:

$$\begin{aligned}\sigma_{\mu\nu}^{\text{SOS-CC2, (1)}} = &\sum_{ai} C_{\mu a} C_{\nu i} \left(\sum_{b} \hat{F}_{ab} R_{bi} \right) - \sum_{ai} C_{\mu a} C_{\nu i} \left(\sum_{j} R_{aj} \hat{F}_{ji} \right) + \sum_{ai} C_{\mu a} C_{\nu i} \bar{F}_{ai} \\ &- c_{\text{os}} \sum_{ai} C_{\mu a} C_{\nu i} \left(\sum_{b} E_{ab} R_{bi} \right) - c_{\text{os}} \sum_{ai} C_{\mu a} C_{\nu i} \left(\sum_{j} R_{aj} E_{ji} \right) \\ &+ \sum_{ai} C_{\mu a} C_{\nu i} \left(\sigma_{ai}^{\text{G, (1)}} + \sigma_{ai}^{\text{H, (1)}} + \sigma_{ai}^{\text{I, (1)}} \right) \end{aligned} \tag{72}$$

The fourth and fifth terms on the right-hand side are rewritten as

$$-c_{\text{os}} \sum_{ai} C_{\mu a} C_{\nu i} \left(\sum_{b} E_{ab} R_{bi} \right) = -c_{\text{os}} \sum_{\mu' \sigma \sigma' \nu'} \hat{E}'_{\mu' \nu'} Q_{\nu' \sigma'} \left[\sum_{\lambda' \lambda} S_{\sigma' \lambda'} R_{\lambda' \lambda} S_{\lambda \sigma} \right] P_{\sigma \nu} \tag{73}$$

$$-c_{\text{os}} \sum_{ai} C_{\mu a} C_{\nu i} \left(\sum_{j} R_{aj} E_{ji} \right) = -c_{\text{os}} \sum_{\mu' \sigma \sigma' \nu'} Q_{\mu \mu'} \left[\sum_{\lambda \lambda'} S_{\mu' \lambda'} R_{\lambda' \lambda} S_{\lambda \sigma} \right] P_{\sigma \sigma'} \hat{E}''_{\sigma' \nu'} \tag{74}$$

where the intermediates **E**, given by

$$E'_{\mu\nu} = \sum_S \Big(\sum_\tau \sum_P \hat{X}^{P,(\mathrm{vo})}_{\mu,\tau} \hat{N}^{PS,(\mathrm{vovo})}_{\tau} \Big) X^{S,(\mathrm{vo})}_{\nu} \tag{75}$$

$$E''_{\mu\nu} = \sum_{\underline{j}\underline{i}} L_{\mu\underline{j}} L_{\nu\underline{i}} \Bigg[\sum_S \Big(\sum_\tau \sum_P \hat{X}^{P,(\mathrm{vo})}_{\underline{i},\tau} \hat{M}^{PS,(\mathrm{vovo})}_{\tau} \Big) X^{S,(\mathrm{vo})}_{\underline{j}} \Bigg] \tag{76}$$

depend only on ground state quantities and hence are computed once and stored on disk. The terms $\boldsymbol{\sigma}^{\mathrm{G},\,(1)}$, $\boldsymbol{\sigma}^{\mathrm{H},\,(1)}$ and $\boldsymbol{\sigma}^{\mathrm{I},\,(1)}$ are given as

$$\begin{aligned}
\sigma^{\mathrm{G},\,(1)}_{\mu\nu} &= -c_{\mathrm{os}} \sum_{\mu'\underline{i}} L_{\nu\underline{i}} \Bigg\{ \sum_\tau e^{\bar{\omega} t_\tau} \sum_{PS} \Big[\hat{X}^{P,(\mathrm{vo})}_{\underline{i},\tau} \bar{M}^{PS,(\mathrm{ovvv})}_{\tau} + \bar{X}^{P,(\mathrm{vo})}_{\underline{i},\tau} \hat{M}^{PS,(\mathrm{ovvv})}_{\tau} \Big] X^{S,(\mathrm{vv})}_{\mu'} \Bigg\} \hat{Q}_{\mu\mu'} \\
&= -c_{\mathrm{os}} \sum_S \sum_{\mu'\underline{i}} L_{\nu\underline{i}} \bar{Y}^{S,(\mathrm{vv})}_{\underline{i}} X^{S,(\mathrm{vv})}_{\mu'} \hat{Q}_{\mu\mu'}
\end{aligned} \tag{77}$$

$$\begin{aligned}
\sigma^{\mathrm{H},\,(1)}_{\mu\nu} &= +c_{\mathrm{os}} \sum_{\underline{i}} L_{\nu\underline{i}} \Bigg\{ \sum_\tau e^{\bar{\omega} t_\tau} \sum_{PS} \Big[\bar{X}^{P,(\mathrm{vo})}_{\mu,\tau} \hat{N}^{PS,(\mathrm{vooo})}_{\tau} + \hat{X}^{P,(\mathrm{vo})}_{\mu,\tau} \bar{N}^{PS,(\mathrm{vooo})}_{\tau} \Big] \hat{X}^{S,(\mathrm{oo})}_{\underline{i}} \Bigg\} \\
&= +c_{\mathrm{os}} \sum_S \sum_{\underline{i}} \bar{Y}^{S,(\mathrm{oo})}_{\mu} \hat{X}^{S,(\mathrm{oo})}_{\underline{i}} L_{\nu\underline{i}}
\end{aligned} \tag{78}$$

$$\begin{aligned}
\sigma^{\mathrm{I},\,(1)}_{\mu\nu} &= -c_{\mathrm{os}} \sum_{\underline{i}} L_{\nu\underline{i}} \Bigg\{ \sum_\tau e^{\bar{\omega} t_\tau} \sum_P \Big[\bar{X}^{P,(\mathrm{vo})}_{\mu,\tau} \hat{X}^{P,(\mathrm{vo})}_{\underline{i},\tau} + \hat{X}^{P,(\mathrm{vo})}_{\mu,\tau} \bar{X}^{P,(\mathrm{vo})}_{\underline{i},\tau} \Big] \hat{I}^{P,(\mathrm{vo})}_{\tau} \Bigg\} \\
&\quad - c_{\mathrm{os}} \sum_{\underline{i}} L_{\nu\underline{i}} \Bigg\{ \sum_\tau \sum_P \hat{X}^{P,\tau}_{\mu} \hat{X}^{P,\tau}_{\underline{i}} \bar{I}^{P,(\mathrm{vo})}_{\tau,(1)} \Bigg\}
\end{aligned} \tag{79}$$

with

$$\bar{I}^{P,(\mathrm{vo})}_{\tau,(1)} = \sum_{\mu\nu\underline{i}} \hat{X}^{P,\tau}_{\mu} \hat{X}^{P,\tau}_{\underline{i}} \bar{F}_{\mu\nu} L_{\nu\underline{i}} \tag{80}$$

The matrices $\bar{M}$ and $\bar{N}$ are defined in eqs. 44-45 and computed as shown in Table 2. The general reasoning of the order of contractions and how to reduce the scaling is similar to the

ideas presented for Table 1. The state-specific THC $\bar{\mathbf{X}}$ matrices are given by

$$\bar{X}^{P,(\mathrm{vo})}_{\mu,\tau} = \sum_{\mu'} \bar{Q}^{\tau}_{\mu\mu'} X^{P,(\mathrm{vo})}_{\mu'} \qquad\qquad \bar{X}^{P,(\mathrm{vo})}_{\underline{i},\tau} = \sum_{\mu} \bar{P}^{\tau}_{\mu\underline{i}} X^{P,(\mathrm{vo})}_{\mu} \tag{81}$$

where the densities $\bar{Q}$ and $\bar{P}$ defined as

$$\bar{Q}^{\tau}_{\mu\nu} = \sum_{a} w_{\tau}^{\frac{1}{4}} C_{\mu a} e^{(-\epsilon_a)t_\tau} \bar{\Lambda}^{p}_{\nu a} = -\sum_{\mu'\nu'\underline{k}} Q^{\tau}_{\mu\mu'} \Big[\sum_{\sigma\lambda} S_{\mu'\sigma} R_{\sigma\lambda} S_{\lambda\nu'} \Big] L_{\nu'\underline{k}} L_{\underline{k}\nu} \tag{82}$$

$$\bar{P}^{\tau}_{\mu\nu} = \sum_{i} w_{\tau}^{\frac{1}{4}} \bar{\Lambda}^{h}_{\mu i} e^{(\epsilon_i)t_\tau} C_{\nu i} = \Bigg\{ \sum_{\mu'\nu'} \sum_{\underline{j}\sigma'\lambda'} Q_{\mu\mu'} \Big[S_{\mu'\lambda} R_{\lambda\sigma} S_{\sigma\nu'} \Big] L_{\nu'\underline{j}} L_{\sigma'\underline{j}} S_{\sigma'\lambda'} P^{\tau}_{\lambda'\underline{i}} \Bigg\} L_{\nu\underline{i}} \tag{83}$$

contain the information about the electronic transition. As discussed in Section 2.3.1, the SOS-ADC(2) matrix-vector product is easily obtained by setting the singles amplitudes to zero and symmetrizing the intermediates in eqs. 75, 76. Notice that, eq. 51 can be reformulated as

$$\begin{aligned}
\sigma^{\mathrm{I},\,(2)}_{\mu\nu} = & -c_{\mathrm{os}} \sum_{\underline{i}} L_{\nu\underline{i}} \Bigg\{ \sum_{\tau} \sum_{P} X^{P,\tau}_{\mu} X^{P,\tau}_{\underline{i}} \bar{I}^{P,(\mathrm{vo})}_{\tau,(1)} \Bigg\} \\
& - c_{\mathrm{os}} \sum_{\mu'\nu'} \sum_{\underline{i}} Q_{\mu\nu'} \Bigg\{ \sum_{\sigma\lambda} [2(\mu'\nu'|\sigma\lambda) - (\mu'\lambda|\sigma\nu')] L_{\sigma\underline{k}} \bar{I}_{\lambda\underline{k}} \Bigg\} L_{\mu'\underline{i}} L_{\nu\underline{i}}
\end{aligned} \tag{84}$$

$$\bar{I}_{\lambda\underline{k}} = \sum_{P} \sum_{\tau} X^{P,\tau}_{\lambda} X^{P,\tau}_{\underline{i}} \bar{I}^{P,(\mathrm{vo})}_{\tau,(2)} \tag{85}$$

$$\bar{I}^{P,(\mathrm{vo})}_{\tau,(2)} = \sum_{\mu\underline{i}} X^{P,\tau}_{\mu} X^{P,\tau}_{\underline{i}} \Bigg[\sum_{\nu\lambda\sigma\nu'} Q_{\mu\nu} S_{\nu\lambda} R_{\lambda\sigma} S_{\sigma\nu'} L_{\nu'\underline{i}} \Bigg] \tag{86}$$

3 Computational Details

The presented CDD-THC-SOS-LR-CC2 and CDD-THC-SOS-ADC(2) methods as well as the MO-based variants are implemented in the FermiONs++[79–81] program. The program was compiled with the Intel C/C++ Compiler 2022.0.2 and linked against the Intel Math

Table 2: Programmable equations for the evaluation of the σ^{G} and σ^{H} contribution to the CDD-THC-SOS-ADC(2)/CC2 matrix-vector product. Throughout this table Einstein's summation convention is used. The ADC(2) equations are easily obtained by setting $\mathbf{t}_{\mu_1} = 0$.

	Intermediates	Asymptotic Scaling
(a)	$\bar{A}_\tau^{QR,(\mathrm{vovo})} = \bar{X}_{\underline{i},\tau}^{Q,(\mathrm{vo})} X_{\underline{i}}^{R,(\mathrm{vo})}$	$\mathcal{O}(N)$
(b)	$\bar{B}_\tau^{QR,(\mathrm{vovo})} = \bar{X}_{\mu,\tau}^{Q,(\mathrm{vo})} X_{\mu}^{R,(\mathrm{vo})}$	$\mathcal{O}(N)$
(c)	$\bar{C}_\tau^{QR,(\mathrm{vovo})} = \bar{A}^{QR,(\mathrm{vovo})} \hat{B}^{QR,(\mathrm{vovo})} + \hat{A}^{QR,(\mathrm{vovo})} \bar{B}^{QR,(\mathrm{vovo})}$	$\mathcal{O}(N)$
(d)	$\bar{D}_\tau^{\alpha\beta} = \Gamma_\alpha^{Q,(\mathrm{vo})} \bar{C}_\tau^{QR,(\mathrm{vovo})} \Gamma_\beta^{R,(\mathrm{vo})}$	$\mathcal{O}(N^2)$
(e)	$\bar{D}_\tau^{PS,(\mathrm{ovvv})} = e^{\bar{\omega} t_\tau} \Gamma_\alpha^{P,(\mathrm{vo})} \bar{D}_\tau^{\alpha\beta} \Gamma_\beta^{S,(\mathrm{vv})}$	$\mathcal{O}(N^2)$
(f)	$\bar{D}_\tau^{PS,(\mathrm{vooo})} = e^{\bar{\omega} t_\tau} \Gamma_\alpha^{P,(\mathrm{vo})} \bar{D}_\tau^{\alpha\beta} \Gamma_\beta^{S,(\mathrm{oo})}$	$\mathcal{O}(N^2)$
(e')	$\bar{D}_\tau^{PS,(\mathrm{ovvv})} = e^{\bar{\omega} t_\tau} Z^{PQ,(\mathrm{vovo})} \bar{C}_\tau^{QR,(\mathrm{vovo})} Z^{RS,(\mathrm{ovvv})}$	$\mathcal{O}(N^2)$
(f')	$\bar{D}_\tau^{PS,(\mathrm{vooo})} = e^{\bar{\omega} t_\tau} Z^{PQ,(\mathrm{vovo})} \bar{C}_\tau^{QR,(\mathrm{vovo})} Z^{RS,(\mathrm{vooo})}$	$\mathcal{O}(N^2)$
(g)	$\bar{A}_\tau^{PS,(\mathrm{vooo})} = \bar{X}_{\underline{i},\tau}^{P,(\mathrm{vo})} X_{\underline{i}}^{S,(\mathrm{oo})}$	$\mathcal{O}(N)$
(h)	$\bar{B}_\tau^{PS,(\mathrm{ovvv})} = \bar{X}_{\mu,\tau}^{P,(\mathrm{vo})} X_{\mu}^{S,(\mathrm{vv})}$	$\mathcal{O}(N)$
(i)	$\bar{M}_\tau^{PS,(\mathrm{ovvv})} = \bar{M}_{\tau,(1)}^{PS,(\mathrm{ovvv})} + \bar{M}_{\tau,(2)}^{PS,(\mathrm{ovvv})}$	$\mathcal{O}(N)$
(j)	$\bar{M}_{\tau,(1)}^{PS,(\mathrm{ovvv})} = \hat{B}_\tau^{PS,(\mathrm{ovvv})} \bar{D}_\tau^{PS,(\mathrm{ovvv})}$	$\mathcal{O}(N)$
(k)	$\bar{M}_{\tau,(2)}^{PS,(\mathrm{ovvv})} = \bar{B}_\tau^{PS,(\mathrm{ovvv})} \hat{D}_\tau^{PS,(\mathrm{ovvv})}$	$\mathcal{O}(N)$
(l)	$\bar{N}_\tau^{PS,(\mathrm{vooo})} = \bar{M}_{\tau,(1)}^{PS,(\mathrm{vooo})} + \bar{M}_{\tau,(2)}^{PS,(\mathrm{vooo})}$	$\mathcal{O}(N)$
(m)	$\bar{N}_{\tau,(1)}^{PS,(\mathrm{vooo})} = \hat{A}_\tau^{PS,(\mathrm{vooo})} \bar{D}_\tau^{PS,(\mathrm{vooo})}$	$\mathcal{O}(N)$
(n)	$\bar{N}_{\tau,(2)}^{PS,(\mathrm{vooo})} = \bar{A}_\tau^{PS,(\mathrm{vooo})} \hat{D}_\tau^{PS,(\mathrm{vooo})}$	$\mathcal{O}(N)$
(o)	$\bar{Y}_{\mu}^{S,(\mathrm{oo})} = \bar{X}_{\mu,\tau}^{P,(\mathrm{vo})} \hat{N}_\tau^{PS,(\mathrm{vooo})} + \hat{X}_{\mu,\tau}^{P,(\mathrm{vo})} \bar{N}_\tau^{PS,(\mathrm{vooo})}$	$\mathcal{O}(N)$
(p)	$\bar{Y}_{\underline{i}}^{S,(\mathrm{vv})} = \hat{X}_{\underline{i},\tau}^{P,(\mathrm{vo})} \bar{M}_\tau^{PS,(\mathrm{ovvv})} + \bar{X}_{\underline{i},\tau}^{P,(\mathrm{vo})} \hat{M}_\tau^{PS,(\mathrm{ovvv})}$	$\mathcal{O}(N)$

Kernel Library 2022.0.2 for the employed matrix algebra. All developed code was – as far as possible – parallelized with OpenMP.[82] The underlying Hartree–Fock calculations have been converged to a maximum element of the error matrix in the direct inversion in the iterative subspace (DIIS) procedure below 10^{-7}. In the SCF, the Coulomb matrix is evaluated using the RI-J approach by Kussmann *et al.*[71] using the cc-pVDZ-JKfit[83] RI-J basis set. For the exchange matrix, the semi-numerical linear scaling exchange method by Laqua *et al.*[68,69] is used. For the solution of the least-squares equations in THC the pivoted Cholesky decomposition ansatz by Matthews[57] is used. The hand-optimized grid for the cc-pVTZ basis set by Kokkila Schumacher *et al.*[84] is used as a parent grid together with a pruning threshold of 10^{-10}, unless otherwise noted. As demonstrated in the SI, it is pivotal to reorder the grid points after the pruning, since the pivoting in the Cholesky decomposition significantly reduces the sparsity of intermediates based on the pruned collocation matrices. The performance of the CDD-THC-SOS-LR-CC2 and CDD-THC-SOS-ADC(2) methods is improved using sparse linear algebra. The current implementation leverages block-sparse (BS) matrices, which divide the matrices into smaller blocks, of maximum size 96×96. Further information about the BS matrix implementation is provided in Ref. 38. The thresholds controlling the sparsity (ϑ_a) and the performance of matrix-matrix multiplications (ϑ_m) are set to 10^{-7} and 10^{-9}, respectively. The singles cluster amplitudes and ground state energy at the SOS-CC2 level are optimized via the DIIS procedure, which terminates when the L2-norm of the singles vector function is lower than 10^{-5} and the variation in the energy is lower than 10^{-6}. For excited-states calculations, the trial excitation vectors and energies are first optimized at the CCS level via the Davidson procedure, until the L2-norm of residuals and the variation in the eigenvalues are below 10^{-3}. Then, SOS-LR-CC2 or SOS-ADC(2) excitation vectors and energies are optimized using the DIIS algorithm, which terminates when the L2-norm of residuals are lower than 10^{-5} and the variations in the eigenvalues are lower than 10^{-6}. It is important to note that the CCS trial vectors and eigenvalues can be pre-optimized at the CC2 or ADC(2) level if the DIIS procedure fails to converge to the

right root. Optimized minimax grids with 7 quadrature points for the Laplace expansion, for both ground and excited states calculations are used. Moreover, we used the frozen-core approximation during the THC fitting, the ground state, and excited states calculations. Throughout, the Dunning cc-pVXZ (X $\in$ {D,T}) basis sets[62,63] are used together with their corresponding RI basis sets.[64] All calculations are performed using a compute node with two AMD EPYC 7302 32-Core 3.0 GHz CPUs, $\sim$1TB of RAM, and $\sim$24 TB of disk space. All runtimes are reported as wall times, not CPU times.

4 Results

4.1 Accuracy

The aim of the present work is to increase the efficiency of the SOS-ADC(2) and SOS-LR-CC2 methods and extend their application to molecules with several hundred atoms while retaining accuracy as far as possible. In order to assess the accuracy of the ground state implementation, the errors produced by the MO-based as well as the CDD-based THC-SOS-MP2/CC2 methods are investigated with respect to MO-RI-SOS-MP2/CC2. Table 3 reports these errors for a set of 12 medium-size molecules, with the THC error ΔE_{THC} defined as $|E_{\text{MO-RI-SOS-MP2/CC2}} - E_{\text{MO-THC-SOS-MP2/CC2}}|$ and the CDD-THC error $\Delta E_{\text{CDD-THC}}$ defined as $|E_{\text{MO-RI-SOS-MP2/CC2}} - E_{\text{CDD-THC-SOS-MP2/CC2}}|$.

On the one hand, both MO- and CDD-THC-SOS-MP2 show only a small deviation on the order of $\sim 10^{-5} - 10^{-6}$ H compared to MO-RI-SOS-MP2 with a linearly growing error for the considered test set in Table 3. On the other hand, the MO- and CDD-THC-SOS-CC2 errors are roughly one order of magnitude larger because – contrary to MP2 – the solution of the CC2 equations requires the fitting of (ov|vv)-type integrals, which results in larger errors as the fitted subspace is much larger than the (ov|ov) integrals in MP2. Moreover, the grid error is carried along the iterative procedure for the optimization of the coupled cluster amplitudes, which is demonstrated in the SI for the propagation of the error along the DIIS

Table 3: Absolute errors of the ground state energies of MO- and CDD-THC-SOS-MP2/CC2 referenced against MO-RI-SOS-MP2/CC2. The THC error ΔE_{THC} is defined as $|E_{\text{MO-RI-SOS-MP2/CC2}} - E_{\text{MO-THC-SOS-MP2/CC2}}|$ while the CDD-THC error $\Delta E_{\text{CDD-THC}}$ is defined as $|E_{\text{MO-RI-SOS-MP2/CC2}} - E_{\text{CDD-THC-SOS-MP2/CC2}}|$. All calculations are performed with the cc-pVDZ/cc-pVDZ-RI basis set combination.

	SOS-MP2		SOS-CC2	
	ΔE_{THC} / mH	$\Delta E_{\text{CDD-THC}}$ / mH	ΔE_{THC} / mH	$\Delta E_{\text{CDD-THC}}$ / mH
LCA_{40}	0.004	0.005	0.400	0.400
LCA_{80}	0.008	0.014	0.408	0.408
LCA_{160}	0.021	0.048	0.405	0.437
AT_2	0.009	0.010	5.170	5.170
AT_4	0.025	0.030	11.500	11.500
Butadiene	< 0.001	< 0.001	0.053	0.052
Hexatriene	< 0.001	< 0.001	0.078	0.078
β-carotene	0.003	0.003	0.352	0.353
15-OPDA	0.002	0.002	0.515	0.513
Metenkephalin	0.002	0.002	2.620	2.620
Dyad	0.003	0.003	2.260	2.260

procedure.

While absolute energies are of interest from a theoretical standpoint, relative energies provide valuable insights into chemical processes, such as reactions or conformational changes. For this, the suitability of the THC-CC2 methods is tested by evaluating the errors of relative energies of 27 tetraalanine conformers in Table 4.[56]

Table 4: Mean absolute errors for conformational energies of 27 tetraalanine conformers.[56] Errors are reported as mean absolute deviations (MAD), maximum deviations (MAX), and root mean square deviations (RMSD) from the difference of the conformational energies as obtained by the MO/CDD-THC-SOS-MP2/CC2 methods relative to the MO-RI-SOS-MP2/CC2 results. All calculations are performed with the cc-pVDZ/cc-pVDZ-RI basis set combination.

	MAD / kcal mol^{-1}	MAX / kcal mol^{-1}	RMSD / kcal mol^{-1}
MO-THC-SOS-MP2	$<$0.001	0.001	$<$0.001
MO-THC-SOS-CC2	0.043	0.241	0.073
CDD-THC-SOS-MP2	$<$0.001	0.001	$<$0.001
CDD-THC-SOS-CC2	0.043	0.241	0.073

As shown in Table 4, THC-SOS-MP2 predicts the relative energies of the tetraalanine conformers with errors on the order of 10^{-3} kcal mol^{-1}. Comparable to the accuracy for absolute

energies, the THC-SOS-CC2 results deviate more significantly with errors on the order of 0.05 kcal mol^{-1}. Despite the fact that using THC-factorized integrals incurs an additional error over the RI-SOS-CC2 reference implementation, Table 4 shows that good accuracy is reached for relative energies.

Going beyond absolute and relative ground state energies, Table 5 shows SOS-LR-CC2 and SOS-ADC(2) excitation energies to singlet (S) and triplet (T) states computed with the previously reported MO-RI-SOS-LR-CC2/ADC(2) methods for representative molecules. Additionally, the deviations of the presented MO/CDD-THC-SOS-LR-CC2/ADC(2) methods are shown to assess the applicability of THC-SOS-CC2/ADC(2) for excitation energy calculations.

As shown in Table 5, the average error originating from the THC approximation (ΔE_{THC}) of the THC-SOS-ADC(2) and THC-SOS-LR-CC2 methods is $\sim$ 0.01 eV and $\sim$ 0.02 eV, respectively, for singlet states. For the triplet excited states in Table 5, THC-SOS-ADC(2) and THC-SOS-LR-CC2 methods show an average ΔE_{THC} error of $\sim$ 0.002 eV and $\sim$ 0.02 eV, respectively. The SOS-LR-CC2 implementation is less accurate than SOS-ADC(2) due to the error in the singles cluster amplitudes propagating to the evaluation of excitation energies. Nonetheless, the error is small enough for most practical applications and does not increase with the molecular size, as exemplarily shown for the series of linear carboxylic acids (LCAs). Furthermore, the observed THC error on the order of $\sim 0.01 - 0.02$ eV is on par with the errors reported by Hohenstein *et al.*[55] for excitation energies based on THC-EOM-CC2.

Moreover, the error ($\Delta E_{\text{CDD-THC}}$) generated by the reformulation in the local Cholesky orbital basis and the use of sparse algebra is small compared to the THC error. The latter then permits the use of sparse linear algebra routines for a reduction of the computational effort, scaling, and memory demands (see Section 4.2) in larger systems without affecting the overall accuracy of the CDD-THC-SOS-ADC(2) and CDD-THC-SOS-LR-CC2 methods.

Table 5: Excitation energies to singlet (S) and triplet (T) excited states obtained with the MO-RI-SOS-LR-CC2/ADC(2) reference implementations E_{ref}, as well as absolute deviations of MO-THC-SOS-CC2/ADC(2) (ΔE_{THC}) and CDD-THC-SOS-LR-CC2/ADC(2) ($\Delta E_{\text{CDD-THC}}$)from the MO-RI-SOS-LR-CC2/ADC(2) results. All calculations are performed with the cc-pVDZ/cc-pVDZ-RI basis set combination. Note that for AT_4, the excitation energies were converged to a threshold of 10^{-5} instead of 10^{-6}.

		SOS-ADC(2)			SOS-LR-CC2		
	State	E_{ref} / eV	ΔE_{THC} / eV	$\Delta E_{\text{CDD-THC}}$ / eV	E_{ref} / eV	ΔE_{THC} / eV	$\Delta E_{\text{CDD-THC}}$ / eV
LCA_{40}	S_1	5.958	0.002	0.002	6.204	0.020	0.020
LCA_{80}	S_1	5.958	0.002	0.002	6.204	0.024	0.024
LCA_{160}	S_1	5.958	0.002	0.002	6.204	0.022	0.022
AT_2^*	S_1	5.155	<0.001	<0.001	5.266	0.016	0.015
	S_2	5.227	0.023	0.024	5.309	0.016	0.016
AT_4^*	S_1	5.112	<0.001	<0.001	5.200	0.021	0.017
Butadiene	S_1	6.793	0.001	0.001	6.857	0.031	0.031
	S_2	8.353	0.002	0.002	8.330	0.005	0.005
Hexatriene	S_1	5.685	<0.001	<0.001	5.745	0.024	0.024
	S_2	7.226	0.007	0.007	7.211	0.037	0.037
β-carotene	S_1	3.556	<0.001	<0.001	3.579	0.002	0.002
	S_2	4.495	0.064	0.064	4.525	0.002	0.002
15-OPDA	S_1	4.497	0.002	0.002	4.679	0.016	0.015
	S_2	6.040	0.002	0.002	6.281	0.024	0.022
	S_3	8.553	0.007	0.007	8.691	0.013	0.013
Metenkephalin	S_1	4.771	<0.001	<0.001	4.775	0.011	0.011
	S_2	4.902	0.001	0.001	4.893	0.003	0.003
	S_3	6.002	<0.001	<0.001	6.020	0.003	0.003
Dyad	S_1	3.263	<0.001	<0.001	3.406	0.044	0.044
	S_2	3.936	0.002	0.002	4.021	0.013	0.013
LCA_{40}	T_1	6.612	0.001	0.001	6.708	0.033	0.340
LCA_{80}	T_1	6.612	0.001	0.001	6.708	0.032	0.330
LCA_{160}	T_1	6.612	0.001	0.001	6.708	0.035	0.360
AT_2^*	T_1	3.717	<0.001	<0.001	3.771	0.014	0.013
AT_4^*	T_1	3.697	<0.001	<0.001	3.754	0.013	0.013
Butadiene	T_1	6.793	0.001	0.001	6.857	0.031	0.031
	T_2	8.353	0.002	0.002	8.330	0.005	0.005
Hexatriene	T_1	5.685	<0.001	<0.001	5.745	0.024	0.024
	T_1	7.226	0.007	0.007	7.211	0.037	0.037
β-carotene	T_1	2.157	<0.001	<0.001	2.154	0.003	0.003
15-OPDA	T_1	4.099	0.002	0.002	4.252	0.014	0.013
	T_2	5.757	0.013	0.013	5.966	0.020	0.020
Metenkephalin	T_1	4.143	<0.001	<0.001	4.142	0.007	0.007
Dyad	T_1	2.664	<0.001	<0.001	2.730	0.021	0.021
Average Error (eV)	Singlet		0.006	0.006		0.018	0.018
	Triplet		0.002	0.002		0.021	0.021

4.2 Scaling

The sparsity of the ground state one-electron density is closely related to the energy gap between the highest occupied (HOMO) and the lowest unoccupied MO (LUMO) of a molecular system. Given a significant HOMO-LUMO gap, asymptotically linear-scaling variants of many common quantum chemistry methods have been proposed.[85,86] In addition, for excited state calculations the transition density $\mathbf{R}$ with elements $R_{\mu\nu}$ in eqs. 82 and 83 must be considered, whose sparsity is related to the locality of the excitation. In order to assess the computational scaling of the newly proposed density-based grid-projection algorithm for LS-THC and the scaling of the resulting CDD-THC-SOS-LR-CC2 and CDD-THC-SOS-ADC(2) methods, linear carboxylic acids (LCAs – see Figure 2) are selected as a best-case scenario showing a local electronic structure as well as a local excitation for the lowest singlet excited state (S_1), which is mostly localized on the carboxyl group. Secondly, the scaling behavior of the implementations of the presented methods is discussed for three-dimensional systems, such as DNA fragments (see Figure 5). DNA double helices provide a valuable model system for evaluating the scaling of a given method, as the system can be viewed as mostly three-dimensional for 4-8 base pairs, but becomes increasingly linear beyond 8 base pairs, for which the method should approach its asymptotic scaling.

4.2.1 Integral-direct Tensor Hypercontraction

First, the efficiency of the proposed density-based, integral-direct algorithm for the grid-projection of the three-center RI integrals, i.e., for the formation of intermediates $\mathbf{Y}$ in eq. 13, is demonstrated. For this, first a comparison between the previously published[58] Cholesky MO-based natural blocking approach (*nat. block.*) and density-based implementations based on the J-engine (*J-engine*), RI-J (*RI-J*), and the newly proposed method in Section 2.2.3 (*this work*) is drawn in Table 6.

For the natural blocking-based algorithm the recommended settings from Ref. 58 are used, most notably, attenuated Coulomb-RI[40] with an attenuation strength of $\omega = 0.1$. The

Table 6: Wall time required for the formation of the $\mathbf{\Gamma}^{(\mathrm{oo})}$, $\mathbf{\Gamma}^{(\mathrm{vo})}$, and $\mathbf{\Gamma}^{(\mathrm{vv})}$ intermediates based on the previously published natural blocking[58] (*nat. block.*) approach as well as density-based and integral-direct using the J-engine (*J-engine*), the RI-J algorithm (*RI-J*), and the proposed algorithm (*this work*) from Section 2.2.3. Since the natural blocking approach was optimized for the formation of $\mathbf{\Gamma}$ in the virtual-occupied subspace, only timings for $\mathbf{\Gamma}^{(\mathrm{vo})}$ are reported. All times are given in hours for LCA_n ($n \in \{20, 40, 80, 160\}$) using the cc-pVXZ (X $\in$ {D,T}) basis sets. Extrapolated values are marked with an asterisk (*).

		cc-pVDZ				cc-pVTZ			
		nat. block.	*J-engine*	*RI-J*	*this work*	*nat. block.*	*J-engine*	*RI-J*	*this work*
$\mathbf{\Gamma}^{(\mathrm{oo})}$									
	LCA_{20}	–	<0.1	<0.1	<0.1	–	0.1	<0.1	<0.1
	LCA_{40}	–	0.1	<0.1	<0.1	–	0.5	0.1	<0.1
	LCA_{80}	–	1.2	0.1	<0.1	–	4.9	0.3	0.1
	LCA_{160}	–	8.8	0.4	0.1	–	53.1	1.4	0.5
$\mathbf{\Gamma}^{(\mathrm{vo})}$									
	LCA_{20}	<0.1	<0.1	<0.1	<0.1	<0.1	1.0	0.2	<0.1
	LCA_{40}	<0.1	0.8	0.1	<0.1	0.1	9.0	0.9	0.1
	LCA_{80}	0.1	9.2	0.5	0.1	0.3	85.3	3.3	0.4
	LCA_{160}	0.4	70.0	2.1	0.5	1.2	924.0*	13.6	3.1
$\mathbf{\Gamma}^{(\mathrm{vv})}$									
	LCA_{20}	–	0.2	0.1	<0.1	–	1.3	0.4	<0.1
	LCA_{40}	–	1.3	0.3	<0.1	–	11.8	1.5	0.1
	LCA_{80}	–	14.6	1.1	0.1	–	114.0	5.9	0.5
	LCA_{160}	–	118.3	4.1	0.6	–	1235.4*	24.6	3.7

latter is required in order to achieve sparsity in the three-center integrals, which makes this approach efficient. In contrast, all density-based approaches use the regular $1/r_{12}$ operator. For smaller molecule sizes like LCA_{20} all algorithms perform roughly equally well, resulting in only an insignificant overhead for forming the THC intermediates. In the limit of the largest LCA molecules, the apparent scaling for forming $\mathbf{\Gamma}$ approaches $\mathcal{O}(N^2)$ for the natural blocking and the RI-J approach, whereas it approaches $\mathcal{O}(N^3)$ scaling for the J-engine version and the newly proposed method. It is noteworthy, that while the J-engine variant and the proposed method both scale cubically with the system size, the J-engine based method has a significantly higher prefactor, which leads to the fact, that it is slower than all other variants. In contrast, for the proposed, likewise cubically scaling approach from Section 2.2.3 the prefactor is low enough to render the method competitive to the natural blocking approach, which heavily relies on screening to be efficient, even for the largest molecule sizes considered. In order to demonstrate the effectiveness of the algorithm, the system size

scaling for the formation of the $\mathbf{Y}^{(\mathrm{oo})}$, $\mathbf{Y}^{(\mathrm{vo})}$, and $\mathbf{Y}^{(\mathrm{vv})}$ intermediate for LCAs up to LCA_{160} is shown in Figure 1 (left).

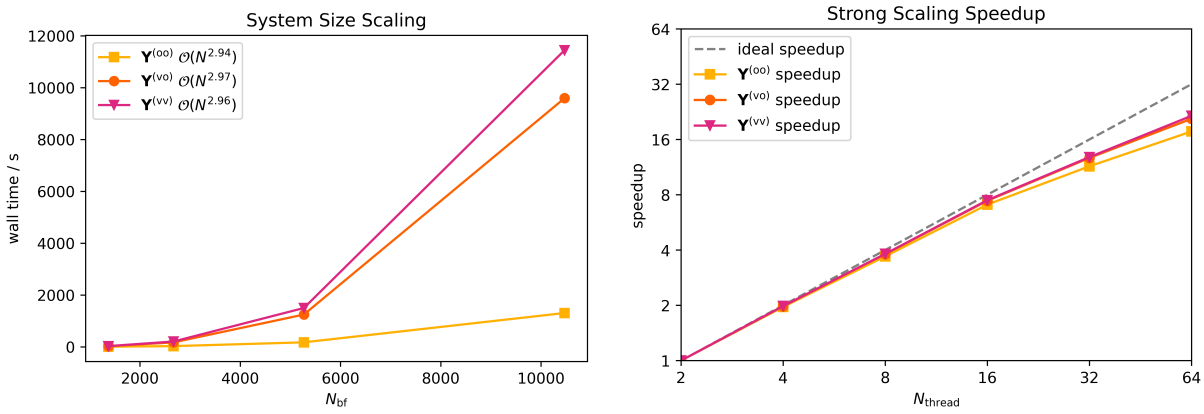

Figure 1: System size scaling (left) and strong scaling speedup (right) of the proposed density-based integral direct grid-projection algorithm for the cc-pVTZ basis set. The scaling of the wall time with respect to the system size is measured for LCAs up to 160 carbon atoms, while the strong scaling analysis is performed with LCA_{40} up to 64 threads.

While for all MO subspaces the scaling is cubic, the applied grid-pruning technique from Matthews[57] reduces the prefactor considerably for the $\mathbf{Y}^{(\mathrm{oo})}$ intermediate due to the compactness of the occupied-occupied subspace. Additionally, the strong scaling, i.e., the time-to-solution behavior for the same molecule size but increasing numbers of threads, was assessed. For this, the strong scaling speedup relative to the baseline solution time for two threads is shown in Figure 1 (right). Two threads were chosen as a baseline since the used node has a dual-socket board and we want to neglect the communication latency when scaling from a single thread on one CPU to a thread per CPU. Keeping the individual workload high enough on all processors is key to ideal strong scaling speedup. In this regard, an almost perfect speedup is observed for up to 15 threads, whereas only diminishing returns are obtained due to decreasing workload per CPU core. In summary, while the proposed grid-projection algorithm scales cubically, its prefactor is diminutive with a good scaling with respect to the number of CPU cores. Furthermore, it is competitive to the previously published natural blocking approach while only relying on the shell-pair sparsity of the atomic orbitals, which makes it better suited for non-sparse three-dimensional systems.

4.2.2 THC-SOS-LR-CC2 and THC-SOS-ADC(2)

Linear Carboxylic Acids

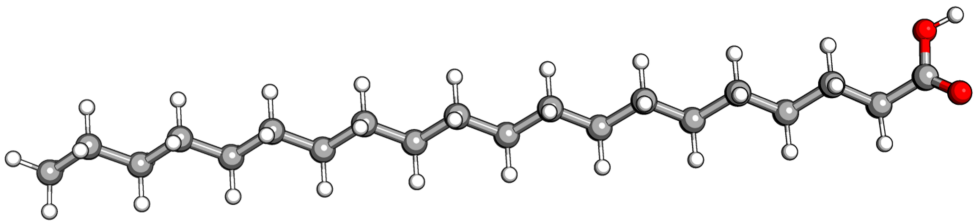

Figure 2: Linear carboxylic acid with 20 carbon atoms.

The scaling behavior of the proposed CDD-THC-SOS-LR-CC2 and CDD-THC-SOS-ADC(2) implementations is investigated by taking into account the number of floating-point operations (FLOP) required to form the singles-manifold CC vector and the matrix-vector product for ground and excited state calculations, respectively. For excited states, it is important to stress that, starting from the CCS transition density, the number of relevant elements $R_{\mu\nu}$ varies during the optimization procedure, as some electronic excitations become more (or less) important to accurately describe the state. Therefore, we decided to take into account the average number of FLOP per iteration (total no. of FLOP / no. of iterations) during the DIIS procedure. In Figure 3 the described scaling of the number of FLOP for the ground (left) as well as the excited state calculations (right) is plotted for the MO-RI-SOS-LR-CC2/ADC(2) reference implementations as well as for the proposed MO/CDD-THC-SOS-LR-CC2/ADC(2) methods for a series of LCAs.

As demonstrated in Figure 3, the MO-based THC-SOS-LR-CC2 and THC-SOS-ADC(2) algorithms allow for a $\mathcal{O}(N^3)$ scaling evaluation of the ground state and excitation energies with an effort that is ~ 7 and ~ 11 times smaller than their MO-RI variant, respectively. Reformulating the equations for the SOS-CC2 singles amplitudes in the local Cholesky/atomic orbitals basis decreases the computational effort and scaling. As shown in Figure 3, the use of sparse linear algebra to solve eq. 64 results in a sub-cubic asymptotic scaling and causes

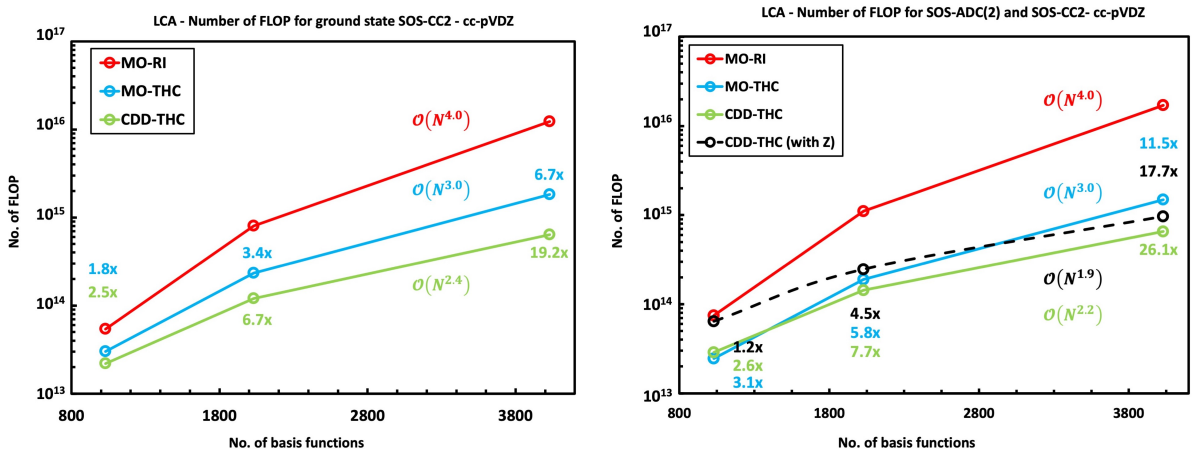

Figure 3: Number of FLOP required to evaluate the SOS-CC2 singles amplitudes (left) and the SOS-LR-CC2/SOS-ADC(2) matrix-vector product (right) for a series of LCAs ($n \in \{40, 80, 160\}$). Labels represent the FLOP reduction compared to the MO-RI-SOS-LR-CC2/ADC(2) implementation and all calculations are performed with the cc-pVDZ/cc-pVDZ-RI basis set combination.

a $\sim$ 19-fold reduction of the effort. Furthermore, CDD-THC-SOS-LR-CC2 and CDD-THC-SOS-ADC(2) show $\mathcal{O}(N^2)$ scaling behavior and a $\sim$ 26-fold diminution for the largest LCA considered. Additionally, as discussed below, it is possible to further decrease the asymptotic computational scaling to sub-quadratic by reintroducing the THC $\mathbf{Z}$ tensor instead of $\mathbf{\Gamma}$, as explained in Sections 2.3.2 and 2.3.3. Figure 3 demonstrates the described situation by showing a higher number of operations when the $\mathbf{Z}$ tensor is used and a crossover with the MO-based implementation at around $\sim$ 60 carbon atoms is observed. Despite the increased prefactor, the CDD-THC-SOS-LR-CC2 and CDD-THC-SOS-ADC(2) implementations using $\mathbf{Z}$ tensor will be more efficient than the $\mathbf{\Gamma}$-based algorithms for larger systems.

In order to understand the computational scaling of the local reformulations, we must discuss their memory demands and hence the number of allocated, i.e., significant blocks for the most important intermediates in both ground and excited state calculations. Focusing on the ground state, Figure 4 shows that the number of significant blocks in the different kinds of (transformed) $\mathbf{X}$ matrices grows linearly with the system size. Therefore, both the memory demand and the effort for the calculation of intermediate $\hat{\mathbf{C}}$ – see eq. (a)-(c) in Table 1 –

scale linearly with the system size. The first time-determining step (d) in Table 1 scales cubically in the asymptotic limit, as $\hat{\mathbf{C}}$ is multiplied with two dense matrices $\mathbf{\Gamma}^{(\mathrm{vo})}$ from the left and right, leading to a dense result matrix. For the other time-determining steps (e)-(f), the effort would scale cubically, as within a regular dense multiplication. However, the fact that the next set of intermediates – $\hat{\mathbf{N}}^{(\mathrm{vooo})}$ and $\hat{\mathbf{M}}^{(\mathrm{ovvv})}$ – will be computed via a Schur product of the $\hat{\mathbf{D}}^{(\mathrm{vooo})}$ and $\hat{\mathbf{A}}^{(\mathrm{vooo})}$ intermediates, and the $\hat{\mathbf{D}}^{(\mathrm{ovvv})}$ and $\hat{\mathbf{B}}^{(\mathrm{ovvv})}$ intermediates, respectively, can be leveraged in steps (e)-(f). Considering that the number of significant blocks in $\hat{\mathbf{A}}$ and $\hat{\mathbf{B}}$ grows linearly, only a fixed number of blocks of the intermediates $\hat{\mathbf{D}}^{(\mathrm{vooo})}$ and $\hat{\mathbf{D}}^{(\mathrm{ovvv})}$ must be computed. Therefore, steps (e)-(f) in Table 1 scale again sub-cubically, as the first multiplication with the THC fitting matrix scales as $\mathcal{O}(N^3)$ and the second one scales as $\mathcal{O}(N^2)$. As shown in Table 1, all the remaining steps scale at most quadratically with the system size. Hence, the overall computational effort for one iteration of CDD-THC-SOS-LR-CC2 and CDD-THC-SOS-MP2 scales sub-cubically in the asymptotic limit.

For the solution of the excited state problem, the matrix-vector product must be formed. To do so, the $\bar{\mathbf{X}}$ matrices that contain information about the electronic excitation need to be computed. For local excitations and local electronic structures, the number of significant blocks in $\bar{\mathbf{X}}$ will be constant in the asymptotic limit, as shown in Figure 4 (left). Consequently, the number of blocks in the $\bar{\mathbf{A}}$, $\bar{\mathbf{B}}$, and $\bar{\mathbf{C}}$ matrices will be constant as well. Again, the time-determining steps are the formation of the intermediates $\hat{\mathbf{D}}$ – (d)-(f) in Table 1 – and $\bar{\mathbf{D}}$ – (d)-(f) in Table 2. Contrary to the ground state intermediates, the effort for evaluating $\bar{\mathbf{D}}$ scales quadratically, if the fact that the $\bar{\mathbf{C}}$, $\bar{\mathbf{A}}$, and $\bar{\mathbf{B}}$ intermediates only contain a constant number of relevant blocks is leveraged. Alternatively, calculating $\bar{\mathbf{D}}$ by contraction with the $\mathbf{Z}$ fitting tensor – steps (e') and (f') in Table 2 – requires an effort that scales quadratically in the asymptotic limit because we first contract $\bar{\mathbf{C}}$ with the dense fitting matrix and secondly evaluate only a fixed number of blocks for $\bar{\mathbf{D}}^{\mathrm{vooo}}$ and $\bar{\mathbf{D}}^{\mathrm{ovvv}}$. The remaining steps scale at most linearly, except for eq. 80 that scales quadratically, albeit with a negligible prefactor.

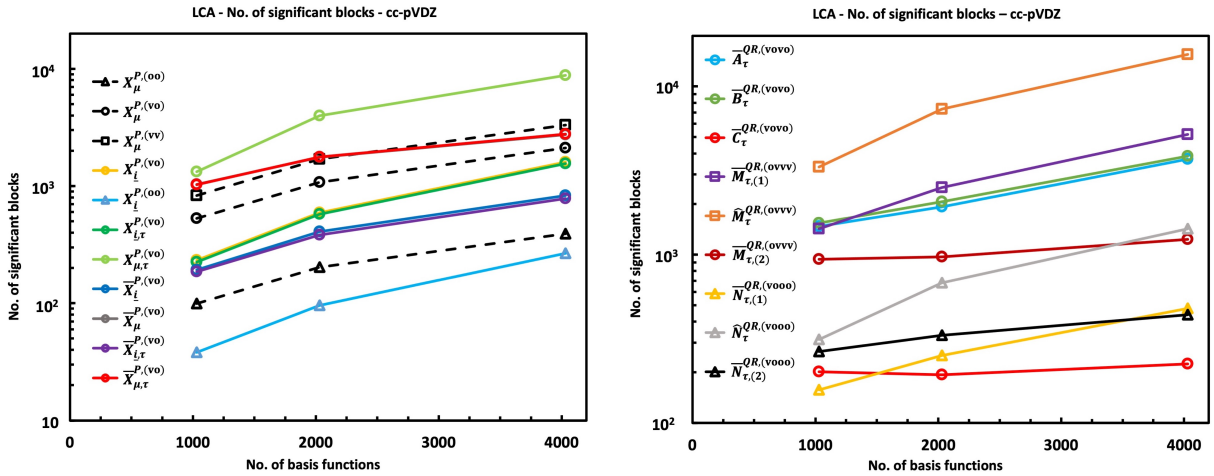

Figure 4: Number of significant blocks for the various THC **X** tensors (left) and the most important Laplace point-dependent intermediates (right) for the CDD-THC-SOS-ADC(2) method. For the Laplace point-dependent intermediates the number of allocated blocks is averaged over the number of quadrature points. All calculations are performed with the cc-pVDZ/cc-pVDZ-RI basis set combination.

DNA Fragments

In order to investigate the scaling behavior in the evaluation of the excitation energy for systems of practical interest, CDD-THC-SOS-ADC(2) was applied to DNA fragments containing up to 16 adenine-thymine-pairs (AT_n), see Figure 5 (left). The smaller DNA fragments can be considered to be three-dimensional systems, which become linear with increasing numbers of base pairs, i.e., in the asymptotic limit. The number of operations performed within one iteration of the MO- and CDD-THC-SOS-ADC(2) is displayed in Figure 5 (right) for the cc-pVDZ basis set and grids generated from the hand-optimized cc-pVDZ- (*grid1*) and cc-pVTZ-based parent grids (*grid2*).

The MO-THC-SOS-ADC(2) implementation shows cubic scaling behavior and a FLOP count reduced by ∼60 times for the fragment with 16 AT-pairs. As demonstrated in the previous section, the computational effort of CDD-THC-SOS-ADC(2) grows quadratically with the system size for both grid types. Contrary to the case of the LCAs, the three-dimensional structure of the DNA fragments does not display sparse one-electron density matrices un-

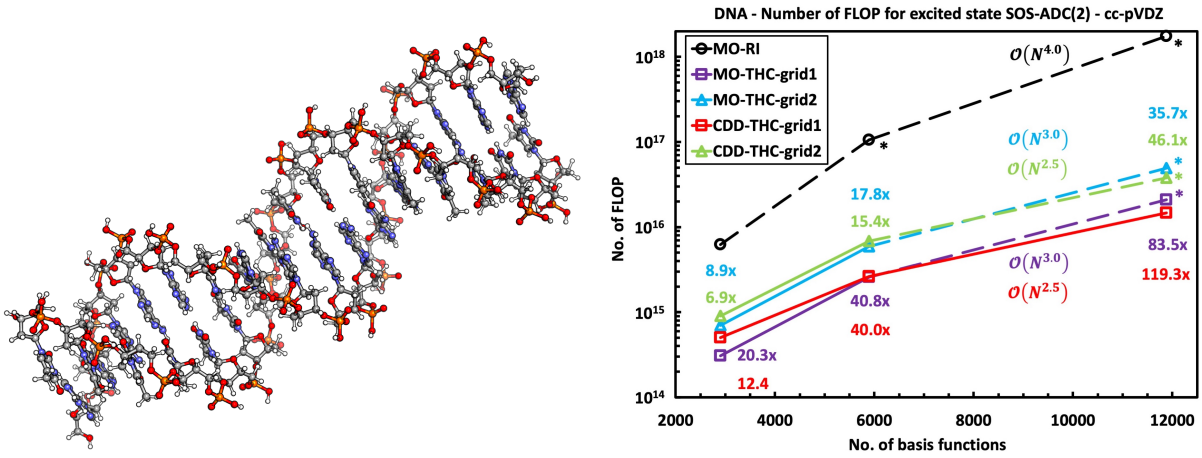

Figure 5: DNA fragment with 16 AT-pairs and 1052 atoms (left). Number of FLOP performed to evaluate the SOS-ADC(2) matrix-vector product for DNA fragments with 4, 8, and 16 AT-pairs using the cc-pVDZ basis set and the grids generated from both the hand-optimized cc-pVDZ- (*grid1*) and cc-pVTZ-based parent grids (*grid2*). Extrapolated values are shown with dashed lines and marked with an asterisk (*). Labels represent the FLOP reduction compared to the MO-RI-SOS-ADC(2) implementation.

til the ∼1000 atoms scale is reached. Thus, the crossover with MO-THC-SOS-ADC(2) is shifted toward ∼6000 basis functions, as shown in Figure 5 (right). The reformulation in the Cholesky basis and the use of sparse linear algebra grant an additional reduction of the prefactor by a factor of ∼2 and hence the newly presented CDD-THC-SOS-ADC(2) method is ∼119-fold faster.

According to the data provided in Figure 5, the THC decomposition is highly recommended for calculations on three-dimensional systems, i.e., when there is not enough sparsity in the electronic structure to reduce the computational effort as well as its scaling with the size. Indeed, MO-THC-SOS-ADC(2) already provides considerable savings in the FLOP count, and the CDD-RI-SOS-ADC(2) reformulation further reduces the effort via sparse linear algebra. In addition, the memory and storage savings should be considered, which extend the applicability of SOS-ADC(2) and SOS-LR-CC2 to much larger systems, without any need of batching the workload until the ∼1000 atoms scale is reached. Taking AT_{16} as an example, one set of MO-based RI integrals using the cc-pVDZ/cc-pVDZ-RI basis set

combination would require ∼6 TB of memory (and disk space) with a ∼20% saving if the Cholesky pseudo-MOs and sparse algebra are put to use. Hence, considering that at least one other set of integrals must be stored in the CDD-RI-SOS-ADC(2) implementation, both the number of input/output operations (I/O) as well as storage demands easily become a bottleneck for common high-performance compute nodes and would render batching – with its intrinsic overhead – mandatory. In contrast, for the same basis set the evaluation of the SOS-ADC(2) and SOS-LR-CC2 excitation energy of AT_{16} using THC only requires ∼500 GB of memory space. In addition, the presented implementation of MO- and CDD-THC-SOS-ADC(2)/CC2 only requires disk I/O for the $\hat{\mathbf{D}}^{\alpha\beta}$ matrices (∼126 GB for AT_{16}/cc-pVDZ/cc-pVDZ-RI) in the Laplace integration, while all other intermediates can be kept in memory.

4.3 Timings

The use of THC grants a reduction of the effort (FLOP) in each iteration and hence runtime speedups are expected for both MO-THC-SOS-ADC(2) and MO-THC-SOS-LR-CC2. Table 7 shows ∼14-fold and ∼7-fold speedups for MO-THC-SOS-MP2 and MO-THC-SOS-CC2 for ground state energy calculations, respectively. Further, speedup of ∼1.5 is achieved by reformulating the methods in the Cholesky pseudo-MO basis and by using sparse linear algebra, as discussed previously.

Table 7: Time required to perform 1 iteration of the respective ground state calculation. Scaling and speedups are reported for the THC-based methods relative to MO-RI-SOS-MP2/CC2.

			MO-RI	MO-THC		CDD-THC	
	System	N_{bf}	Time / h	Time / h	Speedup	Time / h	Speedup
SOS-MP2							
	LCA_{40}	1030	0.01	0.01	2.5	0.01	2.2
	LCA_{80}	2030	0.13	0.02	6.7	0.02	6.8
	LCA_{160}	4030	1.72	0.12	14.3	0.08	22.4
SOS-CC2							
	LCA_{40}	1030	0.03	0.01	2.5	0.02	1.5
	LCA_{80}	2030	0.16	0.07	2.4	0.07	2.4
	LCA_{160}	4030	2.32	0.32	7.2	0.22	10.5

Table 8 reports the speedups for the THC-SOS-ADC(2)/CC2 implementations for excitation energies compared to MO-RI-SOS-ADC(2)/CC2. Since the steps performed to form the CC2 and ADC(2) matrix-vector products are mostly identical, both timings and speedups are similar. For the largest system the MO-based algorithms grant ∼6-fold time savings in each iteration with respect to the MO-RI implementation. As for the ground state step, the local reformulation allows for an additional speedup of a factor of ∼2. Furthermore, THC-based implementation is already faster than MO-RI-SOS-ADC(2)/CC2 for the smallest considered system size, i.e., LCA_{40}, as a crossover is observed at around 40 carbon atoms. Although the CDD reformulation is slower for LCA_{40} due to the lack of sufficient sparsity in the one-electron density matrix, a crossover between the CDD-THC-SOS-ADC(2)/CC2 and the MO-based implementations is observed at around ∼60 carbon atoms.

Table 8: Time required to perform 1 iteration of the excited state calculation. Scaling and speedups are reported for the THC-based methods relative to MO-RI-SOS-LR-CC2/ADC(2).

			MO-RI	MO-THC		CDD-THC	
	System	N_{bf}	Time / h	Time / h	Speedup	Time / h	Speedup
SOS-ADC(2)							
	LCA_{40}	1030	0.02	0.02	1.1	0.03	0.7
	LCA_{80}	2030	0.22	0.09	2.5	0.09	2.4
	LCA_{160}	4030	3.19	0.54	5.9	0.27	12.0
SOS-LR-CC2							
	LCA_{40}	1030	0.04	0.02	1.9	0.04	1.1
	LCA_{80}	2030	0.22	0.09	2.5	0.10	2.3
	LCA_{160}	4030	3.28	0.54	6.0	0.25	13.1

When applied to larger systems, such as DNA fragments, the speedups with respect to the RI-based implementation vastly increase. Table 9 reports the speedup for up to 16 AT-pairs for the two different parent grid types.

First, the timings obtained with the smaller grid originating from the cc-pVDZ basis set are considered. Interestingly, the MO-THC-SOS-ADC(2) method is already ∼9 times faster than MO-RI-SOS-ADC(2) for AT_4, while the speedup for the CDD reformulation is only 4-fold due to the lack of sparsity in the one-electron density matrices. As the size increases

Table 9: Time required to perform 1 iteration of the excited state calculation. Scaling and speedups are reported for the THC-based methods relative to MO-RI-SOS-ADC(2) using the cc-pVDZ/cc-pVDZ-RI basis set combination together with the grids generated from both the hand-optimized cc-pVDZ- (*grid1*) and cc-pVTZ-based parent grids (*grid2*). Extrapolated values are marked with an asterisk (*).

			MO-RI	MO-THC		CDD-THC	
	System	N_{bf}	Time / h	Time / h	Speedup	Time / h	Speedup
grid1							
	AT_4	2904	1.1	0.1	8.9	0.3	4.1
	AT_8	5896	19.0*	0.8	23.4	1.0	18.8
	AT_{16}	11 880	312.2*	6.6*	47.0	4.6	68.1
grid2							
	AT_4	2904	1.1	0.4	2.6	0.5	2.2
	AT_8	5896	19.0*	2.3	8.3	2.5	7.7
	AT_{16}	11 880	312.2*	19.0*	16.4	11.1*	28.1

and simultaneously the densities become more sparse, a crossover between the MO-based and the CDD-THC-SOS-ADC(2) implementations is observed at around ∼6000 basis functions. For the largest considered fragment, i.e., AT_{16}, MO-THC-SOS-ADC(2) is ∼47 times faster than MO-RI-SOS-ADC(2) and is able to perform one iteration of the DIIS procedure in just ∼7 hours, against the 312 hours estimated for MO-RI-SOS-ADC(2). When further taking advantage of the sparsity in the densities with the CDD approach, it is possible to perform one iteration in just ∼5 hours for 16 AT-pairs. When instead the THC-grid is generated from the cc-pVTZ-based parent grid – as used for the LCA calculations – the speedups are reduced due to the larger number of grid points. Nonetheless, it is possible to perform one DIIS iteration of MO- and CDD-THC-SOS-ADC(2) with ∼16-fold and ∼28-fold speedups compared to MO-RI-SOS-ADC(2), respectively. In total, with both the MO-THC-SOS-ADC(2) and the CDD-THC-SOS-ADC(2) methods it is possible to compute the excitation energies to the two lowest singlet states of AT_8 in ∼3 days when using the cc-pVDZ basis set and the THC grid generated from the cc-pVTZ-based parent grid.

Employing CDD-THC-SOS-ADC(2) makes it possible to compute the excitation energy to the lowest singlet excited state of AT_{16} for the cc-pVDZ basis set. The total time required

for the calculation is ∼3.5 days, for which most of the time is spent evaluating the THC $\mathbf{\Gamma}$ matrices, which take up ∼25.5% of the total computation time, and calculation of the ADC(2) excitation energy, which requires ∼57.2% of the total computation time. Notice that the ADC(2) optimization procedure is converged with thresholds of 10^{-6} and 10^{-5} for the excitation vector and the energy, respectively. The SCF procedure, the calculation of the MP2 energy correction, and the evaluation of the ground state intermediates $\mathbf{E}$ from eq. 76 together required ∼4.6% of the total time. Finally, the pre-optimization at the CCS level within the Davidson procedure took ∼12.9% of the time. The generous speedup granted by a smaller grid comes with a reasonable error in the excitation energies. In fact, the error introduced by this grid type for CDD-THC-SOS-ADC(2) calculations on AT_4 is ∼0.01 eV. Despite being larger than the error provided in Table 5, it is known to be small enough for investigating the electronic transition and additionally provides a good starting point for optimizations with larger grids. At this point, it is important to stress that the error in the excitation energies does not increase with the size of the system, as demonstrated in Section 4.1, and hence we expect an error of the same order for the AT_{16} system when using the smaller grid.

5 Conclusion

An efficient reformulation of SOS-LR-CC2 and SOS-ADC(2) for both ground state as well as excitation energies is presented. The implementation leverages the THC-factorized representation of the ERIs together with block-sparse linear algebra for the resulting tensor contractions. The latter is particularly attractive since local Cholesky pseudo-MOs from the CDD approach are employed in the Laplace integration, which cause the number of significant blocks in all ground state-dependent intermediates to grow linearly, while excited state related intermediates here show constant scaling. Since SOS-LR-CC2 and SOS-ADC(2) only involve Coulomb-type integral contractions, no higher than second-order tensors have

to be formed and all FLOP-intensive contractions can be performed by block-sparse matrix-matrix multiplications. Furthermore, a density-based integral-direct approach for the grid-projection of the ERI tensor, which is the most time-consuming step in the THC fitting, is presented. The density-based reformulation allows to use existing code for Coulomb matrix builds in the grid-projection. This facilitates the implementation of LS-THC in quantum chemistry packages, since apart from linear algebra, which is readily available from BLAS implementations, only the ability to evaluate basis functions on a real-space DFT-like grid is required then. Consequently, LS-THC is easily implemented in existing quantum chemistry programs, which already implement a Kohn–Sham SCF. Nonetheless, an optimized kernel for this type of integral contraction can improve the performance of this step significantly, as demonstrated above. Combined with the described optimizations, memory-efficient and effectively sub-quadratically scaling implementations of SOS-LR-CC2 and SOS-ADC(2) for the computation of excitation energies are presented. The efficiency of the presented approach is demonstrated for representative systems up to 1000 atoms and 12000 basis functions.

Acknowledgement

The authors acknowledge financial support by the cluster of excellence (EXC2111-390814868) "Munich Center for Quantum Science and Technology" (MCQST), the Deutsche Forschungsgemeinschaft (DFG) under Grant TRR325 'Assembly Controlled Chemical Photocatalysis' (grant No. 444632635), and the Marie Skłodowska-Curie European Training Network "COSINE - COmputational Spectroscopy In Natural sciences and Engineering," Grant Agreement No. 765739. C.O. acknowledges additional support as Max-Planck-Fellow at the MPI-FKF Stuttgart. F.H.B. thanks the "Fonds der Chemischen Industrie" (FCI) for a graduate fellowship. The authors thank Y. Lemke (LMU Munich) for helpful discussions and Dr. J. Kussmann (LMU Munich) for providing a development version of the FermiONs++ program package.

Supporting Information Available

Details about the sparsity-conserving grid pruning, explicit expressions for the THC-SOS-CC2 ground state energy and the THC-SOS-LR-CC2/ADC(2) triplet excited states, programmable equations for the MO-THC-SOS-LR-CC2 method, and details about the error propagation in the iterative amplitude optimization.

References

(1) Serrano-Andrés, L.; Merchán, M. Quantum Chemistry of the Excited State: 2005 Overview. *J. Mol. Struct. Theochem* **2005**, *729*, 99–108.

(2) Hershenson, H. *Ultraviolet and visible absorption spectra*; Elsevier, 2012.

(3) Rodger, A.; Sanders, K. *Encyclopedia of spectroscopy and spectrometry*; Elsevier, 2017; pp 495–502.

(4) Agarwal, B. K. *X-ray spectroscopy: an introduction*; Springer, 2013; Vol. 15.

(5) Sherrill, C. D.; Schaefer III, H. F. *Advances in quantum chemistry*; Elsevier, 1999; Vol. 34; pp 143–269.

(6) Helgaker, T.; Jorgensen, P.; Olsen, J. *Molecular electronic-structure theory*; John Wiley & Sons, 2013.

(7) Dreuw, A.; Papapostolou, A.; Dempwolff, A. L. Algebraic Diagrammatic Construction Schemes Employing the Intermediate State Formalism: Theory, Capabilities, and Interpretation. *The J. Phys. Chem. A* **2023**, *127*, 6635–6646.

(8) Crawford, T. D.; Kumar, A.; Bazanté, A. P.; Di Remigio, R. Reduced-scaling coupled cluster response theory: Challenges and opportunities. *Wiley Interdiscip. Rev. Comput. Mol. Sci.* **2019**, *9*, e1406.

(9) Head-Gordon, M.; Oumi, M.; Maurice, D. Quasidegenerate second-order perturbation corrections to single-excitation configuration interaction. *Mol. Phys.* **1999**, *96*, 593–602.

(10) Casida, M. E. *Recent Advances in Density Functional Methods*; 1999; Vol. 1.

(11) Casida, M. E.; Huix-Rotllant, M. Progress in time-dependent density-functional theory. *Annu. Rev. Phys. Chem.* **2012**, *63*, 287–323.

(12) Dreuw, A.; Head-Gordon, M. Single-reference ab initio methods for the calculation of excited states of large molecules. **2005**, *105*, 4009–4037.

(13) Roos, B. O.; Taylor, P. R.; Sigbahn, P. E. A complete active space SCF method (CASSCF) using a density matrix formulated super-CI approach. *Chem. Phys.* **1980**, *48*, 157–173.

(14) Roos, B. O.; Andersson, K.; Fulscher, M. P.; Malmqvist, P.-A.; SerranoAndres, L.; Pierloot, K.; Merchán, M. Multiconfigurational perturbation theory: Applications in electronic spectroscopy. *Adv Chem Phys.* **1996**, *93*, 219–331.

(15) Andersson, K.; Malmqvist, P. A.; Roos, B. O.; Sadlej, A. J.; Wolinski, K. Second-order perturbation theory with a CASSCF reference function. *J. Phys. Chem.* **1990**, *94*, 5483–5488.

(16) Schirmer, J. Beyond the random-phase approximation: A new approximation scheme for the polarization propagator. *Phys. Rev. A* **1982**, *26*, 2395.

(17) Dreuw, A.; Wormit, M. The algebraic diagrammatic construction scheme for the polarization propagator for the calculation of excited states. *Wiley Interdisciplinary Reviews: Computational Molecular Science* **2015**, *5*, 82–95.

(18) Mertins, F.; Schirmer, J. Algebraic propagator approaches and intermediate-state representations. I. The biorthogonal and unitary coupled-cluster methods. *Phys. Rev. A* **1996**, *53*, 2140.

(19) Harbach, P. H.; Wormit, M.; Dreuw, A. The third-order algebraic diagrammatic construction method (ADC (3)) for the polarization propagator for closed-shell molecules: Efficient implementation and benchmarking. *J. Phys. Chem.* **2014**, *141*, 064113.

(20) Sekino, H.; Bartlett, R. J. A linear response, coupled-cluster theory for excitation energy. *Int. J. Quantum Chem.* **1984**, *26*, 255–265.

(21) Koch, H.; Jørgensen, P. Coupled cluster response functions. *J. Phys. Chem.* **1990**, *93*, 3333.

(22) Pedersen, T. B.; Koch, H. Coupled cluster response functions revisited. *J. Phys. Chem.* **1997**, *106*, 8059–8072.

(23) Sneskov, K.; Christiansen, O. Excited state coupled cluster methods. *Wiley Interdiscip. Rev. Comput. Mol. Sci.* **2012**, *2*, 566–584.

(24) Christiansen, O.; Koch, H.; Jo/rgensen, P. Response functions in the CC3 iterative triple excitation model. *J. Phys. Chem.* **1995**, *103*, 7429–7441.

(25) Christiansen, O.; Koch, H.; Jørgensen, P. The second-order approximate coupled cluster singles and doubles model CC2. *Chem. Phys. Lett.* **1995**, *243*, 409–418.

(26) Grimme, S. Improved second-order Møller-Plesset perturbation theory by separate scaling of parallel-and antiparallel-spin pair correlation energies. *J. Phys. Chem.* **2003**, *118*, 9095–9102.

(27) Jung, Y.; Lochan, R. C.; Dutoi, A. D.; Head-Gordon, M. Scaled opposite-spin second order Møller-Plesset correlation energy: an economical electronic structure method. *J. Phys. Chem.* **2004**, *121*, 9793–9802.

(28) Jung, Y.; Shao, Y.; Head-Gordon, M. Fast evaluation of scaled opposite spin second-order Møller-Plesset correlation energies using auxiliary basis expansions and exploiting sparsity. *J. Comput. Chem.* **2007**, *28*, 1953–1964.

(29) Winter, N. O. C.; Hättig, C. Scaled Opposite-Spin CC2 for Ground and Excited States with Fourth Order Scaling Computational Costs. *J. Phys. Chem.* **2011**, *134*, 184101.

(30) Krauter, C. M.; Pernpointner, M.; Dreuw, A. Application of the scaled-opposite-spin approximation to algebraic diagrammatic construction schemes of second order. *J. Phys. Chem.* **2013**, *138*.

(31) Whitten, J. L. Coulombic Potential Energy Integrals and Approximations. *J. Phys. Chem.* **1973**, *58*, 4496.

(32) Dunlap, B. I.; Connolly, J. W.; Sabin, J. R. On Some Approximations in Applications of Xα Theory. *J. Chem. Phys.* **1979**, *71*, 3396.

(33) Feyereisen, M.; Fitzgerald, G.; Komornicki, A. Use of Approximate Integrals in Ab Initio Theory. An Application in MP2 Energy Calculations. *Chem. Phys. Lett.* **1993**, *208*, 359–363.

(34) Eichkorn, K.; Treutler, O.; Öhm, H.; Häser, M.; Ahlrichs, R. Auxiliary Basis Sets to Approximate Coulomb Potentials. *Chem. Phys. Lett.* **1995**, *240*, 283–290.

(35) Baudin, P.; Marín, J. S.; Cuesta, I. G.; Sánchez De Merás, A. M. J. Calculation of Excitation Energies from the CC2 Linear Response Theory Using Cholesky Decomposition. *J. Phys. Chem.* **2014**, *140*, 104111.

(36) Almlöf, J. Elimination of energy denominators in Møller—Plesset perturbation theory by a Laplace transform approach. *Chemical physics letters* **1991**, *181*, 319–320.

(37) Häser, M.; Almlöf, J. Laplace transform techniques in Mo/ller–Plesset perturbation theory. *The Journal of chemical physics* **1992**, *96*, 489–494.

(38) Sacchetta, F.; Graf, D.; Laqua, H.; Ambroise, M. A.; Kussmann, J.; Dreuw, A.; Ochsenfeld, C. An Effective Sub-Quadratic Scaling Atomic-Orbital Reformulation of the Scaled

Opposite-Spin RI-CC2 Ground-State Model Using Cholesky-decomposed Densities and an Attenuated Coulomb Metric. *J. Phys. Chem.* **2022**, *157*, 104104.

(39) Ambroise, M. A.; Sacchetta, F.; Graf, D.; Ochsenfeld, C.; Dreuw, A. Scaled Opposite-Spin Atomic-Orbital Based Algebraic Diagrammatic Construction Scheme for the Polarization Propagator with Asymptotic Linear-Scaling Effort: Theory and Implementation. *J. Phys. Chem.* **2023**, *158*, 124121.

(40) Luenser, A.; Schurkus, H. F.; Ochsenfeld, C. Vanishing-Overhead Linear-Scaling Random Phase Approximation by Cholesky Decomposition and an Attenuated Coulomb-Metric. *J. Chem. Theory Comput.* **2017**, *13*, 1647–1655.

(41) Maurer, S. A.; Clin, L.; Ochsenfeld, C. Cholesky-decomposed density MP2 with density fitting: Accurate MP2 and double-hybrid DFT energies for large systems. *J. Phys. Chem.* **2014**, *140*, 224112.

(42) Glasbrenner, M.; Graf, D.; Ochsenfeld, C. Efficient Reduced-Scaling Second-Order Møller-Plesset Perturbation Theory with Cholesky-Decomposed Densities and an Attenuated Coulomb Metric. *J. Chem. Theory Comput.* **2020**, *16*, 6856–6868.

(43) Beer, M.; Ochsenfeld, C. Efficient linear-scaling calculation of response properties: Density matrix-based Laplace-transformed coupled-perturbed self-consistent field theory. 2008.

(44) Beuerle, M.; Graf, D.; Schurkus, H. F.; Ochsenfeld, C. Efficient calculation of beyond RPA correlation energies in the dielectric matrix formalism. *J. Phys. Chem.* **2018**, *148*, 204104.

(45) Graf, D.; Beuerle, M.; Ochsenfeld, C. Low-scaling self-consistent minimization of a density matrix based random phase approximation method in the atomic orbital space. *J. Chem. Theory Comput.* **2019**, *15*, 4468–4477.

(46) Hohenstein, E. G.; Parrish, R. M.; Martínez, T. J. Tensor Hypercontraction Density Fitting. I. Quartic Scaling Second- and Third-Order Møller-Plesset Perturbation Theory. *J. Chem. Phys.* **2012**, *137*, 044103.

(47) Parrish, R. M.; Hohenstein, E. G.; Martínez, T. J.; Sherrill, C. D. Tensor Hypercontraction. II. Least-squares Renormalization. *J. Chem. Phys.* **2012**, *137*, 224106.

(48) Parrish, R. M.; Hohenstein, E. G.; Martínez, T. J.; Sherrill, C. D. Discrete Variable Representation in Electronic Structure Theory: Quadrature Grids for Least-Squares Tensor Hypercontraction. *J. Chem. Phys.* **2013**, *138*, 194107.

(49) Parrish, R. M.; Hohenstein, E. G.; Schunck, N. F.; Sherrill, C. D.; Martínez, T. J. Exact Tensor Hypercontraction: A Universal Technique for the Resolution of Matrix Elements of Local Finite-Range N-body Potentials in Many-Body Quantum Problems. *Phys. Rev. Lett.* **2013**, *111*, 1–5.

(50) Hohenstein, E. G.; Kokkila, S. I.; Parrish, R. M.; Martínez, T. J. Quartic Scaling Second-Order Approximate Coupled Cluster Singles and Doubles via Tensor Hypercontraction: THC-CC2. *J. Chem. Phys.* **2013**, *138*, 124111.

(51) Parrish, R. M.; Sherrill, C. D.; Hohenstein, E. G.; Kokkila, S. I.; Martínez, T. J. Communication: Acceleration of Coupled Cluster Singles and Doubles via Orbital-Weighted Least-Squares Tensor Hypercontraction. *J. Chem. Phys.* **2014**, *140*, 181102.

(52) Schutski, R.; Zhao, J.; Henderson, T. M.; Scuseria, G. E. Tensor-Structured Coupled Cluster Theory. *J. Chem. Phys.* **2017**, *147*, 184113.

(53) Hohenstein, E. G.; Fales, B. S.; Parrish, R. M.; Martínez, T. J. Rank-Reduced Coupled-Cluster. III. Tensor Hypercontraction of the Doubles Amplitudes. *J. Phys. Chem.* **2022**, *156*, 054102.

(54) Jiang, A.; Turney, J. M.; Schaefer, H. F. Tensor Hypercontraction Form of the Perturbative Triples Energy in Coupled-Cluster Theory. *J. Chem. Theory Comput.* **2023**, *19*, 1476–1486.

(55) Hohenstein, E. G.; Kokkila, S. I.; Parrish, R. M.; Martínez, T. J. Tensor Hypercontraction Equation-of-Motion Second-Order Approximate Coupled Cluster: Electronic Excitation Energies in O(N4) Time. *J. Phys. Chem. B* **2013**, *117*, 12972–12978.

(56) DiStasio, R. A.; Jung, Y.; Head-Gordon, M. A resolution-of-the-identity implementation of the local triatomics-in-molecules model for second-order Møller- Plesset perturbation theory with application to alanine tetrapeptide conformational energies. *J. Chem. Theory Comput.* **2005**, *1*, 862–876.

(57) Matthews, D. A. Improved Grid Optimization and Fitting in Least Squares Tensor Hypercontraction. *J. Chem. Theory Comput.* **2020**, *16*, 1382–1385.

(58) Bangerter, F. H.; Glasbrenner, M.; Ochsenfeld, C. Low-Scaling Tensor Hypercontraction in the Cholesky Molecular Orbital Basis Applied to Second-Order Møller-Plesset Perturbation Theory. *J. Chem. Theory Comput.* **2021**, *17*, 211–221.

(59) Maurer, S. A.; Kussmann, J.; Ochsenfeld, C. Communication: A Reduced Scaling J-engine Based Reformulation of SOS-MP2 Using Graphics Processing Units. *J. Chem. Phys.* **2014**, *141*.

(60) Kussmann, J.; Laqua, H.; Ochsenfeld, C. Highly Efficient Resolution-of-Identity Density Functional Theory Calculations on Central and Graphics Processing Units. *J. Chem. Theory Comput.* **2021**, *17*, 1512–1521.

(61) Drontschenko, V.; Graf, D.; Laqua, H.; Ochsenfeld, C. Lagrangian-Based Minimal-Overhead Batching Scheme for the Efficient Integral-Direct Evaluation of the RPA Correlation Energy. *J. Chem. Theory Comput.* **2021**, *17*, 5623–5634.

(62) Dunning, T. H. Gaussian basis sets for use in correlated molecular calculations. I. The atoms boron through neon and hydrogen. *J. Chem. Phys.* **1989**, *90*, 1007–1023.

(63) Woon, D. E.; Dunning, T. H. Gaussian basis sets for use in correlated molecular calculations. III. The atoms aluminum through argon. *J. Chem. Phys.* **1993**, *98*, 1358–1371.

(64) Weigend, F.; Köhn, A.; Hättig, C. Efficient Use of the Correlation Consistent Basis Sets in Resolution of the Identity MP2 Calculations. *The Journal of Chemical Physics* **2002**, *116*, 3175–3183.

(65) Obara, S.; Saika, A. Efficient recursive computation of molecular integrals over Cartesian Gaussian functions. *J. Chem. Phys.* **1986**, *84*, 3963–3974.

(66) Obara, S.; Saika, A. General recurrence formulas for molecular integrals over Cartesian Gaussian functions. *J. Chem. Phys.* **1988**, *89*, 1540–1559.

(67) Laqua, H.; Kussmann, J.; Ochsenfeld, C. Efficient and Linear-Scaling Seminumerical Method for Local Hybrid Density Functionals. *J. Chem. Theory Comput.* **2018**, *14*, 3451–3458.

(68) Laqua, H.; Thompson, T. H.; Kussmann, J.; Ochsenfeld, C. Highly efficient, linear-scaling seminumerical exact-exchange method for graphic processing units. *J. Chem. Theory Comput.* **2020**, *16*, 1456–1468.

(69) Laqua, H.; Kussmann, J.; Ochsenfeld, C. Accelerating seminumerical Fock-exchange calculations using mixed single-and double-precision arithmethic. *J. Phys. Chem.* **2021**, *154*.

(70) Meurer, A.; Smith, C. P.; Paprocki, M.; Čertík, O.; Kirpichev, S. B.; Rocklin, M.; Kumar, A.; Ivanov, S.; Moore, J. K.; Singh, S.; Rathnayake, T.; Vig, S.; Granger, B. E.; Muller, R. P.; Bonazzi, F.; Gupta, H.; Vats, S.; Johansson, F.; Pedregosa, F.;

Curry, M. J.; Terrel, A. R.; Roučka, v.; Saboo, A.; Fernando, I.; Kulal, S.; Cimrman, R.; Scopatz, A. SymPy: symbolic computing in Python. *PeerJ Computer Science* **2017**, *3*, e103.

(71) Kussmann, J.; Laqua, H.; Ochsenfeld, C. Highly efficient resolution-of-identity density functional theory calculations on central and graphics processing units. *J. Chem. Theory Comput.* **2021**, *17*, 1512–1521.

(72) Hättig, C.; Weigend, F. CC2 excitation energy calculations on large molecules using the resolution of the identity approximation. *J. Phys. Chem.* **2000**, *113*, 5154–5161.

(73) Hättig, C. Structure optimizations for excited states with correlated second-order methods: CC2 and ADC (2). *Adv. Quantum Chem.* **2005**, *50*, 37–60.

(74) Pulay, P. Improved SCF convergence acceleration. *J. Comput. Chem.* **1982**, *3*, 556–560.

(75) Kats, D.; Schütz, M. A multistate local coupled cluster CC2 response method based on the Laplace transform. *J. Phys. Chem.* **2009**, *131*.

(76) Higham, N. J. Cholesky factorization. *Wiley Interdiscip. Rev. Comput. Stat.* **2009**, *1*, 251–254.

(77) Harbrecht, H.; Peters, M.; Schneider, R. On the low-rank approximation by the pivoted Cholesky decomposition. *Appl. Numer. Math.* **2012**, *62*, 428–440.

(78) Bangerter, F. H.; Glasbrenner, M.; Ochsenfeld, C. Tensor-Hypercontracted MP2 First Derivatives: Runtime and Memory Efficient Computation of Hyperfine Coupling Constants. *J. Chem. Theory Comput.* **2022**, acs.jctc.2c00118.

(79) Kussmann, J.; Ochsenfeld, C. Pre-selective screening for matrix elements in linear-scaling exact exchange calculations. *J. Chem. Phys.* **2013**, *138*, 134114.

(80) Kussmann, J.; Ochsenfeld, C. Preselective screening for linear-scaling exact exchange-gradient calculations for graphics processing units and general strong-scaling massively parallel calculations. *J. Chem. Theory Comput.* **2015**, *11*, 918–922.

(81) Kussmann, J.; Ochsenfeld, C. Hybrid CPU/GPU Integral Engine for Strong-Scaling Ab Initio Methods. *J. Chem. Theory Comput.* **2017**, *13*, 3153–3159.

(82) Dagum, L.; Menon, R. OpenMP: an industry standard API for shared-memory programming. *Computational Science & Engineering, IEEE* **1998**, *5*, 46–55.

(83) Weigend, F. A Fully Direct RI-HF Algorithm: Implementation, Optimised Auxiliary Basis Sets, Demonstration of Accuracy and Efficiency. *Phys. Chem. Chem. Phys.* **2002**, *4*, 4285–4291.

(84) Kokkila Schumacher, S. I.; Hohenstein, E. G.; Parrish, R. M.; Wang, L. P.; Martínez, T. J. Tensor Hypercontraction Second-Order Møller-Plesset Perturbation Theory: Grid Optimization and Reaction Energies. *J. Chem. Theory Comput.* **2015**, *11*, 3042–3052.

(85) Maslen, P. E.; Ochsenfeld, C.; White, C. A.; Lee, M. S.; Head-Gordon, M. Locality and sparsity of ab initio one-particle density matrices and localized orbitals. *The J. Phys. Chem. A* **1998**, *102*, 2215–2222.

(86) Ochsenfeld, C.; Kussmann, J.; Lambrecht, D. S. Linear-scaling methods in quantum chemistry. *Rev. Comput. Chem.* **2007**, *23*, 1.

TOC Graphic

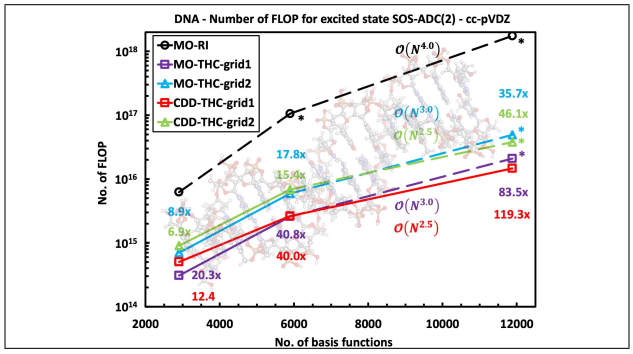
DNA - Number of FLOP for excited state SOS-ADC(2) - cc-pVDZ
MO-RI
MO-THC-grid1
MO-THC-grid2
CDD-THC-grid1
CDD-THC-grid2
$O(N^{4.0})$
$O(N^{3.0})$
$O(N^{2.5})$
$O(N^{3.0})$
$O(N^{2.5})$
35.7x
46.1x
17.8x
15.4x
8.9x
6.9x
83.5x
119.3x
40.8x
40.0x
20.3x
12.4
No. of FLOP
No. of basis functions
10^{18}
10^{17}
10^{16}
10^{15}
10^{14}
2000
4000
6000
8000
10000
12000

Supporting Information: Efficient Low-scaling Calculation of THC-SOS-CC2 and THC-SOS-ADC(2) Excitation Energies Through Density-based Integral-direct Tensor Hypercontraction

Filippo Sacchetta,[†] Felix H. Bangerter,[†] Henryk Laqua,[†] and Christian Ochsenfeld[*,†,‡]

†*Chair of Theoretical Chemistry, Department of Chemistry, University of Munich (LMU), D-81377 Munich, Germany*

‡*Max Planck Institute for Solid State Research, D-70569 Stuttgart, Germany*

E-mail: christian.ochsenfeld@cup.uni-muenchen.de

Contents

1 Sparsity-conserving Grid Pruning **S-3**

2 Ground State Equations **S-5**

3 Excited State Equations - Triplet States **S-6**

4 Programmable Equations for the MO-based algorithm **S-8**

5 Growth of the error in the T1 amplitudes during the CC2 optimization **S-9**

6 DNA Scaling **S-9**

References **S-9**

1 Sparsity-conserving Grid Pruning

Throughout this work the grid pruning technique by Matthews[S1] was used, which serves two purposes: 1) a removal of unnecessary linear combinations of grid points and 2) the solution of the system of linear equations required for forming the final $\mathbf{\Gamma}$ intermediates. Instead of defining novel parent grids from which to prune from, the hand-optimized grid for the cc-pVTZ basis set by Kokkila Schumacher *et al.*[S2] is used as a parent grid. In the following, the influence of the pruning threshold ε, i.e., the rank threshold in the underlying pivoted Cholesky decomposition (PCD), on the accuracy is assessed. Figure S1 shows the behavior of the error (solid lines) of THC-SOS-RI-MP2 compared to SOS-RI-MP2 as well as the growth of the numerical rank (dashed lines), i.e., the resulting number of grid points N_{grid} after pruning, for LCAs up to 160 carbon atoms.

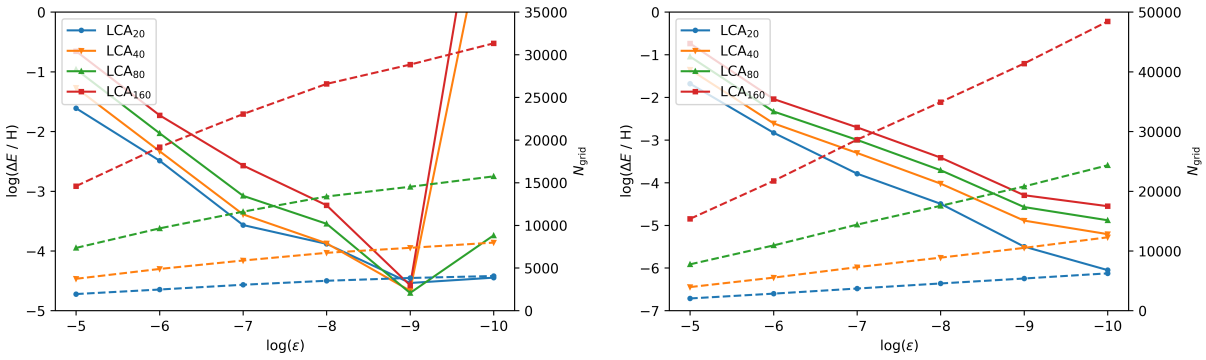

Figure S1: Behavior of the error (solid lines) of THC-SOS-RI-MP2 compared to SOS-RI-MP2 as well as the growth of the numerical rank (dashed lines) with an increasingly tight pruning threshold ε. All calculations were performed with the cc-pVDZ/cc-pVDZ-RI basis set combination and with the hand-optimized grids for the cc-pVDZ (left) and cc-pVTZ (right) basis set as parent grids.

In general a smooth linear reduction of the error and a linear growth of the number of resulting grid points is observed with increasingly tight pruning thresholds, like previously reported by Matthews.[S1] Also, with the hand-optimized grid for the cc-pVDZ basis set serving as a parent grid, the accuracy deteriorates beyond a threshold of 10^{-9}. While with the tightest reasonable threshold an acceptable accuracy on the order of 10^{-5} H for absolute

energies is achieved for both parent grids, the cc-pVTZ based parent grid was chosen for all calculations in the main part of this paper because of the more well-behaved error. Additionally note that by comparing the errors between the LCAs of different chain length, it is observed that the error grows linearly with the molecule size, as reported previously.[S1,S3] One potential drawback of the PCD-based grid pruning is the pivoting, which changes the order of the grid points, or rather linear combinations thereof. To increase sparsity in the one-particle density matrix it is custom to reorder atoms according to the reverse Cuthill–McKee (RCM)[S4] algorithm in order to minimize the bandwidth of the resulting density matrix. Likewise, this reordering also reduces the bandwidth of grid-based intermediates like the grid metric $\mathbf{S}$, for which the order of the grid points is predominately determined by the order of the atoms since the constituting grids are atom-centered. However, the pivoting in the PCD causes are reordering of the grid points which results in unwanted fill-in. To preserve sparsity, all resulting grid points after pruning are assigned to their closest neighboring atom and then ordered according to their parent atom in the order determined by the RCM algorithm. Figure S2 demonstrates the described situation for the THC grid metric tensor $\mathbf{S}$ for LCA_{80} and highlights the importance of the reordering of the grid points after pivoting.

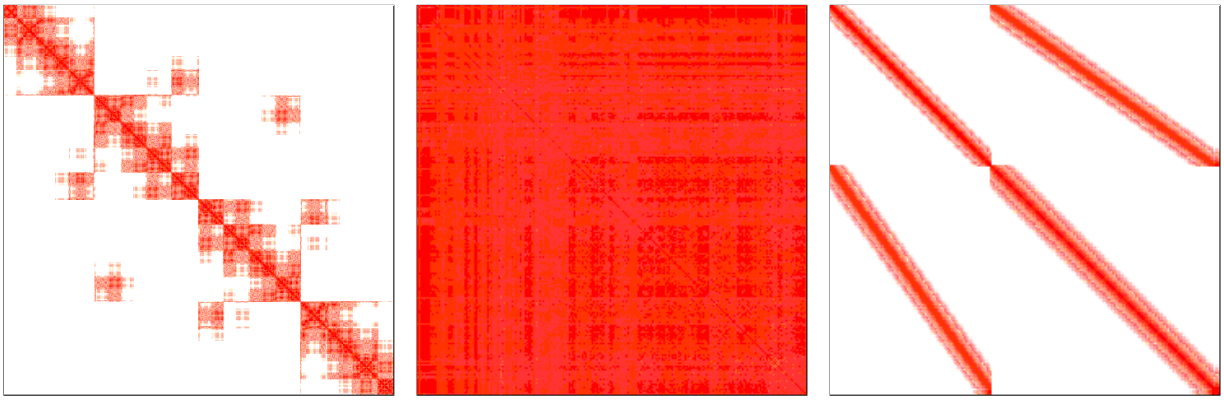

Figure S2: Block sparsity pattern of the THC grid metric **S** in the AO basis before (left) and after pruning (center), as well as after reordering of the grid points (right). Red pixels indicate significant blocks while white pixels represent blocks for which the norm is less than 10^{-10}. All sparsity patterns are obtained from LCA_{80} using the cc-pVDZ basis set and pruning from the hand-optimized cc-pVTZ based grid for the occupied-virtual subspace. Note that the images for the **S** tensor after pruning are scaled up; before pruning **S** was of size 45411×45411 and after pruning of size 22906×22906.

2 Ground State Equations

$$
\begin{aligned}
\Omega^{\mathrm{G}}_{ai} &= -c_{\mathrm{os}} \sum_{\tau} w_\tau \sum_{cbj} \sum_{\alpha,P,Q} \sum_{\beta,R,S} \hat{X}^{P,(\mathrm{vo})}_{c} \hat{X}^{P,(\mathrm{vo})}_{i} \Gamma^{P,(\mathrm{vo})}_{\alpha} \Gamma^{Q,(\mathrm{vo})}_{\alpha} \hat{X}^{Q,(\mathrm{vo})}_{b} \hat{X}^{Q,(\mathrm{vo})}_{j} e^{-\epsilon_{ci} t_\tau} e^{-\epsilon_{bj} t_\tau} \\
&\quad \cdot \left(X^{R,(\mathrm{vo})}_{j} X^{R,(\mathrm{vo})}_{b} \Gamma^{R,(\mathrm{vo})}_{\beta} \Gamma^{S,(\mathrm{vv})}_{\beta} \hat{X}^{S,(\mathrm{vv})}_{a} X^{S,(\mathrm{vv})}_{c} \right) \\
&= -c_{\mathrm{os}} \sum_{\tau} \sum_{P,S} \hat{X}^{P,(\mathrm{vo})}_{i,\tau} \left[\sum_{\alpha,\beta} \sum_{Q,R} \hat{B}^{PS,(\mathrm{ovvv})}_{\tau} \Gamma^{P,(\mathrm{vo})}_{\alpha} \Gamma^{Q,(\mathrm{vo})}_{\alpha} \hat{A}^{QR,(\mathrm{vovo})}_{\tau} \hat{B}^{QR,(\mathrm{vovo})}_{\tau} \Gamma^{R,(\mathrm{vo})}_{\beta} \Gamma^{S,(\mathrm{vv})}_{\beta} \right] \hat{X}^{S,(\mathrm{vv})}_{a} \\
&= -c_{\mathrm{os}} \sum_{\tau} \sum_{P,S} \hat{X}^{P,(\mathrm{vo})}_{i,\tau} M^{PS,(\mathrm{ovvv})}_{\tau} \hat{X}^{S,(\mathrm{vv})}_{a} \qquad (1)
\end{aligned}
$$

$$
\begin{aligned}
\Omega^{\mathrm{H}}_{ai} &= c_{\mathrm{os}} \sum_{\tau} w_\tau \sum_{kbj} \sum_{\alpha,P,Q} \sum_{\beta,R,S} \hat{X}^{P,(\mathrm{vo})}_{a} \hat{X}^{P,(\mathrm{vo})}_{k} \Gamma^{P,(\mathrm{vo})}_{\alpha} \Gamma^{Q,(\mathrm{vo})}_{\alpha} \hat{X}^{Q,(\mathrm{vo})}_{b} \hat{X}^{Q,(\mathrm{vo})}_{j} e^{-\epsilon_{ak} t_\tau} e^{-\epsilon_{bj} t_\tau} \\
&\quad \cdot \left(X^{R,(\mathrm{vo})}_{j} X^{R,(\mathrm{vo})}_{b} \Gamma^{R,(\mathrm{vo})}_{\beta} \Gamma^{S,(\mathrm{oo})}_{\beta} X^{S,(\mathrm{oo})}_{k} \hat{X}^{S,(\mathrm{oo})}_{i} \right) \\
&= c_{\mathrm{os}} \sum_{\tau} \sum_{P,S} \hat{X}^{P,(\mathrm{vo})}_{a,\tau} \left[\sum_{\alpha,\beta} \sum_{Q,R} \hat{A}^{PS,(\mathrm{vooo})}_{\tau} \Gamma^{P,(\mathrm{vo})}_{\alpha} \Gamma^{Q,(\mathrm{vo})}_{\alpha} \hat{A}^{QR,(\mathrm{vovo})}_{\tau} \hat{B}^{QR,(\mathrm{vovo})}_{\tau} \Gamma^{R,(\mathrm{vo})}_{\beta} \Gamma^{S,(\mathrm{vv})}_{\beta} \right] \hat{X}^{S,(\mathrm{oo})}_{i} \\
&= c_{\mathrm{os}} \sum_{\tau} \sum_{P,S} \hat{X}^{P,(\mathrm{vo})}_{a,\tau} N^{PS,(\mathrm{vooo})}_{\tau} \hat{X}^{S,(\mathrm{vv})}_{i} \qquad (2)
\end{aligned}
$$

$$
\begin{aligned}
E^{\text{SOS-CC2}} &= c_{\text{os}} \sum_{aibj} \sum_{\beta,P,Q} t_{ai} t_{bj} X_a^{R,(\text{vo})} X_i^{R,(\text{vo})} \Gamma_\alpha^{R,(\text{vo})} \Gamma_\alpha^{S,(\text{vo})} X_b^{S,(\text{vo})} X_j^{S,(\text{vo})} \\
&- c_{\text{os}} \sum_\tau w_\tau \sum_{\alpha,P,Q} \sum_{\beta,R,S} \hat{X}_a^{P,(\text{vo})} \hat{X}_i^{P,(\text{vo})} \Gamma_\alpha^{P,(\text{vo})} \Gamma_\alpha^{Q,(\text{vo})} \hat{X}_b^{Q,(\text{vo})} \hat{X}_j^{Q,(\text{vo})} e^{-\epsilon_{ai} t_\tau} e^{-\epsilon_{bj} t_\tau} \\
&\cdot \left(\hat{X}_a^{R,(\text{vo})} \hat{X}_i^{R,(\text{vo})} \Gamma_\beta^{R,(\text{vo})} \Gamma_\beta^{S,(\text{vo})} \hat{X}_b^{S,(\text{vo})} \hat{X}_j^{S,(\text{vo})} \right) \\
&= c_{\text{os}} \sum_{aibj} \sum_{\beta,P,Q} t_{ai} t_{bj} X_a^{R,(\text{vo})} X_i^{R,(\text{vo})} \Gamma_\alpha^{R,(\text{vo})} \Gamma_\alpha^{S,(\text{vo})} X_b^{S,(\text{vo})} X_j^{S,(\text{vo})} - c_{\text{os}} \sum_\tau w_\tau \sum_{\alpha,\beta} \hat{C}_\tau^{\alpha\beta,(\text{ovov})} \hat{C}_\tau^{\alpha\beta,(\text{ovov})}
\end{aligned}
\tag{3}
$$

3 Excited State Equations - Triplet States

The matrix-vector products for triplet (T) states are given by:

$$
\begin{aligned}
\sigma_{ai}^{\text{SOS-CC2,(T)}} &= \hat{F}_{ab} R_{bi} - R_{aj} \hat{F}_{ji} - \sum_{ck} \hat{(ac|ki)} R_{ck} - c_{\text{os}} \sum_b E_{ab} R_{bi} - c_{\text{os}} \sum_j R_{aj} E_{ji} \\
&+ \sigma_{ai}^{\text{G, (T)}} + \sigma_{ai}^{\text{H, (T)}} + \sigma_{ai}^{\text{I, (T)}}
\end{aligned}
\tag{4}
$$

$$
\begin{aligned}
\sigma_{ai}^{\text{SOS-ADC(2),(T)}} &= (\epsilon_a - \epsilon_i) R_{ai} - \sum_{ck} (ac|ki) R_{ck} - c_{\text{os}} \sum_b E_{ab} R_{bi} - c_{\text{os}} \sum_j R_{aj} E_{ji} \\
&+ \sigma_{ai}^{\text{G, (T)}} + \sigma_{ai}^{\text{H, (T)}} + \sigma_{ai}^{\text{I, (T)}}
\end{aligned}
\tag{5}
$$

The derivation of the singlet equations is discussed in the paper. In order to derive the equations for the triplet states it is necessary to consider the following spin-symmetry relationships for singlet

$$
R_{a_\alpha i_\alpha} = R_{a_\beta i_\beta} \tag{6}
$$

and triplet state:

$$
R_{a_\alpha i_\alpha} = -R_{a_\beta i_\beta} \tag{7}
$$

where α, β here are the spin of the electrons. Accordingly, the intermediates to the matrix-vector product are given by:

$$\begin{aligned}
\bar{M}_{\tau}^{PS,(\mathrm{ovvv})} &= -\bar{M}_{\tau,(1)}^{PS,(\mathrm{ovvv})} + \bar{M}_{\tau,(2)}^{PS,(\mathrm{ovvv})} \\
&= -\hat{B}_{\tau}^{PS,(\mathrm{ovvv})} \bar{D}_{\tau}^{PS,(\mathrm{ovvv})} + \bar{B}_{\tau}^{PS,(\mathrm{ovvv})} \hat{D}_{\tau}^{PS,(\mathrm{ovvv})} \qquad (8) \\
\bar{N}_{\tau}^{PS,(\mathrm{vooo})} &= -\bar{N}_{\tau,(1)}^{PS,(\mathrm{vooo})} + \bar{N}_{\tau,(2)}^{PS,(\mathrm{vooo})} \\
&= -\hat{A}_{\tau}^{PS,(\mathrm{vooo})} \bar{D}_{\tau}^{PS,(\mathrm{vooo})} + \bar{A}_{\tau}^{PS,(\mathrm{vooo})} \hat{D}_{\tau}^{PS,(\mathrm{vooo})} \qquad (9) \\
\sigma_{ai}^{\text{I, SOS-CC2, (T)}} &= +c_{\mathrm{os}} \sum_{bj} t_{aibj}^{(os)} \bar{F}_{jb} + \sum_{bj} c_{\mathrm{os}} R_{ij}^{ab}(\bar{\omega}) \hat{F}_{jb} \\
&= +c_{\mathrm{os}} \sum_{\tau} \sum_{P} \hat{X}_{a}^{P,\tau} \hat{X}_{i}^{P,\tau} \bar{I}_{\tau,(1)}^{P,(\mathrm{vo})} \\
&\quad - c_{\mathrm{os}} \sum_{\tau} e^{\bar{\omega} t_{\tau}} \sum_{P} \Big[\bar{X}_{a,\tau}^{P,(\mathrm{vo})} \hat{X}_{i,\tau}^{P,(\mathrm{vo})} + \hat{X}_{a,\tau}^{P,(\mathrm{vo})} \bar{X}_{i,\tau}^{P,(\mathrm{vo})} \Big] \hat{I}_{\tau}^{P,(\mathrm{vo})} \qquad (10) \\
\sigma_{ai}^{\text{I, ADC(2), (T)}} &= +\frac{c_{\mathrm{os}}}{2} \sum_{bj} t_{aibj}^{(os)} \bar{F}_{jb} - \frac{c_{\mathrm{os}}}{2} \sum_{bj} (ib|ja) \Big[\sum_{ck} t_{ckbj}^{(os)} R_{ck} \Big] \\
&= +\frac{c_{\mathrm{os}}}{2} \sum_{\tau} \sum_{P} X_{a}^{P,\tau} X_{i}^{P,\tau} \bar{I}_{\tau,(1)}^{P,(\mathrm{vo})} - \frac{c_{\mathrm{os}}}{2} \sum_{bj} (ib|ja) \bar{I}_{bj} \qquad (11)
\end{aligned}$$

where for triplet states:

$$\bar{F}_{ib} = -(jc\hat{|}kb) R_{ck} \qquad (12)$$

4 Programmable Equations for the MO-based algorithm

Table S1: Programmable equations of the intermediates for the solution of eq. **??** and **??**. Notice that, for SOS-MP2 calculations, $t_{ai} = 0$ and only eq. (a)-(d) need to be solved.

Intermediates	Formal Scaling
$\hat{A}_\tau^{QR,(\mathrm{vovo})} = \hat{X}_{i,\tau}^{Q,(\mathrm{vo})} X_i^{R,(\mathrm{vo})}$	$N_{\mathrm{occ}} N_{\text{grid-ov}}^2$
$\hat{B}_\tau^{QR,(\mathrm{vovo})} = \hat{X}_{a,\tau}^{Q,(\mathrm{vo})} X_a^{R,(\mathrm{vo})}$	$N_{\mathrm{virt}} N_{\text{grid-ov}}^2$
$\hat{A}_\tau^{PS,(\mathrm{vooo})} = \hat{X}_{i,\tau}^{P,(\mathrm{vo})} X_i^{S,(\mathrm{oo})}$	$N_{\mathrm{occ}} N_{\text{grid-ov}} N_{\text{grid-oo}}$
$\hat{B}_\tau^{PS,(\mathrm{ovvv})} = \hat{X}_{a,\tau}^{P,(\mathrm{vo})} X_a^{S,(\mathrm{vv})}$	$N_{\mathrm{virt}} N_{\text{grid-ov}} N_{\text{grid-vv}}$
$\hat{Y}_a^{S,(\mathrm{oo})} = \hat{X}_{a,\tau}^{P,(\mathrm{vo})} \hat{N}_\tau^{PS,(\mathrm{vooo})}$	$N_{\mathrm{virt}} N_{\text{grid-ov}} N_{\text{grid-oo}}$
$\hat{Y}_i^{S,(\mathrm{vv})} = \hat{X}_{i,\tau}^{P,(\mathrm{vo})} \hat{M}_\tau^{PS,(\mathrm{ovvv})}$	$N_{\mathrm{occ}} N_{\text{grid-ov}} N_{\text{grid-vv}}$
$\hat{I}_{j,\tau}^{P,(\mathrm{ov})} = \hat{X}_{b,\tau}^{P,(\mathrm{vo})} \hat{F}_{jb}$	$N_{\mathrm{virt}} N_{\mathrm{occ}} N_{\text{grid-ov}}$
$\hat{n}_\tau^{P,(\mathrm{ov})} = \hat{X}_{j,\tau}^{P,(\mathrm{vo})} \hat{I}_{j,\tau}^{P,(\mathrm{ov})}$	$N_{\mathrm{occ}} N_{\text{grid-ov}}$

Table S2: Programmable equations of the intermediates for the solution of the MO-SOS-THC-CC2 excited states equations.

Intermediates	Formal Scaling
$\bar{A}_\tau^{QR,(\mathrm{vovo})} = \bar{X}_{i,\tau}^{Q,(\mathrm{vo})} X_i^{R,(\mathrm{vo})}$	$N_{\mathrm{occ}} N_{\text{grid-ov}}^2$
$\bar{B}_\tau^{QR,(\mathrm{vovo})} = \bar{X}_{a,\tau}^{Q,(\mathrm{vo})} X_a^{R,(\mathrm{vo})}$	$N_{\mathrm{virt}} N_{\text{grid-ov}}^2$
$\bar{A}_\tau^{PS,(\mathrm{vooo})} = \bar{X}_{i,\tau}^{P,(\mathrm{vo})} X_i^{S,(\mathrm{oo})}$	$N_{\mathrm{occ}} N_{\text{grid-ov}} N_{\text{grid-oo}}$
$\bar{B}_\tau^{PS,(\mathrm{ovvv})} = \bar{X}_{a,\tau}^{P,(\mathrm{vo})} X_a^{S,(\mathrm{vv})}$	$N_{\mathrm{virt}} N_{\text{grid-ov}} N_{\text{grid-vv}}$
$\bar{Y}_a^{S,(\mathrm{oo})} = \hat{X}_{a,\tau}^{P,(\mathrm{vo})} \hat{N}_\tau^{PS,(\mathrm{vooo})}$	$N_{\mathrm{virt}} N_{\text{grid-ov}} N_{\text{grid-oo}}$
$\bar{Y}_i^{S,(\mathrm{vv})} = \hat{X}_{i,\tau}^{P,(\mathrm{vo})} \hat{M}_\tau^{PS,(\mathrm{ovvv})}$	$N_{\mathrm{occ}} N_{\text{grid-ov}} N_{\text{grid-vv}}$

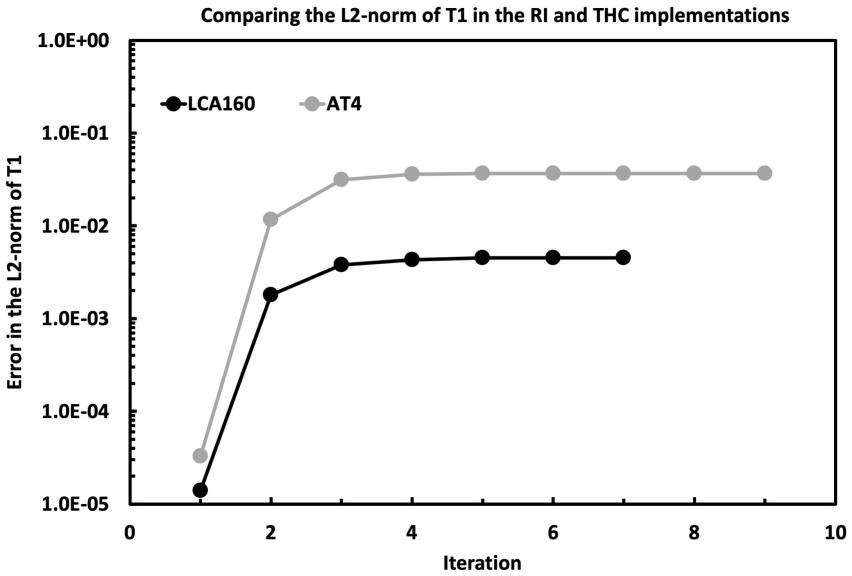

Figure S3: The plot shows the error in the single amplitudes T1 (in the $\log_{10}$ scale) along the DIIS iterative procedure, defined as the difference of its L2-norm within the RI- and THC-fitted implementations for LCA_{160}.

5 Growth of the error in the T1 amplitudes during the CC2 optimization

6 DNA Scaling

References

(S1) Matthews, D. A. Improved Grid Optimization and Fitting in Least Squares Tensor Hypercontraction. *J. Chem. Theory Comput.* **2020**, *16*, 1382–1385.

(S2) Kokkila Schumacher, S. I.; Hohenstein, E. G.; Parrish, R. M.; Wang, L. P.; Martínez, T. J. Tensor Hypercontraction Second-Order Møller-Plesset Perturbation Theory: Grid Optimization and Reaction Energies. *J. Chem. Theory Comput.* **2015**, *11*, 3042–3052.

(S3) Parrish, R. M.; Hohenstein, E. G.; Martínez, T. J.; Sherrill, C. D. Tensor Hypercon-

Table S3: Average number of PFLOPs (10^{15} FLOPs) required per DIIS iteration to form the matrix-vector product in CDD-THC-SOS-ADC(2) and MO-THC-SOS-ADC(2). Additionally, the x-fold reduction in the number of FLOPs is shown with respect to MO-RI-SOS-ADC(2). All calculations are performed using the cc-pVDZ/cc-pVDZ-RI basis set combinations and the grids generated from both the hand-optimized cc-pVDZ- (*grid1*) and cc-pVTZ-based parent grids (*grid2*).

			MO-RI	MO-THC			CDD-THC		
	System	N_{bf}	PFLOPs	PFLOPs	Scaling	Reduction	PFLOPs	Scaling	Reduction
grid1									
	AT_{04}	2904	6.2	0.3	—	20.3x	0.5	—	12.4x
	AT_{08}	5896	110.0*	2.6	**3.0**	41.0x	2.6	**2.3**	40.0x
	AT_{16}	11880	1800.0*	21.0*	**3.0**	83.5x	15.0	**2.5**	119.3x
grid2									
	AT_{04}	2904	6.2	0.7	—	8.9x	0.9	—	6.9x
	AT_{08}	5896	110.0*	5.9	**3.0**	17.8x	6.8	**2.8**	15.4x
	AT_{16}	11880	1800.0*	49.1*	**3.0**	35.7x	38.0*	**2.5**	46.1x

traction. II. Least-squares Renormalization. *Journal of Chemical Physics* **2012**, *137*, 224106.

(S4) Cuthill, E.; McKee, J. Reducing the Bandwidth of Sparse Symmetric Matrices. *Proceedings of the 1969 24th National Conference, ACM 1969* **1969**, 157–172.

6 Ongoing Projects

In **Publications I-III** local-orbitals reformulations of the Laplace-transformed SOS-LR-CC2 and SOS-ADC(2) are presented within the RI and THC approximations. They efficiently decrease the computational effort for the evaluation of excitation energies and extend the application of these methods to molecules with several hundreds of atoms by exploiting block-sparse linear algebra. In Section 6.1, we will discuss an improved implementation of the $\mathcal{O}(N)$ scaling ω-CDD-RI-SOS-ADC(2) method proposed in **Publication II** which has been extended to the closely related ω-CDD-RI-SOS-LR-CC2 for the first time. However, as quantum chemists, we are also interested in the properties of the computed excited states as well as the transition itself. Therefore, in Section 6.2, we provide the low-scaling equations for the calculations of the one-particle reduced density matrix and transition density matrix at the SOS-ADC(2) level. The algorithm for their fast and memory-efficient evaluation is currently under development, and we will not provide information about it. Nonetheless, it will be clear that the formation of the one-particle reduced density matrix and transition density matrix requires intermediates similar or equal to those for the energies. Accordingly, the introduction of Cholesky decomposed density matrices[63,64,104] is expected to reduce the $\mathcal{O}(N^4)$ scaling to $\mathcal{O}(N^2)$, or even $\mathcal{O}(N)$, in the asymptotic limit – for systems with significant HOMO-LUMO gap and local excitations. That is, we will be able to compute the transition moments, oscillator strengths, and natural transition orbitals, and hence to study the photochemistry of large systems (i.e., hundreds of atoms) with sparse electronic structure and localized excitations. In addition, the approach used for the calculation of the one-particle reduced density matrix and transition density matrix can be easily extended to the analytic evaluation of the nuclear gradients required to investigate the potential energy surface and thus study the process a given system undergoes after the excitation.

6.1 Linear-Scaling Evaluation of Closed-Shell RI-SOS-LR-CC2 and RI-SOS-ADC(2) Excitation Energies

As discussed in Section 3.3, the calculation of excitation energies requires the formation of the matrix-vector product (MVP) in the single excitations manifold:[23,38]

$$\left[A_{\mu_1\nu_1} - \frac{A_{\mu_1\gamma_2}A_{\gamma_2\nu_1}}{\varepsilon_{\gamma_2} - \bar{\omega}}\right] R_{\nu_1} = \sigma_{\mu_1} = \bar{\omega} R_{\mu_1} \tag{6.1}$$

where R_{μ_1} is the singles part of the right eigenvector. The doubles part of the excitation vector is defined as

$$R_{\mu_2} = -\frac{A_{\mu_2\nu_1}R_{\nu_1}}{\varepsilon_{\gamma_2} - \bar{\omega}} \tag{6.2}$$

Notice that, contrary to Chapter 3, we used **R** to indicate the excitation vector to avoid confusion with the THC **X** matrices.
In order to solve the nonlinear eq. (6.1), the solutions (i.e., excitation energy $\bar{\omega}$) have to be found until self-consistency is reached. If the initial guess of the eigenvectors and eigenvalues is close enough to the final results, a common choice for the solution of the nonlinear problem is the DIIS algorithm, which turned out to be stable and rapidly convergent.[23,38] In addition, it has the advantage of being a single root algorithm, thus it is possible to aim for high-lying excited states without converging all the lower states. On the other hand, if the initial guess is far from the converged CC2 – or ADC(2) – results, the eigenvalues, and the eigenvectors must be pre-optimized using an alternative algorithm. For this purpose we use a modification of the Davidson algorithm.[23,47] Both DIIS and Davidson procedures for CC2 and ADC(2) are described in literature[23,38,47] and will not be further discussed here.
The calculation of the matrix-vector product $\sigma_{\mu_1}(\bar{\omega}, R_{\nu_1})$ is required in both optimization procedures and represents the time-determining step. The original implementation in the MO basis of RI-SOS-LR-CC2[38] scales with the fourth power of the system size. Here, we will reformulate the equations for the matrix-vector product in a local basis reducing the scaling behavior of the method to $\mathcal{O}(N)$. The explicit expressions for SOS-LR-CC2 and SOS-ADC(2) can be easily obtained by neglecting the same-spin contributions and scaling the remaining terms in the equations of Section 3.3.1 by a factor $c_{\text{os}} = 1.3$.

6.1.1 Low-scaling reformulation: ω-SOS-RI-CDD-LR-CC2 and ω-SOS-RI-CDD-ADC(2)

As proposed in **Publications I-III**, in order to reduce both computational and memory scaling with the system size, we back-transform the contributions to the matrix-vector product of singlet (S) and triplet (T) states in the AO basis:

$$\begin{aligned}\sigma_{\mu\nu}^{(\text{S})/(\text{T})} = \sum_{ai} C_{\mu a}\sigma_{ai}^{(\text{S})/(\text{T})}C_{\nu i} &= \sum_{ai} C_{\mu a}(\sigma_{ai}^{0,(\text{S})/(\text{T})} + \sigma_{ai}^{G,(\text{S})/(\text{T})} + \sigma_{ai}^{H,(\text{S})/(\text{T})} + \sigma_{ai}^{I,(\text{S})/(\text{T})} + \sigma_{ai}^{J,(\text{S})/(\text{T})})C_{\nu i} \\ &= \sigma_{\mu\nu}^{0,(\text{S})/(\text{T})} + \sigma_{\mu\nu}^{G,(\text{S})/(\text{T})} + \sigma_{\mu\nu}^{H,(\text{S})/(\text{T})} + \sigma_{\mu\nu}^{I,(\text{S})/(\text{T})} + \sigma_{\mu\nu}^{J,(\text{S})/(\text{T})} \end{aligned} \tag{6.3}$$

Introducing the Laplace transform[34,35,37] that decomposes the orbital energy denominator

$$\frac{1}{\varepsilon_a - \varepsilon_i + \varepsilon_b - \varepsilon_j} = \int_0^\infty e^{-t(\varepsilon_a - \varepsilon_i + \varepsilon_b - \varepsilon_j)}dt \approx \sum_\tau w_\tau e^{-t_\tau(\varepsilon_a - \varepsilon_i + \varepsilon_b - \varepsilon_j)} \tag{6.4}$$

with the integral in eq. (6.4) accurately approximated with 5-8 integration points τ,[35] the intermediates of eq. (6.3) are expressed in terms of ground state one-electron density matrices

$$P_{\mu\nu} = \sum_i C_{\mu i}C_{\nu i} \qquad\qquad Q_{\mu\nu} = \sum_a C_{\mu a}C_{\nu a} \tag{6.5}$$

as well as ground state pseudo-density matrices

$$Q_{\mu\nu}^\tau = w_\tau^{\frac{1}{4}} C_{\mu a} e^{-\varepsilon_a t_\tau} C_{\nu a} \qquad\qquad P_{\mu\nu}^\tau = w_\tau^{\frac{1}{4}} C_{\mu i} e^{\varepsilon_i t_\tau} C_{\nu i} \tag{6.6}$$

and excitation vectors in the AO basis

$$R_{\mu\nu}^{(\mathrm{S})/(\mathrm{T})} = \sum_{ai} C_{\mu a} R_{ai}^{(\mathrm{S})/(\mathrm{T})} C_{\nu i} \tag{6.7}$$

Note that **C** matrix contains the coefficients obtained as the solution of the SCF procedure (i.e., the molecular orbitals). As previously discussed in **Publications I-III**, the resulting pure-AO reformulations are only suited for large systems and moderate basis sets. Its applicability to large basis sets is hampered by the scaling with the basis set size ($\mathrm{N_{bf}}$) and auxiliary basis set size ($\mathrm{N_{aux}}$). In fact, the formal scaling is increased from $N_{\mathrm{occ}}N_{\mathrm{virt}}N_{\mathrm{aux}}^2$ to $N_{\mathrm{bf}}^2N_{\mathrm{aux}}^2$ for a fixed molecular size, shifting the crossover with the MO-based method to large sizes. This problem is overcome using the Cholesky decomposition of **P** in eq. (6.5) with complete pivoting[63,104] and the idempotency relation of the occupied pseudo-density matrix[64]

$$\mathbf{P} = \mathbf{L}\mathbf{L}^T \qquad\qquad \mathbf{P}^{\tau} = \mathbf{P}^{\tau}\mathbf{S}\mathbf{P} = \mathbf{P}^{\tau}\mathbf{S}\mathbf{L}\mathbf{L}^T \tag{6.8}$$

that reduce the scaling with the basis set size to $N_{\mathrm{occ}}N_{\mathrm{bf}}N_{\mathrm{aux}}^2$, as previously proposed by our group.[64] The columns of **L** can be considered as the coefficients of localized occupied MOs that are also known as Cholesky orbitals[163] which inherit the locality from the density matrix.[164] Moreover, it is important to stress that the number of Cholesky MOs – obtained from the Cholesky decomposition of **P** – is equal to the number of occupied canonical MOs. From this point, the Einstein summation convention[63,64,104] will be employed in this section.

Transformation of the three-index integrals

The RI decomposition is performed according to Sec. 4.1. For the sake of simplicity, we will use **B** to indicate the three-index integrals in eq. (4.4) or eq. (4.6), while **J** refers to the two-index integrals in either eq. (4.5) or eq. (4.9). Although the effort for computing the three- and two-index integrals scales as $\mathscr{O}(N^2)$ (see Table 6.1), it does not affect the overall scaling of the method as the integrals **B** and **J** are evaluated only once at the beginning and stored on disk.
The scaling behavior of RI-SOS-CC2 and RI-SOS-ADC(2) is reduced by transforming the three-index integrals with the one-electron density matrices and taking advantage of their locality through our block-sparse linear algebra routines. According to eq. (6.8), the ground state T1-dependent virtual $\hat{\mathbf{Q}}$ and occupied $\hat{\mathbf{P}}$ density matrices are given by

$$\hat{Q}_{\mu\nu} = C_{\mu d}\Lambda_{\nu d}^{p} = Q_{\mu\nu} - Q_{\mu\mu'}S_{\mu'\sigma}t_{\sigma\lambda}S_{\lambda\nu'}P_{\nu'\nu} \tag{6.9}$$

$$\begin{aligned}\hat{P}_{\mu\nu} &= \Lambda_{\mu l}^{h}C_{\nu l} = P_{\mu\nu} + Q_{\mu\mu'}S_{\mu'\sigma}t_{\sigma\lambda}S_{\lambda\nu'}P_{\nu'\nu} \\ &= \left(L_{\mu\underline{i}} + Q_{\mu\mu'}S_{\mu'\sigma}t_{\sigma\lambda}S_{\lambda\nu'}L_{\nu'\underline{i}}\right)L_{\nu\underline{i}} = \hat{P}_{\mu\underline{i}}L_{\nu\underline{i}}\end{aligned} \tag{6.10}$$

where **S** is the overlap matrix. Thus, the Laplace-independent three-index integrals are transformed using eq. (6.9) and eq. (6.10) for the ground state:

$$\hat{B}_{\mu\underline{i}}^{\alpha} = B_{\mu'\nu'}^{\alpha}\left(L_{\nu'\underline{j}} + Q_{\nu'\nu}S_{\nu\sigma}t_{\sigma\lambda}S_{\lambda\nu''}L_{\nu''\underline{j}}\right) \tag{6.11}$$

$$\hat{B}_{\underline{k}\underline{i}}^{\alpha} = L_{\mu\underline{k}}B_{\mu\nu}^{\alpha}\hat{P}_{\nu\underline{i}} \tag{6.12}$$

$$B_{\mu\underline{i}}^{\alpha} = B_{\mu\nu}^{\alpha}L_{\nu\underline{i}} \tag{6.13}$$

The ground state T1-dependent virtual and occupied pseudo-density matrices are obtained according to

$$\hat{Q}^{\tau}_{\mu\nu} = w_{\tau}^{\frac{1}{4}} C_{\mu d} e^{-\varepsilon_d t_\tau} \Lambda^{p}_{\nu d} = Q^{\tau}_{\mu\nu} - Q^{\tau}_{\mu\mu'} S_{\mu'\sigma} \boldsymbol{t}_{\sigma\lambda} S_{\lambda\nu'} P_{\nu'\nu} \tag{6.14}$$

$$\hat{P}^{\tau}_{\mu\nu} = w_{\tau}^{\frac{1}{4}} \Lambda^{h}_{\mu i} e^{(\varepsilon_i) t_\tau} C_{\nu i} = \left[\left(L_{\mu \underline{j}} + Q_{\mu\nu'} S_{\nu'\sigma} \boldsymbol{t}_{\sigma\lambda} S_{\lambda\nu''} L_{\nu'' \underline{j}} \right) L_{\sigma' \underline{j}} S_{\sigma'\lambda'} P^{\tau}_{\lambda' \underline{i}} \right] L_{\nu \underline{i}} \tag{6.15}$$

and used to compute the ground state Laplace-dependent three-index integrals:

$$\hat{B}^{\alpha,\tau}_{\mu \underline{i}} = \hat{Q}^{\tau}_{\mu\mu'} \hat{B}^{\alpha}_{\mu' \underline{j}} \left(L_{\sigma' \underline{j}} S_{\sigma'\lambda'} P^{\tau}_{\lambda' \underline{i}} \right) \tag{6.16}$$

Similarly to the ground state, the pseudo-density matrices containing the information about the electronic excitation

$$\bar{Q}^{\tau}_{\mu\nu} = w_{\tau}^{\frac{1}{4}} C_{\mu a} e^{(-\varepsilon_a) t_\tau} \bar{\Lambda}^{p}_{\nu a} = -Q^{\tau}_{\mu\mu'} S_{\mu'\sigma} R^{(\mathrm{S})/(\mathrm{T})}_{\sigma\lambda} S_{\lambda\nu'} L_{\nu' \underline{k}} L_{\underline{k}\nu} \tag{6.17}$$

$$\bar{P}^{\tau}_{\mu\nu} = w_{\tau}^{\frac{1}{4}} \bar{\Lambda}^{h}_{\mu i} e^{(\varepsilon_i) t_\tau} C_{\nu i} = \left[\left(Q_{\mu\mu'} S_{\mu'\lambda} R^{(\mathrm{S})/(\mathrm{T})}_{\lambda\sigma} S_{\sigma\nu'} L_{\nu' \underline{j}} \right) L_{\sigma' \underline{j}} S_{\sigma'\lambda'} P^{\tau}_{\lambda' \underline{i}} \right] L_{\nu \underline{i}} \tag{6.18}$$

are used to evaluate the Laplace-dependent excited states three-index integrals, according to

$$\bar{B}^{\alpha,\tau}_{\mu \underline{i}} = Q^{\tau}_{\mu\sigma} S_{\sigma\lambda} \bar{B}^{\alpha}_{\lambda \underline{j}} \left(L_{\sigma' \underline{j}} S_{\sigma'\nu} P^{\tau}_{\nu \underline{i}} \right) \tag{6.19}$$

where we exploited the idempotency relation of the pseudo-density matrices to form the half-transformed and Laplace-independent integrals,[61,64] in order to reduce the number of operations as well as the I/O effort and the space requirements:

$$\begin{aligned} \bar{B}^{\alpha}_{\mu \underline{i}} = {} & \hat{Q}_{\mu\mu'} B^{\alpha}_{\mu'\nu'} \left(Q_{\nu'\mu''} S_{\mu''\lambda} R^{(\mathrm{S})/(\mathrm{T})}_{\lambda\sigma} S_{\sigma\lambda'} L_{\lambda' \underline{j}} \right) \\ & + \bar{Q}_{\mu\mu'} B^{\alpha}_{\mu'\nu'} \left(L_{\nu' \underline{j}} + Q_{\nu'\lambda} S_{\lambda\sigma} t_{\sigma\lambda'} S_{\lambda'\mu''} L_{\mu'' \underline{j}} \right) \end{aligned} \tag{6.20}$$

with

$$\bar{Q}_{\mu\nu} = C_{\mu a} \bar{\Lambda}^{p}_{\nu a} = -Q_{\mu\mu'} S_{\mu'\sigma} R^{(\mathrm{S})/(\mathrm{T})}_{\sigma\lambda} S_{\lambda\nu'} L_{\nu' \underline{k}} L_{\underline{k}\nu} \tag{6.21}$$

For systems with significant HOMO-LUMO gap and local excitations, the transformation of the AO-based three-index integrals into the Cholesky orbitals basis – see eqs. (6.11)-(6.13), eq. (6.16), and eqs. (6.19)-(6.20) – scales as $\mathscr{O}(N^2)$ and $\mathscr{O}(N)$ in the standard RI Coulomb metric ($\omega = 0.0$) and the attenuated RI Coulomb metric ($\omega = 0.1$), respectively.

Contributions to the singlet matrix-vector product

The single-single block of the Jacobian matrix provides zeroth-, first-, and second-order contributions to the matrix-vector product

$$\sigma^{0,(\mathrm{S})}_{\mu\nu} = \hat{Q}_{\mu\lambda} \hat{F}_{\lambda\nu} R^{(\mathrm{S})}_{\nu' \underline{i}} - R^{(\mathrm{S})}_{\mu \underline{j}} \hat{P}_{\nu \underline{j}} \hat{F}_{\mu\nu} L_{\mu \underline{i}} + E_{\mu\nu'} R^{(\mathrm{S})}_{\nu' \underline{i}} - R^{(\mathrm{S})}_{\mu \underline{j}} E_{\underline{j}\underline{i}} + \sigma^{I,(\mathrm{S})}_{\mu\nu} + \sigma^{J,(\mathrm{S})}_{\mu\nu} \tag{6.22}$$

with

$$R^{(\mathrm{S})/(\mathrm{T})}_{\mu\underline{i}} = Q_{\mu\nu} S_{\nu\lambda} R^{(\mathrm{S})/(\mathrm{T})}_{\lambda\sigma} S_{\sigma\nu'} L_{\nu'\underline{i}} \tag{6.23}$$

$$\sigma^{J,(\mathrm{S})}_{\mu\nu} = \left\{ \hat{Q}_{\mu\mu'} \hat{P}_{\nu'\underline{i}} \Big[2(\mu'\nu'|\sigma\lambda) - (\mu'\lambda|\sigma\nu') \Big] R^{(\mathrm{S})}_{\lambda\underline{k}} L_{\sigma\underline{k}} \right\} L_{\nu\underline{i}} \tag{6.24}$$

The **E** intermediates only depend on ground state quantities and hence they are computed once and stored on disk:

$$E_{\mu\nu} = -\hat{Y}^{\beta}_{\mu\underline{k}} B^{\beta}_{\underline{k}\nu} \qquad\qquad E_{\underline{j}\underline{i}} = +B^{\beta}_{\nu\underline{j}} \hat{Y}^{\beta}_{\nu\underline{i}} \tag{6.25}$$

where the $\hat{\mathbf{Y}}$ intermediate is formed according to

$$\hat{Y}^{\beta}_{\mu\underline{i}} = -c_{\mathrm{os}} \hat{B}^{\alpha,\tau}_{\mu\underline{i}} \hat{M}^{\alpha\beta}_{\tau} \tag{6.26}$$

with

$$\hat{M}^{\alpha\beta}_{\tau} = -c_{\mathrm{os}} e^{\bar{\omega} t_\tau} \Big[J^{-1}_{\alpha\gamma} \hat{N}^{\gamma\gamma'}_{\tau} J^{-1}_{\gamma'\beta} \Big] \tag{6.27}$$

$$\hat{N}^{\gamma\gamma'}_{\tau} = \hat{B}^{\gamma,\tau}_{\mu\underline{j}} B^{\gamma'}_{\mu\underline{j}} \tag{6.28}$$

The last contribution from the single-single block is defined as

$$\sigma^{I,(\mathrm{S})}_{\mu\nu} = \Big[\hat{m}^{\alpha}_{\tau} \bar{B}^{\alpha,\tau}_{\mu\underline{i}} + \bar{m}^{\alpha,(\mathrm{S})}_{\tau} \hat{B}^{\alpha,\tau}_{\mu'\underline{i}} \Big] L_{\nu\underline{i}} \qquad\qquad \bar{m}^{\alpha,(\mathrm{S})}_{\tau} = \bar{m}^{\alpha}_{\tau}(A) + \bar{m}^{\alpha}_{\tau}(B) \tag{6.29}$$

where the intermediates are given by

$$\hat{m}^{\alpha}_{\tau} = -c_{\mathrm{os}} e^{\bar{\omega} t_\tau} \Big[\hat{n}^{\alpha'}_{\tau} J^{-1}_{\alpha\alpha'} \Big] \qquad\qquad \hat{n}^{\alpha'}_{\tau} = \hat{F}_{\underline{j}\mu} \hat{B}^{\alpha',\tau}_{\mu\underline{j}} \tag{6.30}$$

$$\bar{m}^{\alpha}_{\tau}(A) = -c_{\mathrm{os}} e^{\bar{\omega} t_\tau} \Big[\bar{n}^{\alpha'}_{\tau}(A) J^{-1}_{\alpha\alpha'} \Big] \qquad\qquad \bar{n}^{\alpha'}_{\tau}(A) = \hat{F}_{\underline{j}\mu} \bar{B}^{\alpha',\tau}_{\mu\underline{j}} \tag{6.31}$$

$$\bar{m}^{\alpha}_{\tau}(B) = -c_{\mathrm{os}} \Big[\bar{n}^{\alpha'}_{\tau}(B) J^{-1}_{\alpha\alpha'} \Big] \qquad\qquad \bar{n}^{\alpha'}_{\tau}(B) = \bar{F}_{\underline{j}\mu} \hat{B}^{\alpha',\tau}_{\mu\underline{j}} \tag{6.32}$$

Finally, the coupling-block contributes to the matrix-vector product through the $\sigma^{G}_{\mu\nu}$ and $\sigma^{H}_{\mu\nu}$ terms, which are reformulated in the following fashion:

$$\sigma^{G,(\mathrm{S})}_{\mu\nu} = \hat{Q}_{\mu\mu'} \big(B^{\beta}_{\mu'\nu'} \bar{Y}^{\beta,(\mathrm{S})}_{\nu'\underline{i}} \big) L_{\nu\underline{i}} \qquad\qquad \sigma^{H,(\mathrm{S})}_{\mu\nu} = \big(-\bar{Y}^{\beta,(\mathrm{S})}_{\mu\underline{k}} \hat{B}^{\beta}_{\underline{k}\underline{i}} \big) L_{\nu\underline{i}} \tag{6.33}$$

with the formation of the Laplace-independent $\bar{\mathbf{Y}}$ tensor being the most expensive step:

$$\bar{Y}^{\beta,(\mathrm{S})}_{\mu\underline{i}} = \bar{B}^{\alpha,\tau}_{\mu\underline{i}} \hat{M}^{\alpha\beta}_{\tau} + \hat{B}^{\alpha,\tau}_{\mu\underline{i}} \bar{M}^{\alpha\beta}_{\tau} \tag{6.34}$$

The $\hat{\mathbf{M}}$ matrix is given in eq. (6.27), while the excited state intermediate $\bar{\mathbf{M}}$ is equal to

$$\bar{M}^{\alpha\beta}_{\tau} = -c_{\mathrm{os}} e^{\bar{\omega} t_\tau} \Big[J^{-1}_{\alpha\gamma} \bar{N}^{\gamma\gamma'}_{\tau} J^{-1}_{\gamma'\beta} \Big] \qquad\qquad \bar{N}^{\gamma\gamma'}_{\tau} = \bar{B}^{\gamma,\tau}_{\mu\underline{j}} B^{\gamma'}_{\mu\underline{j}} \tag{6.35}$$

Notice that we postpone the multiplication with the two-index integrals to the steps in eqs. (6.35), (6.27), (6.31), (6.32), and (6.39), in order to exploit and preserve the locality of the three-index integrals, as long as possible.

The CDD-RI-SOS-ADC(2) equations are obtained by setting $t_{\mu\nu} = 0$ and by symmetrization of the Jacobian single-single block:

$$\sigma_{\mu\nu}^{0,\text{SOS-ADC(2),(S)}} = Q_{\mu\lambda}F_{\lambda\nu}R_{\nu'\underline{i}}^{(\text{S})} - R_{\mu\underline{j}}^{(\text{S})}P_{\nu\underline{j}}F_{\mu\nu}L_{\mu\underline{i}} + \frac{1}{2}\Big(E_{\mu\nu'} + E_{\nu'\mu}\Big)R_{\nu'\underline{i}}^{(\text{S})} - \frac{1}{2}R_{\mu\underline{j}}^{(\text{S})}\Big(E_{\underline{j}\underline{i}} + E_{\underline{i}\underline{j}}\Big) + \sigma_{\mu\nu}^{I,(\text{S})} + \sigma_{\mu\nu}^{J,(\text{S})} \tag{6.36}$$

$$\sigma_{\mu\nu}^{I,\text{SOS-ADC(2),(S)}} = \frac{1}{2}\Big[\bar{m}_{\tau}^{P}(B)B_{\mu\underline{i}}^{\alpha,\tau} + Q_{\mu\nu'}L_{\mu'\underline{i}}[2(\mu'\nu'|\sigma\lambda) - (\mu'\lambda|\sigma\nu')]L_{\sigma\underline{k}}I_{\lambda\underline{k}}^{(\text{S})}\Big]L_{\nu\underline{i}} \tag{6.37}$$

where

$$I_{\mu\underline{i}} = \bar{m}^{\alpha}(C)B_{\mu\underline{i}}^{\alpha,\tau} \tag{6.38}$$

$$\bar{m}_{\tau}^{\alpha}(C) = -c_{\text{os}}\Big[\bar{n}_{\tau}^{\alpha'}(C)J_{\alpha\alpha'}^{-1}\Big] \tag{6.39}$$

$$\bar{n}_{\tau}^{\alpha'}(C) = R_{\mu\underline{j}}^{(\text{S})}B_{\mu\underline{j}}^{\alpha',\tau} \tag{6.40}$$

For systems with a significant HOMO-LUMO gap and local excitations, the overall computational scaling of CDD-RI-SOS-LR-CC2 and CDD-RI-SOS-ADC(2) is asymptotically quadratic, due to the slow long-range $\frac{1}{r_{12}}$ decay within the standard Coulomb metric ($\omega = 0.0$) that couples the auxiliary functions to the AO basis-function pairs.[108,109] On the other hand, the attenuated-Coulomb metric has the property of combining the accuracy of the Coulomb metric and the sparsity of the local overlap metric[108–110] as described in Section 4.1. The erfc-Coulomb metric with $\omega = 0.1$ increases the sparsity of the ω-CDD-RI-SOS-LR-CC2 and ω-CDD-RI-SOS-ADC(2) intermediates and grants a further reduction of the scaling. Hence, one achieves $\mathcal{O}(N)$ scaling behavior. The computational behavior for each step is reported in Table 6.1.

Contributions to the triplet matrix-vector product

The evaluation of excitation energies to triplet states at the SOS-LR-CC2 and SOS-ADC(2) levels of theory requires minor modifications of the equations derived for singlet states. Considering the following spin-symmetry relationships for the transition vector

$$R_{ai}^{(\text{T})} = -R_{\overline{ai}}^{(\text{T})} \tag{6.41}$$

with the (ai) and $(\overline{ai})$ orbitals having opposite spins, one obtains the expressions for the triplet intermediates. First, the ω-CDD-RI-SOS-LR-CC2 contributions $\boldsymbol{\sigma^J}$ and $\boldsymbol{\sigma^I}$ for triplet states are obtained as

$$\sigma_{\mu\nu}^{J,(\text{T})} = \Big\{\hat{Q}_{\mu\mu'}\hat{P}_{\nu'\underline{i}}\Big[-(\mu'\lambda|\sigma\nu')\Big]R_{\lambda\underline{k}}^{(\text{T})}L_{\sigma\underline{k}}\Big\}L_{\nu\underline{i}} \tag{6.42}$$

$$\sigma_{\mu\nu}^{I,(\text{T})} = \Big[\hat{m}_{\tau}^{\alpha}\bar{B}_{\mu\underline{i}}^{\alpha,\tau} + \bar{m}_{\tau}^{\alpha,(\text{T})}\hat{B}_{\mu'\underline{i}}^{\alpha,\tau}\Big]L_{\nu\underline{i}} \tag{6.43}$$

with

$$\bar{m}_\tau^{\alpha,(\mathrm{T})} = \bar{m}_\tau^\alpha(A) - \bar{m}_\tau^\alpha(B) \tag{6.44}$$

Finally, the $\boldsymbol{\sigma}^G$ and $\boldsymbol{\sigma}^H$ terms, for triplet states, are given in the following fashion:

$$\sigma_{\mu\nu}^{G,(\mathrm{T})} = \hat{Q}_{\mu\mu'}\big(B^\beta_{\mu'\nu'}\bar{Y}^{\beta,(\mathrm{T})}_{\nu'\underline{i}}\big)L_{\nu\underline{i}} \qquad \sigma_{\mu\nu}^{H,(\mathrm{T})} = \big(-\bar{Y}^{\beta,(\mathrm{T})}_{\mu\underline{k}}\hat{B}^\beta_{\underline{k}\underline{i}}\big)L_{\nu\underline{i}} \tag{6.45}$$

with the Laplace-independent $\bar{\mathbf{Y}}$ tensor evaluated as

$$\bar{Y}^{\beta,(\mathrm{T})}_{\mu\underline{i}} = \bar{B}^{\alpha,\tau}_{\mu\underline{i}}\hat{M}^{\alpha\beta}_\tau - \hat{B}^{\alpha,\tau}_{\mu\underline{i}}\bar{M}^{\alpha\beta}_\tau \tag{6.46}$$

Note that, for ω-CDD-RI-SOS-ADC(2), the triplet states contributions to the matrix-vector product are obtained by setting $t_{\mu\nu} = 0$ in eqs. (6.42)-(6.46) and by symmetrization of the $\boldsymbol{\sigma}^I$ in eq. (6.43):

$$\sigma_{\mu\nu}^{I,\text{SOS-ADC(2)},(\mathrm{T})} = \frac{1}{2}\Big[-\bar{m}^P_\tau(B)B^{\alpha,\tau}_{\mu\underline{i}} + Q_{\mu\nu'}L_{\mu'\underline{i}}[-(\mu'\lambda|\sigma\nu')]L_{\sigma\underline{k}}I^{(\mathrm{T})}_{\lambda\underline{k}}\Big]L_{\nu\underline{i}} \tag{6.47}$$

with $I^{(\mathrm{T})}_{\lambda\underline{k}} = I^{(\mathrm{S})}_{\lambda\underline{k}}$. The other intermediates are equal for both the singlet and triplet states. The computational effort for the evaluation of triplet intermediates is slightly reduced compared to the singlet state because the Coulomb term in the Fock-like terms is not computed. Overall, for triplet states, ω-CDD-RI-SOS-CC2 and ω-CDD-RI-SOS-ADC(2) show $\mathcal{O}(N^2)$ and $\mathcal{O}(N)$ computational scaling behavior for systems with significant HOMO-LUMO gap and local excitations.

6.1.2 Outline of the implementation

The equations for the excitation energies can be implemented as for the underlying ground state ω-SOS-RI-CDD-CC2 method in **Publication I**. For the sake of simplicity, we will assume that ground state calculations have been carried out and that the ground state three-index integrals – $B^\beta_{\underline{j}\mu}$ and $\hat{B}^\beta_{\mu\underline{i}}$ in eqs. (6.13) and (6.16) – and intermediates –$\hat{M}^{\alpha\beta}_\tau$ and $\hat{m}^\alpha_\tau$ in eqs. (6.27) and (6.30) – are stored on disk. The high memory demands of excited-states calculations easily exceed the available memory on a single computing node. Therefore, as in **Publication I**, we employ an optimized batching scheme based on a Lagrangian formulation[61] for evaluating the excited states intermediates (e.g., the three-index integrals, $\bar{N}^{\alpha\beta}_\tau$ and $\bar{Y}^\beta_{\mu\underline{i}}$) and the contributions to the matrix-vector product. The implementation of the equations for the state-specific matrix-vector product can be summarized in three main algorithms:

- We compute the intermediates $\bar{N}^{\alpha\beta}_\tau$ and $\bar{n}^\alpha_\tau$, as shown in Algorithm 1 by reading integrals in lines 13, 27, and 39 in batches of auxiliary and basis functions indices, at the cost of a batching overhead proportional to the number of auxiliary and basis functions batches $\mathrm{b_{aux}}$ and $\mathrm{b_{AO}}$. In the optimal batching, $\mathrm{b_{aux}}$ and $\mathrm{b_{AO}}$ are equal. Once the intermediates are formed (lines 20, 22, 34, and 43), they are multiplied by the RI metric (lines 49-52) and stored on disk. Notice that these intermediates, as well as their ground state homologues $\hat{M}^{\alpha\beta}_\tau$ and $\hat{m}^\alpha_\tau$, do not depend on the eigenvalues $\bar{\omega}$ and are computed only once for each macro-iteration of the Davidson procedure.

- The intermediates formed in Algorithm 1 and the ground state matrices $\hat{M}_\tau^{\alpha\beta}$ and $\hat{m}_\tau^\alpha$ are read and scaled by the updated $\bar{\omega}$. Then, the intermediates $\bar{Y}_{\mu\underline{i}}^\beta$, $\Omega_{\mu\underline{i}}^I$, and $I_{\mu\underline{i}}$ are computed by batching occupied indices (see Algorithm 2). The three-index integrals $\hat{B}_{\mu\underline{j}}^\alpha$ and $\bar{B}_{\mu\underline{j}}^\alpha$ are read with an overhead proportional to the number of occupied batches $\mathrm{b_{occ}}$. Notice that we keep in memory the $\bar{Y}_{\mu\underline{i}}^\beta$ intermediate until both contributions from lines 23 and 35 are computed, and we write it on disk only once.
- The $\sigma_{\mu\underline{i}}^G$ and $\sigma_{\mu\underline{i}}^H$ contributions to the matrix-vector product are computed as the $\Omega_{\mu\underline{i}}^G$ and $\Omega_{\mu\underline{i}}^H$ contributions to the ground state vector-function proposed in **Publication I**. Therefore, the algorithm is not discussed here.

As can be seen in Algorithm 1, the minimal overhead is obtained if there is only one τ-batch containing all Laplace quadrature points.[61] We also used only one τ-batch in the simpler batching scheme in Algorithm 2. Finally, in order to increase the efficiency, the three-index integrals are read and simultaneously transformed in parallel using all the available threads (i.e., lines 12 and 26 in Algorithm 1, and lines 12 and 25 in Algorithm 2). Finally, the Coulomb and exchange terms in, e.g., the $\sigma_{\mu\nu}^J$ contribution are computed by using the same routines used to build the Fock matrices. The Coulomb term is computed in a quadratic scaling fashion as proposed by Kussmann *et al.*,[161] while the exchange term is calculated via the linear-scaling sn-Link method by Laqua *et al.*.[79,165] Due to the high efficiency of the routines, the resulting overall scaling of these steps is linear with the system size (considering timings).

Algorithm 1 Singlet states ω-CDD-RI-SOS-LR-CC2 and ω-CDD-RI-SOS-ADC(2): calculation of $\bar{M}_\tau^{\alpha\beta}$ and $\bar{m}_\tau^\alpha$

for aux-batch-1 **do**
  for $\alpha \in$ aux-batch-1 **do**
    read $B^\alpha_{\mu\nu}\ \forall\mu,\nu$
    $\bar{B}^\alpha_{\mu\underline{j}} = \hat{Q}_{\mu\mu'}B^\alpha_{\mu'\nu'}(Q_{\nu'\mu''}S_{\mu''\lambda}R_{\lambda\sigma}S_{\sigma\lambda'}L_{\lambda'\underline{j}}) + \bar{Q}_{\mu\mu'}B^\alpha_{\mu'\nu'}(L_{\nu'\underline{j}} + Q_{\nu'\lambda}S_{\lambda\sigma}t_{\sigma\lambda'}S_{\lambda'\mu''}L_{\mu''\underline{j}})\ \forall\underline{j},\mu$
    write $\bar{B}^\alpha_{\mu\underline{j}}$ on disk
  end for
end for
for aux-batch-1 **do**
  for AO-batch **do**
    for $\alpha \in$ aux-batch-1 **do**
      read $\hat{B}^\alpha_{\mu'\underline{j}}\ \forall\mu',\underline{j}$, if do_adc: $t_{\mu\nu}=0$
      for all τ **do**
        $\hat{B}^{\alpha,\tau}_{\mu\underline{i}} = \hat{Q}^\tau_{\mu\mu'}\hat{B}^\alpha_{\mu'\underline{j}}(L_{\sigma\underline{j}}S_{\sigma\lambda}P^\tau_{\lambda\underline{i}})\forall\underline{i},\mu \in$ AO-batch;
      end for
    end for
    for all τ **do**
      for $\alpha \in$ aux-batch-1 **do**
        $\bar{n}^\alpha_\tau(B) += \hat{B}^{\alpha,\tau}_{\mu\underline{i}}\bar{F}_{\underline{i}\mu}\forall\underline{i},\mu \in$ AO-batch
        if do_adc **then**
          $\bar{n}^\alpha_\tau(C) += \hat{B}^{\alpha,\tau}_{\mu\underline{i}}R_{\mu\underline{i}}\forall\underline{i},\mu \in$ AO-batch
        end if
      end for
    end for
    for $\alpha \in$ aux-batch-1 **do**
      read $\bar{B}^\alpha_{\mu'\underline{j}}\ \forall\mu',\underline{j}$
      for all τ **do**
        $\bar{B}^{\alpha,\tau}_{\mu\underline{i}} = Q^\tau_{\mu\mu'}\bar{B}^\alpha_{\mu'\underline{j}}(L_{\sigma\underline{j}}S_{\sigma\lambda}P^\tau_{\lambda\underline{i}})\forall\underline{i},\mu \in$ AO-batch;
      end for
    end for
    for all τ **do**
      for $\alpha \in$ aux-batch-1 **do**
        $\bar{n}^\alpha_\tau(A) += \bar{B}^{\alpha,\tau}_{\mu\underline{i}}\hat{F}_{\underline{i}\mu}\forall\underline{i},\mu \in$ AO-batch, if do_adc: $n^\alpha_\tau(A)=0$
      end for
    end for
    for aux-batch-2 **do**
      for $\beta \in$ aux-batch-2 **do**
        read $B^\beta_{\underline{i}\mu}\forall\underline{i},\mu \in$ AO-batch;
      end for
      for all τ **do**
        for i $\in$ rank_occ **do**
          $\bar{N}^{\alpha\beta}_\tau += \bar{B}^{\alpha,\tau}_{\mu\underline{i}}B^\beta_{\mu\underline{i}}\ \forall\mu \in$ AO-batch and $\alpha,\beta \in$ aux-batch-1/-2
        end for
      end for
    end for
  end for
end for
$\bar{M}^{\alpha\beta}_\tau = J^{-1}_{\alpha'\alpha}\bar{N}^{\alpha'\beta'}_\tau J^{-1}_{\beta'\beta}\ \forall\tau \rightarrow$ write on disk
$\bar{m}^\alpha_\tau(A) = \bar{n}^{\alpha'}_\tau(A)J^{-1}_{\alpha'\alpha}\ \forall\tau \rightarrow$ write on disk
$\bar{m}^\alpha_\tau(B) = \bar{n}^{\alpha'}_\tau(B)J^{-1}_{\alpha'\alpha}\ \forall\tau \rightarrow$ write on disk
$\bar{m}^\alpha_\tau(C) = \bar{n}^{\alpha'}_\tau(C)J^{-1}_{\alpha'\alpha}\ \forall\tau \rightarrow$ write on disk

Algorithm 2 Singlet states ω-CDD-RI-SOS-LR-CC2 and ω-CDD-RI-SOS-ADC(2): calculation of $\bar{Y}^{\beta}_{\mu\underline{i}}$, $\sigma^{I}_{\mu\underline{i}}$ and $I_{\mu\underline{i}}$

for all τ **do**
  read $\hat{M}^{\alpha\beta}_{\tau}$ and $\bar{M}^{QP}_{\tau}$ and scale it by $-c_{\mathrm{os}}e^{\bar{\omega}t_{\tau}}$
  read $\bar{m}^{\alpha}_{\tau}(B)$ and scale it by $-c_{\mathrm{os}}$
  if do_adc2 **then**
    read $\bar{m}^{\alpha}_{\tau}(C)$ and scale it by $-c_{\mathrm{os}}$
  else
    read $\bar{m}^{\alpha}_{\tau}(A)$ and scale it by $-c_{\mathrm{os}}e^{\bar{\omega}t_{\tau}}$
    read $\hat{m}^{\alpha}_{\tau}$ and scale it by $-c_{\mathrm{os}}e^{\bar{\omega}t_{\tau}}$
  end if
end for
for occ-batch **do**
  for all $\alpha \in$ naux **do**
    read $\hat{B}^{\alpha}_{\mu'\underline{j}}\ \forall\mu',\underline{j}$
    for all τ **do**
      $\hat{B}^{\alpha,\tau}_{\mu\underline{i}} = \hat{Q}^{\tau}_{\mu\mu'}\hat{B}^{\alpha}_{\mu'\underline{j}}(L_{\sigma\underline{j}}S_{\sigma\lambda}P^{\tau}_{\lambda\underline{i}})\forall\mu,\underline{i} \in$ occ-batch;
    end for
  end for
  for all τ **do**
    $\Omega^{I}_{\mu\underline{i}} += \hat{B}^{\alpha,\tau}_{\mu\underline{i}}\bar{m}^{\alpha}_{\tau}\ \forall\mu,\underline{i} \in$ occ-batch
    if do_adc2 **then**
      $I_{\mu\underline{i}} += B^{\alpha,\tau}_{\mu\underline{i}}\bar{m}^{\alpha}_{\tau}(C)\ \forall\mu,\underline{i} \in$ occ-batch
    end if
    $\bar{Y}^{\beta}_{\mu\underline{i}} += \hat{B}^{\alpha,\tau}_{\mu\underline{i}}\bar{M}^{\alpha\beta}_{\tau}$
  end for
  for all $\alpha \in$ naux **do**
    read $\bar{B}^{\alpha}_{\mu'\underline{j}}\ \forall\mu',\underline{j}$
    for all τ **do**
      $\bar{B}^{\alpha,\tau}_{\mu\underline{i}} = Q^{\tau}_{\mu\mu'}\bar{B}^{\alpha}_{\mu'\underline{j}}(L_{\sigma'\underline{j}}S_{\sigma'\lambda'}P^{\tau}_{\lambda'\underline{i}})\ \forall\mu,\underline{i} \in$ occ-batch;
    end for
  end for
  for all τ **do**
    if !do_adc2 **then**
      $\Omega^{I}_{\mu\underline{i}} += \bar{B}^{\alpha,\tau}_{\mu\underline{i}}\hat{m}^{\alpha}_{\tau}\forall\mu,\underline{i} \in$ occ-batch, $\forall\alpha \in$ aux-batch-1
    end if
    $\bar{Y}^{\beta}_{\mu\underline{i}} += \bar{B}^{\alpha,\tau}_{\mu\underline{i}}\tilde{N}^{\alpha\beta}_{\tau}$
  end for
  write $\bar{Y}^{Q}_{\mu\underline{i}}\ \forall\mu,\underline{i} \in$ occ-batch
end for
if do_adc2 **then**
  scale $\Omega^{I}_{\mu\underline{i}}$ and $I_{\mu\underline{i}}$ by 0.5
end if

Table 6.1: Formal and asymptotic computational scaling (with the number of orbitals N) for key steps of ω-CDD-RI-SOS-LR-CC2 and ω-CDD-RI-SOS-ADC(2) within the RI standard-Coulomb metric ($\omega = 0$) and overlap metric ($\omega \to \infty$).

	Formal Scaling	Asymptotic Scaling	
		$\omega = 0$	$\omega \to \infty$
Cholesky decompose $\mathbf{P}$	N^3	$\mathcal{O}(N)$	$\mathcal{O}(N)$
Compute $\mathbf{J}$	N^2	$\mathcal{O}(N^2)$	$\mathcal{O}(N^2)$
Invert $\mathbf{J}$	N^3	$\mathcal{O}(N^3)$	$\mathcal{O}(N^3)$
Compute $B^{\alpha}_{\mu\nu}$	N^2	$\mathcal{O}(N^2)$	$\mathcal{O}(N^2)$
Compute $\sigma^{G}_{\mu\nu}$	N^4	$\mathcal{O}(N^2)$	$\mathcal{O}(N)$
Compute $\sigma^{H}_{\mu\nu}$	N^4	$\mathcal{O}(N^2)$	$\mathcal{O}(N)$
Compute $\sigma^{I}_{\mu\nu}$	N^3	$\mathcal{O}(N^2)$	$\mathcal{O}(N)$
Compute $\sigma^{J}_{\mu\nu}$	N^4	$\mathcal{O}(N^2)$	$\mathcal{O}(N^2)$
Compute $I_{\mu\underline{i}}$	N^3	$\mathcal{O}(N^2)$	$\mathcal{O}(N)$
Transform $B^{\alpha}_{\mu\nu}$	N^4	$\mathcal{O}(N^2)$	$\mathcal{O}(N)$
Compute $\bar{n}^{\alpha}_{\tau}$	N^3	$\mathcal{O}(N^2)$	$\mathcal{O}(N)$
Compute $\bar{m}^{P}_{\tau}$	N^2	$\mathcal{O}(N^2)$	$\mathcal{O}(N^2)$
Compute $N^{\alpha\beta}_{\tau}$	N^4	$\mathcal{O}(N^3)$	$\mathcal{O}(N)$
Compute $\bar{N}^{\alpha\beta}_{\tau}$	N^4	$\mathcal{O}(N^2)$	$\mathcal{O}(N)$
Compute $\hat{M}^{\alpha\beta}_{\tau}$	N^3	$\mathcal{O}(N^3)$	$\mathcal{O}(N^3)$
Compute $\bar{M}^{\alpha\beta}_{\tau}$	N^3	$\mathcal{O}(N^3)$	$\mathcal{O}(N^3)$
Compute $\hat{Y}^{\beta}_{\mu\nu}$	N^4	$\mathcal{O}(N^3)$	$\mathcal{O}(N^2)$
Compute $\bar{Y}^{\beta}_{\mu\nu}$	N^4	$\mathcal{O}(N^3)$	$\mathcal{O}(N)$

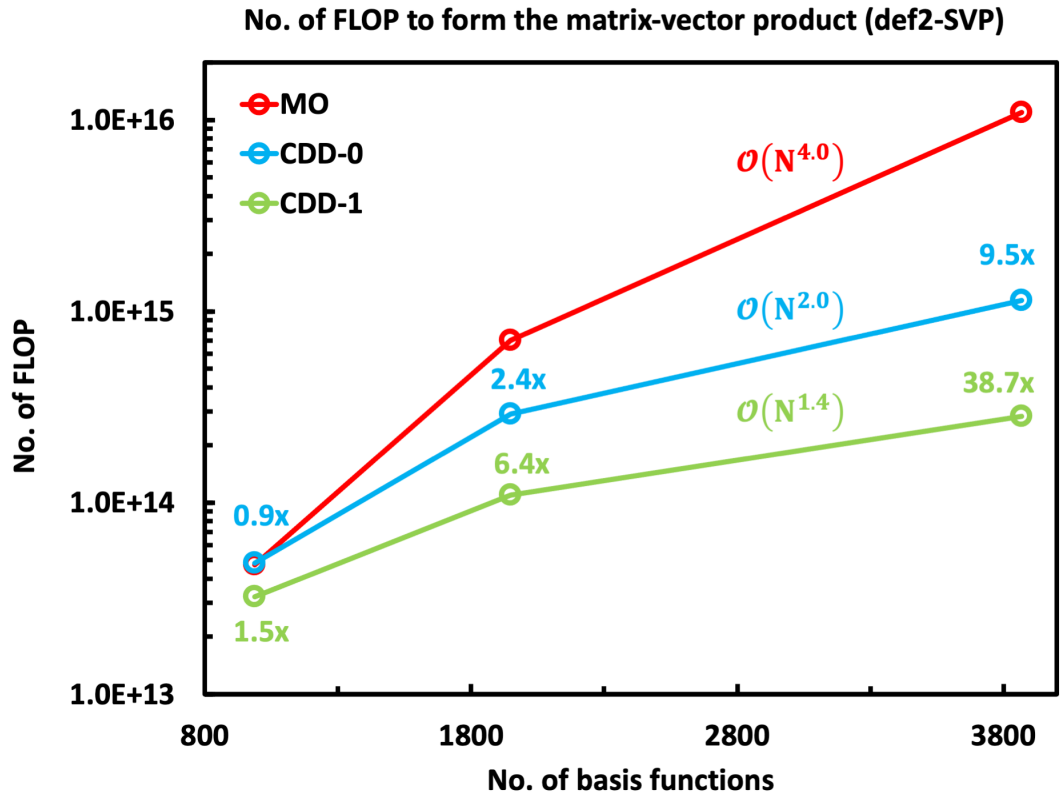

Figure 6.1: Number FLOP for the evaluation of the matrix-vector product of MO-RI-SOS-LR-CC2 and MO-RI-SOS-ADC(2) (MO) and ω-CDD-SOS-RI-SOS-LR-CC2 ω-CDD-SOS-RI-SOS-ADC(2) with $\omega = 0.0$ (CDD-0) and $\omega = 0.1$ (CDD-1) in the def2-SVP basis. The computational scaling and speedups are also reported.

6.1.3 Scaling Behavior

The sparsity of the ground state one-electron density is closely related to the HOMO-LUMO gap of molecular systems and the asymptotic linear-scaling behavior holds only for systems with a non-vanishing HOMO–LUMO gap.[14,40] In addition, when calculating excitation energies, one must consider the sparsity of the transition vector in eq. (6.7) as it is related to the locality of the excitation. In order to discuss the computational scaling of ω-CDD-RI-SOS-LR-CC2 and ω-CDD-RI-SOS-ADC(2), we first consider linear carboxylic acids (LCAs) showing a local electronic structure and a local excitation for the lowest singlet excited state S_1 (see Figure 4.1) – mostly localized on the carboxyl group. Although the LCAs represent the best-case scenario, the asymptotic scaling behavior discussed in this section can be translated to three-dimensional systems with localized excitations as well. For the test calculation on the LCAs, we used the def2-SVP[162] basis set and the related def2-SVP-RI[166] and def2-universal-RI-J[167] auxiliary basis sets. Note that the formation of the intermediates for singlet and triplet state calculations shows the same computational effort and scaling behavior with the system size. Thus, only the singlet state calculations are discussed here.

Linear Carboxylic Acids

The scaling behavior of our ω-CDD-RI-SOS-LR-CC2 and ω-CDD-RI-SOS-ADC(2) implementations is investigated by taking into account the number of floating-point operations (FLOP) required to form the matrix-vector product with $\omega = 0.0$ and $\omega = 0.1$. Notice that, starting from the CCS transition density, the number of relevant elements $R_{\mu\nu}$ might slowly increase during the optimization procedure, as some electronic excitations can become more important to accurately describe the state. Therefore, we decided to take into account the average number of FLOPS per iteration (total no. of FLO / no. of iterations) during the DIIS procedure. The results are summarized in Figure 6.1, where the number of FLOP of ω-CDD-RI-SOS-ADC(2) and ω-CDD-RI-SOS-LR-CC2 overlap and display $\mathscr{O}(N^2)$ and $\mathscr{O}(N)$ computational scaling behavior with $\omega = 0.0$ ($\frac{1}{r_{12}}$) and $\omega = 0.1$ ($\frac{\mathrm{erfc}(\omega r_{12})}{r_{12}}$), respectively. Alongside the lowering of the scaling, Figure 6.1 shows that a significant diminution of the effort is achieved when ω-CDD-RI-SOS-ADC(2) and ω-CDD-RI-SOS-LR-CC2 are used on systems with local electronic structure and excitation, such that $\sim$10-fold and $\sim$39-fold less operations are performed with $\omega = 0.0$ and $\omega = 0.1$, respectively. However, it is important to stress that for larger basis sets, i.e., def2-TZVP,[162] the linear scaling regime is reached at larger system sizes and a smaller reduction of the effort is seen for fixed sizes. In addition, we remember from **Publication I** that the calculation of the ω-CDD-RI-SOS-MP2 ground-state energy scales quadratically (with $\omega = 0$) or even linearly ($\omega = 0.1$) in the asymptotic limit. On the other hand, the ω-CDD-RI-SOS-CC2 ground state energy is computed with a sub-cubic and sub-quadratic scaling effort, for $\omega = 0.0$ and $\omega = 0.1$, respectively.

In order to understand the scaling behavior of our local implementations, we must discuss the memory demands for the formation of the matrix-vector product. To do so, we consider the number of allocated blocks for the important intermediates during both ground and excited state calculations. Again, for the excited state quantities, we look at the average number of allocated blocks per iteration (total no. of blocks / no. of iterations) during the DIIS procedure. Since the memory demands of ω-CDD-RI-SOS-LR-CC2 and ω-CDD-RI-SOS-ADC(2) implementations only differ for the storage of the $\hat{B}^{\alpha}_{\mu\underline{i}}$ integrals in eq. (6.11), whose number of relevant blocks is the same of $B^{\alpha}_{\mu\underline{i}}$ in eq. (6.13), we will only report the memory demands of the latter one. Considering the use of the standard Coulomb operator ($\omega = 0.0$), Figure 6.2A shows that the number of relevant blocks in the ground state intermediates ($B^{\alpha}_{\mu\underline{i}}$, $\hat{Y}^{\beta}_{\mu\underline{i}}$, and $\hat{N}^{\alpha\beta}_{\tau}$) scales quadratically with the system size, due to the long-range nature of the standard Coulomb metric. On the other hand, the number of significant blocks in $\bar{B}^{\alpha}_{\mu\underline{i}}$ and $\bar{N}^{\alpha\beta}_{\tau}$ scales linearly with the system size as they depend on the transition density matrix – see eq. (6.34) and eq. (6.35) – whose number of relevant blocks becomes constant for large systems and local excitations. The time-determining calculation of $\bar{Y}^{\beta}_{\mu\underline{i}}$ scales as $\mathscr{O}(N^2)$ because we multiply $B^{\alpha}_{\mu\underline{i}}$ with $\bar{M}^{\alpha\beta}_{\tau}$ and $\bar{B}^{\alpha}_{\mu\underline{i}}$ with $\hat{M}^{\alpha\beta}_{\tau}$. Notice that the $\bar{\mathbf{M}}$ and $\hat{\mathbf{M}}$ matrices are obtained from the multiplication with the RI two-index integrals in eq. (6.35) and eq. (6.27), respectively, and the number of their relevant blocks grows quadratically with the system size. The computed $\bar{Y}^{\beta}_{\mu\underline{i}}$ tensor contains a quadratically growing number of blocks.

If the attenuated Coulomb operator with $\omega = 0.1$ is used (see Figure 6.2B), the memory demands for the ground state three-index integrals $B^{\alpha}_{\mu\underline{i}}$ and the intermediates $\hat{N}^{\alpha\beta}_{\tau}$ scale as $\mathscr{O}(N)$, while the number of allocated blocks in $\hat{Y}^{\beta}_{\mu\underline{i}}$ scales sub-quadratically with the size of the system with

significant HOMO-LUMO gap as LCAs. On the contrary, the number of blocks within the $\bar{B}^{\alpha}_{\mu\underline{i}}$ and $\bar{N}^{\alpha\beta}_{\tau}$ becomes constant in the asymptotic limit for localized excitations. Accordingly, the time-determining evaluation of eq. (6.34) scales linearly with the system size due to the constant number of elements in $\bar{N}^{\alpha\beta}_{\tau}$ that introduces sparsity in the matrix $\bar{M}^{\alpha\beta}_{\tau}$. Hence both terms in eq. (6.34) show computational linear scaling for large systems and local excitations. The memory demands of $\bar{Y}^{\beta}_{\mu\underline{i}}$ scale linearly in the asymptotic limit.
For three-dimensional systems with local excitations, ω-CDD-RI-SOS-LR-CC2 and ω-CDD-RI-SOS-ADC(2) are expected to reach the computational linear scaling regime only for larger system sizes. Similarly, the memory demands for the three-index integrals and the other intermediates are expected to be severely affected by the decreased sparsity of the one-electron densities. In such cases, as well as when diffuse basis functions are involved, the THC-based implementations presented in **Publication III** would be a better choice in terms of computational and memory efficiency since they have been proven to yield chemically accurate results.

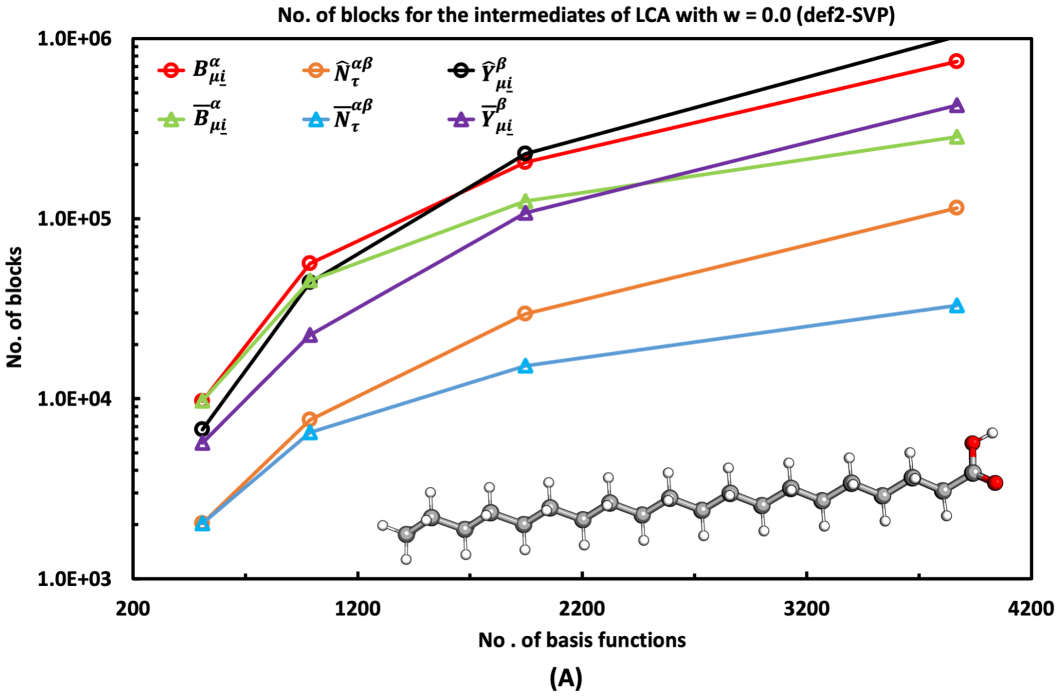

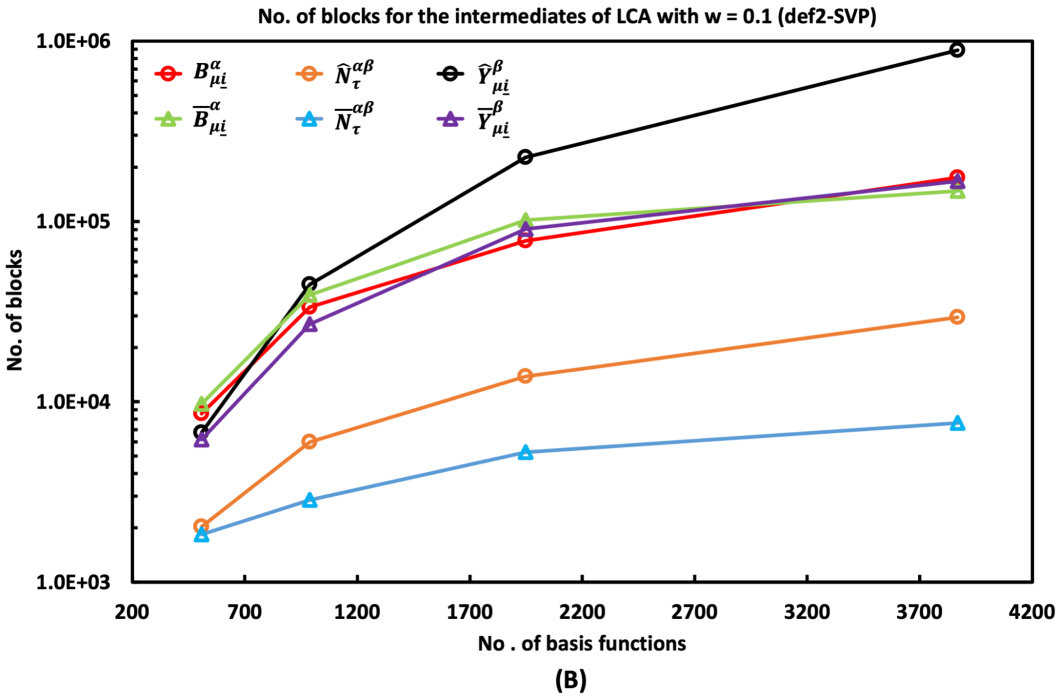

Figure 6.2: Number of relevant blocks in the most important intermediates of ω-CDD-RI-SOS-ADC(2) with $\omega = 0.0$ (A) and $\omega = 0.1$ (B) for the def2-SVP basis.

6.2 Low-scaling Evaluation of Closed-Shell SOS-ADC(2) Density Matrices

In Sec. 6.1 and in **Publications I-III**, we proposed several ways of reducing both computational and memory demands of the SOS-LR-CC2 and SOS-ADC(2) methods. The implemented algorithms proved to be fast and accurate even for molecules with hundreds of atoms. In this section, we discuss the evaluation of the one-particle reduced density matrix and transition density matrix – that depend on the solutions to the eigenvalue problem – in order to gather knowledge about the electronic transitions to singlet excited states. We will focus on the ADC(2) method since it is a Hermitian and size-consistent method,[22,25,168,169] and contrary to LR-CC2 does not require the solution of the left eigenvalue problem.[48,170,171] To the best of our knowledge, low-scaling reformulations based on the Cholesky decomposed density matrices within either the RI or the THC approximation (see Sec. 6.2.3 and Sec. 6.2.5, respectively) have not been published for SOS-ADC(2) density matrices and transition density matrices.

Following the solution of the eigenvalue problem for an excited state I, the normalized[56] ADC(2) wave function is used to evaluate the one-particle reduced density matrix $\boldsymbol{\rho}^I$ and transition density matrix $\boldsymbol{\rho}^{I\leftarrow 0}$ from the MP2 ground state to the excited state I according to:[146,154,169,170,172]

$$\rho^I_{pq} = \langle \Psi^{\mathrm{ADC(2)}}_I | \hat{a}^\dagger_p \hat{a}_q | \Psi^{\mathrm{ADC(2)}}_I \rangle \tag{6.48}$$

$$\rho^{I\leftarrow 0}_{pq} = \langle \Psi^{\mathrm{ADC(2)}}_I | \hat{a}^\dagger_p \hat{a}_q | \mathrm{MP1} \rangle \tag{6.49}$$

With the ADC(2) one-electron density matrices at hand we can investigate any excited state property T_I or transition property $\mathrm{T}_{I\leftarrow 0}$ that can be expressed in terms of a one-particle operator $\hat{O}$[146,154,170,173]

$$T_I = \langle \Psi^{\mathrm{ADC(2)}}_I | \hat{O} | \Psi^{\mathrm{ADC(2)}}_I \rangle = \sum_{pq} O_{pq} \rho^I_{pq} \tag{6.50}$$

$$T_{I\leftarrow 0} = \langle \Psi^{\mathrm{ADC(2)}}_I | \hat{O} | \mathrm{MP1} \rangle = \sum_{pq} O_{pq} \rho^{I\leftarrow 0}_{pq} \tag{6.51}$$

for instance, dipole transition moments and oscillator strengths.[48,170] Furthermore, a visual analysis of the electronic excitation is enabled by the evaluation of, e.g., the one-particle reduced transition density

$$T(r) = \sum_{pq} \phi^*_p(r) \phi_q(r) \rho^{I\leftarrow 0}_{pq} \tag{6.52}$$

as well as the one-particle reduced difference density

$$\Delta\rho(r) = \sum_{pq} \phi^*_p(r) \phi_q(r) \left(\rho^I_{pq} - \rho^0_{pq} \right) \tag{6.53}$$

or attachment and detachment densities that derive from the difference density.[170] Moreover, the one-particle reduced density matrix yields the natural transition orbitals (NTOs) via diagonal-

ization of its occupied-occupied $\boldsymbol{\rho}^{\boldsymbol{I}}_{\mathrm{occ}}$ and virtual-virtual $\boldsymbol{\rho}^{\mathbf{I}}_{\mathrm{virt}}$ blocks:[58–60,174–176]

$$\boldsymbol{\rho}^{\boldsymbol{I}}_{\mathrm{occ}}\boldsymbol{U}_k = \boldsymbol{\lambda}_k\boldsymbol{U}_k \tag{6.54}$$

$$\boldsymbol{\rho}^{\boldsymbol{I}}_{\mathrm{virt}}\boldsymbol{V}_{k'} = \boldsymbol{\lambda}'_{k'}\boldsymbol{V}_{k'} \tag{6.55}$$

where $k = 1,2,\ldots,N_{\mathrm{occ}}$, $k' = 1,2,\ldots,N_{\mathrm{virt}}$, and the $\mathbf{U}$ and $\mathbf{V}$ are the unitary transformation matrices,[59,60] used to transform the canonical MO basis to the NTO basis. The eigenvalues represent the importance of occupied and virtual NTOs for the description of the transition to the excited state I.[59,60]

6.2.1 Closed-shell expressions of the one-particle density matrices

The converged closed-shell SOS-ADC(2) wave function describing an excited state I

$$\Psi_I^{\text{SOS-ADC(2)}} = (\hat{R}^I_{\mu_1} + \hat{R}^{I,\mathrm{os}}_{\mu_2})(1+\hat{T}^{\mathrm{os}}_{\mu_2})|\mathrm{HF}\rangle \tag{6.56}$$

is normalized dividing the transition vectors $\mathbf{R}_{\boldsymbol{\mu_1}}$ and $\mathbf{R}_{\boldsymbol{\mu_2}}$ by the normalization factor[56]

$$c = \left[\sum_{ai} R^I_{ai}R^I_{ai} + \frac{1}{2}c_{\mathrm{os}}\sum_{aibj} R^{I,\mathrm{os}}_{aibj}R^{I,\mathrm{os}}_{aibj}\right]^{\frac{1}{2}} \tag{6.57}$$

The zeroth-order contributions to the SOS-ADC(2) excited state one-particle density matrix are

$$\rho^I_{ij} = -\sum_a R^I_{ai}R^I_{aj} - c_{\mathrm{os}}\sum_{abk} R^{I,\mathrm{os}}_{aibk}R^{I,\mathrm{os}}_{ajbk} \tag{6.58}$$

$$\rho^I_{ab} = +\sum_i R_{ai}R_{bi} + c_{\mathrm{os}}\sum_{ijc} R^{\mathrm{os}}_{aicj}R^{\mathrm{os}}_{bicj} \tag{6.59}$$

$$\rho^I_{ia} = \rho^I_{ai} = c_{\mathrm{os}}\sum_{bj} R^I_{jb}R^{\mathrm{os}}_{aibj} \tag{6.60}$$

while the first-order contributions vanish and the second-order contributions to $\boldsymbol{\rho}^{\mathbf{I}}$ are neglected. The evaluation of the transition one-particle density matrix requires the calculation of contributions up to second-order. In this work, we neglect the most expensive among the second-order contributions as they scale up to $\mathcal{O}(N^6)$ with the system size. Hence, the SOS-ADC(2) density matrix is correct up to first-order and consistent with the LR-CC theory.[56] The zeroth-order contribution to $\rho^{I\leftarrow 0}_{pq}$ is simply the transition vector in the singles manifold

$$\rho^{I\leftarrow 0}_{ai} = R^I_{ai} \tag{6.61}$$

and the first-order contribution is computed as

$$\rho^{I\leftarrow 0}_{ia} = c_{\mathrm{os}}\sum_{jb} R^I_{bj}t^{\mathrm{os}}_{aibj} \tag{6.62}$$

The second-order contributions to $\rho^{I\leftarrow 0}_{pq}$ involve the doubles part of the excitation vector

$$\rho^{I\leftarrow 0}_{ij} = -c_{\mathrm{os}}\sum_{abk} R^{I,\mathrm{os}}_{aibk}t^{\mathrm{os}}_{ajbk} \tag{6.63}$$

$$\rho^{I\leftarrow 0}_{ab} = c_{\mathrm{os}}\sum_{ijc} R^{I,\mathrm{os}}_{aicj}t^{\mathrm{os}}_{bicj} \tag{6.64}$$

as well as the SOS-MP2 corrections to the ground state one-particle density matrix

$$\rho_{ai}^{I\leftarrow 0} = +\sum_{k} R_{ak}\rho_{ki}^{0} - \sum_{b}\rho_{ab}^{0}R_{bi} \tag{6.65}$$

$$\rho_{ij}^{0} = -c_{\mathrm{os}}\sum_{abk} t_{aibk}^{\mathrm{os}} t_{ajbk}^{\mathrm{os}} \tag{6.66}$$

$$\rho_{ab}^{0} = c_{\mathrm{os}}\sum_{ijc} t_{aicj}^{\mathrm{os}} t_{bicj}^{\mathrm{os}} \tag{6.67}$$

Notice that the doubles part of the SOS-ADC(2) excitation vector and the SOS-MP2 doubles amplitudes are formed according to

$$R_{aibj}^{I,\mathrm{os}} = -\frac{S_{ij}^{ab}(ai|\bar{b}j)}{\varepsilon_a - \varepsilon_i + \varepsilon_b - \varepsilon_j - \bar{\omega}} \tag{6.68}$$

$$t_{aibj}^{\mathrm{os}} = -\frac{(ai|bj)}{\varepsilon_a - \varepsilon_i + \varepsilon_b - \varepsilon_j} \tag{6.69}$$

with the ERIs defined in eq. (3.49) and eq. (2.73), respectively. Hence a key role in deriving the RI- and THC-decomposed formulations for the density matrices is played by the cross-multiplication:[177–179]

$$\frac{1}{(\varepsilon_a - \varepsilon_i + \varepsilon_b - \varepsilon_k)(\varepsilon_a - \varepsilon_j + \varepsilon_b - \varepsilon_k)} = \left[\frac{1}{\varepsilon_a - \varepsilon_i + \varepsilon_b - \varepsilon_k} - \frac{1}{\varepsilon_a - \varepsilon_j + \varepsilon_b - \varepsilon_k}\right]\frac{1}{\varepsilon_i - \varepsilon_j} \tag{6.70}$$

Upon the Laplace transformation of the energy denominators, eq. (6.70) becomes:

$$\frac{1}{(\varepsilon_a - \varepsilon_i + \varepsilon_b - \varepsilon_k)(\varepsilon_a - \varepsilon_j + \varepsilon_b - \varepsilon_k)} = \sum_{\tau} w_\tau g_{ij}^{\tau}\left[e^{-\varepsilon_b t_\tau} e^{\varepsilon_k t_\tau} e^{-\varepsilon_a t_\tau}\right] \tag{6.71}$$

where the energy exponentials for the i and j orbitals are included in the coefficient g_{ij}^{τ}, for each Laplace quadrature point. Considering both the occupied-occupied and virtual-virtual blocks of the density matrices, we obtain the following Laplace-dependent scaling coefficients:

$$g_{ij}^{\tau} = \frac{e^{\varepsilon_i t_\tau} - e^{\varepsilon_j t_\tau}}{\varepsilon_i - \varepsilon_j} \qquad g_{ab}^{\tau} = -\frac{e^{-\varepsilon_a t_\tau} - e^{-\varepsilon_b t_\tau}}{\varepsilon_a - \varepsilon_b} \tag{6.72}$$

$$g_{ij}^{\tau}(\bar{\omega}) = \frac{e^{\varepsilon_i t_\tau} - e^{\varepsilon_j t_\tau}}{\varepsilon_i - \varepsilon_j} e^{\bar{\omega} t_\tau} \qquad g_{ab}^{\tau}(\bar{\omega}) = -\frac{e^{-\varepsilon_a t_\tau} - e^{-\varepsilon_b t_\tau}}{\varepsilon_a - \varepsilon_b} e^{\bar{\omega} t_\tau} \tag{6.73}$$

$$\bar{g}_{ij}^{\tau}(\bar{\omega}) = \frac{e^{\varepsilon_i t_\tau} e^{\bar{\omega} t_\tau} - e^{\varepsilon_j t_\tau}}{(\varepsilon_i + \bar{\omega}) - \varepsilon_j} \qquad \bar{g}_{ab}^{\tau}(\bar{\omega}) = -\frac{e^{-\varepsilon_a t_\tau} e^{\bar{\omega} t_\tau} - e^{\varepsilon_b t_\tau}}{(\varepsilon_a - \bar{\omega}) - \varepsilon_b} \tag{6.74}$$

6.2.2 Quartic-scaling RI-MO-based formulation of the one-particle density matrices

The RI decomposition of the ERIs and Laplace transformation of the energy denominators allows for quartic-scaling evaluation of the SOS-ADC(2) excitation energies.[25,38] The memory

demand scales with the cubic power of the size of the system.[25,38] Although an efficient implementation of the equations for the MO-RI-SOS-ADC(2) densities has already been published in literature,[38,178] we propose the explicit equations to be used as a reference for the low-scaling reformulation. Before deriving the MO-based expressions of the density matrices, we introduce the transformed three-index integrals

$$B^{\alpha}_{ai} = \sum_{\mu\nu} C_{\mu a} C_{\nu i} B^{\alpha}_{\mu\nu} \tag{6.75}$$

$$\bar{B}^{\alpha}_{ai} = \sum_{\mu\nu} \left(\bar{\Lambda}^{\mathrm{h}}_{\mu a} C_{\nu i} + C_{\mu a} \bar{\Lambda}^{\mathrm{h}}_{\nu i} \right) B^{\alpha}_{\mu\nu} \tag{6.76}$$

obtained with a quartic-scaling computational cost. The $\bar{\mathbf{\Lambda}}$ matrices are defined in eqs. (3.50) and (3.51) and depend on the singles part of the transition vector.

One-particle reduced density matrix

The elements of the occupied-occupied and virtual-virtual blocks in the one-particle reduced density matrix of an excited state I are evaluated with a quartic scaling effort

$$\begin{aligned}
\rho^{I}_{ij} &= -c_{\mathrm{os}} \sum_{abk} R^{I,\mathrm{os}}_{aibk} R^{I,\mathrm{os}}_{ajbk} \\
&= -c_{\mathrm{os}} \sum_{\tau} w^{\frac{1}{2}}_{\tau} g^{\tau}_{ij}(\bar{\omega}) \sum_{a} \sum_{\alpha\beta} \left\{ \left[\bar{B}^{\alpha}_{ai} M^{\alpha\beta}_{\tau} + B^{\alpha}_{ai} \bar{M}^{\alpha\beta}_{\tau} \right] \bar{B}^{\beta}_{aj} + \left[\bar{B}^{\alpha}_{ai} \bar{M}^{\beta\alpha}_{\tau} + B^{\alpha}_{ai} \bar{\bar{M}}^{\alpha\beta}_{\tau} \right] B^{\beta}_{aj} \right\} e^{-\varepsilon_a t_\tau} \\
&= -c_{\mathrm{os}} \sum_{\tau} w^{\frac{1}{2}}_{\tau} g^{\tau}_{ij}(\bar{\omega}) \sum_{a} \sum_{\beta} \left[\bar{Y}^{\beta,\tau}_{ai} \bar{B}^{\beta}_{aj} e^{-\varepsilon_a t_\tau} + \bar{\bar{Y}}^{\beta,\tau}_{ai} B^{\beta}_{aj} e^{-\varepsilon_a t_\tau} \right]
\end{aligned} \tag{6.77}$$

$$\begin{aligned}
\rho^{I}_{ab} &= +c_{\mathrm{os}} \sum_{ijc} R^{\mathrm{os}}_{aicj} R^{\mathrm{os}}_{bicj} \\
&= +c_{\mathrm{os}} \sum_{\tau} w^{\frac{1}{2}}_{\tau} g^{\tau}_{ab}(\bar{\omega}) \sum_{i} \sum_{\alpha\beta} \left\{ \left[\bar{B}^{\alpha}_{ai} M^{\alpha\beta}_{\tau} + B^{\alpha}_{ai} \bar{M}^{\alpha\beta}_{\tau} \right] \bar{B}^{\beta}_{bi} + \left[\bar{B}^{\alpha}_{ai} \bar{M}^{\beta\alpha}_{\tau} + B^{\alpha}_{ai} \bar{\bar{M}}^{\alpha\beta}_{\tau} \right] B^{\beta}_{bi} \right\} e^{\varepsilon_i t_\tau} \\
&= +c_{\mathrm{os}} \sum_{\tau} w^{\frac{1}{2}}_{\tau} g^{\tau}_{ab}(\bar{\omega}) \sum_{i} \sum_{\beta} \left[\bar{Y}^{\beta,\tau}_{ai} \bar{B}^{\beta}_{bi} e^{\varepsilon_i t_\tau} + \bar{\bar{Y}}^{\beta,\tau}_{ai} B^{\beta}_{bi} e^{\varepsilon_i t_\tau} \right]
\end{aligned} \tag{6.78}$$

with the intermediates computed as:

$$\bar{Y}^{\beta,\tau}_{ai} = \sum_{\alpha} \left(\bar{B}^{\alpha}_{ai} M^{\alpha\beta}_{\tau} + B^{\alpha}_{ai} \bar{M}^{\alpha\beta}_{\tau} \right) \qquad \bar{\bar{Y}}^{\beta,\tau}_{ai} = \sum_{\alpha} \left(\bar{B}^{\alpha}_{ai} \bar{M}^{\beta\alpha}_{\tau} + B^{\alpha}_{ai} \bar{\bar{M}}^{\alpha\beta}_{\tau} \right) \tag{6.79}$$

$$M^{\alpha\beta}_{\tau} = J^{-1}_{\alpha\alpha'} \left[w^{\frac{1}{2}}_{\tau} \sum_{bj} B^{\alpha'}_{bj} B^{\beta'}_{bj} e^{-\varepsilon_{bj} t_\tau} \right] J^{-1}_{\beta'\beta} \tag{6.80}$$

$$\bar{M}^{\alpha\beta}_{\tau} = J^{-1}_{\alpha\alpha'} \left[w^{\frac{1}{2}}_{\tau} \sum_{bj} \bar{B}^{\alpha'}_{bj} B^{\beta'}_{bj} e^{-\varepsilon_{bj} t_\tau} \right] J^{-1}_{\beta'\beta} \tag{6.81}$$

$$\bar{\bar{M}}^{\alpha\beta}_{\tau} = J^{-1}_{\alpha\alpha'} \left[w^{\frac{1}{2}}_{\tau} \sum_{bj} \bar{B}^{\alpha'}_{bj} \bar{B}^{\beta'}_{bj} e^{-\varepsilon_{bj} t_\tau} \right] J^{-1}_{\beta'\beta} \tag{6.82}$$

The $\mathbf{M}$ and $\bar{\mathbf{M}}$ matrices are formed – and stored on disk – while evaluating the ground state energy and the excitation energies, respectively. Thus, only the $\bar{\bar{\mathbf{M}}}$ matrices must be computed for each excited state I. Moreover, it is important to stress that the elements ρ^I_{ij} and ρ^I_{ab} can be evaluated within the same algorithm as they differ only in the last summation over the occupied or virtual index, respectively. The calculation of the off-diagonal blocks of the density matrix $\boldsymbol{\rho}^{\boldsymbol{I}}$ requires cubic-scaling steps:

$$\rho^I_{ai} = c_{\rm os} \sum_{bj} R^I_{jb} R^{\rm os}_{aibj} = c_{\rm os} \sum_{\tau} w_\tau^{\frac{1}{2}} \sum_{\alpha} \left[\bar{B}^\alpha_{ai} \bar{m}^\alpha_\tau + \bar{\bar{m}}^\alpha_\tau B^\alpha_{ai} \right] e^{\bar{\omega} t_\tau} e^{-\varepsilon_{ai} t_\tau} \tag{6.83}$$

with

$$\bar{m}^\alpha_\tau = J^{-1}_{\alpha\beta} \left[w_\tau^{\frac{1}{2}} \sum_{bj} R_{jb} B^\beta_{bj} e^{-\varepsilon_{bj} t_\tau} \right] \tag{6.84}$$

$$\bar{\bar{m}}^\alpha_\tau = J^{-1}_{\alpha\beta} \left[w_\tau^{\frac{1}{2}} \sum_{bj} R_{jb} \bar{B}^\beta_{bj} e^{-\varepsilon_{bj} t_\tau} \right] \tag{6.85}$$

Notice that the intermediate in eq. (6.84) is formed and stored on disk during the evaluation of the excitation energies.

One-particle reduced transition density matrix

Similar expressions to eqs. (6.77), (6.78), and (6.83) are obtained for the contributions to the one-electron reduced transition density matrix. In fact, to form the transition density matrix only part of the intermediates from the previous Section are required. It follows that the density matrix and the transition density matrix are obtained in the same algorithm, with the second one being considered as a by-product of the matrix $\boldsymbol{\rho}^I$.
The elements of the first-order off-diagonal block of $\boldsymbol{\rho}^{I\leftarrow 0}$ are computed with a cubic-scaling effort:

$$\rho^{I\leftarrow 0}_{ia} = c_{\rm os} \sum_{\tau} w_\tau^{\frac{1}{2}} \sum_{\alpha} \bar{m}^\alpha_\tau B^\alpha_{ai} e^{-\varepsilon_{ai} t_\tau} \qquad \bar{m}^\alpha_\tau = J^{-1}_{\alpha\beta} \left[w_\tau^{\frac{1}{2}} \sum_{bj} R_{bj} B^\beta_{bj} e^{-\varepsilon_{bj} t_\tau} \right] \tag{6.86}$$

with the intermediate $\bar{\mathbf{m}}$ defined in eq. (6.84). On the other hand, the elements of the diagonal occupied-occupied and virtual-virtual blocks can be evaluated with a quartic-scaling behavior, according to:

$$\begin{aligned} \rho^{I\leftarrow 0}_{ij} &= -c_{\rm os} \sum_{abk} R^{I,{\rm os}}_{aibk} t^{\rm os}_{ajbk} \\ &= -c_{\rm os} \sum_{\tau} w_\tau^{\frac{1}{2}} \bar{g}^\tau_{ij}(\bar{\omega}) \sum_a \sum_{\alpha\beta} \left\{ \left[\bar{B}^\alpha_{ai} M^{\alpha\beta}_\tau + B^\alpha_{ai} \bar{M}^{\alpha\beta}_\tau \right] B^\beta_{aj} \right\} e^{-\varepsilon_a t_\tau} \end{aligned} \tag{6.87}$$

$$\begin{aligned} \rho^{I\leftarrow 0}_{ab} &= c_{\rm os} \sum_{ijc} R^{I,{\rm os}}_{aicj} t^{\rm os}_{bicj} \\ &= +c_{\rm os} \sum_{\tau} w_\tau^{\frac{1}{2}} \bar{g}^\tau_{ab}(\bar{\omega}) \sum_i \sum_{\alpha\beta} \left\{ \left[\bar{B}^\alpha_{ai} M^{\alpha\beta}_\tau + B^\alpha_{ai} \bar{M}^{\alpha\beta}_\tau \right] B^\beta_{bi} \right\} e^{\varepsilon_i t_\tau} \end{aligned} \tag{6.88}$$

The matrices $\mathbf{M}$ and $\bar{\mathbf{M}}$ in eqs. (6.80) and (6.81) are computed and stored while evaluating the energy of the state I. Finally, the second-order off-diagonal block of the transition density matrix in eq. (6.65) is formed with a $\mathscr{O}(N^4)$ scaling effort since it depends on the SOS-MP2 correction to the ground state density matrix:

$$\begin{aligned}\rho^0_{ij} &= -c_{\mathrm{os}} \sum_{abk} t^{\mathrm{os}}_{aibk} t^{\mathrm{os}}_{ajbk} \\ &= -c_{\mathrm{os}} \sum_{\tau} w_\tau^{\frac{1}{2}} g^\tau_{ij} \sum_a \sum_{\alpha\beta} \left\{ B^\alpha_{ai} M^{\alpha\beta}_\tau B^\beta_{aj} \right\} e^{-\varepsilon_a t_\tau} \qquad (6.89)\\ \rho^0_{ab} &= c_{\mathrm{os}} \sum_{ijc} t^{\mathrm{os}}_{aicj} t^{\mathrm{os}}_{bicj} \\ &= +c_{\mathrm{os}} \sum_{\tau} w_\tau^{\frac{1}{2}} g^\tau_{ab} \sum_i \sum_{\alpha\beta} \left\{ B^\alpha_{ai} M^{\alpha\beta}_\tau B^\beta_{bi} \right\} e^{\varepsilon_i t_\tau} \qquad (6.90)\end{aligned}$$

6.2.3 Low-scaling RI-CDD-based formulation of the one-particle density matrices

A low-scaling reformulation of the contributions to the one-electron reduced density matrix and transition density matrix is obtained by rewriting the equations from Sec. 6.2.2 in terms of Cholesky decomposed density matrices[63,64,104] – see eq. (6.8). The computational cost is expected to scale as $\mathscr{O}(N^2)$ and $\mathscr{O}(N)$ with the attenuation factor of the Coulomb metric equal to $\omega = 0.0$ and $\omega = 0.1$, respectively, and for systems with a significant HOMO-LUMO gap and a local electronic excitation. As discussed in **Publications I-III** and in Sec. 6.1, the reformulation is enabled by back-transforming the MO-based blocks of $\boldsymbol{\rho}^I$ and $\boldsymbol{\rho}^{I\leftarrow 0}$ into the AO basis:

$$\rho^I_{\mu\nu} = \sum_{pq} C_{\mu p} \rho^I_{pq} C_{\nu q} \qquad (6.91)$$

$$\rho^{I\leftarrow 0}_{\mu\nu} = \sum_{pq} C_{\mu p} \rho^{I\leftarrow 0}_{pq} C_{\nu q} \qquad (6.92)$$

Before presenting the reformulation of the equations, we introduce the following symmetric pseudo-density matrices which depend on the singles part of the transition vector:

$$\begin{aligned}\bar{\tilde{Q}}^\tau_{\mu\nu} &= w_\tau^{\frac{1}{4}} \sum_a \bar{\Lambda}^{\mathrm{p}}_{\mu a} \bar{\Lambda}^{\mathrm{p}}_{\nu a} e^{-\varepsilon_a t_\tau} = \sum_a \Big[\sum_i C_{\mu i} R_{ai} \Big] \Big[\sum_j C_{\mu j} R_{aj} \Big] \\ &= (\mathbf{PSR^T SQ^\tau SRSP})_{\mu\nu} \qquad (6.93)\\ \bar{\tilde{P}}^\tau_{\mu\nu} &= w_\tau^{\frac{1}{4}} \sum_i \bar{\Lambda}^{\mathrm{h}}_{\mu i} \bar{\Lambda}^{\mathrm{h}}_{\nu i} e^{\varepsilon_i t_\tau} = \sum_i \Big[\sum_a C_{\mu a} R_{ai} \Big] \Big[\sum_b C_{\mu b} R_{bi} \Big] \\ &= (\mathbf{QSRSP^\tau SR^T SQ})_{\mu\nu} \qquad (6.94)\end{aligned}$$

where $Q^\tau_{\mu\nu} = w_\tau^{\frac{1}{4}} \sum_a C_{\mu a} C_{\nu a} e^{-\varepsilon_a t_\tau}$ and $P^\tau_{\mu\nu} = w_\tau^{\frac{1}{4}} \sum_i C_{\mu i} C_{\nu i} e^{\varepsilon_i t_\tau}$. Additionally, in order to obtain efficient programmable equations, we rewrite eqs. (6.93) and (6.94) as follows:

$$\bar{\tilde{Q}}^\tau_{\mu\nu} = -\sum_{\sigma''} \tilde{Q}^\tau_{\mu\sigma''} \bar{Q}_{\sigma''\nu} \qquad \bar{\tilde{P}}^\tau_{\mu\nu} = \sum_{\underline{i}} \bar{P}^\tau_{\mu\underline{i}} \bar{P}_{\nu\underline{i}} \qquad (6.95)$$

with the virtual densities formed as

$$\tilde{Q}^{\tau}_{\mu\nu} = (\mathbf{PSR^{T}SQ^{\tau}S})_{\mu\nu} \tag{6.96}$$

$$\bar{Q}_{\mu\nu} = -(\mathbf{QSRSP})_{\mu\nu} \tag{6.97}$$

and the occupied densities formed as

$$\bar{P}^{\tau}_{\mu\underline{i}} = \sum_{\underline{k}} (\mathbf{QSRSL})_{\mu\underline{k}} (\mathbf{L^{T}SP^{\tau}SL})_{\underline{k}\underline{i}} \tag{6.98}$$

$$\bar{P}_{\mu\underline{i}} = (\mathbf{QSRSL})_{\mu\underline{i}} \tag{6.99}$$

$$P^{\tau}_{\underline{k}\underline{i}} = (\mathbf{L^{T}SP^{\tau}SL})_{\underline{k}\underline{i}} \tag{6.100}$$

Finally, using the density matrices in eqs. (6.99), (6.97), and (6.8), one can transform the Laplace-independent three-index integrals to reduce the computational cost and the I/O effort, as discussed in Sec. 6.1:

$$\bar{B}^{\alpha}_{\mu\underline{i}} = \sum_{\mu'\nu} \bar{Q}_{\mu\mu'} B^{\alpha}_{\mu'\nu} L_{\nu\underline{i}} + \sum_{\mu\nu} Q_{\mu'\mu} B^{\alpha}_{\mu\nu} \bar{P}_{\nu\underline{i}} \qquad\qquad B^{\alpha}_{\mu\underline{i}} = \sum_{\nu} B^{\alpha}_{\mu\nu} L_{\nu\underline{i}} \tag{6.101}$$

Notice that the three-index integrals in eq. (6.101) are also used to form the contributions of the matrix-vector product in Sec. 6.1 and hence they are already stored on disk and are not recomputed to form the ω-CDD-RI-SOS-ADC(2) one-particle excited state density matrix and transition density matrix.

One-particle reduced density matrix

The elements of the occupied-occupied and virtual-virtual diagonal blocks of the one-particle reduced density matrix are obtained by performing the time-consuming steps in the local Cholesky orbital basis, which result in the intermediate matrix $\mathbf{\Omega}$. For the occupied-occupied block, we obtain the following intermediates:

$$\begin{aligned}\Omega^{\tau,(1)}_{\underline{i}\underline{j}} = \sum_{\alpha\beta} \Bigg\{ \sum_{\lambda} \Big[\sum_{\mu'} \Big(\sum_{\sigma'} Q^{\tau}_{\lambda\sigma'} S_{\sigma'\mu'} \Big) \bar{B}^{\alpha}_{\mu'\underline{i}} \Big] M^{\alpha\beta}_{\tau} \Big[\sum_{\sigma} B^{\beta}_{\lambda\sigma} \bar{P}_{\sigma\underline{j}} \Big] \\ + \sum_{\lambda} \Big[\sum_{\mu'} \tilde{Q}^{\tau}_{\lambda\mu'} \bar{B}^{\alpha}_{\mu'\underline{i}} \Big] M^{\alpha\beta}_{\tau} \Big[\sum_{\sigma} B^{\beta}_{\lambda\sigma} L_{\sigma\underline{i}} \Big] \Bigg\}\end{aligned} \tag{6.102}$$

$$\Omega^{\tau,(2)}_{\underline{i}\underline{j}} = \sum_{\alpha\beta} \Bigg\{ \sum_{\mu} \Big[\sum_{\nu} B^{\alpha}_{\mu\nu} L_{\nu\underline{i}} \Big] \bar{M}^{\alpha\beta}_{\tau} \Big[\sum_{\lambda'} \Big(\sum_{\sigma'} Q^{\tau}_{\mu\sigma'} S_{\sigma'\lambda'} \Big) \bar{B}^{\alpha}_{\lambda'\underline{i}} \Big] \Bigg\}_{\underline{i} \longleftrightarrow \underline{j}} \tag{6.103}$$

$$\Omega^{\tau,(3)}_{\underline{i}\underline{j}} = \sum_{\alpha\beta} \Bigg\{ \sum_{\lambda} \Big[\sum_{\mu\nu} Q^{\tau}_{\mu\nu} B^{\alpha}_{\mu\nu} L_{\nu\underline{i}} \Big] \bar{\bar{M}}^{\alpha\beta}_{\tau} \Big[\sum_{\sigma} B^{\beta}_{\lambda\sigma} L_{\sigma\underline{j}} \Big] \Bigg\} \tag{6.104}$$

where $\underline{i} \leftrightarrow \underline{j}$ symmetrizes an intermediate according to $(\Omega_{\underline{ij}})_{\underline{i}\leftrightarrow\underline{j}} = \Omega_{\underline{ij}} + \Omega_{\underline{ji}}$. On the other hand, the intermediates for the virtual-virtual block are formed as:

$$\Omega^{\tau,(4)}_{\mu'\nu'} = \sum_{\alpha\beta}\Bigg\{\sum_{\underline{i}}\Big[\sum_{\underline{k}}\bar{B}^{\alpha}_{\mu'\underline{k}}P^{\tau}_{\underline{ki}}\Big]M^{\alpha\beta}_{\tau}\Big[\sum_{\lambda\sigma}\bar{Q}_{\nu'\lambda}B^{\beta}_{\lambda\sigma}L_{\sigma\underline{i}}\Big] + \sum_{\underline{i}}\Big[\sum_{\underline{k}}\bar{B}^{\alpha}_{\mu'\underline{k}}P^{\tau}_{\underline{ki}}\Big]M^{\alpha\beta}_{\tau}\Big[\sum_{\lambda\sigma}Q_{\nu'\lambda}B^{\beta}_{\lambda\sigma}\bar{P}_{\sigma\underline{i}}\Big]\Bigg\} \tag{6.105}$$

$$\Omega^{\tau,(5)}_{\mu'\nu'} = \sum_{\alpha\beta}\Bigg\{\sum_{\underline{i}}\Big[\sum_{\mu\nu}Q_{\mu'\mu}B^{\alpha}_{\mu\nu}L_{\nu\underline{i}}\Big]\bar{M}^{\alpha\beta}_{\tau}\Big[\sum_{\underline{k}}\bar{B}^{\alpha}_{\nu'\underline{k}}P^{\tau}_{\underline{ki}}\Big]\Bigg\}_{\mu'\leftrightarrow\nu'} \tag{6.106}$$

$$\Omega^{\tau,(6)}_{\mu'\nu'} = \sum_{\alpha\beta}\Bigg\{\sum_{\underline{i}}\Big[\sum_{\mu\nu}Q_{\mu'\mu}B^{\alpha}_{\mu\nu}L_{\nu\underline{k}}P^{\tau}_{\underline{ki}}\Big]\bar{\bar{M}}^{\alpha\beta}_{\tau}\Big[Q_{\nu'\lambda}B^{\beta}_{\lambda\sigma}L_{\sigma\underline{i}}\Big]\Bigg\} \tag{6.107}$$

It is important to stress again that the $\mathbf{M}$ and $\bar{\mathbf{M}}$ matrices are computed and stored while evaluating the excited state energies – see eqs. (6.27) and (6.35) respectively. The remaining matrix $\bar{\bar{\mathbf{M}}}$ must be computed for each excited state density matrix $\boldsymbol{\rho}^I$, according to:

$$\bar{\bar{M}}^{\alpha\beta}_{\tau} = \sum_{\alpha'\beta'}J^{-1}_{\alpha\alpha'}\Bigg\{\sum_{\lambda\underline{j}}\Big[\sum_{\lambda'}\sum_{\underline{k}}\tilde{Q}^{\tau}_{\lambda\lambda'}\bar{B}^{\alpha'}_{\lambda'\underline{k}}P^{\tau}_{\underline{kj}}\Big]\Big[\sum_{\sigma}B^{\beta'}_{\lambda\sigma}L_{\sigma\underline{j}}\Big] + \sum_{\lambda\underline{j}}\Big[\sum_{\lambda'}\sum_{\underline{k}}\Big(\sum_{\mu'}Q^{\tau}_{\lambda\mu'}S_{\mu'\lambda'}\Big)\bar{B}^{\alpha'}_{\lambda'\underline{k}}P^{\tau}_{\underline{kj}}\Big]\Big[\sum_{\sigma}B^{\beta'}_{\lambda\sigma}\bar{P}_{\sigma\underline{k}}\Big]\Bigg\}J^{-1}_{\beta'\beta} \tag{6.108}$$

Note that the intermediates $\bar{\bar{\mathbf{M}}}$ can be evaluated within Algorithm 1 with minor changes. Once the intermediates $\boldsymbol{\Omega}$ are formed, we can collect them:

$$\Omega^{\tau,(\mathrm{occ})}_{\mu\nu} = \sum_{\underline{ij}}L_{\mu\underline{i}}\Big[\Omega^{\tau,(1)}_{\underline{ij}} + \Omega^{\tau,(2)}_{\underline{ij}} + \Omega^{\tau,(3)}_{\underline{ij}}\Big]L_{\nu\underline{j}} \tag{6.109}$$

$$\Omega^{\tau,(\mathrm{virt})}_{\mu\nu} = \Omega^{\tau,(4)}_{\mu\nu} + \Omega^{\tau,(5)}_{\mu\nu} + \Omega^{\tau,(6)}_{\mu\nu} \tag{6.110}$$

Eventually, the matrices $\Omega^{\tau,(\mathrm{occ})}_{\mu\nu}$ and $\Omega^{\tau,(\mathrm{virt})}_{\mu\nu}$ are formed by multiplying intermediates whose sparsity has been discussed in Sec. 6.1 – except the matrices $\bar{\bar{\mathbf{M}}}$. Therefore, we expect to compute $\Omega^{\tau,(\mathrm{occ})}_{\mu\nu}$ and $\Omega^{\tau,(\mathrm{virt})}_{\mu\nu}$ with asymptotical quadratic and linear scaling computational effort – in the standard and attenuated Coulomb metric, respectively, and for systems with sparse electronic structure and a local excitation. The memory demands of the intermediate $\bar{\bar{\mathbf{M}}}$ are expected to show the same scaling behavior discussed for $\bar{\mathbf{M}}$. The diagonal blocks of the one-particle reduced

density matrix $\boldsymbol{\rho}^I$ are given by:

$$\rho^I_{ij} = -c_{\text{os}} \sum_\tau w_\tau^{\frac{1}{4}} g^\tau_{ij}(\bar{\omega}) \left\{ \sum_{\mu\mu'} \sum_{\nu\nu'} C_{\mu' i} S_{\mu'\mu} \Omega^{\tau,(\text{occ})}_{\mu\nu} S_{\nu\nu'} C_{\nu' j} \right\} \tag{6.111}$$

$$\rho^I_{ab} = c_{\text{os}} \sum_\tau w_\tau^{\frac{1}{4}} g^\tau_{ab}(\bar{\omega}) \left\{ \sum_{\mu\mu'} \sum_{\nu\nu'} C_{\mu' a} S_{\mu'\mu} \Omega^{\tau,(\text{virt})}_{\mu\nu} S_{\nu\nu'} C_{\nu' b} \right\} \tag{6.112}$$

Finally, the off-diagonal blocks of $\boldsymbol{\rho}^I$ are evaluated with $\mathscr{O}(N^2)$ and $\mathscr{O}(N)$ for $\omega = 0.0$ and $\omega = 0.1$, respectively:

$$\rho^I_{ai} = \rho^I_{ia} = \sum_{\mu\mu'} \sum_{\nu\nu'} C_{\mu' a} S_{\mu'\mu} \Big[\sum_{\underline{i}} \rho^I_{\mu\underline{i}} L_{\nu\underline{i}} \Big] S_{\nu\nu'} C_{\nu' i} \tag{6.113}$$

$$\rho^I_{\mu\underline{i}} = c_{\text{os}} \sum_\tau \sum_\alpha \left[\bar{\bar{m}}^\alpha_\tau \Big(\sum_{\mu'\underline{k}} Q^\tau_{\mu\mu'} B^\alpha_{\mu'\underline{k}} P^\tau_{\underline{k}i} \Big) + \Big(\sum_{\mu'\nu'} \sum_{\underline{k}} Q^\tau_{\mu\nu'} S_{\nu'\mu'} \bar{B}^\alpha_{\mu'\underline{k}} P^\tau_{\underline{k}i} \Big) \bar{m}^\alpha_\tau \right] e^{\bar{\omega} t_\tau} \tag{6.114}$$

with $R_{\mu\underline{j}}$ defined in eq. (6.23), and the intermediates $\bar{\mathbf{m}}$ and $\bar{\bar{\mathbf{m}}}$ given by

$$\bar{m}^\alpha_\tau = J^{-1}_{\alpha\beta} \left[\sum_{\nu\underline{j}} R_{\nu\underline{j}} \Big(\sum_{\mu'\underline{k}} Q^\tau_{\nu\mu'} B^\beta_{\mu'\underline{k}} P^\tau_{\underline{k}\underline{j}} \Big) \right] \quad \bar{\bar{m}}^\alpha = J^{-1}_{\alpha\beta} \left[\sum_{\nu\underline{j}} R_{\nu\underline{j}} \Big(\sum_{\mu'\nu'} \sum_{\underline{k}} Q^\tau_{\nu\nu'} S_{\nu'\mu'} \bar{B}^\beta_{\mu'\underline{k}} P^\tau_{\underline{k}\underline{j}} \Big) \right] \tag{6.115}$$

One-particle reduced transition density matrix

As discussed for the MO-based formulation in Sec. 6.2.2, the one-particle transition density matrix $\boldsymbol{\rho}^{I\leftarrow 0}$ can be obtained as a by-product of computing the one-particle density matrix $\boldsymbol{\rho}^I$. For systems with a significant HOMO-LUMO gap and a local electronic transition, the second-order diagonal blocks of $\boldsymbol{\rho}^{I\leftarrow 0}$ are formed according to:

$$\rho^{I\leftarrow 0}_{ij} = -c_{\text{os}} \sum_\tau w_\tau^{\frac{1}{4}} \bar{g}^\tau_{ij}(\bar{\omega}) \Omega^\tau_{ij} \qquad \rho^{I\leftarrow 0}_{ab} = -c_{\text{os}} \sum_\tau w_\tau^{\frac{1}{4}} \bar{g}^\tau_{ab}(\bar{\omega}) \Omega^\tau_{ab} \tag{6.116}$$

where the $\boldsymbol{\Omega}$ intermediates are evaluated with an effort scaling as $\mathscr{O}(N^2)$ – with the standard RI Coulomb metric – or $\mathscr{O}(N)$ – with the attenuated Coulomb metric and $\omega = 0.1$:

$$\begin{aligned} \Omega^\tau_{ij} = \sum_{\sigma\lambda} \sum_{\sigma'\lambda'} \sum_{\underline{i}\underline{j}} C_{\sigma i} S_{\sigma\lambda} L_{\lambda\underline{i}} \Bigg\{ & \sum_{\alpha\beta} \sum_\mu \Big[\sum_{\nu'} \Big(\sum_{\mu'} Q^\tau_{\mu\mu'} S_{\mu'\nu'} \Big) \bar{B}^\alpha_{\nu'\underline{i}} M^{\alpha\beta}_\tau \\ & + \sum_{\nu'} Q^\tau_{\mu\nu'} B^\alpha_{\nu'\underline{i}} \bar{M}^{\alpha\beta}_\tau \Big] B^\beta_{\mu\underline{j}} \Bigg\} L_{\sigma'\underline{j}} S_{\sigma'\lambda'} C_{\lambda' j} \end{aligned} \tag{6.117}$$

$$\Omega^\tau_{ab} = \sum_{\mu\nu} \sum_{\sigma\lambda} C_{\lambda a} S_{\lambda\mu} \left\{ \sum_{\alpha\beta} \sum_{\underline{i}} \Big[\Big(\sum_{\underline{k}} \bar{B}^\alpha_{\mu\underline{k}} P^\tau_{\underline{k}i} \Big) M^{\alpha\beta}_\tau + \Big(\sum_{\underline{k}} B^\alpha_{\mu\underline{k}} P^\tau_{\underline{k}i} \Big) \bar{M}^{\alpha\beta}_\tau \Big] B^\beta_{\nu\underline{i}} \right\} S_{\nu\sigma} C_{\sigma b} \tag{6.118}$$

The first-order off-diagonal block of the transition density matrix is evaluated according to

$$\rho^{I\leftarrow 0}_{ia} = \sum_{\mu\mu'\nu\nu'} C_{\mu' a} S_{\mu'\mu} \left\{ c_{\text{os}} \sum_{\underline{i}} \Big[\sum_\tau \sum_\alpha \bar{m}^\alpha_\tau B^{\alpha,\tau}_{\mu\underline{i}} \Big] L_{\nu\underline{i}} \right\} S_{\nu\nu'} C_{\nu' i} \quad \bar{m}^\alpha_\tau = J^{-1}_{\alpha\beta} \left[\sum_{\nu\underline{j}} R_{\nu\underline{j}} B^{\beta,\tau}_{\nu\underline{j}} \right] \tag{6.119}$$

where $R_{\nu\underline{j}}$ is defined in eq. (6.23). Notice that this block is equivalent to the first term in the right-hand side of eq. (6.37). Therefore, it is not recomputed to form the transition density matrix. Finally, the second-order off-diagonal block, depending on the SOS-MP2 correction to the ground state density matrices, is evaluated with a $\mathcal{O}(N^3)$ and sub-quadratic asymptotic scaling for the standard and the attenuated RI Coulomb metric, respectively:

$$\rho^0_{ij} = -c_{\mathrm{os}} \sum_\tau g^\tau_{ij} \left\{ C_{\mu' i} S_{\mu'\mu} L_{\mu\underline{i}} \Omega^{\tau,(0)}_{\underline{i}\underline{j}} L_{\nu\underline{j}} S_{\nu\nu'} C_{\nu' j} \right\} \tag{6.120}$$

$$\rho^0_{ab} = c_{\mathrm{os}} \sum_\tau g^\tau_{ab} \left\{ C_{\mu' a} S_{\mu'\mu} \Omega^{\tau,(0)}_{\mu\nu} S_{\nu\nu'} C_{\nu' b} \right\} \tag{6.121}$$

with

$$\Omega^{\tau,(0)}_{\underline{i}\underline{j}} = \sum_{\alpha\beta} \sum_\nu \left[\sum_{\mu\nu'} Q^\tau_{\nu\mu} B^\alpha_{\mu\nu'} L_{\nu'\underline{i}} \right] M^{\alpha\beta}_\tau B^\beta_{\nu\underline{j}} \tag{6.122}$$

$$\Omega^{\tau,(0)}_{\mu\nu} = \sum_{\alpha\beta} \sum_{\underline{i}} \left[\sum_{\mu\underline{k}} Q_{\mu\mu'} B^\alpha_{\mu'\underline{k}} P^\tau_{\underline{k}\underline{i}} \right] M^{\alpha\beta}_\tau B^\beta_{\nu\underline{i}} \tag{6.123}$$

Despite the higher computational asymptotic scaling for the matrices in eqs. (6.122) and (6.123), it is important to stress that the prefactor for these steps is smaller compared to the evaluation of the other blocks. Moreover, the corrections ρ^0 are evaluated only once for the ground state and can be obtained as a by-product during the computation of the intermediates in eq. (6.25). Therefore, for systems with a local electronic structure and a local excitation, the overall computational effort to form $\rho^{I\leftarrow 0}$ is expected to scale as $\mathcal{O}(N^2)$ within the standard RI Coulomb metric and as $\mathcal{O}(N)$ in the attenuated RI Coulomb metric with $\omega = 0.1$.

6.2.4 Cubic-scaling THC-MO-based formulation of the one-particle density matrices

Before deriving the THC decomposed equations, we should define the THC **X** matrices transformed into the MO basis as:

$$X^P_i = \sum_\mu X^P_\mu C_{\mu i} \qquad \bar{X}^P_i = \sum_\mu X^P_\mu \bar{\Lambda}^{\mathrm{h}}_{\mu i} \tag{6.124}$$

$$X^P_a = \sum_\mu X^P_\mu C_{\mu a} \qquad \bar{X}^P_a = \sum_\mu X^P_\mu \bar{\Lambda}^{\mathrm{p}}_{\mu a} \tag{6.125}$$

with the $\bar{\mathbf{\Lambda}}$ matrices given in eqs. (3.50) and (3.51). Using eqs. (6.124) and (6.125), the THC-approximated MO-based SOS-MP2 doubles amplitudes and the doubles part of the SOS-ADC(2) excitation vector are rewritten according to

$$t^{(\mathrm{os})}_{aibj} = -\sum_\tau w_\tau \sum_{PQ} \sum_\alpha X^P_a X^P_i \Gamma^P_\alpha \Gamma^Q_\alpha X^Q_b X^Q_j e^{-\varepsilon_a t_\tau} e^{\varepsilon_i t_\tau} e^{-\varepsilon_b t_\tau} e^{\varepsilon_j t_\tau} \tag{6.126}$$

$$R^{(\mathrm{os})}_{aibj} = -\sum_\tau w_\tau S^{ab}_{ij} \left[\sum_{PQ} \sum_\alpha \left(\bar{X}^P_a X^P_i + X^P_a \bar{X}^P_i \right) \Gamma^P_\alpha \Gamma^Q_\alpha X^Q_b X^Q_j \right] e^{-\varepsilon_a t_\tau} e^{\varepsilon_i t_\tau} e^{-\varepsilon_b t_\tau} e^{\varepsilon_j t_\tau} \tag{6.127}$$

Notice that contrary to **Publication III**, only (ov|ov) ERIs appear in the equations for the SOS-ADC(2) density matrix and transition density matrix, and hence only one kind of THC-fitting matrix $\mathbf{\Gamma}$ is required.

One-particle reduced density matrix

According to eq. (6.127), the THC decomposition of the diagonal blocks of the one-particle reduced density matrix results in the following expressions:

$$\begin{aligned}\rho^I_{ij} = -\sum_\tau w_\tau^{\frac{1}{4}} g^\tau_{ij}(\bar{\omega}) \sum_{PR} \Bigg\{ &\Big(X_i^P \bar{B}_\tau^{PR} X_j^R + X_i^P \bar{B}_\tau^{PR} \bar{X}_j^R + \bar{X}_i^P \bar{B}_\tau^{RP} X_j^R + \bar{X}_i^P B_\tau^{PR} \bar{X}_j^P \Big) D_\tau^{PR} \\ &+ \Big(X_i^P \bar{B}_\tau^{RP} X_j^R + X_i^P B_\tau^{PR} \bar{X}_j^P \Big) \bar{D}_\tau^{PR} + \Big(X_i^P \bar{B}_\tau^{PR} X_j^R + \bar{X}_i^P B_\tau^{PR} X_j^R \Big) \bar{D}_\tau^{RP} \\ &+ X_i^P \bar{\bar{D}}_\tau^{PR} B_\tau^{PR} X_j^R \Bigg\} = -\sum_\tau w_\tau^{\frac{1}{4}} g^\tau_{ij}(\bar{\omega}) \sum_R \left\{ \bar{\bar{Y}}^{R,(1)}_{i,\tau} X_j^R + \bar{\bar{Y}}^{R,(2)}_{i,\tau} \bar{X}_j^R \right\}\end{aligned} \tag{6.128}$$

$$\begin{aligned}\rho^I_{ab} = \sum_\tau w_\tau^{\frac{1}{4}} g^\tau_{ab}(\bar{\omega}) \sum_{PR} \Bigg\{ &\Big(\bar{X}_a^P A_\tau^{PR} \bar{X}_b^R + \bar{X}_a^P \bar{A}_\tau^{RP} X_b^R + X_a^P \bar{A}_\tau^{PR} \bar{X}_b^R + X_a^P \bar{\bar{A}}_\tau^{PR} X_b^R \Big) D_\tau^{PR} \\ &+ \Big(X_a^P A_\tau^{PR} \bar{X}_b^R + X_a^P \bar{A}_\tau^{RP} X_b^R \Big) \bar{D}_\tau^{PR} + \Big(\bar{X}_a^P A_\tau^{PR} X_b^R + X_a^P \bar{A}_\tau^{PR} X_b^R \Big) \bar{D}_\tau^{RP} \\ &+ X_a^P \bar{\bar{D}}_\tau^{PR} A_\tau^{PR} X_b^R \Bigg\} = \sum_\tau w_\tau^{\frac{1}{4}} g^\tau_{ab}(\bar{\omega}) \sum_R \left\{ \bar{\bar{Y}}^{R,(1)}_{a,\tau} X_b^R + \bar{\bar{Y}}^{R,(2)}_{a,\tau} \bar{X}_b^R \right\}\end{aligned} \tag{6.129}$$

The calculation of ρ^I_{ij} and ρ^I_{ab} elements scales as $\mathcal{O}(N^3)$ with the size of the system. As discussed in **Publication III**, we expect the formation of the intermediates $\mathbf{D}$, $\bar{\mathbf{D}}$, and $\bar{\bar{\mathbf{D}}}$ to be the time-determining step, because it involves the multiplication of the corresponding matrices $\mathbf{C}$, $\bar{\mathbf{C}}$, and $\bar{\bar{\mathbf{C}}}$ with the THC-fitting matrix $\mathbf{\Gamma}$:

$$D_\tau^{PR} = \sum_{QS} \sum_{\alpha\beta} \Gamma_\alpha^P \Gamma_\alpha^Q C_\tau^{QS} \Gamma_\beta^S \Gamma_\beta^R \qquad C_\tau^{QS} = A_\tau^{QS} B_\tau^{QS} \tag{6.130}$$

$$\bar{D}_\tau^{PR} = \sum_{QS} \sum_{\alpha\beta} \Gamma_\alpha^P \Gamma_\alpha^Q \bar{C}_\tau^{QS} \Gamma_\beta^S \Gamma_\beta^R \qquad \bar{C}_\tau^{QS} = \bar{A}_\tau^{QS} B_\tau^{QS} + A_\tau^{QS} \bar{B}_\tau^{QS} \tag{6.131}$$

$$\bar{\bar{D}}_\tau^{PR} = \sum_{QS} \sum_{\alpha\beta} \Gamma_\alpha^P \Gamma_\alpha^Q \bar{\bar{C}}_\tau^{QS} \Gamma_\beta^S \Gamma_\beta^R \qquad \bar{\bar{C}}_\tau^{QS} = \bar{\bar{B}}_\tau^{QS} A_\tau^{QS} + \bar{B}_\tau^{QS} \bar{A}_\tau^{SQ} + \bar{B}_\tau^{SQ} \bar{A}_\tau^{QS} + B_\tau^{QS} \bar{\bar{A}}_\tau^{QS} \tag{6.132}$$

The matrices required to evaluate $\mathbf{C}$, $\bar{\mathbf{C}}$, and $\bar{\bar{\mathbf{C}}}$, via Schur product, are given by

$$A_\tau^{QS} = w_\tau^{\frac{1}{4}} \sum_k X_k^Q e^{\varepsilon_k t_\tau} X_k^S \qquad B_\tau^{QS} = w_\tau^{\frac{1}{4}} \sum_b X_b^Q e^{-\varepsilon_b t_\tau} X_b^S \tag{6.133}$$

$$\bar{A}_\tau^{QS} = w_\tau^{\frac{1}{4}} \sum_k \bar{X}_k^Q e^{\varepsilon_k t_\tau} X_k^S \qquad \bar{B}_\tau^{QS} = w_\tau^{\frac{1}{4}} \sum_b \bar{X}_b^Q e^{-\varepsilon_b t_\tau} X_b^S \tag{6.134}$$

$$\bar{\bar{A}}_\tau^{QS} = w_\tau^{\frac{1}{4}} \sum_i \bar{X}_i^Q e^{\varepsilon_i t_\tau} \bar{X}_i^S \qquad \bar{\bar{B}}_\tau^{QS} = w_\tau^{\frac{1}{4}} \sum_a \bar{X}_a^Q e^{-\varepsilon_a t_\tau} \bar{X}_a^S \tag{6.135}$$

where eq. (6.133) only depends on ground state quantities, while eqs. (6.134) and (6.135) contain information about the electronic excitation. The intermediates $\bar{\bar{\mathbf{Y}}}$ in eqs. (6.128) and (6.129) are computed with a cubic computational scaling effort, according to:

$$\bar{\bar{Y}}^{R,(1)}_{i,\tau} = X^P_i \left[\bar{\bar{B}}^{PR}_\tau D^{PR}_\tau + \bar{B}^{RP}_\tau \bar{D}^{PR}_\tau + B^{PR}_\tau \bar{D}^{PR}_\tau + \bar{B}^{PR}_\tau \bar{D}^{RP}_\tau + B^{PR}_\tau \bar{\bar{D}}^{PR}_\tau \right] + \bar{X}^P_i \left[\bar{B}^{RP}_\tau \bar{D}^{PR}_\tau \right] \tag{6.136}$$

$$\bar{\bar{Y}}^{R,(2)}_{i,\tau} = X^P_i \left[\bar{B}^{PR}_\tau D^{PR}_\tau \right] + \bar{X}^P_i \left[B^{PR}_\tau D^{PR}_\tau + B^{PR}_\tau \bar{D}^{RP}_\tau \right] \tag{6.137}$$

$$\bar{\bar{Y}}^{R,(1)}_{a,\tau} = X^P_a \left[\bar{\bar{A}}^{PR}_\tau D^{PR}_\tau + \bar{A}^{RP}_\tau \bar{D}^{PR}_\tau + \bar{A}^{PR}_\tau \bar{D}^{RP}_\tau + A^{PR}_\tau \bar{\bar{D}}^{PR}_\tau \right] + \bar{X}^P_a \left[\bar{A}^{RP}_\tau D^{PR}_\tau + A^{PR}_\tau \bar{D}^{RP}_\tau \right] \tag{6.138}$$

$$\bar{\bar{Y}}^{R,(2)}_{a,\tau} = X^P_a \left[\bar{A}^{PR}_\tau D^{PR}_\tau + A^{PR}_\tau \bar{D}^{PR}_\tau \right] + \bar{X}^P_a \left[A^{PR}_\tau D^{PR}_\tau \right] \tag{6.139}$$

The less expensive off-diagonal blocks of the one-particle reduced density matrix are computed according to

$$\rho^I_{ia} = \rho^I_{ai} = \sum_\tau w_\tau^{\frac{1}{2}} \sum_P \left\{ \left(\bar{X}^P_a X^P_i + X^P_a \bar{X}^P_i \right) e^{-\varepsilon_a t_\tau} e^{\varepsilon_i t_\tau} \bar{m}^{P,(1)}_\tau + X^P_a X^P_i e^{-\varepsilon_a t_\tau} e^{\varepsilon_i t_\tau} \bar{m}^{P,(2)}_\tau \right\} \tag{6.140}$$

with a cubic scaling computational effort and with the intermediates $\bar{\mathbf{m}}$ equal to

$$\bar{m}^{P,(1)}_\tau = w_\tau^{\frac{1}{2}} \Gamma^P_\alpha \Gamma^Q_\alpha \left[\sum_{bj} X^Q_b X^Q_j R_{bj} e^{-\varepsilon_b t_\tau} e^{\varepsilon_j t_\tau} \right] \tag{6.141}$$

$$\bar{m}^{P,(2)}_\tau = w_\tau^{\frac{1}{2}} \Gamma^P_\alpha \Gamma^Q_\alpha \left[\sum_{bj} \bar{X}^Q_b X^Q_j R_{bj} e^{-\varepsilon_b t_\tau} e^{\varepsilon_j t_\tau} + X^Q_b \bar{X}^Q_j R_{bj} e^{-\varepsilon_b t_\tau} e^{\varepsilon_j t_\tau} \right] \tag{6.142}$$

One-particle reduced transition density matrix

The first-order off-diagonal block of the one-particle reduced transition density matrix is already computed during the evaluation of the excitation energies, according to

$$\rho^I_{ia} = \sum_\tau w_\tau^{\frac{1}{2}} \sum_P \left\{ X^P_a X^P_i e^{-\varepsilon_a t_\tau} e^{\varepsilon_i t_\tau} \bar{m}^{P,(1)}_\tau \right\} \tag{6.143}$$

with $\bar{m}^{P,(1)}_\tau$ computed as in eq. (6.141). On the other hand, the diagonal blocks of the one-particle reduced transition density matrix are computed as a by-product of eqs. (6.128) and (6.129), according to

$$\rho^{I\leftarrow 0}_{ij} = -c_{\mathrm{os}} \sum_\tau w_\tau^{\frac{1}{4}} \bar{g}^\tau_{ij}(\bar{\omega}) \sum_{PR} \left\{ X^P_i \left[\bar{B}^{PR}_\tau D^{PR}_\tau + B^{PR}_\tau \bar{D}^{PR}_\tau \right] + \bar{X}^P_i \left[B^{PR}_\tau D^{PR}_\tau \right] \right\} X^R_j \tag{6.144}$$

$$\rho^{I\leftarrow 0}_{ab} = c_{\mathrm{os}} \sum_\tau w_\tau^{\frac{1}{4}} \bar{g}^\tau_{ab}(\bar{\omega}) \sum_{PR} \left\{ X^P_a \left[\bar{A}^{PR}_\tau D^{PR}_\tau + A^{PR}_\tau \bar{D}^{PR}_\tau \right] + \bar{X}^P_a \left[A^{PR}_\tau D^{PR}_\tau \right] \right\} X^R_b \tag{6.145}$$

The second-order off-diagonal block depends on the SOS-MP2 one-particle density matrix, whose MO-based THC reformulation has been already published by Hohenstein *et al.*:[180]

$$\rho^0_{ij} = -c_{\text{os}} \sum_\tau w_\tau^{\frac{1}{4}} g^\tau_{ij} \sum_{PR} \left\{ X_i^P \left[B^{PR}_\tau D^{PR}_\tau \right] \right\} X_j^R \tag{6.146}$$

$$\rho^0_{ab} = c_{\text{os}} \sum_\tau w_\tau^{\frac{1}{4}} g^\tau_{ab} \sum_{PR} \left\{ X_a^P \left[A^{PR}_\tau D^{PR}_\tau \right] \right\} X_b^R \tag{6.147}$$

6.2.5 Low-scaling THC-CDD-based formulation of the one-particle density matrices

The THC decomposition allows for a straightforward low-scaling reformulation of the equations. Indeed, upon back-transformation of $\boldsymbol{\rho}^I$ and $\boldsymbol{\rho}^{I\leftarrow 0}$, in eqs. (6.91) and (6.92), we can easily reformulate the expressions for the THC **X** matrices in eqs. (6.136)-(6.139), the **A/B** intermediates in eqs. (6.133)-(6.135), and the $\bar{\bar{\mathbf{Y}}}$ intermediates in eqs. (6.136)-(6.139) in terms of Cholesky decomposed density matrices. For systems with a significant HOMO-LUMO gap and local excitations, the formation of the density matrices is expected to scale quadratically if our block-sparse linear algebra is used, as it will involve intermediates whose sparsity has been discussed in **Publication III**. However, in order to obtain efficient low-scaling implementations, particular care should be put into sorting the evaluation of the intermediates because the computational and memory efficiency strictly depends on the ability to avoid the redundant calculation of the same matrices as well as to store the minimum amount of them. Our group is currently testing different ways of performing the presented steps.

One-particle reduced density matrix

First, the THC **X** matrices are transformed using the densities defined in eqs. (6.93)-(6.100) and eq. (6.8):

$$X^P_{\underline{i}} = \sum_\mu X^P_\mu L_{\mu \underline{i}} \qquad X^{P,\tau}_{\underline{i}} = \sum_\mu X^P_\mu \left(\sum_{\sigma\lambda} P^\tau_{\mu\sigma} S_{\sigma\lambda} L_{\lambda \underline{i}} \right) \tag{6.148}$$

$$\bar{X}^P_{\underline{i}} = \sum_\mu X^P_\mu \bar{P}_{\mu \underline{i}} \qquad \bar{X}^{P,\tau}_{\underline{i}} = \sum_\mu X^P_\mu \bar{P}^\tau_{\mu \underline{i}} \tag{6.149}$$

$$X^{P,\tau}_\mu = \sum_{\mu'} Q^\tau_{\mu\mu'} X^Q_{\mu'} \qquad \bar{\bar{X}}^{P,\tau}_\mu = \sum_{\mu'} \bar{\bar{Q}}^\tau_{\mu\mu'} X^P_{\mu'} \tag{6.150}$$

$$\bar{X}^P_\mu = \sum_{\mu'} \bar{Q}_{\mu\mu'} X^P_{\mu'} \qquad \bar{X}^{P,\tau}_\mu = \sum_{\mu'} \bar{Q}^\tau_{\mu\mu'} X^P_{\mu'} \tag{6.151}$$

with $\bar{Q}^\tau_{\mu\nu} = \sum_{\lambda\sigma} Q^\tau_{\mu\lambda} S_{\lambda\sigma} \bar{Q}_{\sigma\nu}$. For systems with a significant HOMO-LUMO gap, the ground state **X** matrices contain a number of relevant blocks that grows linearly with the size of the system. On the other hand, for localized excitations, the excited state $\bar{\mathbf{X}}$ and $\bar{\bar{\mathbf{X}}}$ matrices contain a constant number of significant blocks in the asymptotic limit, as discussed in **Publication III**. Once the Laplace-dependent **X** matrices are obtained, the **A/B** intermediates are computed

according to

$$A_\tau^{QS} = \sum_{\underline{k}} X_{\underline{k}}^{Q,\tau} X_{\underline{k}}^{S} \qquad B_\tau^{QS} = \sum_{\mu} X_\mu^{Q,\tau} X_\mu^{S} \tag{6.152}$$

$$\bar{A}_\tau^{QS} = \sum_{k} \bar{X}_{\underline{k}}^{Q,\tau} X_{\underline{k}}^{S} \qquad \bar{B}_\tau^{QS} = \sum_{\mu} \bar{X}_\mu^{Q,\tau} X_\mu^{S} \tag{6.153}$$

$$\bar{\bar{A}}_\tau^{QS} = \sum_{i} \bar{X}_{\underline{k}}^{Q,\tau} \bar{X}_{\underline{k}}^{S} \qquad \bar{\bar{B}}_\tau^{QS} = \sum_{\mu} \bar{\bar{X}}_\mu^{Q,\tau} X_\mu^{S} \tag{6.154}$$

The **A/B** intermediates in eqs. (6.152) and (6.153) are formed with a cost that scales linearly with the size of systems with a significant HOMO-LUMO gap and local excitations. On the other hand, the effort to form the intermediates in eq. (6.154) is expected to be constant in the asymptotic limit, since the THC $\bar{\mathbf{X}}$ matrices contain a constant number of relevant blocks in the asymptotic limit, as shown **Publication III**, for systems with local excitations. Accordingly, for systems with a significant HOMO-LUMO gap and local excitations, the **C** intermediates in eq. (6.130) are computed with a linear scaling effort, while those in eqs. (6.131)-(6.132) are formed with a constant effort in the asymptotic limit.

The fact that the $\hat{\mathbf{D}}$ matrices are Schur multiplied with either the **A/B** matrices in eqs. (6.155)-(6.158) can be exploited. Since intermediates **A/B** intermediates are sparse and the Schur product will only involve blocks – since we are using block-sparse algebra – which are significant in both **A/B** and $\hat{\mathbf{D}}$, only the blocks in **D** which are significant in **A/B** need to be computed in eqs. (6.130)-(6.132). In the end, this enables the formation of the expensive $\hat{\mathbf{D}}$ intermediates with $\mathcal{O}(N^2)$ asymptotic scaling.

For systems with local electronic structure and excitations, the $\bar{\bar{\mathbf{Y}}}$ intermediates are reformulated into the local basis and computed with a linear scaling behavior:

$$\bar{\bar{Y}}_{\underline{i},\tau}^{R,(1)} = X_{\underline{i}}^{P} \left[\bar{\bar{B}}_\tau^{PR} D_\tau^{PR} + \bar{B}_\tau^{RP} \bar{D}_\tau^{PR} + B_\tau^{PR} \bar{D}_\tau^{PR} + \bar{B}_\tau^{PR} \bar{D}_\tau^{RP} + B_\tau^{PR} \bar{\bar{D}}_\tau^{PR} \right] + \bar{X}_{\underline{i}}^{P} \left[\bar{B}_\tau^{RP} \bar{D}_\tau^{PR} \right] \tag{6.155}$$

$$\bar{\bar{Y}}_{\underline{i},\tau}^{R,(2)} = X_{\underline{i}}^{P} \left[\bar{B}_\tau^{PR} D_\tau^{PR} \right] + \bar{X}_{\underline{i}}^{P} \left[B_\tau^{PR} D_\tau^{PR} + B_\tau^{PR} \bar{D}_\tau^{RP} \right] \tag{6.156}$$

$$\bar{\bar{Y}}_{\mu,\tau}^{R,(1)} = \sum_{\nu} Q_{\mu\nu} X_\nu^{P} \left[\bar{\bar{A}}_\tau^{PR} D_\tau^{PR} + \bar{A}_\tau^{RP} \bar{D}_\tau^{PR} + \bar{A}_\tau^{PR} \bar{D}_\tau^{RP} + A_\tau^{PR} \bar{\bar{D}}_\tau^{PR} \right] + \bar{X}_\mu^{P} \left[\bar{A}_\tau^{RP} D_\tau^{PR} + A_\tau^{PR} \bar{D}_\tau^{RP} \right] \tag{6.157}$$

$$\bar{\bar{Y}}_{\mu,\tau}^{R,(2)} = \sum_{\nu} Q_{\mu\nu} X_\nu^{P} \left[\bar{A}_\tau^{PR} D_\tau^{PR} + A_\tau^{PR} \bar{D}_\tau^{PR} \right] + \bar{X}_\mu^{P} \left[A_\tau^{PR} D_\tau^{PR} \right] \tag{6.158}$$

Then, the diagonal blocks of the one-particle reduced density matrix are obtained by multiplying the $\bar{\bar{\mathbf{Y}}}$ intermediates with the THC **X** matrices to form the $\boldsymbol{\Omega}$ matrices as

$$\Omega_{\mu\nu}^{\tau,(\mathrm{occ})} = \sum_{\underline{i}\underline{j}} L_{\mu\underline{i}} \left\{ \sum_{R} \left[\bar{\bar{Y}}_{\underline{i},\tau}^{R,(1)} X_{\underline{j}}^{R} + \bar{\bar{Y}}_{\underline{i},\tau}^{R,(2)} \bar{X}_{\underline{j}}^{R} \right] \right\} L_{\mu\underline{j}} \tag{6.159}$$

$$\Omega_{\mu\nu}^{\tau,(\mathrm{virt})} = \sum_{R} \sum_{\nu'} \bar{\bar{Y}}_{\mu,\tau}^{R,(1)} X_{\nu'}^{R} Q_{\nu'\nu} + \sum_{R} \bar{\bar{Y}}_{\mu,\tau}^{R,(2)} \bar{X}_\nu^{R} \tag{6.160}$$

with a $\mathscr{O}(N)$ scaling effort, and hence multiply them with the Laplace dependent coefficients $g^{\tau}_{ij}(\bar{\omega})$ and $g^{\tau}_{ab}(\bar{\omega})$ while adding the contributions from each Laplace quadrature point:

$$\rho^{I}_{ij} = -\sum_{\tau} w^{\frac{1}{4}}_{\tau} g^{\tau}_{ij}(\bar{\omega}) \left\{ \sum_{\mu\nu}\sum_{\sigma\lambda} C_{\sigma i} S_{\sigma\mu} \Omega^{\tau,(\mathrm{occ})}_{\mu\nu} S_{\nu\lambda} C_{\lambda j} \right\} \tag{6.161}$$

$$\rho^{I}_{ab} = \sum_{\tau} w^{\frac{1}{4}}_{\tau} g^{\tau}_{ab}(\bar{\omega}) \sum_{R} \left\{ \sum_{\mu\nu}\sum_{\sigma\lambda} C_{\sigma a} S_{\sigma\mu} \Omega^{\tau,(\mathrm{virt})}_{\mu\nu} S_{\nu\lambda} C_{\lambda b} \right\} \tag{6.162}$$

At last, the less expensive off-diagonal blocks of the one-particle reduced density matrix are computed with a linear scaling effort, according to

$$\rho^{I}_{ia} = \sum_{\mu\nu}\sum_{\nu'\mu'} C_{\nu' i} S)\nu'\nu \Big[\sum_{\underline{i}} L_{\nu \underline{i}} \rho^{I}_{\underline{i}\mu} \Big] S_{\mu\mu'} C_{\mu' a} \tag{6.163}$$

$$\rho^{I}_{\underline{i}\mu} = \rho^{I}_{\mu\underline{i}} = \sum_{\tau} w^{\frac{1}{4}}_{\tau} \sum_{P} \left\{ \Big[\bar{X}^{P,\tau}_{\mu} X^{P,\tau}_{\underline{i}} + \Big(\sum_{\nu} Q^{\tau}_{\mu\nu} X^{P}_{\nu} \Big) \bar{X}^{P,\tau}_{\underline{i}} \Big] \bar{m}^{P,(1)}_{\tau} + \Big(\sum_{\nu} Q^{\tau}_{\mu\nu} X^{P}_{\nu} \Big) X^{P,\tau}_{\underline{i}} \bar{m}^{P,(2)}_{\tau} \right\} \tag{6.164}$$

with the $\bar{\mathbf{m}}$ terms depending on the elements $R_{\mu \underline{j}}$ defined in eq. (6.23):

$$\bar{m}^{P,(1)}_{\tau} = \sum_{Q}\sum_{\alpha} \Gamma^{P}_{\alpha} \Gamma^{Q}_{\alpha} \left[\sum_{\nu \underline{j}} \Big(\sum_{\mu} Q^{\tau}_{\mu\nu} X^{Q}_{\mu} \Big) X^{Q,\tau}_{\underline{j}} R_{\nu \underline{j}} \right] \tag{6.165}$$

$$\bar{m}^{P,(2)}_{\tau} = \sum_{Q}\sum_{\alpha} \Gamma^{P}_{\alpha} \Gamma^{Q}_{\alpha} \left\{ \sum_{\nu \underline{j}} \Big[\bar{X}^{Q,\tau}_{\nu} X^{Q,\tau}_{\underline{j}} + \Big(\sum_{\mu} Q^{\tau}_{\mu\nu} X^{Q}_{\mu} \Big) \bar{X}^{Q,\tau}_{\underline{j}} \Big] R_{\nu \underline{j}} \right\} \tag{6.166}$$

Notice that for systems with delocalized electronic structure and excitations, the computational effort to form the matrix $\boldsymbol{\rho}^{I}$ scales as $\mathscr{O}(N^3)$.

One-particle reduced transition density matrix

The THC-based expressions for the diagonal blocks of the one-particle reduced transition density matrix are simpler and depend on the intermediates discussed for the density matrix $\boldsymbol{\rho}^{I}$. Once the local intermediates $\boldsymbol{\Omega}$ are obtained

$$\Omega^{\tau,(\mathrm{occ})}_{\mu\nu} = \sum_{\underline{i}\underline{j}} L_{\mu \underline{i}} L_{\nu \underline{j}} \sum_{PR} \left\{ X^{P}_{\underline{i}} \Big[\bar{B}^{PR}_{\tau} D^{PR}_{\tau} + B^{PR}_{\tau} \bar{D}^{PR}_{\tau} \Big] + \bar{X}^{P}_{\underline{i}} \Big[B^{PR}_{\tau} D^{PR}_{\tau} \Big] \right\} X^{R}_{\underline{j}} \tag{6.167}$$

$$\Omega^{\tau,(\mathrm{virt})}_{\mu\nu} = \sum_{PR} \left\{ \sum_{\mu'} Q_{\mu\mu'} X^{P}_{\mu'} \Big[\bar{A}^{PR}_{\tau} D^{PR}_{\tau} + A^{PR}_{\tau} \bar{D}^{PR}_{\tau} \Big] + \bar{X}^{P}_{\mu} \Big[A^{PR}_{\tau} D^{PR}_{\tau} \Big] \right\} \sum_{\nu'} Q_{\nu\nu'} X^{R}_{\nu'} \tag{6.168}$$

they are back-transformed to the MO basis and scaled by the Laplace-dependent factors $\bar{g}^{\tau}_{ij}(\bar{\omega})$ and $\bar{g}^{\tau}_{ab}(\bar{\omega})$, in order to collect the contributions from each quadrature point:

$$\rho^{I\leftarrow 0}_{ij} = -\sum_{\tau} w_{\tau}^{\frac{1}{4}} \bar{g}^{\tau}_{ij}(\bar{\omega}) \left\{ \sum_{\mu\nu}\sum_{\sigma\lambda} C_{\sigma i} S_{\sigma\mu} \Omega^{\tau,(\mathrm{occ})}_{\mu\nu} S_{\nu\lambda} C_{\lambda j} \right\} \tag{6.169}$$

$$\rho^{I\leftarrow 0}_{ab} = \sum_{\tau} w_{\tau}^{\frac{1}{4}} \bar{g}^{\tau}_{ab}(\bar{\omega}) \sum_{R} \left\{ \sum_{\mu\nu}\sum_{\sigma\lambda} C_{\sigma a} S_{\sigma\mu} \Omega^{\tau,(\mathrm{virt})}_{\mu\nu} S_{\nu\lambda} C_{\lambda b} \right\} \tag{6.170}$$

The first-order off-diagonal elements are obtained according to

$$\rho^{I\leftarrow 0}_{i\underline{a}} = \sum_{\mu\nu}\sum_{\nu'\mu'} C_{\nu' i} S_{\nu'\nu} \Big[\sum_{\underline{i}} L_{\nu\underline{i}} \rho^{I\leftarrow 0}_{\underline{i}\mu} \Big] S_{\mu\mu'} C_{\mu' a} \tag{6.171}$$

$$\rho^{I\leftarrow 0}_{\underline{i}\mu} = \rho^{I}_{\mu\underline{i}} = \sum_{\tau} w_{\tau}^{\frac{1}{4}} \sum_{P} \left\{ \Big(\sum_{\nu} Q^{\tau}_{\mu\nu} X^{P}_{\nu} \Big) X^{P,\tau}_{\underline{i}} \bar{m}^{P,(1)}_{\tau} \right\} \tag{6.172}$$

with the $\bar{\mathbf{m}}$ term defined in eq. (6.165). Finally, the second-order off-diagonal block depends on the CDD-SOS-MP2 one-particle density matrices which are computed as:

$$\rho^{0}_{ij} = -c_{\mathrm{os}} \sum_{\tau} w_{\tau}^{\frac{1}{4}} g^{\tau}_{ij} \left\{ \sum_{\mu\nu}\sum_{\sigma\lambda} C_{\sigma i} S_{\sigma\mu} \Omega^{\tau,(\mathrm{occ},\,0)}_{\mu\nu} S_{\nu\lambda} C_{\lambda j} \right\} \tag{6.173}$$

$$\rho^{0}_{ab} = c_{\mathrm{os}} \sum_{\tau} w_{\tau}^{\frac{1}{4}} g^{\tau}_{ab} \sum_{PR} \left\{ \sum_{\mu\nu}\sum_{\sigma\lambda} C_{\sigma a} S_{\sigma\mu} \Omega^{\tau,(\mathrm{virt},\,0)}_{\mu\nu} S_{\nu\lambda} C_{\lambda b} \right\} \tag{6.174}$$

$$\Omega^{\tau,(\mathrm{occ},\,0)}_{\mu\nu} = \sum_{\underline{i}\underline{j}} L_{\mu\underline{i}} L_{\nu\underline{j}} \sum_{PR} \left\{ X^{P}_{\underline{i}} \Big[B^{PR}_{\tau} D^{PR}_{\tau} \Big] \right\} X^{R}_{\underline{j}} \tag{6.175}$$

$$\Omega^{\tau,(\mathrm{virt},\,0)}_{\mu\nu} = \sum_{PR} \left\{ \sum_{\mu'} Q_{\mu\mu'} X^{P}_{\mu'} \Big[A^{PR}_{\tau} D^{PR}_{\tau} \Big] \right\} \sum_{\nu'} Q_{\nu\nu'} X^{R}_{\nu'} \tag{6.176}$$

Notice that for systems with delocalized electronic structure and excitation, the computational effort to form the matrix $\boldsymbol{\rho}^{I\leftarrow 0}$ scales as $\mathscr{O}(N^3)$.

7 Conclusion

In this thesis, various solutions aiming to improve on the most important bottlenecks of CC2[23,24,38] and ADC(2),[25,145,170] being the high computational cost, the high memory requirements, the scaling behavior with the size of the system, and the I/O effort, were proposed. Inspired by the previous works on the MP2,[64,103,105,113,163] RPA,[110,181–183] CP-SCF,[184] and CC[89] theories, we took advantage of the Laplace transformation of the energy denominator to reformulate the molecular orbitals (MOs)-based scaled opposite-spin (SOS)-CC2 projected equations[38] –within the resolution of the identity (RI) framework[38,185–188] – into the local atomic orbital (AO) basis. For systems with a significant HOMO-LUMO gap, the computational and memory demands of the newly derived density-based AO-RI-SOS-CC2 method scale as $\mathscr{O}(N^3)$ and $\mathscr{O}(N^2)$, respectively, upon screening via the block-sparse linear algebra routines developed in our group. Note that our block-sparse linear algebra routines allow for direct control of both the block-sparsity and accuracy of the method. Although the AO-RI-SOS-CC2 implementation is suitable for large systems and small basis sets, the use of large basis sets is hindered by the scaling with basis set size. Therefore, as previously proposed for MP2 and RPA,[64,110,163,182–184] we introduced the local Cholesky MOs – from the Cholesky decomposed densities (CDD) – enabling the transformation of the large three-index electron integrals at an early stage and hence decreasing the memory requirements by a factor of $N_{\text{bf}}/N_{\text{occ}}$. Overall, the formal scaling of memory requirements for the three-index integrals is slightly increased from $N_{\text{aux}}N_{\text{virt}}N_{\text{occ}}$ in MO-RI-SOS-CC2 to $N_{\text{aux}}N_{\text{bf}}N_{\text{occ}}$ in CDD-RI-SOS-CC2. A further reduction of the scaling of CDD-RI-SOS-CC2 was achieved by introducing, for the first time in coupled cluster theory, the local attenuated Coulomb RI-metric[64,108–110] which increases the sparsity within the three-index integrals at the cost of slightly reduced accuracy – both controlled by varying the attenuation factor ω. The resulting ω-CDD-RI-SOS-CC2 model shows computational and memory demands scaling quadratically with the size of systems with local electronic structure. Despite the reduced scaling and the use of block-sparse linear algebra, the memory demands of the three-index integrals exceed the capability of a single computing node for large systems and large basis sets. Therefore, particularly for systems with three-dimensional structures, the three-index integrals must be stored on disk, and one is forced to batch the workload. In order to minimize the overhead related to the batching and the I/O of the integrals, we applied a Lagrangian-based optimized bathing.[61] The strategies outlined so far have been extended to the efficient local treatment of electron excitations, previously limited to local molecular orbitals and natural (transition) orbitals approaches which require state-specific localization techniques. In this work, we proposed the first local linear response (LR) RI-SOS-CC2 and RI-SOS-ADC(2) models based on the Cholesky decomposed density matrices. By exploiting the locality of both the electronic structure and excitation, combined with the local attenuated Coulomb metric, we demonstrated that the evaluation of excitation energies scales linearly when using ω-CDD-RI-SOS-LR-CC2 and ω-CDD-RI-SOS-ADC(2). In addition, we showed that the memory demands of the three-index integrals scale as $\mathscr{O}(1)$ if they contain

information about the local excitation, while the other excited state intermediates scale linearly with the system size. Within the RI approximation, we also studied the quasi-robust approach[68] to achieve the linear scaling behavior within ω-CDD-RI-SOS-ADC(2) while retaining the same accuracy of the dense standard-Coulomb metric.

Although ω-CDD-RI-SOS-LR-CC2 and ω-CDD-RI-SOS-ADC(2) show linear scaling behavior, their application is hampered by the use of large basis sets with diffuse basis functions that severely impact – in particular for three-dimensional systems – the sparsity of the densities and hence negatively affects the overall scaling behavior. That is, the low-scaling regime is only reached for very large systems – i.e., more than 1000 atoms – in either the ground or excited state calculations, and thus not only the computational effort but also the memory demands and I/O become relevant. In addition, it should be stressed that in the case of dense electronic structure, i.e. small HOMO-LUMO gap, the low-scaling regime will not be reached and the computational cost of ω-CDD-RI-SOS-LR-CC2 and ω-CDD-RI-SOS-ADC(2) will surpass the cost of the MO-based implementations. In order to overcome the drawbacks of the RI-based implementations, we employed the least-squares (LS) tensor hypercontraction (THC) approach[189–192] to decompose the electron-repulsion integrals into two-index tensors, as previously proposed for MP2,[113,114] CC2,[193] CCSD,[194–196] CCSD(T),[197] and EOM-CC2.[198] The LS-THC approximation led to a reformulation of the equations of SOS-LR-CC2 and SOS-ADC(2) that require only the use of matrix linear algebra as it circumvents the necessity to store and contract three-index tensors completely. This means that, as opposed to the RI approximation, LS-THC not only considerably reduces the memory requirements and the computational effort but also reduces the scaling of the SOS-LR-CC2 and SOS-ADC(2) methods. Accordingly, the computational cost and the memory demands of MO-THC-SOS-LR-CC2 and MO-THC-SOS-ADC(2) scale as $\mathscr{O}(N^3)$ and $\mathscr{O}(N^2)$, respectively. In the case of large basis sets with diffuse basis functions, they already represent the most efficient choice among the approximated models reported so far. In order to make use of the locality of the electronic structure and of the excitations, and further reduce the scaling, we combined the LS-THC approximation with local Cholesky MOs in the Laplace integration and block-sparse linear algebra obtaining the efficient $\mathscr{O}(N^2)$ scaling CDD-THC-SOS-LR-CC2 and CDD-THC-SOS-ADC(2) formulations. As for the RI-based algorithm, we showed that, assuming local electronic structure and excitations, the memory demands for the intermediates of the local THC-SOS-LR-CC2 and THC-SOS-ADC(2) scale as $\mathscr{O}(N)$ or even $\mathscr{O}(1)$ with the system size. Benefitting from the reduced memory demands and computational effort of CDD-THC-SOS-ADC(2), it was possible to evaluate chemically accurate excitation energies to the lowest singlet and triplet states of DNA fragments in the thousand atoms scale. Finally, in this work, we provided low-scaling expressions for the excited states one-particle reduced density matrix and transition density matrix for the CDD-RI-SOS-ADC(2) and CDD-THC-SOS-ADC(2) models. Although we could not yet present results to show the performance, the intermediates appearing in the working equations were already encountered in the equations for the excitation energies and hence we can efficiently form the density matrices via algorithms discussed in **Publications I-III**.

Despite the fact that we focused on the opposite-spin contributions, the concepts discussed in this work can be extended to the same-spin contributions as well as to the ADC(2)-x[25,145,150] variant and the higher-order ADC(3)[142,143,171,199,200] schemes, as well as combined with dif-

ferent approximations – i.e., core-valence separation (CVS)-ADC(2),[201–203] spin-flip (SF)-ADC.[152,204,205] Another valid contribution to the field of approximate and fast electronic structure methods is represented by our density-based integral-direct implementation for the evaluation of the THC fitting described in Sec. 4.2. We proposed two different approaches based on the J-engine[103] and the RI-J kernels[161,206] providing an easy way to implement the least-squares THC in any quantum chemistry packages, since apart from linear algebra, only the ability to evaluate basis functions on a real-space DFT-like grid is required then.

8 Appendix

Notation

Throughout this thesis, we employ the following notation:

- $\mu, \nu, \lambda, \sigma$: atomic orbital indices belonging to the AO basis $\{\chi_\mu\}$ of size N_{bf}.
- $\alpha, \beta, \gamma, \delta$: auxiliary basis function indices belonging to the density fitting basis $\{\chi_\alpha\}$ of size N_{aux} (usually $N_{\text{aux}} \approx 3 \cdot N_{\text{bf}}$).
- P, Q, R, S: auxiliary basis function indices belonging to the THC basis of size $N_{\text{aux-THC}}$; in the context of least-squares THC gridpoint indices belonging to the least-squares THC grid of size N_{grid} (usually $N_{\text{grid}} \approx 3 \cdot N_{\text{aux}}$).
- i, j, k: occupied molecular orbital indices belonging to the MO basis $\{\phi_i\}$ of size N_{occ}.
- a, b, c: virtual molecular orbital indices belonging to the MO basis $\{\phi_a\}$ of size N_{virt} ($N_{\text{virt}} \gg N_{\text{occ}}$).
- $\underline{i}, \underline{k}, \underline{j}$: occupied local Cholesky orbitals basis $\{\phi_{\underline{i}}\}$ of size N_{occ}; they are obtained via Cholesky decomposition of the occupied one-electron density.
- p, q, r, s: general orbital indices
- τ: Laplace quadrature point of size N_τ (usually $5 \leq N_\tau \leq 10$ is sufficiently accurate).

Bibliography

[1] E. Schrödinger, *Phys. Rev.* **1926**, *28*, 1049–1070.

[2] M. Born, R. Oppenheimer, *Ann. Phys.* **1927**, *389*, 457–484.

[3] J. A. Pople, *Angew. Chem. Int. Ed.* **1999**, *38*, 1894–1902.

[4] T. Helgaker, P. Jorgensen, J. Olsen, *Molecular electronic-structure theory*, John Wiley & Sons, **2013**.

[5] O. Sinanoğlu, *J. Chem. Phys.* **1962**, *36*, 706–717.

[6] J. Čızek, *J. Chem. Phys.* **1966**, *45*, 4256–4266.

[7] J. Čížek, *Adv. Chem. Phys.* **1969**, 35–89.

[8] F. E. Harris, *Int. J. Quantum Chem.* **1977**, *12*, 403–411.

[9] G. D. Purvis III, R. J. Bartlett, *J. Chem. Phys.* **1982**, *76*, 1910–1918.

[10] J. Noga, R. J. Bartlett, *J. Chem. Phys.* **1987**, *86*, 7041–7050.

[11] G. E. Scuseria, H. F. Schaefer III, *Chem. Phys. Lett.* **1988**, *152*, 382–386.

[12] C. Møller, M. S. Plesset, *Phys. Rev.* **1934**, *46*, 618.

[13] E. Schrödinger, *Ann. Phys.* **1926**, *385*, 437–490.

[14] C. Ochsenfeld, J. Kussmann, D. S. Lambrecht, *Rev. Comput. Chem.* **2007**, *23*, 1.

[15] O. Christiansen, H. Koch, P. Jørgensen, *Chem. Phys. Lett.* **1995**, *243*, 409–418.

[16] H. Koch, P. Jørgensen, *J. Chem. Phys.* **1990**, *93*, 3333.

[17] H. Koch, H. J. A. Jensen, P. Jørgensen, T. Helgaker, *J. Chem. Phys.* **1990**, *93*, 3345–3350.

[18] R. J. Rico, M. Head-Gordon, *Chem. Phys. Lett.* **1993**, *213*, 224–232.

[19] J. Geertsen, M. Rittby, R. J. Bartlett, *Chem. Phys. Lett.* **1989**, *164*, 57–62.

[20] I. Shavitt, R. J. Bartlett, *Many-body methods in chemistry and physics: MBPT and coupled-cluster theory*, Cambridge University Press, **2009**.

[21] D. R. Nascimento, A. E. DePrince III, *J. Chem. Theory Comput.* **2016**, *12*, 5834–5840.

[22] J. Schirmer, *Phys. Rev. A* **1982**, *26*, 2395.

[23] C. Hättig, F. Weigend, *J. Chem. Phys.* **2000**, *113*, 5154–5161.

[24] C. Hättig, *Adv. Quantum Chem.* **2005**, *50*, 37–60.

[25] C. M. Krauter, M. Pernpointner, A. Dreuw, *J. Chem. Phys.* **2013**, *138*.

[26] R. A. Kendall, H. A. Früchtl, *Theoret. Chem. Acc.* **1997**, *97*, 158–163.

[27] M. Feyereisen, G. Fitzgerald, A. Komornicki, *Chem. Phys. Lett.* **1993**, *208*, 359–363.

[28] R. M. Parrish, E. G. Hohenstein, T. J. Martınez, C. D. Sherrill, *J. Chem. Phys.* **2012**, *137*.

[29] R. M. Parrish, E. G. Hohenstein, T. J. Martınez, C. D. Sherrill, *J. Chem. Phys.* **2013**, *138*.

[30] C. Song, T. J. Martınez, *J. Chem. Phys.* **2016**, *144*.

[31] C. Song, T. J. Martınez, *J. Chem. Phys.* **2017**, *146*.

[32] E. G. Hohenstein, S. I. Kokkila, R. M. Parrish, T. J. Martınez, *J. Chem. Phys.* **2013**, *138*.

[33] Y. Jung, R. C. Lochan, A. D. Dutoi, M. Head-Gordon, *J. Chem. Phys.* **2004**, *121*, 9793–9802.

[34] J. Almlöf, *Chem. Phys. Lett.* **1991**, *181*, 319–320.

[35] M. Häser, J. Almlöf, *J. Chem. Phys.* **1992**, *96*, 489–494.

[36] D. Braess, W. Hackbusch, *IMA J. Num. Analys.* **2005**, *25*, 685–697.

[37] A. Takatsuka, S. Ten-No, W. Hackbusch, *J. Chem. Phys.* **2008**, *129*.

[38] N. O. Winter, C. Hättig, *J. Chem. Phys.* **2011**, *134*.

[39] E. G. Hohenstein, S. I. Kokkila, R. M. Parrish, T. J. Martınez, *The J. Phys. Chem. B* **2013**, *117*, 12972–12978.

[40] P. E. Maslen, C. Ochsenfeld, C. A. White, M. S. Lee, M. Head-Gordon, *The J. Phys. Chem. A* **1998**, *102*, 2215–2222.

[41] P. Pulay, *Chem. Phys. Lett.* **1983**, *100*, 151–154.

[42] S. Sæbø, P. Pulay, *Chem. Phys. Lett.* **1985**, *113*, 13–18.

[43] S. Saebo, P. Pulay, *Annu. Rev. Phys. Chem.* **1993**, *44*, 213–236.

[44] M. Schütz, G. Hetzer, H.-J. Werner, *J. Chem. Phys.* **1999**, *111*, 5691–5705.

[45] M. Schütz, H.-J. Werner, *J. Chem. Phys.* **2001**, *114*, 661–681.

[46] D. Kats, T. Korona, M. Schütz, *J. Chem. Phys.* **2006**, *125*.

[47] D. Kats, M. Schütz, *J. Chem. Phys.* **2009**, *131*.

[48] M. Schütz, *J. Chem. Phys.* **2015**, *142*.

[49] A. G. Taube, R. J. Bartlett, *J. Chem. Phys.* **2008**, *128*.

[50] P. R. Nagy, G. Samu, M. Kállay, *J. Chem. Theory Comput.* **2018**, *14*, 4193–4215.

[51] Z. Rolik, L. Szegedy, I. Ladjánszki, B. Ladóczki, M. Kállay, *J. Chem. Phys.* **2013**, *139*.

[52] F. Neese, A. Hansen, D. G. Liakos, *J. Chem. Phys.* **2009**, *131*.

[53] F. Neese, F. Wennmohs, A. Hansen, *J. Chem. Phys.* **2009**, *130*.

[54] A. Hansen, D. G. Liakos, F. Neese, *J. Chem. Phys.* **2011**, *135*.

[55] D. Mester, P. R. Nagy, M. Kállay, *J. Chem. Phys.* **2017**, *146*.

[56] D. Mester, P. R. Nagy, M. Kállay, *J. Chem. Phys.* **2018**, *148*.

[57] D. Mester, M. Kállay, *J. Chem. Theory Comput.* **2023**, *19*, 2850–2862.

[58] R. L. Martin, *J. Chem. Phys.* **2003**, *118*, 4775–4777.

[59] P. Baudin, K. Kristensen, *J. Chem. Phys.* **2016**, *144*.

[60] P. Baudin, K. Kristensen, *J. Chem. Phys.* **2017**, *146*.

[61] V. Drontschenko, D. Graf, H. Laqua, C. Ochsenfeld, *J. Chem. Theory Comput.* **2021**, *17*, 5623–5634.

[62] N. J. Higham, *WIREs Comput. Stat.* **2009**, *1*, 251–254.

[63] H. Harbrecht, M. Peters, R. Schneider, *Appl. Numer. Math.* **2012**, *62*, 428–440.

[64] M. Glasbrenner, D. Graf, C. Ochsenfeld, *J. Chem. Theory Comput.* **2020**, *16*, 6856–6868.

[65] J. Kussmann, C. Ochsenfeld, *J. Chem. Phys.* **2013**, *138*.

[66] J. Kussmann, C. Ochsenfeld, *J. Chem. Theory Comput.* **2015**, *11*, 918–922.

[67] J. Kussmann, C. Ochsenfeld, *J. Chem. Theory Comput.* **2017**, *13*, 3153–3159.

[68] D. P. Tew, *J. Chem. Phys.* **2018**, *148*.

[69] J. C. Slater, *Phys. Rev.* **1929**, *34*, 1293–1322.

[70] W. Pauli, *Z. Phys.* **1925**, *31*, 765–783.

[71] A. Szabo, N. S. Ostlund, *Modern quantum chemistry: introduction to advanced electronic structure theory*, Courier Corporation, **2012**.

[72] C. C. J. Roothaan, *Rev. Mod. Phys.* **1951**, *23*, 69–89.

[73] J. Almlöf, K. Fægri Jr, K. Korsell, *J. Comput. Chem.* **1982**, *3*, 385–399.

[74] C. A. White, B. G. Johnson, P. M. Gill, M. Head-Gordon, *Chem. Phys. Lett.* **1994**, *230*, 8–16.

[75] C. A. White, M. Head-Gordon, *J. Chem. Phys.* **1994**, *101*, 6593–6605.

[76] C. A. White, M. Head-Gordon, *J. Chem. Phys.* **1996**, *105*, 5061–5067.

[77] C. A. White, B. G. Johnson, P. M. Gill, M. Head-Gordon, *Chem. Phys. Lett.* **1996**, *253*, 268–278.

[78] C. Ochsenfeld, C. A. White, M. Head-Gordon, *J. Chem. Phys.* **1998**, *109*, 1663–1669.

[79] H. Laqua, T. H. Thompson, J. Kussmann, C. Ochsenfeld, *J. Chem. Theory Comput.* **2020**, *16*, 1456–1468.

[80] D. K. Jordan, D. A. Mazziotti, *J. Chem. Phys.* **2005**, *122*.

[81] A. Niklasson, V. Weber, M. Challacombe, *J. Chem. Phys.* **2005**, *123*.

[82] E. H. Rubensson, E. Rudberg, P. Sałek, *J. Chem. Phys.* **2008**, *128*.

[83] P. Suryanarayana, *Chem. Phys. Lett.* **2013**, *555*, 291–295.

[84] P. Jordan, O. Klein, *Z. Phys.* **1927**, *45*, 751–765.

[85] P. Jordan, E. P. Wigner, *Z. Phys* **1928**, *47*, 14–75.

[86] V. Fock, *Z. Phys.* **1932**, *75*, 622–647.

[87] A. Fetter, J. Walecka, Quantum theory of many particle systems New York, **1971**.

[88] H. Koch, O. Christiansen, R. Kobayashi, P. Jørgensen, T. Helgaker, *Chem. Phys. Lett.* **1994**, *228*, 233–238.

[89] G. E. Scuseria, P. Y. Ayala, *J. Chem. Phys.* **1999**, *111*, 8330–8343.

[90] E. G. Hohenstein, R. M. Parrish, C. D. Sherrill, T. J. Martınez, *J. Chem. Phys.* **2012**, *137*.

[91] N. Handy, P. Knowles, K. Somasundram, *Theor. Chim. Acta* **1985**, *68*, 87–100.

[92] J. Olsen, O. Christiansen, H. Koch, P. Jørgensen, *J. Chem. Phys.* **1996**, *105*, 5082–5090.

[93] P. Pulay, S. Saebø, *Theor. Chim. Acta* **1986**, *69*, 357–368.

[94] G. Hetzer, M. Schütz, H. Stoll, H.-J. Werner, *J. Chem. Phys.* **2000**, *113*, 9443–9455.

[95] K. Kristensen, I.-M. Høyvik, B. Jansik, P. Jørgensen, T. Kjærgaard, S. Reine, J. Jakowski, *Phys. Chem. Chem. Phys.* **2012**, *14*, 15706–15714.

[96] P. Baudin, P. Ettenhuber, S. Reine, K. Kristensen, T. Kjærgaard, *J. Chem. Phys.* **2016**, *144*.

[97] P. Y. Ayala, G. E. Scuseria, *J. Chem. Phys.* **1999**, *110*, 3660–3671.

[98] D. S. Lambrecht, B. Doser, C. Ochsenfeld, *J. Chem. Phys.* **2005**, *123*.

[99] D. S. Lambrecht, B. Doser, C. Ochsenfeld, *J. Chem. Phys.* **2012**, *136*.

[100] B. Doser, D. S. Lambrecht, C. Ochsenfeld, *Phys. Chem. Chem. Phys.* **2008**, *10*, 3335–3344.

[101] B. Doser, D. S. Lambrecht, J. Kussmann, C. Ochsenfeld, *J. Chem. Phys.* **2009**, *130*.

[102] S. A. Maurer, D. S. Lambrecht, J. Kussmann, C. Ochsenfeld, *J. Chem. Phys.* **2013**, *138*.

[103] S. Maurer, J. Kussmann, C. Ochsenfeld, *J. Chem. Phys.* **2014**, *141*.

[104] N. J. Higham, *Wiley Interdiscip. Rev. Comput. Stat.* **2009**, *1*, 251–254.

[105] J. Zienau, L. Clin, B. Doser, C. Ochsenfeld, *J. Chem. Phys.* **2009**, *130*.

[106] S. A. Maurer, D. S. Lambrecht, D. Flaig, C. Ochsenfeld, *J. Chem. Phys.* **2012**, *136*, 144107.

[107] S. Reine, E. Tellgren, A. Krapp, T. Kjærgaard, T. Helgaker, B. Jansik, S. Høst, P. Salek, *J. Chem. Phys.* **2008**, *129*, 104101.

[108] Y. Jung, Y. Shao, M. Head-Gordon, *J. Comput. Chem.* **2007**, *28*, 1953–1964.

[109] Y. Jung, A. Sodt, P. M. Gill, M. Head-Gordon, *Proc. Natl. Acad. Sci.* **2005**, *102*, 6692–6697.

[110] A. Luenser, H. F. Schurkus, C. Ochsenfeld, *J. Chem. Theory Comput.* **2017**, *13*, 1647–1655.

[111] E. G. Hohenstein, R. M. Parrish, T. J. Martınez, *J. Chem. Phys.* **2012**, *137*.

[112] S. I. Kokkila Schumacher, E. G. Hohenstein, R. M. Parrish, L.-P. Wang, T. J. Martınez, *J. Chem. Theory Comput.* **2015**, *11*, 3042–3052.

[113] F. H. Bangerter, M. Glasbrenner, C. Ochsenfeld, *J. Chem. Theory Comput.* **2020**, *17*, 211–221.

[114] F. H. Bangerter, M. Glasbrenner, C. Ochsenfeld, *J. Chem. Theory Comput.* **2022**, *18*, 5233–5245.

[115] S. Grimme, *J. Chem. Phys.* **2003**, *118*, 9095–9102.

[116] C. Song, T. J. Martınez, *J. Chem. Phys.* **2017**, *147*.

[117] O. Christiansen, P. Jørgensen, C. Hättig, *Int. J. Quantum Chem.* **1998**, *68*, 1–52.

[118] N. O. Winter, N. K. Graf, S. Leutwyler, C. Hättig, *Phys. Chem. Chem. Phys.* **2013**, *15*, 6623–6630.

[119] A. Hellweg, S. A. Grün, C. Hättig, *Phys. Chem. Chem. Phys.* **2008**, *10*, 4119–4127.

[120] A. Tajti, P. G. Szalay, *J. Chem. Theory Comput.* **2019**, *15*, 5523–5531.

[121] K. Ledermüller, D. Kats, M. Schütz, *J. Chem. Phys.* **2013**, *139*.

[122] B. Helmich, C. Haettig, *J. Chem. Phys.* **2013**, *139*.

[123] E. V. Anslyn, D. A. Dougherty, *Modern physical organic chemistry*, University science books, **2006**.

[124] E. Dalgaard, H. J. Monkhorst, *Phys. Rev. A* **1983**, *28*, 1217.

[125] T. B. Pedersen, H. Koch, *J. Chem. Phys.* **1997**, *106*, 8059–8072.

[126] O. Christiansen, H. Koch, P. Jørgensen, *J. Chem. Phys.* **1995**, *103*, 7429–7441.

[127] R. J. Bartlett, *Mol. Phys.* **2010**, *108*, 2905–2920.

[128] H. Sekino, R. J. Bartlett, *Int. J. Quantum Chem.* **1984**, *26*, 255–265.

[129] J. F. Stanton, R. J. Bartlett, *J. Chem. Phys.* **1993**, *98*, 7029–7039.

[130] R. J. Bartlett, *Wiley Interdiscip. Rev. Comput. Comp. Sci.* **2012**, *2*, 126–138.

[131] A. I. Krylov, *Annu. Rev. Phys. Chem.* **2008**, *59*, 433–462.

[132] H. Nakatsuji, K. Hirao, *Chem. Phys. Lett.* **1977**, *47*, 569–571.

[133] H. Nakatsuji, *Chem. Phys. Lett.* **1979**, *67*, 329–333.

[134] H. Nakatsuji, *Chem. Phys. Lett.* **1979**, *67*, 334–342.

[135] M. Hodecker, D. R. Rehn, A. Dreuw, *J. Chem. Phys.* **2020**, *152*.

[136] J. Liu, A. Asthana, L. Cheng, D. Mukherjee, *J. Chem. Phys.* **2018**, *148*.

[137] M. Hodecker, S. M. Thielen, J. Liu, D. R. Rehn, A. Dreuw, *J. Chem. Theory Comput.* **2020**, *16*, 3654–3663.

[138] J. Schirmer, F. Mertins, *Theor. Chem. Acc.* **2010**, *125*, 145–172.

[139] H. Koch, R. Kobayashi, A. Sanchez de Merás, P. Jørgensen, *J. Chem. Phys.* **1994**, *100*, 4393–4400.

[140] F. Mertins, J. Schirmer, *Phys. Rev. A* **1996**, *53*, 2140.

[141] M. Head-Gordon, M. Oumi, D. Maurice, *Mol. Phys.* **1999**, *96*, 593–602.

[142] A. Trofimov, G. Stelter, J. Schirmer, *J. Chem. Phys.* **1999**, *111*, 9982–9999.

[143] A. Trofimov, G. Stelter, J. Schirmer, *J. Chem. Phys.* **2002**, *117*, 6402–6410.

[144] H. Koch, O. Christiansen, P. Jørgensen, A. M. Sanchez de Merás, T. Helgaker, *J. Chem. Phys.* **1997**, *106*, 1808–1818.

[145] A. Dreuw, M. Wormit, *Wiley Interdiscip. Rev. Comput. Comp. Sci.* **2015**, *5*, 82–95.

[146] J. Schirmer, *Many-body methods for atoms, molecules and clusters*, Springer, **2018**.

[147] J. Schirmer, L. Cederbaum, O. Walter, *Phys. Rev. A* **1983**, *28*, 1237.

[148] A. Trofimov, J. Schirmer, *J. Chem. Phys.* **2005**, *123*.

[149] W. H. Dickhoff, D. V. Van Neck, *Many-body theory exposed! Propagator description of quantum mechanics in many-body systems*, World Scientific Publishing Company, **2008**.

[150] A. Dreuw, A. Papapostolou, A. L. Dempwolff, *The Journal of Physical Chemistry A* **2023**.

[151] J. Schirmer, *Phys. Rev. A* **1991**, *43*, 4647.

[152] D. Lefrancois, M. Wormit, A. Dreuw, *J. Chem. Phys.* **2015**, *143*.

[153] D. Mukherjee, W. Kutzelnigg in Many-Body Methods in Quantum Chemistry: Proceedings of the Symposium, Tel Aviv University 28–30 August 1988, Springer, **1989**, pp. 257–274.

[154] J. Schirmer, A. Trofimov, *J. Chem. Phys.* **2004**, *120*, 11449–11464.

[155] J. Wenzel, PhD thesis, **2016**.

[156] D. Mester, P. R. Nagy, M. Kállay, *J. Chem. Theory Comput.* **2019**, *15*, 6111–6126.

[157] H.-J. Werner, F. R. Manby, P. J. Knowles, *J. Chem. Phys.* **2003**, *118*, 8149–8160.

[158] O. Vahtras, J. Almlöf, M. Feyereisen, *Chem. Phys. Lett.* **1993**, *213*, 514–518.

[159] R. M. Parrish, E. G. Hohenstein, N. F. Schunck, C. D. Sherrill, T. J. Martınez, *Phys. Rev. Lett.* **2013**, *111*, 132505.

[160] D. A. Matthews, *J. Chem. Theory Comput.* **2020**, *16*, 1382–1385.

[161] J. Kussmann, H. Laqua, C. Ochsenfeld, *J. Chem. Theory Comput.* **2021**, *17*, 1512–1521.

[162] F. Weigend, R. Ahlrichs, *Phys. Chem. Chem. Phys.* **2005**, *7*, 3297.

[163] S. A. Maurer, L. Clin, C. Ochsenfeld, *J. Chem. Phys.* **2014**, *140*.

[164] F. Aquilante, T. Bondo Pedersen, A. Sánchez de Merás, H. Koch, *J. Chem. Phys.* **2006**, *125*.

[165] H. Laqua, J. Kussmann, C. Ochsenfeld, *J. Chem. Phys.* **2021**, *154*, 214116.

[166] F. Weigend, M. Häser, H. Patzelt, R. Ahlrichs, *Chem. Phys. Lett.* **1998**, *294*, 143–152.

[167] F. Weigend, *Phys. Chem. Chem. Phys.* **2006**, *8*, 1057.

[168] A. Trofimov, J. Schirmer, *J. Phys. B - At. Mol. Opt. Phys.* **1995**, *28*, 2299.

[169] A. Trofimov, I. Krivdina, J. Weller, J. Schirmer, *Chem. Phys.* **2006**, *329*, 1–10.

[170] M. Wormit, D. R. Rehn, P. H. Harbach, J. Wenzel, C. M. Krauter, E. Epifanovsky, A. Dreuw, *Mol. Phys.* **2014**, *112*, 774–784.

[171] D. R. Rehn, A. Dreuw, *J. Chem. Phys.* **2019**, *150*.

[172] J. Schirmer, A. Thiel, *J. Chem. Phys.* **2001**, *115*, 10621–10635.

[173] B. Lunkenheimer, A. Köhn, *J. Chem. Theory Comput.* **2013**, *9*, 977–994.

[174] A. Luzanov, A. Sukhorukov, V. Umanskii, *Theor. Exp. Chem.* **1976**, *10*, 354–361.

[175] S. D. Folkestad, H. Koch, *J. Chem. Theory Comput.* **2019**, *16*, 179–189.

[176] S. D. Folkestad, E. F. Kjønstad, L. Goletto, H. Koch, *J. Chem. Theory Comput.* **2021**, *17*, 714–726.

[177] C. M. Aikens, S. P. Webb, R. L. Bell, G. D. Fletcher, M. W. Schmidt, M. S. Gordon, *Theor. Chem. Acc.* **2003**, *110*, 233–253.

[178] N. O. Winter, C. Hättig, *Chem. Phys.* **2012**, *401*, 217–227.

[179] R. C. Lochan, Y. Shao, M. Head-Gordon, *J. Chem. Theory Comput.* **2007**, *3*, 988–1003.

[180] E. G. Hohenstein, B. S. Fales, R. M. Parrish, T. J. Martınez, *J. Chem. Phys.* **2022**, *156*.

[181] D. Graf, M. Beuerle, H. F. Schurkus, A. Luenser, G. Savasci, C. Ochsenfeld, *J. Chem. Theory Comput.* **2018**, *14*, 2505–2515.

[182] M. Beuerle, D. Graf, H. F. Schurkus, C. Ochsenfeld, *J. Chem. Phys.* **2018**, *148*.

[183] D. Graf, M. Beuerle, C. Ochsenfeld, *J. Chem. Theory Comput.* **2019**, *15*, 4468–4477.

[184] M. Beer, C. Ochsenfeld, *J. Chem. Phys.* **2008**, *128*.

[185] J. L. Whitten, *J. Phys. Chem.* **1973**, *58*, 4496.

[186] B. I. Dunlap, J. W. Connolly, J. R. Sabin, *J. Chem. Phys.* **1979**, *71*, 3396.

[187] M. Feyereisen, G. Fitzgerald, A. Komornicki, *Chem. Phys. Lett.* **1993**, *208*, 359–363.

[188] K. Eichkorn, O. Treutler, H. Öhm, M. Häser, R. Ahlrichs, *Chem. Phys. Lett.* **1995**, *240*, 283–290.

[189] E. G. Hohenstein, R. M. Parrish, T. J. Martínez, *J. Chem. Phys.* **2012**, *137*, 044103.

[190] R. M. Parrish, E. G. Hohenstein, T. J. Martínez, C. D. Sherrill, *J. Chem. Phys.* **2012**, *137*, 224106.

[191] R. M. Parrish, E. G. Hohenstein, T. J. Martínez, C. D. Sherrill, *J. Chem. Phys.* **2013**, *138*, 194107.

[192] R. M. Parrish, E. G. Hohenstein, N. F. Schunck, C. D. Sherrill, T. J. Martínez, *Phys. Rev. Lett.* **2013**, *111*, 1–5.

[193] E. G. Hohenstein, S. I. Kokkila, R. M. Parrish, T. J. Martínez, *J. Chem. Phys.* **2013**, *138*, 124111.

[194] R. M. Parrish, C. D. Sherrill, E. G. Hohenstein, S. I. Kokkila, T. J. Martínez, *J. Chem. Phys.* **2014**, *140*, 181102.

[195] R. Schutski, J. Zhao, T. M. Henderson, G. E. Scuseria, *J. Chem. Phys.* **2017**, *147*, 184113.

[196] E. G. Hohenstein, B. S. Fales, R. M. Parrish, T. J. Martínez, *J. Phys. Chem.* **2022**, *156*, 054102.

[197] A. Jiang, J. M. Turney, H. F. Schaefer, *J. Chem. Theory Comput.* **2023**, *19*, 1476–1486.

[198] E. G. Hohenstein, S. I. Kokkila, R. M. Parrish, T. J. Martínez, *J. Phys. Chem. B* **2013**, *117*, 12972–12978.

[199] P. H. Harbach, M. Wormit, A. Dreuw, *J. Chem. Phys.* **2014**, *141*.

[200] J. Wenzel, A. Holzer, M. Wormit, A. Dreuw, *J. Chem. Phys.* **2015**, *142*.

[201] J. Wenzel, M. Wormit, A. Dreuw, *J. Comput. Chem.* **2014**, *35*, 1900–1915.

[202] J. Wenzel, A. Dreuw, *J. Chem. Theory Comput.* **2016**, *12*, 1314–1330.

[203] I. E. Brumboiu, D. R. Rehn, A. Dreuw, Y. M. Rhee, P. Norman, *J. Chem. Phys.* **2021**, *155*.

[204] D. Lefrancois, D. R. Rehn, A. Dreuw, *J. Chem. Phys.* **2016**, *145*.

[205] D. Lefrancois, D. Tuna, T. J. Martınez, A. Dreuw, *J. Chem. Theory Comput.* **2017**, *13*, 4436–4441.

[206] H. Laqua, J. C. Dietschreit, J. Kussmann, C. Ochsenfeld, *J. Chem. Theory Comput.* **2022**, *18*, 6010–6020.